Technology of THERMO FORMING

James L. Throne

© 1996 Carl Hanser Verlag. All rights reserved.
No unauthorized disclosure or reproduction; licensed to purchaser only.

EX1008 (Part 1 of 3)
Yita v. MacNeil
IPR2020-01139

Throne

Technology of Thermoforming

© 1996 Carl Hanser Verlag. All rights reserved.
No unauthorized disclosure or reproduction; licensed to purchaser only.

© 1996 Carl Hanser Verlag. All rights reserved.
No unauthorized disclosure or reproduction; licensed to purchaser only.

James L. Throne

Technology of Thermoforming

Hanser Publishers, Munich Vienna New York

Hanser/Gardner Publications, Inc., Cincinnati

© 1996 Carl Hanser Verlag. All rights reserved.
No unauthorized disclosure or reproduction; licensed to purchaser only.

The Author:
Dr. James L. Throne, Sherwood Technologies, Inc., 158 Brookside Blvd., Hinckley, OH 44233-9676, USA

Distributed in the USA and in Canada by
Hanser/Gardner Publications, Inc.
6600 Clough Pike, Cincinnati, Ohio 45244-4090, USA
Fax: (513) 527-8950
Phone: (513) 527-8977 or 1-800-950-8977

Distributed in all other countries by
Carl Hanser Verlag
Postfach 86 04 20, 81631 München, Germany
Fax: +49 (89) 98 12 64

The use of general descriptive names, trademarks, etc., in this publication, even if the former are not especially identified, is not to be taken as a sign that such names, as understood by the Trade Marks and Merchandise Marks Act, may accordingly be used freely by anyone.

While the advice and information in this book are believed to be true and accurate at the date of going to press, neither the authors nor the editors nor the publisher can accept any legal responsibility for any errors or omissions that may be made. The publisher makes no warranty, express or implied, with respect to the material contained herein.

Library of Congress Cataloging-in-Publication Data

Throne, James L., 1937-
Technology of thermoforming / James L. Throne.
p. cm.
Includes bibliographical references and index.
ISBN 1-56990-198-8
1. Plastics–Molding. I. Title.
TP1150.T48 1996
668.4'12–dc20 96-24175

Die Deutsche Bibliothek-CIP-Einheitsaufnahme
Throne, James L.:
Technology of thermoforming / James L. Throne.–Munich ;
Vienna ; New York : Hanser ; Cincinnati : Hanser / Gardner,
1996
ISBN 3-446-17812-0

All rights reserved. No part of this book may be reproduced or transmitted in any form or by any means, electronic or mechanical, including photocopying or by any information storage and retrieval system, without permission in writing from the publisher.

© Carl Hanser Verlag, Munich Vienna New York, 1996
Typeset in Ireland by Datapage International Ltd., Dublin
Printed and bound in Germany by Kösel, Kempten

© 1996 Carl Hanser Verlag. All rights reserved.
No unauthorized disclosure or reproduction; licensed to purchaser only.

Preface

I completed the monograph, *Thermoforming*, in 1985 and Carl Hanser Verlag published it in 1987. At the time it was written, there were no up-to-date monographs devoted solely to thermoforming. Two monographs devoted to thermoforming appeared about the same time as the *Thermoforming* monograph. They are:

J. Florian, *Practical Thermoforming: Principles and Applications*, Marcel Dekker, Inc., New York (1987).

G. Gruenwald, *Thermoforming: A Plastics Processing Guide*. Technomic Publishing Co., Inc., Lancaster PA (1987).

Reviewers of the three monographs remarked at the time that while there was some overlap, the three monographs provided separate and unique insights to the industry and that technologists would do well to have access to all three.

In the preface to that monograph, I stated that:

"Thermoforming is not an easy process. It just looks easy."

In many respects, the industry has verified this over and over in the last decade. I further stated that:

"... [Thermoforming] is becoming challenging as newer process variations, newer materials, tighter sheet and part tolerances, more critical applications and more sophisticated controls are developed."

In the last decade, the industry has successfully tackled many of these very difficult problems. The core business has been helped greatly by improved heaters, more accurate process controls, cooperative interaction between extruders and formers, more easily thermoformable polymers, advanced trimming techniques, and to a great degree, the acceptance of thermoforming as a process by OEMs. In addition, thermoforming has gained the attention of many universities, technical writers, consultants and software companies. And the industry has grown dramatically in size. As an example, the Society of Plastics Engineers Thermoforming Division held a fall conference in Wisconsin in 1991. About 100 people attended. In Midland MI in 1992 more than 200 attended. In South Bend IN in 1993, more than 400 attended, in Atlanta in 1994, more than 600 attended, and in Cleveland in 1995, nearly 700 attended. And plans are being made for nearly 800 in Cincinnati in 1996. There are more than 200 custom thermoformers in the US today and some estimate that a new thermoforming company is born every week.

The industry seems to have come of age in the last ten years. This work was intended to be a revision and update of the 1987 monograph. Readers of that monograph will note that this book is much larger. This book is also an overview of the technical aspects of thermoforming and generally follows the outline of the *Thermoforming* monograph. However, I have included worked-out examples and many guidelines to illustrate and support the technical aspects. As with the 1987 monograph, the material in each chapter of this book moves from relatively simple concepts to more technical, in-depth considerations. This book has ten chapters:

© 1996 Carl Hanser Verlag. All rights reserved.
No unauthorized disclosure or reproduction; licensed to purchaser only.

Chapter 1, "Thermoforming—Definitions, History, Methods and Equipment", is a proper introduction to the subject. The chapter includes some history, some market information, a glossary of definitions, the traditional methods of forming and some technical considerations about the machinery.

Chapter 2, "Polymeric Materials", briefly reviews the nature of thermoformable polymers and their adducts. General concepts of polymer response to applied loads and temperatures are considered. Some important new information on infrared energy absorption is detailed.

Chapter 3, "Heating the Sheet", reviews the three general ways of heating sheet—conduction, convection and radiation. Since infrared radiation is the most popular and efficient means of heating sheet, fundamental aspects are discussed. This chapter becomes quite technical with general guidelines for determining heating cycles and a new section on computer-generated prediction of sheet temperature.

Chapter 4, "Stretching the Sheet", is concerned with fundamentals of multiaxial sheet deformation. Polymer hot strength is related to tensile characteristics of rubbery solids and viscosity of elastic liquids. Sheet sag is shown to be strongly related to polymer hot strength. Again, the material is quite technical.

Chapter 5, "Cooling and Trimming the Sheet", deals with heat removal from the sheet while against the mold surface. Some new material on computer-generated mold temperature prediction is given. The mechanics of cutting the molded part from the web are considered in detail.

Chapter 6, "Thermoforming Molds", considers mold materials and mold designs. Vacuum or vent hole sizes and numbers are arithmetically determined and plug materials and designs are also discussed.

Chapter 7, "Parts Design", first considers the economics of parts design. Draw ratios are then defined and wall thickness prediction methods discussed. Regrind and material property loss are considered in detail, and an extensive section on part design guidelines follows.

Chapter 8, "Producing Sheet and Film", is a new chapter. Since the thermoformer is the customer of the extruder, he/she should know some rudimentary extrusion concepts. This chapter is a brief summary of the extrusion process, with emphasis on sheet quality and quality control. A sheet quality checklist is discussed in detail.

Chapter 9, "Newer Thermoforming Technologies", is also a new chapter, written in response to many requests for forming information in several new processing areas. In the 1987 monograph. I said:

> **"... [E]ngineers seeking the latest information on pressure forming, the heating of foam sheet or forming crystallizing PET will be disappointed."**

This is no longer the case. Chapter 9 presents vignettes on the following forming techniques:

- CPET,
- Pressure forming,
- Forming filled and reinforced polymers,
- Laminated sheet forming,

© 1996 Carl Hanser Verlag. All rights reserved.
No unauthorized disclosure or reproduction; licensed to purchaser only.

- Twin-sheet forming,
- Forming PP,
- Thermoforming foam sheet, and
- Other semi-thermoforming technologies.

Chapter 10, "Set-Up Protocols, Troubleshooting, and the Economics of Thermoforming", is an assemblage of production and economic issues that were scattered through several chapters of the 1987 monograph. Guidelines to setting up a new mold, forming a new polymer and troubleshooting both the thin-gage and heavy-gage forming process are found here. Thermoforming is an energy intensive process that uses only a portion of its raw material, sheet, to make the part. To be competitive, the thermoformer must know what things cost, in detail. This chapter focuses on this theme.

Caveats are in order. Some of the engineering details are quite technical. The monograph is designed to provide a technical foundation for the industry. Nevertheless, the casual reader should find ample guidelines, protocols, tips and rules-of-thumb to help him/her with specific processing problems or new product planning.

The decade or so since I wrote the *Thermoforming* monograph has been marked by retirement and deaths of many thermoforming leaders. Most notably, Dr. Herman "Dick" Osmers, SPE Thermoformer-of-the-Year, fellow PhD chemical engineer-consultant-teacher and critical reviewer of the 1985 book, died shortly after it was published. I will always miss his technical accuracy, his thoroughness, and his up-beat enthusiasm. This book is dedicated to his memory.

January 1996 James L. Throne, PhD

© 1996 Carl Hanser Verlag. All rights reserved.
No unauthorized disclosure or reproduction; licensed to purchaser only.

© 1996 Carl Hanser Verlag. All rights reserved.
No unauthorized disclosure or reproduction; licensed to purchaser only.

Contents

© 1996 Carl Hanser Verlag. All rights reserved.
No unauthorized disclosure or reproduction; licensed to purchaser only.

© 1996 Carl Hanser Verlag. All rights reserved.
No unauthorized disclosure or reproduction; licensed to purchaser only.

© 1996 Carl Hanser Verlag. All rights reserved.
No unauthorized disclosure or reproduction; licensed to purchaser only.

© 1996 Carl Hanser Verlag. All rights reserved.
No unauthorized disclosure or reproduction; licensed to purchaser only.

© 1996 Carl Hanser Verlag. All rights reserved.
No unauthorized disclosure or reproduction; licensed to purchaser only.

© 1996 Carl Hanser Verlag. All rights reserved.
No unauthorized disclosure or reproduction; licensed to purchaser only.

© 1996 Carl Hanser Verlag. All rights reserved.
No unauthorized disclosure or reproduction; licensed to purchaser only.

© 1996 Carl Hanser Verlag. All rights reserved.
No unauthorized disclosure or reproduction; licensed to purchaser only.

1 Thermoforming—Definitions, History, Methods and Equipment

© 1996 Carl Hanser Verlag. All rights reserved.
No unauthorized disclosure or reproduction; licensed to purchaser only.

1.1 Introduction

Thermoforming is a generic term encompassing many techniques for producing useful plastic articles from flat sheet. In its simplest concept, thermoforming is simply the manual draping of a temporarily softened sheet over a simple mold shape. In one of its more advanced forms, it involves automatic high-speed indexing of a freshly extruded sheet having very accurately known temperature into a forming and in-situ trimming station, with integral web regrind and automatic parts counting, packaging and shipping. In another, it involves automatic placement, plug and/or pneumatic stretching and pressure forming, with multi-axis router trimming.

Thermoforming is one of a family of processes that deal with the pressing or squeezing of pliable plastic into final shape. More than a century ago, celluloid or camphor-solvated cellulose nitrate, was the only malleable semi-synthetic plastic [1]. It was cut or rolled into sheet and made pliable with steam. When soft, it was squeezed into shape in matched dies or rolled into tubes and inflated against metal walls to produce parts. It was also draped over wooden forms. Cosmetic cases, baby rattles, and piano keys were typical of earliest thermoformed parts. The earliest processing of synthetic plastics, included common types of modern thermoforming, albeit restricted to one polymer and very limited processing conditions.

Thermoforming always begins with a contiguous sheet of rubbery plastic. The sheet is produced from:

- Resin liquid by casting as with PMMA, or
- Pellets or powder by:
  Calendering, as with PVC,
  Biaxially blowing film as with PE and PP,
  Extruding as with PS and ABS,
  Compression molding as with cellulosics and high temperature polyimides,

or by similar plastics processing techniques[1]. Thermoforming is differentiated by other processes in the following ways:

- From injection molding, where the initial resin state ispellet or powder and the shaping is done on the polymer as a liquid. As a result, the patented Monoblow process that injects a disk of plastic that is then compressed to a shape is not considered as a thermoforming variant [2].
- From compression molding, where pressures are substantially higher than those employed in traditional vacuum or low pressure thermoforming and where the polymer is shaped as a liquid between matched metal molds. This differentiation blurs when thermoforming technologies are used to form continuous fiber-reinforced composites. The Allied process described in Chapter 9 is a classic example of this blurring. Glass-reinforced nylon 6 or PA-6 sheet is heated to temperatures

[1] Throughout the text, plastics are referred to in abbreviations. Thus PMMA is *polymethyl methacrylate* and so on. A list of common polymer abbreviations is given as Appendix A, at the end of the book.

© 1996 Carl Hanser Verlag. All rights reserved.
No unauthorized disclosure or reproduction; licensed to purchaser only.

above the polymer melt temperature, then forged at relatively high pressures of 150 to 1500 lb_f/in^2 or 0.1 to 1 MPa [3].

Nontraditional thermoforming processes include the Dow scrapless thermoforming process or STP, where the extruded sheet is cut into squares that are then heated and forged into shapes. Other non-traditional and newer processes are discussed in Chapter 9.

1.2 History

Keratin, as a component in tortoise shell, was probably the first material to be thermoformed [4,5]. Keratin is also found in animal horn and hoof. It can be softened by immersing it in boiling water or oil. The sheet is then manually draped over a form and held until cool. Natural cellulose, primary element in tree bark, was shaped in a similar fashion by native Americans.

Although others experimented with natural and extracted cellulosics in the 1800s, J.W. Hyatt is credited with first recognizing the full *commercial potential* of camphor-solvated cellulose nitrate, which he called "celluloid". Most nineteenth century semi-synthetic plastic products were produced of celluloid or products of similar recipes simply by drape forming softened sheet. Sharps piano keys, formed over captive wooden blocks, are an example. A chronology of the early days in plastics as they pertain to thermoforming is given in Table 1.1.

Modern thermoforming began about 60 years ago, shortly before, during, and shortly after the second world war, with major developments in two important areas. Research in thermoplastic resin chemistry led to commercialization of extrusion grade flexible PVC or FPVC, CA and PS and the development of cell-cast PMMA. And continuous forming was achieved with the invention of the screw extruder and the roll-fed thermoformer. These breakthroughs allowed a wide variety of prewar domestic products, particularly thin-gage packages, to be developed. This in turn prepared formers for war product developments such as airplane canopies and war survey relief maps. The packaging industry adopted thermoforming as a basic process in the late 1940s to such an extent that the thermoformed package was considered the most significant packaging development of the 1950s decade [6]. In the 1970s, demand for convenience food containers, ovenable portion servings, and more ductile disposable drink cups spurred development of foam PS, CPET, and PP pressure forming processes. Shower stalls, tub surrounds, and refrigerator liners were thermoformed from heavy-gage sheet. The development of the interstate system led to production of large, light-weight illuminated plastic signs and fast food franchises adopted thermoformed plastics as a way of producing such signs. Engineers developed ways of forming plastic sheets for the transportation industry from reinforced and fire-retardant polymers. Ahead lies further opportunities to replace injection molded plastics in many applications such as packaging lids and containers, welded steel in food cans, glass in jars, aluminum in beverage cans, and hand-laid thermoset

© 1996 Carl Hanser Verlag. All rights reserved.
No unauthorized disclosure or reproduction; licensed to purchaser only.

Table 1.1 Chronology on Thermoforming[1]

Period	Event
Prehistory—Egypt	Heating tortoise shell, keratin, in hot oil, then shaping to produce food containers.
Prehistory—Micronesia	Heating tortoise shell, keratin, in hot water, then shaping to produce bowls.
Prehistory—Americas	Heating tree bark, natural cellulose, in hot water, then shaping to produce bowls, boats, canoes.
1845	Extrusion process commercialized from forerunners of today's plastics. Alfred P. Critchlow, Florence MA develops molding presses, dies for gutta-percha, shellacs.
1850s	Gutta-percha replaces ivory for billiard balls.
1856	First moldable plastic, fibrous cellulosic pulp and gum shellac by Peck.
1862	Cellulose nitrate solvated with camphor to produce "Parkesine" by Alexander Parkes.
1868	Celluloid, molding grade Pyroxylin by John Wesley Hyatt.
1870s	Hydraulic planer for cutting thin sheets by Charles Burroughs Co., MJ, USA.
1870s	Celluloid tubes steam-heated, placed in metal form, inflated with steam pressure yielding blow molding, pressure forming.
1907	Compression molded phenolic bobbin ends, Richard Seabury, Boonton Rubber, Boonton NJ.
1910	Sharps piano keys drape-formed over captive wooden cores.
1930	Bottle formed from two thermoformed halves by Fernplas Corp.
1930s	Relief maps for US Coast & Geodetic Survey.
1938	Blister pack of cellulose acetate.
1938	Roll-fed automatic thermoformer developed by Clauss B. Strauch Co.
1938	Cigarette tips, ice-cube trays automatically thermoformed.
1942	Cast PMMA acrylic thermoformed for fighter/bomber windows, gun closures, windscreens.
1942	Standard mold bases, Detroit Mold Engineering (D-M-E).
1948	Cast PMMA acrylic bathtubs thermoformed by Troman Bros., England.
1954	Skin-packaged products shown at Hardware Manufacturers Association, Chicago.
1970	Thermoformed ABS automobile body by Borg-Warner.

[1] Adapted from [4,5,32]

composites in aircraft and other transports. The prospects for advanced thermoforming systems are discussed in detail in Chapter 9.

1.3 Markets

A best estimate of the entire US consumption of thermoformed shapes in 1992 is about 1181 Mkg or 2600 Mlb. About 800 Mkg or 1760 Mlb is thermoformed into disposables. The fraction of plastics thermoformed into disposables has dropped steadily in the past decade from about 74% in 1983-1984 to about 68% today [7-9].

© 1996 Carl Hanser Verlag. All rights reserved.
No unauthorized disclosure or reproduction; licensed to purchaser only.

Table 1.2 US Polymers Converted via Thermoforming

Polymer	Amount thermoformed (Mkg)						Annual growth (%)
	1962	1969	1977	1983–1984	1992	1995	1984–1992
ABS	NA	40	70	127	202	240	6
PMMA	NA	21	36	38	42	50	2
Cellulosics	8	5	8	4	5	5	0
LDPE	NA	0.7	0.4	0.6	0.7	0.8	0
HDPE	NA	7	10	26	59	87	11
PP**	NA	1	8	22	72	115	16
PS	69	166	392	480	640	720	4
PVC	4	13	24	45	60	72	4
PET	NA	NA	NA	40	80	110	9
Other*	1	NA	NA	NA	20	50	–
Totals	82	254	544	782	1181	1450	5

* Includes K-resin, PAN, XT, TPO polymers
** Does not include stampable PP for automotive applications
NA = Not available (not included)

An estimate of the amounts of plastic consumed in thermoforming in the US in the 30 years from 1962 to 1992 is given in Table 1.2. The data are obtained from several sources [8-10]. In 1969, the industry was projected to grow at about 8.5% to 9% per year during the 1970s. It was then estimated that 527 Mkg or 1180 Mlb would be consumed by 1978 (Fig. 1.1). About 550 Mkg or 1230 Mlb was actually consumed in 1977. In 1969, it was predicted that consumption in 1984 would be 780 to 830 Mkg or 1750 to 1860 Mlb. In 1986, it was determined that about 773 Mkg or 1732 Mlb were actually consumed in 1983-1984 [11]. In 1986, it was predicted that consumption would reach 1045 Mkg or 2300 Mlb in 1992. The prediction is about 13% below actual consumption (Fig. 1.1). The 1986 projection also indicated that 1290 Mkg or 2840 Mlb would be thermoformed in the year 2000. From Fig. 1.1, current, 1994 projection indicates 1860 Mkg or 4100 Mlb will be consumed in the year 2000. This is a continuing annual growth rate of more than 5%.

As seen in Table 1.2, polystyrene accounts for more than half the plastic thermoformed into parts. The growth in this established polymer is less than 3% per year. As expected, PP and PET are experiencing double digit annual growth as new polymers and forming processes are developed. Surprisingly, HDPE growth is also very high, with outdoor products contributing to the growth. As an example, there were no HDPE truck bed liners used in the early 1980s. In 1992, the size of this market alone is approaching 23 Mkg or 50 Mlb. Cellulosics continue to lose market share to PP, PVC and PS, particularly in packaging. In 1984, 7 Mkg or 16 Mlb thermoplastic polyesters or PETs were thermoformed. Only a very small fraction, less than 1%, was crystallized PET. Since the development of CPET thermoforming processes in the 1980s, CPET has become a staple in the disposable food serving and heating tray and dish markets. In 1984, it was estimated that the development of CPET would spur the consumption of PET to double in five years, to 14 Mkg or

© 1996 Carl Hanser Verlag. All rights reserved.
No unauthorized disclosure or reproduction; licensed to purchaser only.

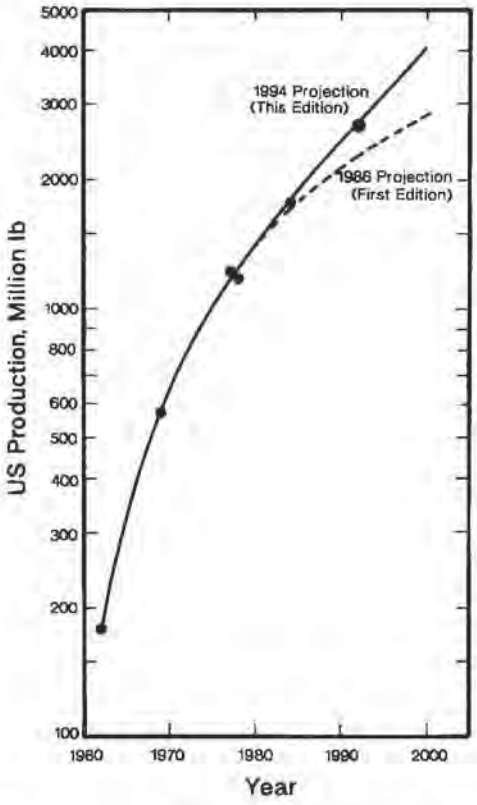

Figure 1.1 US Production of thermoformed products. Adapted from [7-11]

Table 1.3 Approximate Conversion Level of Thermoplastic Polymers to Thermoformed Produces[1]

Polymer	Amount of polymer converted to sheet (%)	Amount of sheet thermoformed (%)	Total amount of polymer formed into product (%)
ABS	25	60	15
PMMA	50	30	15
Cellulosics	25	50	12.5
HDPE	2	30	0.6
LDPE	0.25	5	0.01
PP	1	25	0.25
PS	30	65	19.5
PVC	10	20	2.0

[1] Adapted from [7,8]

© 1996 Carl Hanser Verlag. All rights reserved.
No unauthorized disclosure or reproduction; licensed to purchaser only.

32 Mlb. In actuality, in 1992, this market is about 70 Mkg or 154 Mlb, a ten-fold increase in less than a decade. In 1992, the consumption of CPET is estimated to be about 19 Mkg or 42 Mlb, or about 27% of the total thermoformed PET consumption.

About half of all sheet stock is converted to product by thermoforming [12]. The amount of resin converted into sheet varies from about half of all PMMA polymers to less than 1% of all LDPE polymers (Table 1.3). Only about 5% of all LDPE sheet and film is converted to product by thermoforming whereas 65% of all polystyrene sheet is converted. These are mid-1980s data but the percentages have held relatively constant since the 1960s. Similarly, major markets have remained relatively obvious for nearly two decades. Major new packaging markets continue to be in disposables, as illustrated by the development of PP and CPET food packages and the commercial realization of convenience food foam carryout containers. Applications have also broadened to include packaging of heavier items such as power tools and medical items such as critical care emergency packages. Nearly all packaging applications rely on roll-fed thin-gage sheet stock. In heavy-gage discrete sheet forming, the market traditionally has focussed on economic production of a few, large pieces. As a result, applications include:

- Major appliance components, such as refrigerator cabinet and door liners,
- Recreation products such as swimming and wading pools,
- Vehicles such as snow mobiles and all-terrain vehicles, automotive inner-door panels, truck and tractor cab kick panels,
- Home products such as tube and shower stalls that are backed with GR-UPE, luggage shells, and
- Display items such as advertising, exterior signs and point-of-purchase stands.

Table 1.4 Markets for Thermoformed Products

Packaging and related items
Blister packs, point-of-purchase containers
Bubble packs—slip sleeve, vacuum carded containers
Electronics—audio/video cassette holders
Tool cases—hand, power
Cosmetics—cases, packages
Foams—meat, poultry trays
Unit serving—foodstuffs
Convenience—carry-out, cooking-box trays
Convertible-oven food serving trays
Wide-mouth jars
Vending machine hot drink cups
Cold drink cups—beer, soda
Egg cartons
Wine bottle protectors
Produce separators—apples, grapefruit
Portion—medical unit dose
Form-fill-seal—jelly, crackers, nuts and bolts

(Continued)

© 1996 Carl Hanser Verlag. All rights reserved.
No unauthorized disclosure or reproduction; licensed to purchaser only.

Table 1.4 (Continued)

Vehicular
Automotive door innerliners, headliners
Automotive utility shelves, liners
Automotive instrument panel skins
Aircraft cabin wall panels, overhead compartment doors
Snowmobile shrouds, windshields
Motorcycle windshields, farings, scooter shrouds, mudguards
All-terrain vehicle exterior components
Golf cart shrouds, seats, trays
Tractor shrouds, door fascia
Camper hardtops, interior components such as doors, cabinet tops
Truck cab door fascia, instrument cluster fascia
Recreational vehicle interior components, window blasters
Industrial
Tote bins
Pallets, single deck, double deck
Parts trays, transport trays
Equipment cases
Building products
Shutters, window fascia
Skylights, translucent domes
Exterior lighting shrouds
Storage modules—bath, kitchen, pantry
Lavys
Bath and shower surrounds, GR-UPE backed
Soaking tubs, GR-UPE backed
Retrofit shower components, shower trays
Others
Exterior signs
Advertising signs, lighted indoor signs
Swimming and wading pools
Tray, baskets, hampers, carrying cases
Luggage
Gun cases, golf club cases
Boat hulls, surf-boards, with PUR foams
Animal containers
Prototype concepts for other plastic processes

The recent rediscovery of pressure forming of sheet against a female mold offers an entre into the economically important market of business machine housings [13]. Some major markets are listed in Table 1.4 [14]. The sizes and annual percent growth rates or APR are given in Table 1.5 for several of these markets.

Most of the fully developed, mature thermoforming markets are developed around amorphous polymers such as PVC, PS, ABS and PMMA. These polymers are processed quite successfully over rather wide temperature ranges. Amorphous polymers are usually quite forgiving in this respect. Crystalline polymers and reinforced amorphous polymers, on the other hand, have narrower forming

© 1996 Carl Hanser Verlag. All rights reserved.
No unauthorized disclosure or reproduction; licensed to purchaser only.

© 1996 Carl Hanser Verlag. All rights reserved.
No unauthorized disclosure or reproduction; licensed to purchaser only.

Table 1.5 Selected Growth Markets for Thermoforming

Market	77	78	79	80	81	82	83	84	85	86	87	88	89	90	91	92	93	94	95	96	97	98	99	Average annual growth (%) (years)
Thermoforming machinery (US$ × 10^6) [35]	22												91					121						5.9 (94/89)
Rigid plastic packaging (US$ × 10^9) [36]													6.6											–
Plastic containers (× 10^9 units) [37]									27.2					38					51					6.5 (95/85)
Multilayer containers (× 10^9 units) [37]									0.3					11					29					58.0 (95/85)
Business machine housings (× 10^6 lb) [38]	55			115				178	160					231										8.6 (90/85)
Retortable plastic containers (× 10^9 units) [39]											0.25	0.3	0.6	1.1	2.8									62 (91/86)
Automotive sheet stamping (× 10^6 lb) [40]					4					25					60					90				19 (91/86)
Polystyrene in packaging (× 10^9 16) [41]															2.38				2.74				3.1	2.8 (95/90)
Nucleated PP—sheet extrusion (× 10^6 lb) [42]															3.3					10				25 (96/91)
Barrier packaging polymers (× 10^6 lb) [43]														940					1475					9.4 (95/90)
Modified atmosphere packaging (× 10^6 lb) [44]														800					1400					11.8 (95/90)
Controlled atmosphere packaging (× 10^6 lb) [44]														400					800					14.9 (95/90)

(Continued)

© 1996 Carl Hanser Verlag. All rights reserved.
No unauthorized disclosure or reproduction; licensed to purchaser only.

Table 1.5 (Continued)

Market	77 78 79	80 81 82	83 84 85	86 87 88	89 90 91	92 93 94	95 96	97 98 99	Average annual growth (%) (years)
PP sheet—non-automotive ($\times 10^6$ lb) [45]			44		141				21 (90/84)
PP sheet—auto/appliance ($\times 10^6$ lb) [45]			35		125				24 (90/84)
Plastics in appliances ($\times 10^6$ lb) [46]						888	1047		4.1 (97/92)
Microwavable plastic containers ($\times 10^6$ units) [47]				96		310			26 (93/88)
Non-disposable polyolefin foam ($\times 10^6$ lb) [48]				20	23				4.8 (92/89)
Medical plastics ($\times 10^9$ lb) [49]	0.65			2.05		2.86			6.9 (94/89)
Transport plastics ($\times 10^9$ lb) [50]				1.20	1.19	1.55			5.4 (94/89)
Plastics in appliances (US$ $\times 10^9$) [51]				1.16	1.30				2.4 (91/86)
Plastics in packaging (US$ $\times 10^9$) [52]				7.3		8.1			2.1 (94/89)

windows, usually require higher forming pressures, and/or usually cannot be consistently formed on conventional thermoforming equipment. Only recently has the forming industry begun to apply fundamental processing principles to the development of machinery capable of holding accurate sheet temperatures and forming pressures.

1.4 Some Definitions

The technology of thermoforming is rapidly changing. Old ideas about process limitations are being challenged daily. In 1992, one machinery manufacturer said that:

> "More innovations have been made in thermoforming machinery in the last half-dozen years than in all the years before." [15].

As noted below, machinery innovations include:

- Improved and more reliable ways of clamping sheet,
- Improved heaters,
- Improved heat distribution patterns,
- Adaptation of infrared sensors for monitoring and controlling sheet residence time in ovens,
- Improved clamping systems,
- New plug assist materials,
- Better control of stretching forces and pressures,
- Improved trim dies, and
- Many new mold materials and mold making techniques.

Of course, innovations are not just restricted to machinery. The past decade has seen extensive efforts to produce uniform-property extruded sheet, newer polymers with superior sag resistance and oxidative resistance, regrind monitoring techniques and computer programs to predict time-dependent sheet temperature and local wall thickness. However, there are certain guidelines about the thermoforming process that are relatively generic. For example, thermoforming has become economically important since it offers processing advantages over competitive processes such as:

- Accumulator blow molding,
- Injection blow molding,
- Rotational molding, and
- Injection molding.

Relatively low forming pressures are needed and so mold costs are low and products of relatively large size are fabricated economically. Parts with very small thickness-to-area ratio are fabricated. For thin-walled products, fabrication time is very short, making the process economical for products requiring high multiplication factors.

© 1996 Carl Hanser Verlag. All rights reserved.
No unauthorized disclosure or reproduction; licensed to purchaser only.

For a few thick-walled parts, molds are made of wood, plaster or other easily shaped, relatively inexpensive materials. Mold fabrication time and thus lead time are very short. Thermoforming is the method most usually selected for prototype and display products to be made of other processes.

Gage

Typical thermoforming steps are:

- Clamping,
- Heating,
- Shaping,
- Cooling, and
- Trimming.

The general process of thermoforming is loosely separated by sheet thickness or *gage*. There are two broad categories—thin-gage and heavy-gage. Recently, sub-categories have been introduced to further classify the process.

Thin-gage thermoforming means that the sheet thickness is less than about 0.060 in or 1.5 mm. This category is further classified into:

- Film forming, where the sheet thickness is less than about 0.010 in or 0.25 mm.
- Thin sheet forming, where the sheet thickness is between about 0.10 in or 0.25 mm and 0.060 in or 1.5 mm.

Heavy-gage thermoforming means the sheet thickness is greater than about 0.120 in or 3 mm. This category is further classified into:

- Heavy sheet forming, where the sheet thickness is between about 0.120 in or 3 mm and about 0.400 in or 10 mm.
- Plate forming, where the sheet thickness is greater than about 0.400 in or 10 mm.

There is a gray area between thin-gage ($\leq$0.060 in or 1.5 mm) and heavy-gage ($\geq$0.120 in or 3 mm). In some instances, sheet in this mid-gage range of 0.060 in to 0.120 in or 1.5 mm to 3.0 mm behaves as if it is thin-gage, and in others, as if it is heavy-gage. This gray area is most apparent during handling of the sheet, heating the sheet and trimming the part from the web.

Polystyrene and polyolefin foam sheet thicknesses are usually greater than 0.120 in or 3 mm but these foams are usually treated as thin-gage sheet stock.

Clamping of Thin-Gage Sheet

Thin-gage sheet is usually supplied to the former in rolls. The majority of packaging applications such as blister pack, form-fill-seal packaging, foam sheet forming and biaxially oriented forming uses thin-gage sheet. Formers that use roll sheet stock are

© 1996 Carl Hanser Verlag. All rights reserved.
No unauthorized disclosure or reproduction; licensed to purchaser only.

called *roll-fed* or *continuous sheet* formers. Clamping is by parallel continuous loop chain-fed pins or pin-chains that pierce the sheet at 1 in or 25 mm intervals at about 1 in or 25 mm from each edge. For high-temperature forming of CPET or PP, the rails are shielded from the sheet heating source or are actively cooled. The edges of the sheet and the plastic between the formed product are trimmed, reground and reextruded into sheet for forming.

Clamping of Heavy-Gage Sheet

Heavy-gage sheet is usually supplied as cut, stacked and palleted sheet. The demand for large numbers of large, heavy-wall parts such as refrigerator door liners and vehicle interior components, has led to the development of an in-line heavy-gage sheet extrusion and thermoforming concept (Fig. 1.2) [16]. The sheet extruder is placed in-line with the thermoformer, thus obviating problems associated with handling cut-sheet materials. Formers that use discrete heavy-gage sheet are called *cut-sheet* formers. Cut-sheet clamping frames are usually held closed with mechanical spring-loaded toggle clamps or pneumatic hold-down bars. Shuttle clamps are also used.

Heating of Thin-Gage Sheet

There are three ways of heating sheet:

Conduction, where the sheet is placed in direct contact with the heating medium, such as a hot plate,
Convection, where the sheet is heated with hot air, and
Radiation, where infrared heat from metal wires, ceramic plates, or gas-fired combustion is the primary means of heating the sheet.

Thin-gage, roll-fed sheet is usually heated by passing the sheet between banks of infrared radiant heaters. Combinations of radiation and convection heating are used

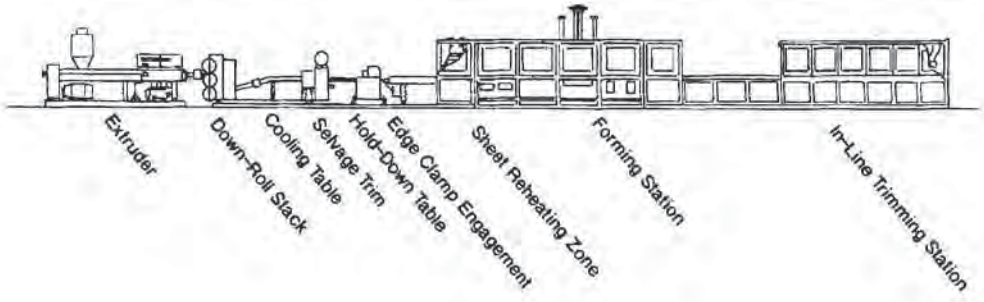

Figure 1.2 In-line heavy-gage sheet extrusion and thermoforming line—Cannon-Shelly [16]

© 1996 Carl Hanser Verlag. All rights reserved.
No unauthorized disclosure or reproduction; licensed to purchaser only.

as well. These are detailed in Chapter 4. Most plastics formed today, such as PS, PVC and ABS, are formed at relatively low temperatures such as 250°F to 450°F or 120°C to 230°C.

Heating Heavy-Gage Sheet

Intense energy input from radiant heaters is unwarranted and is potentially a problem for heavy-gage sheet. Conduction of the energy from the surface of the sheet to its interior controls the heating time. As a result, heavy-gage sheet is frequently heated with forced convection hot air or reradiated energy from fine mesh metal screens or hot plates. Heater types and temperatures are selected on the basis of optimizing the amount of energy transferred to the sheet per unit time.

Shaping Thin-Gage Sheet

In the earliest days of thermoforming, the rubbery sheet was manually stretched or draped over a male mold. *Drape forming* or male mold forming, requires no forming pressure and no difference in pressure across the sheet thickness. Certain aspects of drape forming are used today, whenever male portions of female molds are employed. *Vacuum forming* is the application of differential pressure across the sheet thickness of up to 0.1 MPa or 15 lb_f/in^2 or one atmosphere absolute. In modern commercial machines, the applied vacuum is on the order of 0.05 to 0.09 MPa or 7.3 to 14 lb_f/in^2. Since thin-gage sheet surface-to-volume ratio is very large, thin-gage sheet loses heat to its surroundings very rapidly. As a result, thin-gage sheet is usually formed very rapidly (in seconds). Furthermore, more than one part is formed at a time. Special clamps called cavity isolators are used to minimize nonuniformity in individual part wall thickness due to polymer pulling from one cavity to another during forming. Foams are normally very resilient or stiff at their forming temperatures and so matched die molding is used.

Shaping Heavy-Gage Sheet

Drape forming and vacuum forming are common ways of stretching heavy-gage sheet as well. Usually the mold has a single cavity. Sheet manipulation or prestretching with air or with mechanical assists called *plugs* is a common way of redistributing the plastic across the mold surface to minimize thin spots. In addition, *pressure forming* has been rediscovered. Historically, steam pressure was used to force celluloid against mold surfaces [17]. Air is used today in place of steam [18]. Although forming pressures to 3.5 MPa or 500 lb_f/in^2 are used when shaping continuous fiber-reinforced composites, the pressure forming range of 0.14 to 0.56 MPa or 20 to 80 lb_f/in^2 is commercial with 1.4 MPa or 200 lb_f/in^2 considered the practical upper limit. Pressure forming is combined with vacuum forming to gain additional differential

© 1996 Carl Hanser Verlag. All rights reserved.
No unauthorized disclosure or reproduction; licensed to purchaser only.

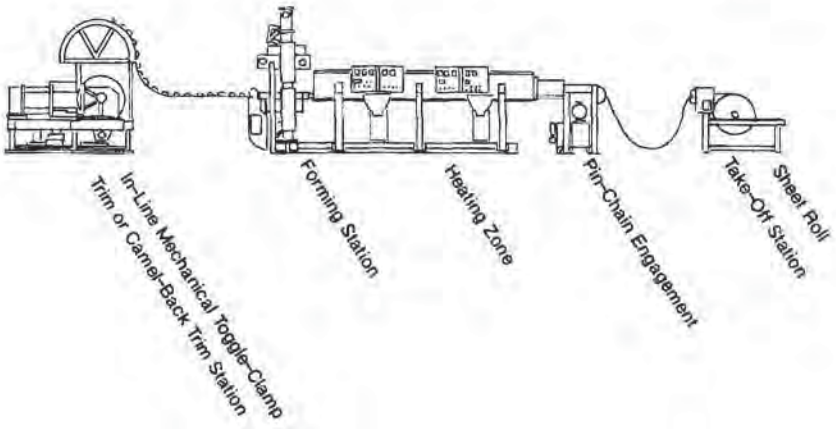

Figure 1.3 Roll-fed thin-gage thermoforming line with in-line trimming station—Battenfeld-Glencoe

pressure and to minimize air pockets between the mold and the sheet. Pressure forming is best suited to heavy-gage sheet forming into female molds. Higher forming pressures require more substantial mold construction. This increases the mold cost and the lead time.

Trimming the Thin-Gage Sheet

Thin-gage sheet can be trimmed in the mold or in a separate in-line hydromechanical trimming device. A camel-back or hump-back trimmer is shown in line with a roll-fed former in Fig. 1.3.

Trimming the Heavy-Gage Sheet

On occasion, heavy-gage sheet is also trimmed in the press. The more common trimming scenario is the transfer of the sheet from the forming press to a trimming fixture. Trimming follows one of the following:

- Manual with a hook-knife or hand-held router,
- Manual with a bandsaw,
- Automatic with a multi-axis trimming fixture, or
- Automatic with a water jet or laser.

Depth-of-Draw

Historically, thermoforming rules-of-thumb are based on the *depth-of-draw* of a given polymer into a given mold configuration. The depth of draw concept is loosely

© 1996 Carl Hanser Verlag. All rights reserved.
No unauthorized disclosure or reproduction; licensed to purchaser only.

understood among formers as the ratio of the depth a sheet could be drawn into a female mold to the minimum dimension at the rim. It is frequently given the notation *h*:*d*. Unfortunately, this definition is easily misinterpreted, is vague for non-cylindrical shapes, and does not truly describe the stretching process. Other definitions based on areal draw ratio and linear stretching are more accurate, as discussed in Chapter 7. For reference, the areal draw ratio is the ratio of the area of the formed sheet to that of the unformed sheet. The linear draw ratio is the length of an imaginary line drawn on the formed sheet to its original length.

1.5 Methods of Forming

In its simplest form, thermoforming is the stretching of a heated rubbery sheet into a final shape. As the sheet is stretched against the mold surface, it stops drawing. As a result, the final part has thick walls where the sheet touched the mold first and thin walls where it touched last (Fig. 1.4). In many thin-gage forming applications, the extent of sheet that is stretching is small and so the areal draw ratio is small. The package integrity and durability are therefore uncompromised. Typical applications are in packaging areas such as blister and bubble packs, form/fill/seal packages and fast food containers and picnic plates. If a high degree of stretching is needed, as with disposable drink cups or for heavy-gage sheet forming, simple stretching techniques are insufficient. The methods of forming are divided into the number of sequential steps needed to form the part once the sheet is at the forming temperature.

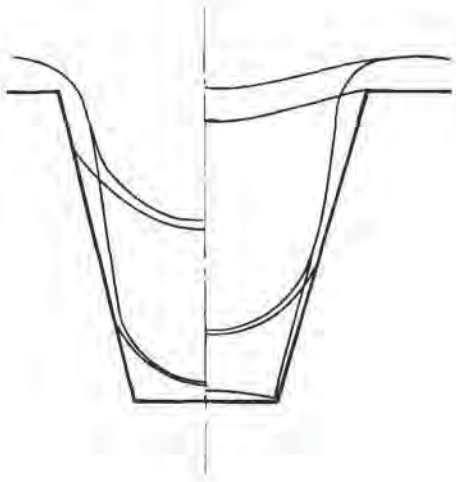

Figure 1.4 Wall thickness variation during draw-down in simple female vacuum forming

© 1996 Carl Hanser Verlag. All rights reserved.
No unauthorized disclosure or reproduction; licensed to purchaser only.

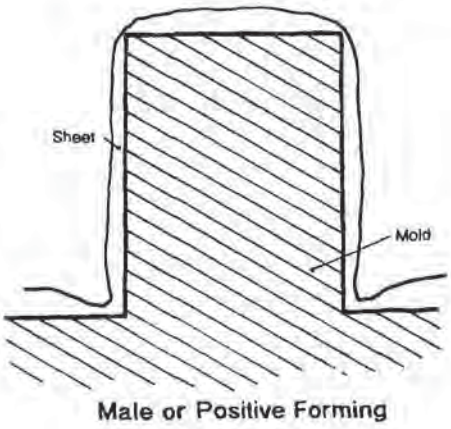

Figure 1.5 Drape forming onto a positive or male mold

One-Step Forming

There are at least five types of one-step forming:

- In *drape forming*, Fig. 1.5, the clamped, heated rubbery sheet is either lowered onto the male mold or the mold is raised into the sheet. The sheet in contact with the mold does not stretch. For modern drape forming, the air trapped between the sheet and the mold is evacuated as the mold penetrates and stretches the sheet against the mold flange. Either vacuum or air pressure is used to produce the differential pressure needed to force the sheet against the male mold. In drape forming, the formed part has a thick bottom and thin sidewalls. The part is thinnest at the rim. Drape forming is also called *male molding*.
- In *vacuum forming*, Fig. 1.6, the clamped, heated rubbery sheet is sealed against the rim of the female mold. Vacuum is then applied. The differential pressure presses the sheet against the mold surface. As noted before, the formed part has

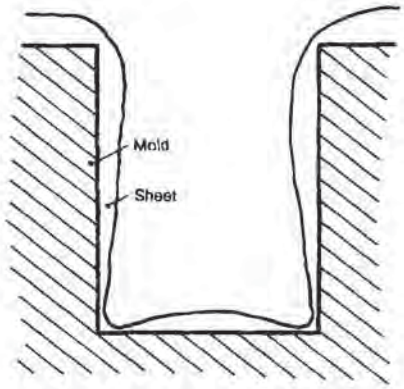

Figure 1.6 Vacuum forming into a negative or female cavity

© 1996 Carl Hanser Verlag. All rights reserved.
No unauthorized disclosure or reproduction; licensed to purchaser only.

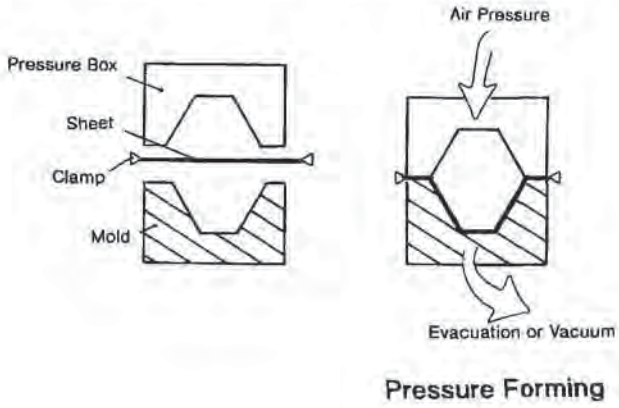

Figure 1.7 Pressure forming

a thick rim and is thinnest in the bottom corners. This is also called *cavity forming* or *female molding*.

- *Pressure forming*, Fig. 1.7, is similar to vacuum forming. A pressure box is fitted over the sheet as it is held against the mold rim and positive air pressure is used to push the sheet into the mold corners. Since air pressure to 1.4 MPa or 200 lb_f/in^2 is used, the pressure box must seal against the free surface of the sheet. Pressure forming is used for difficult-to-form roll-fed thin-gage polymers such as PP and for production of highly detailed heavy-gage parts [18].
- In *free blowing*, Fig. 1.8, the clamped heated rubbery sheet is stretched with air into a free-form shape. The amount of air pressure is controlled with a photocell that senses the height of the expanding bubble. Since the environmental air is slightly cooler than the sheet, the sheet cools in the free-form shape. This

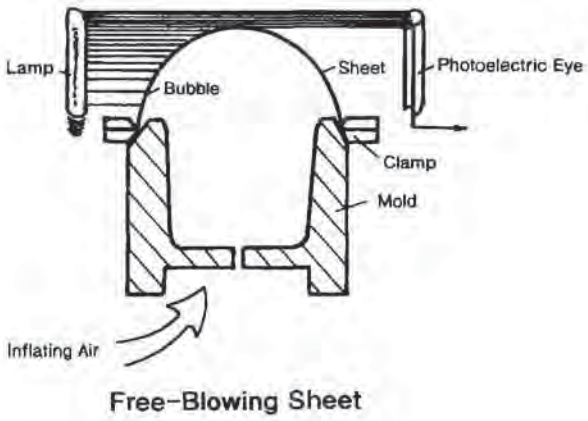

Figure 1.8 Free-blowing to produce domes

© 1996 Carl Hanser Verlag. All rights reserved.
No unauthorized disclosure or reproduction; licensed to purchaser only.

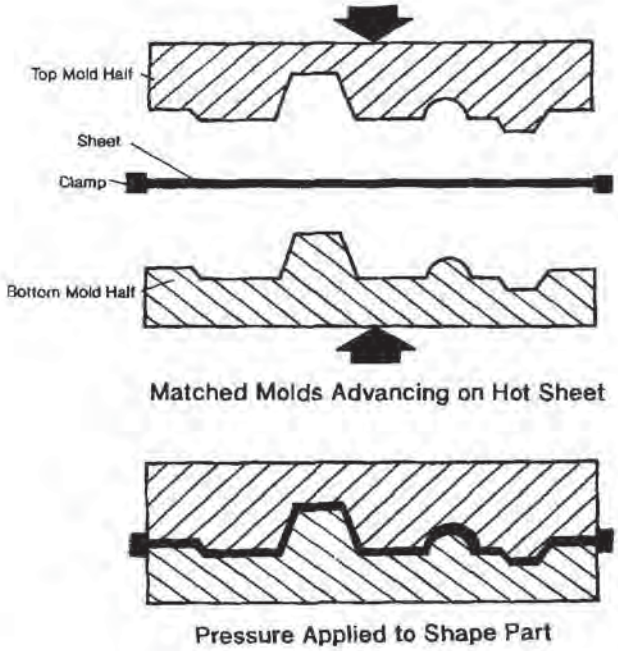

Figure 1.9 Matched die molding with trapped sheet formed at applied pressures less than 1 MPa or 150 lb_f/in^2

technique was pioneered for aircraft gun enclosures. Since the sheet does not touch a solid surface during forming, it remains mar-free. The bubble wall thickness is quite uniform except near the clamping area. Freely blown roll-fed thin-gage bubbles are used for blister packs.

- *Matched die molding*, Fig. 1.9, is a common way of forming shapes from relatively stiff polymers, such as PS foam or filled polymers. The clamped heated rubbery sheet is positioned between two mold halves. As the mold halves close, vacuum is applied to the female half of the mold to assist with forming. Part wall thickness depends on the mating tolerances of the two mold halves. Appreciable material movement is possible if applied forces are relatively large. Usually the applied pressures do not exceed about 1 MPa or 150 lb_f/in^2 and are usually about 0.34 MPa or 50 lb_f/in^2.

Two-Step Forming with Prestretching

Multi-step forming was developed primarily for heavy-gage sheet where single parts are often quite complex and deep and where cost considerations make wall thickness uniformity a significant design parameter. In thin-gage thermoforming, forming times are very short and shapes are relatively simple. Until a few years ago, thin-gage

© 1996 Carl Hanser Verlag. All rights reserved.
No unauthorized disclosure or reproduction; licensed to purchaser only.

forming was restricted to one of the one-step techniques described above. In the 1970s, the development of plug assisted pressure forming of PP below its melting temperature led the way to highly automated multi-step forming of thin-gage roll-fed sheet. The first step in multi-step forming is usually a form of sheet stretching, such as *plug assist* or *billowing*. The prestretched sheet is then pressed against the mold surface. Some examples of multi-step forming follow:

- There are many variations of bubble or billow prestretching. The first step is to pneumatically inflate the clamped heated rubbery sheet to a controlled height with internal air pressure. Typically the differential pressure is 0.014 to 0.055 MPa or 2 to 8 lb_f/in^2 gauge. The bubble height is controlled either by touching a microswitch or by intercepting a photoelectric eye. At this point, the mold can interact with the stretched sheet in one of several ways:
  - In *billow drape forming*, Fig. 1.10, the male mold is pressed into the top of the prestretched sheet. This technique yields a part with wall thicknesses that are much more uniform than that obtained with straight drape forming.
  - When a female mold is used, in *billow vacuum forming*, Fig. 1.11, the differential pressure that has inflated the bubble is reversed. This causes the prestretched sheet to snap into the female mold. Again, the part wall thickness

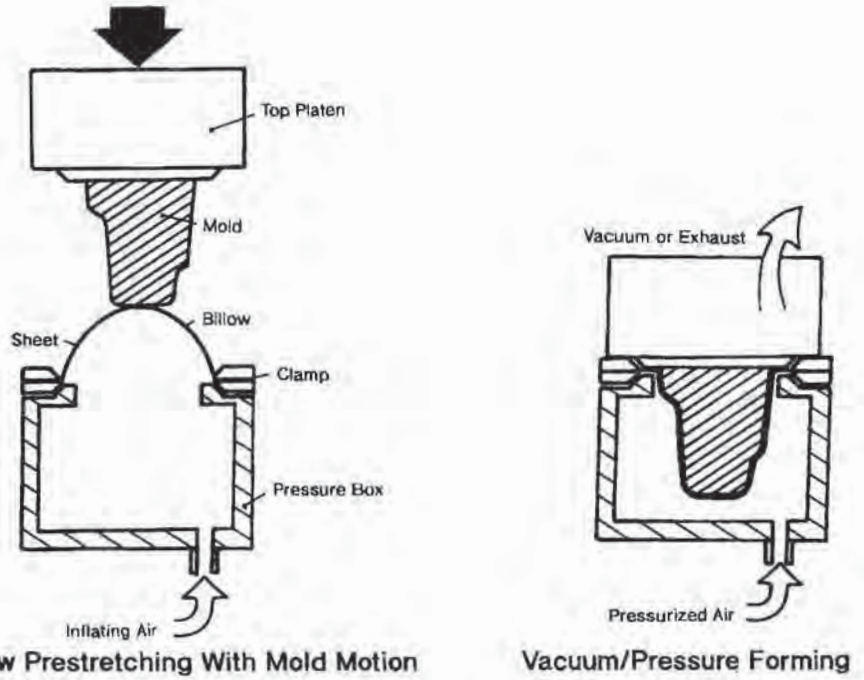

Figure 1.10 Billow drape forming, with either vacuum or applied air pressure shaping the sheet against the mold surface

© 1996 Carl Hanser Verlag. All rights reserved.
No unauthorized disclosure or reproduction; licensed to purchaser only.

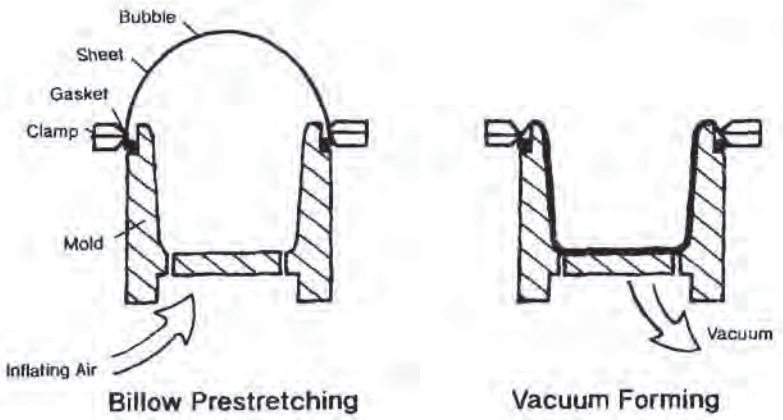

Figure 1.11 Billow vacuum forming

is much more uniform than that obtained with conventional vacuum forming. The eversion of the bubble can be tricky, so this technique is difficult.

- If vacuum is used to pull the bubble, a vacuum box is needed (Fig. 1.12). The male mold is immersed or plunged into the prestretched bubble and the vacuum released and air pressure applied. The bubble then snaps against the mold. The technique is called *vacuum snap-back forming*.
  The billow drape forming and the vacuum snap-back forming methods work well as pressure forming techniques as well.

- The heated rubbery sheet can also be stretched with a mechanically driven plug. There are several plug assisted methods:

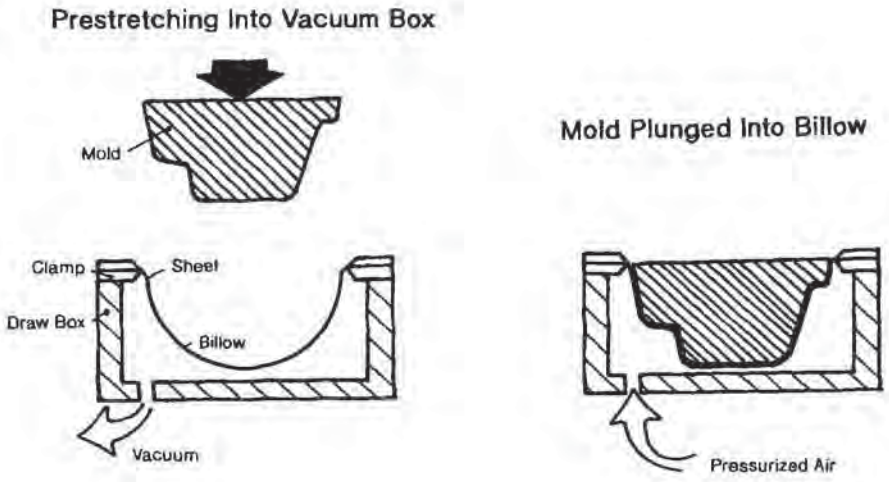

Figure 1.12 Vacuum snap-back forming

© 1996 Carl Hanser Verlag. All rights reserved.
No unauthorized disclosure or reproduction; licensed to purchaser only.

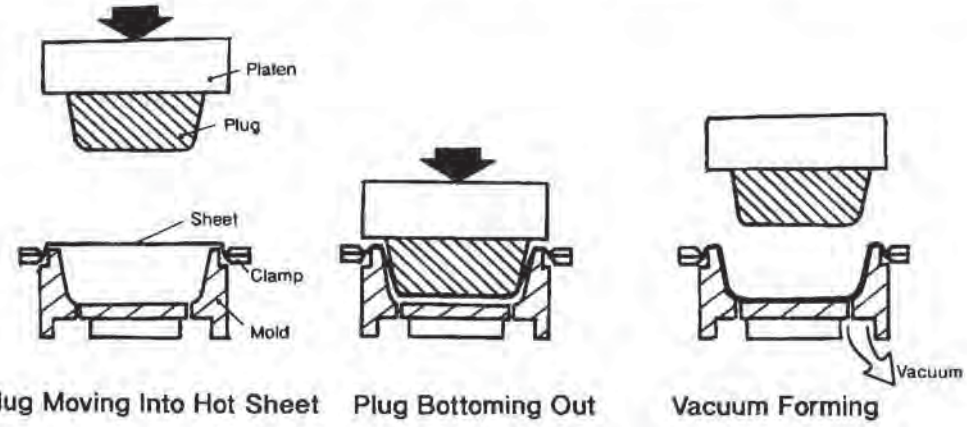

Figure 1.13 Plug-assisted vacuum forming into a female mold

- The most common form of plug-assisted thermoforming is *plug assisted vacuum forming* with a female mold (Fig. 1.13). The sheet is prestretched by pressing the plug into it and forcing the sheet toward the bottom of the female mold cavity. Vacuum is then applied to pull the sheet against the mold surface.
- If the sheet is forced against the female mold surface with air pressure applied through the plug, the technique is known as *plug assist pressure forming* (Fig. 1.14).
- *Plug-assisted drape forming* onto a male mold (Fig. 1.15) is used when the draped sheet must be tucked into three-dimensional corners or into an undercut. It is also used to stretch plastic sheet away from a male portion of a female mold to minimize webbing.

Multi-Step Forming

Billow forming and plug assist forming are occasionally combined with drape forming and vacuum forming to obtain unique wall thickness distributions. One example is *reverse draw forming with plug assist*. Fig. 1.16 illustrates the multiple step process, where a bubble is blown first. The plug is then plunged into the bubble, everting it under control. Once the plug has stretched the bubble nearly to the female mold bottom, vacuum or pressure is applied to force the sheet against the mold surface. This technique requires much patience since a stable bubble without excessive stretching is key to uniform and consistent part wall thickness distribution. Fig. 1.17 illustrates the male mold variation of this, with the mold initially acting as the plug. This technique is sometimes called *pressure bubble immersion forming* or just *immersion forming*. Again, the bubble can be formed with vacuum in a vacuum box that also serves as a pressure box for pressure forming. Table 1.6 [19] summarizes many aspects of the thermoforming process.

© 1996 Carl Hanser Verlag. All rights reserved.
No unauthorized disclosure or reproduction; licensed to purchaser only.

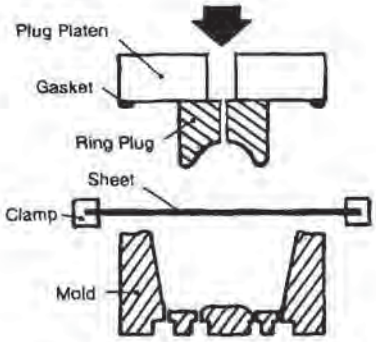

Ring Plug Moving Into Hot Sheet

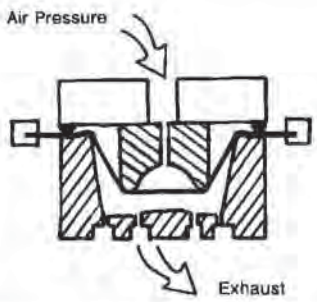

Pressure Balance During Plugging

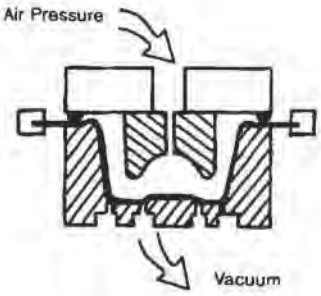

Vacuum/Pressure Forming

Figure 1.14 Plug-assisted pressure forming, using a ring plug

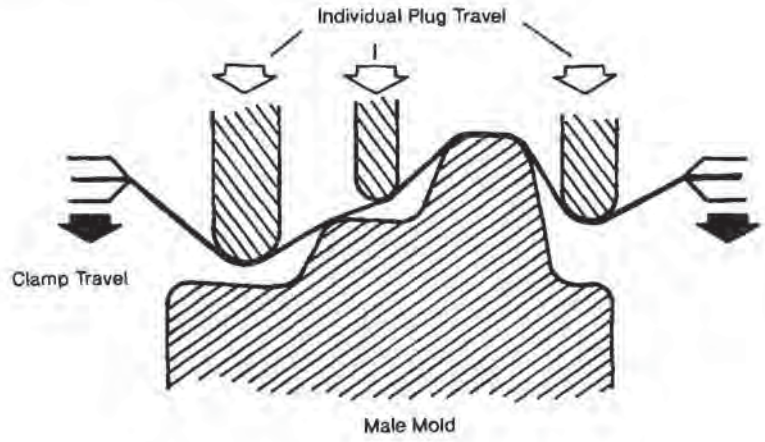

Figure 1.15 Plug-assisted drape forming, using a wire frame plug

© 1996 Carl Hanser Verlag. All rights reserved.
No unauthorized disclosure or reproduction; licensed to purchaser only.

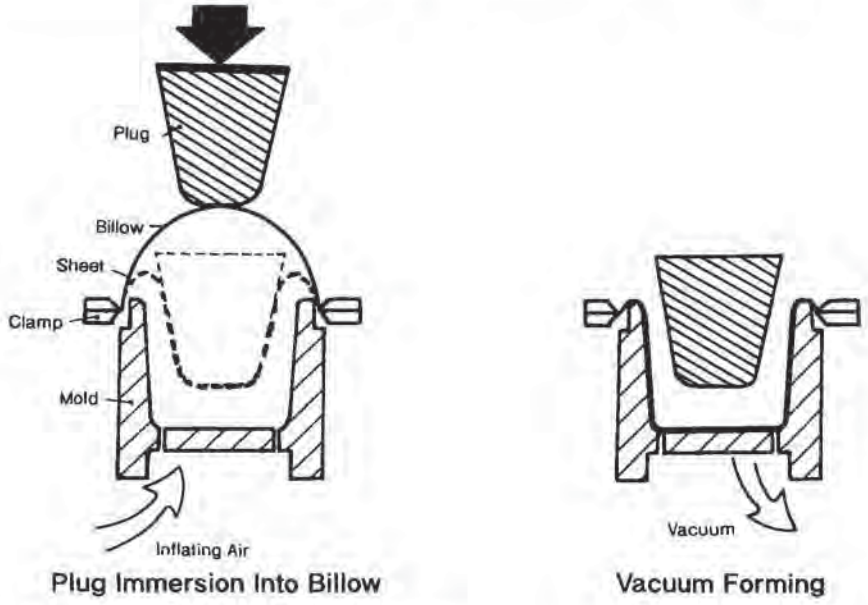

Figure 1.16 Reverse-draw forming with plug assist

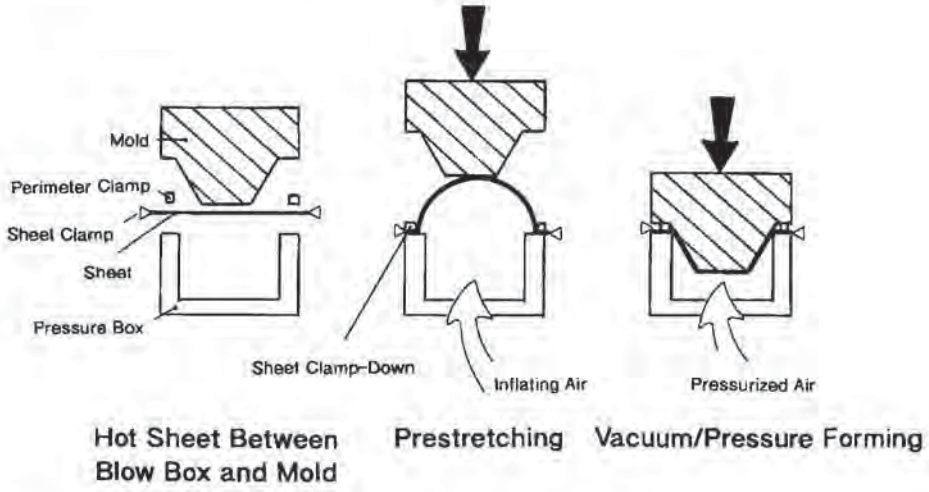

Figure 1.17 Pressure bubble immersion forming or immersion forming

© 1996 Carl Hanser Verlag. All rights reserved.
No unauthorized disclosure or reproduction; licensed to purchaser only.

Table 1.6 Characteristics of the Thermoforming Process[1]

Process	Mold configuration		Plug assist	Inflation
	Male	Female		
Vacuum forming		X		
Drape forming	X			
Matched mold	X	X		
Inflation-plug assist vacuum forming		X	X	X
Plug assist		X	X	
Vacuum snap-back	Plug	Vacuum		
Inflation snap-back	Plug	Pressure		X
Trapped sheet, pressure		X		X
Slip forming	X	X		Mold Rises

[1] Adapted from [19]

Other Variations

In order to form certain types of polymers, techniques other than those discussed above have been devised:

- *Trapped sheet forming*, Fig. 1.18, is used when:
  The polymer is thermally sensitive, such as certain types of PVC,
  The polymer is excessively saggy, as with PP and certain types of LDPE and LLDPE,
  The polymer sheet is highly oriented, as with oriented PS and PP,
  The sheet is flocked or metallized on one side,
  The sheet is laminated with a temperature-sensitive adhesive,

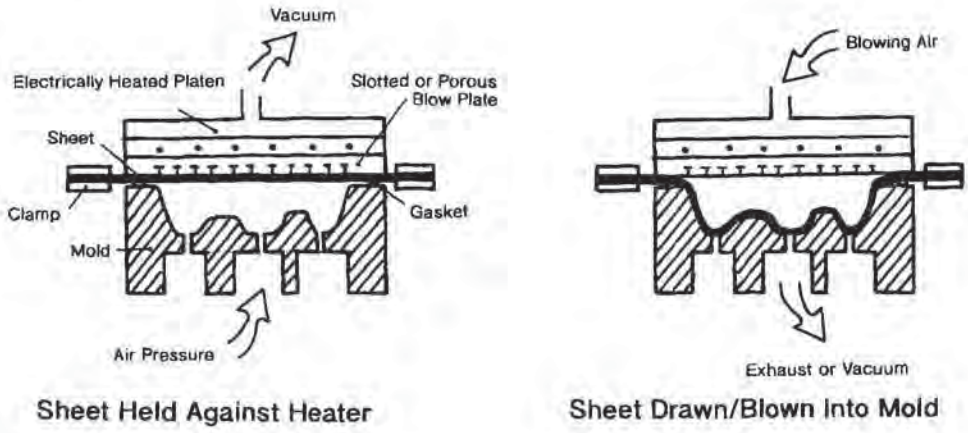

Figure 1.18 Trapped sheet forming with heating against a slotted or porous heated blow plate

© 1996 Carl Hanser Verlag. All rights reserved.
No unauthorized disclosure or reproduction; licensed to purchaser only.

The sheet contains wires or printed circuits that are temperature-sensitive,
The sheet is very thin and printed or embossed on one side, or
The sheet is less than about 0.005 in or 0.13 mm.

The clamped sheet is held against a heated plate until the polymer reaches its forming temperature. Pressure is then applied through holes drilled in the plate, forcing the sheet away from the plate and against the female mold. Alternately, vacuum is applied, sucking the sheet away from the heater and against the mold. The plates are heated with electric rod heaters. Although drilled plate is usually used, there is growing interest in porous bronze or stainless steel plates. Zonal or pattern heating is possible by using insulating plate sections that are heated to different temperatures.

- In *slip forming*, the heated rubbery sheet is not tightly clamped. As the differential pressure is applied, instead of the sheet being stretched, it is drawn from the clamp, over the mold rim and into the cavity. At a predetermined time, the sliding is stopped by increasing the clamp force. This is done by compressing springs as shown in Fig. 1.19, or by using cam-type rockers that squeeze against the sheet after a predetermined amount of rotation. Slip forming parallels deep-draw metal forming practice. It is used to form continuous-fiber reinforced polymer composite sheet. This is described in Chapter 9.
- Splitty plastics such as PET and PA or nylon and certain multilayer structures are best formed without splitting using *diaphragm forming* (Fig. 1.20). A warmed thick-walled neoprene bladder or diaphragm is placed against the clamped heated rubbery plastic sheet. The bladder is inflated with air or with a liquid such as hydraulic fluid or hot water. The inflating bladder stretches the plastic sheet into a female mold. Very uniform wall thicknesses and relatively deep draws are obtained for plastics that cannot be formed in other ways.

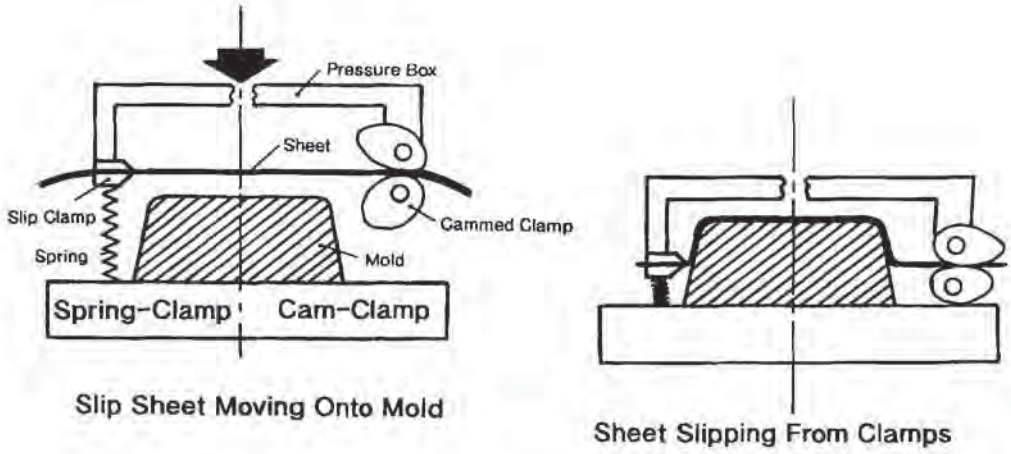

Figure 1.19 Slip forming. Spring-loaded sheet clamp on the left and cam-loaded sheet clamp on the right

© 1996 Carl Hanser Verlag. All rights reserved.
No unauthorized disclosure or reproduction; licensed to purchaser only.

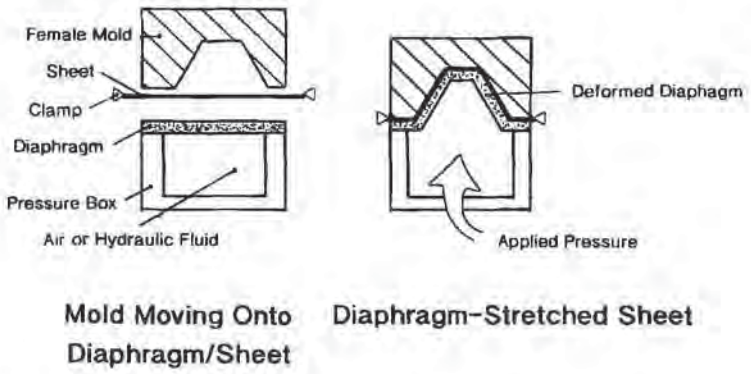

Figure 1.20 Diaphragm forming for splitty or weak polymers

- *Twin-sheet thermoforming* has been a technically viable process for many years. There are several variations on this process, described in greater detail in Chapter 9. One approach is called simultaneous twin-sheet forming. Two sheets are kept separate while heating, then brought together in a double female mold arrangement (Fig. 1.21). Blow pins are inserted between the sheets. Air inflation begins as the sheets are clamped together and the mold halves close. The air pressure keeps the sheets from initially touching and then provides the force needed to press the sheets against the mold surfaces.

  Twin-sheet forming produces a relatively flat hollow part that with proper design of kiss-offs and pinch-offs is light weight and very strong. The hollow cavity can also be filled with PUR foam for additional stiffness and insulation.

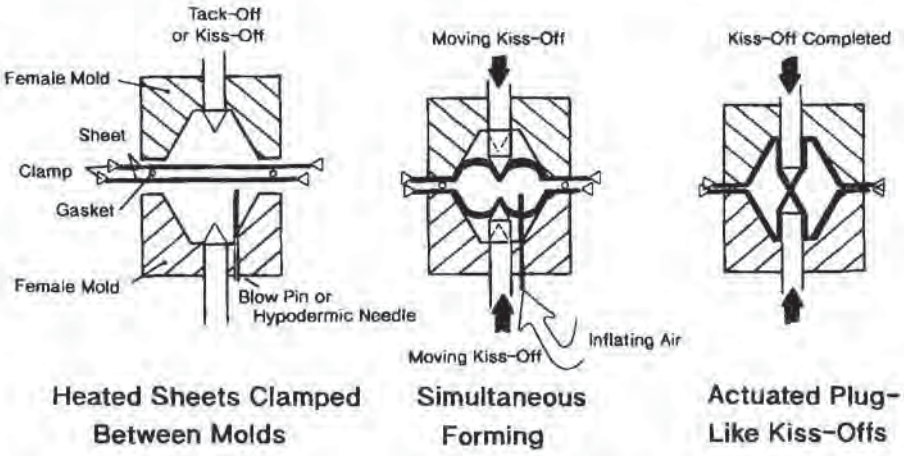

Figure 1.21 Heavy-gage, simultaneous twin cut sheet thermoforming. Here, blow pins extend through sheet surface and kiss-offs are pneumatically driven during forming

© 1996 Carl Hanser Verlag. All rights reserved.
No unauthorized disclosure or reproduction; licensed to purchaser only.

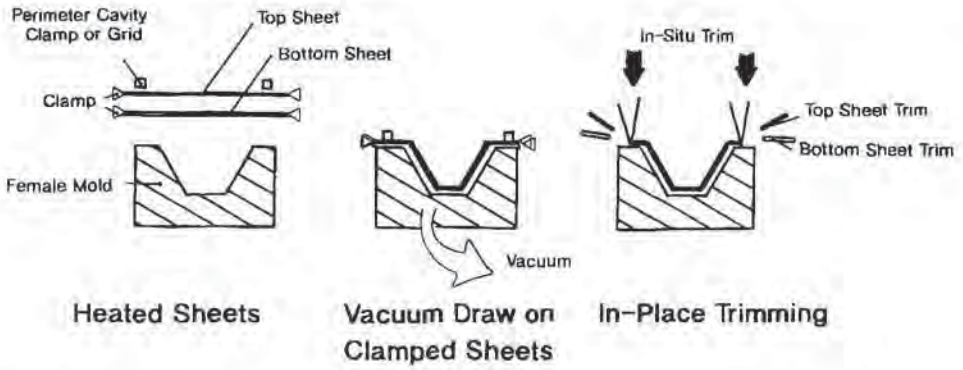

Figure 1.22 Thin-gage, simultaneous twin roll-fed sheet thermoforming. Here, sheets are heated separately and brought together at the forming station

For large, heavy-gage parts, the technique competes with blow molding and rotational molding.

In roll-fed thermoforming, twin-sheet forming is used in a different way (Fig. 1.22). Packages that provide oxygen and moisture barrier are sought. The most effective barrier materials such as PAN, EVOH and PVDC are usually quite expensive and so are used as thin films between layers of less expensive but durable polymers such as PP, HDPE, PET and PS. The results are usually laminates of essentially incompatible plastics glued together with polymers such as EVA that behave as hot-melt adhesives. The web and trim from coextruded laminates of some of these polymers cannot be reprocessed successfully without degradation and gel formation. As a result, a variation on the twin-sheet thermoforming process was developed wherein separate sheets of the candidate polymers are fed from individual rolls, through sandwich heaters and then brought together right at the forming station. Once the multi-layer formed product has been trimmed, the individual layers in the web and trim are stripped from one another. Each polymer web is therefore "clean" and is recycled to produce new sheet. The diverse layers of material in the formed product are only contact-adhered and so will delaminate through misuse.

If the force applied to the sheet increases, thermoforming begins to mimic metal forming techniques. At pressures of 1.73 MPa or 250 lb_f/in^2, the process is similar to tin metal embossing. At pressures of 6.9 MPa or 1000 lb_f/in^2, the process resembles coining. At pressures of 13.8 MPa or 2000 lb_f/in^2, the process is like compression molding or forging [20]. It has been adequately demonstrated in the Dow scrapless thermoforming or STP process, that useful products can be fabricated with high-speed *impact forming*. High pressure forming is described in detail in Chapter 9.

The incentive to achieve more uniform part wall thickness even in very deep draw parts continues to spur development of these multi-step procedures. The more

© 1996 Carl Hanser Verlag. All rights reserved.
No unauthorized disclosure or reproduction; licensed to purchaser only.

sophisticated these procedures become, the more difficult it is to adapt them to high-speed forming without exacting process controls. And yet many new packaging applications, for example, are seeking just such designs. Thermoforming process innovation remains a lively art.

1.6 Thermoforming Machinery

As noted, there are two general thermoforming categories. Typically, heavy-gage sheet is handled as discrete cut sections and the forming equipment are called cut-sheet thermoformers. Thin-gage sheet is handled in continuous rolls and the forming equipment is usually called roll-fed thermoformers. The equipment in both categories includes:

- Some form of sheet handling device,
- A way of moving the sheet from one station to another,
- A means of controlling the various elements that allow the sheet to be heated, formed and moved from station to station,
- A sheet heating oven,
- A vacuum system,
- A forming press, and
- A formed part removal region.

In addition, the equipment may include:

- Some form of prestretching such as:
  preblowing or
  plug assist,
- A pressure system,
- A trimming press, and
- Some form of trim removal.

Certain guidelines pertain to both categories of forming equipment. Table 1.7 gives an overview for thermoforming equipment in general [20]. Some of these are summarized below.

Heating Source

The various heating methods are detailed in Chapter 3. Sheet temperature should be controlled to within $\pm$ 5°C or $\pm$ 10°F. During transfer to the forming station, the sheet temperature drop should not exceed 5 to 10°C or 10 to 20°F. Infrared heating is most popular today. The various heating methods include [21]:

- Simple nickel-chrome heating wires,
- Metal resistance rods, sometimes called calrods,

© 1996 Carl Hanser Verlag. All rights reserved.
No unauthorized disclosure or reproduction; licensed to purchaser only.

Table 1.7 General Specifications for Thermoformers[1]

Platen size, W × L (in × in or mm × mm)
Maximum depth of draw (in or mm)
Forming process (vacuum, pressure, matched mold, plug assist, twin-sheet capability)
Platen power drive (pneumatic, hydraulic, mechanical, electric)
Indexing power drive (pneumatic, hydraulic, mechanical, electric)
Floor space (ft^2 or m^2)
Heater type (metal rod, quartz, ceramic, radiant, gas, nichrome wire)
Heater controls (proportioning, percentage timers, timer controlled, zone controlled, programmable controlled, machine controlled)
Maximum heater output (kW/ft^2 or kW/m^2)
Special features (purpose, type such as shuttle or rotary, number of stations, number of ovens, etc.)

[1] [20] with permission of John Wiley & Sons

- Ceramic bricks or tiles,
- Quartz heaters in rod, spiral or square plate form,
- Direct gas-fired burners,
- Indirect gas-fired catalytic burners,
- Heat lamps,
- Quartz glass plates,
- Halogen bulbs, and
- Wire or rod heated metal plates.

Heater surface temperature is usually measured with thermocouples, thermistors or infrared pyrometric devices. Heating wires and resistance wires are inexpensive but oxidize rapidly and so lose heating efficiency. Quartz heaters are quite efficient, can be turned on and off like light bulbs but are quite expensive and fragile. Quartz is preferred for high temperature and "shaped heating" needs as described in Chapter 3.

Sheet is also heated by direct contact with a hot metal plate (trapped sheet heating), by placing the sheet in a hot air oven (convection heating), or by passing it through a high-frequency electromagnetic field (RF or microwave heating). In the last case, the plastic must absorb the high-frequency energy. PVC is heated by radio-frequency energy in the flow-molding embossing process. Other polymers must be doped with "lossy" substances such as inorganic hydrates or even carbon black.

There are certain elements that pertain to the ovens for all forming presses. For example:

- There must be a way of separating the sheet from the heater source at shut-down. Baffles and dampers are used for heavy-gage sheet and fly-open and extracting shuttles are used for thin-gage sheet.
- There should be adequate means for rapid replacement of burned-out heater elements on both top and bottom heater banks.

© 1996 Carl Hanser Verlag. All rights reserved.
No unauthorized disclosure or reproduction; licensed to purchaser only.

Forming Platform

The forming station should include all elements necessary to prestretch the sheet, form it, cool it and eject it from the mold. Some of these elements include:

- Substantial guide-rods are needed. For vacuum molds greater than 12 in or 300 mm by 24 in or 600 in dimension and for all pressure forming applications, four guide-rods are recommended.
- Clamp tonnage should be in proportion to mold size, that is:
  Typically >100 lb_f/in^2 or 0.7 MPa for straight vacuum forming, and
  Typically >200 lb_f/in^2 or 1.4 MPa for pressure forming.
- The press frame pit should not be deeper than 4 ft or 1.3 m. In many areas, pits deeper than this must be entered by people wearing self-contained breathing apparatus.
- The overhead press frame structure should be robust enough to support such elements as:
  The entire weight of the mold, if it is desired to mold in an "up" position,
  In-mold trimming components including cylinders and framework,
  Ancillary mold elements such as:
    Plug assist cylinders and frames,
    Ejector cylinders and frames, and
    Cavity isolator cylinders and frames, and
    Pressure boxes.
- The press should allow for easy mold removal and maintenance.
- The press platens should allow for easily adjustable mold daylight.
- There should be adequate headroom for overhead ancillary equipment.
- There should be adequate space around the presses for vacuum lines, vacuum and air pressure lines, and adequate mold temperature hoses and manifolds.
- There should be adequate provision for prestretching and billowing, sheet lock-down and stripping and ejecting.
- There should be allowance for free surface temperature control, including chilled air.
- The frame should be adequately reinforced and gusseted to carry heavy molds, ancillary hardware, and day-to-day vibration and shaking.
- There should be adequate provision for part removal and trim or web takeaway.

The drive system that raises and lowers the platens is the key to forming station performance. Depending on the application, the drive unit can be as inexpensive as a simple air cylinder or as complex as the hydromechanical clamps used on injection molding presses. Table 1.8 [21] rates some of the drives used in thermoforming presses. Many high-speed presses use electric toggle clamps and cams. For high-speed pressure forming of polypropylene, double toggle clamps are used. Some straight hydraulic clamps are used in high pressure applications. Electrically driven clamps are being developed that are touted to be more accurate with less maintenance than conventional clamp systems. Most vacuum forming drive systems are designed to close and clamp at maximum pressures of 20 to 40 lb_f/in^2 or 0.15 to 0.30 MPa. For

© 1996 Carl Hanser Verlag. All rights reserved.
No unauthorized disclosure or reproduction; licensed to purchaser only.

Table 1.8 Comparison of Forming Table Drive Units[1]

Characteristic	Pneumatic air cylinder	Geared motor-cogwheel	Hydraulic	Pneumatic driven toggle	Eccentric motor-cams	Motor-driven spindle
Uniformity	0	5	4	0	3	5
Stroke limit control	1	5	5	3	3	5
Timing control	2	5	4	1	2	4
Repeatability	0	5	4	0	3	5
Speed control	3/4	0/2/5	5	1	0	2
Forming force	3	3	5	0	1	5
Clamping force	3	3	5	5	5	4
Stability—tracking	0/3	3/4	0/3	4	4	5
Energy consumption	0	5	1	0	3	2
Trouble-free nature	3	5	0	2	4	3
Maintenance	4	5	0	2	3	3
Noise level	0	5	3	0	4	1
Construction quality	1	3	1	5	5	5
Cost	5/2	4/1	0	3	1	1
Preblowing capacity	5	5	5	0	0	0
Total	30/31	61/65	42/45	26	41	50

[1] From [21: Table 8] by permission of Carl Hanser Verlag
Key: 0 = Low or poor; 3 = Moderate or average; 5 = High or excellent

pressure forming, the drive system must clamp against the forming air pressure. Safety factors of 3 to 4 are recommended. If 30 lb_f/in^2 or 2 MPa air pressure is used in forming, the drive system should be designed to remain closed against 90 to 120 lb_f/in^2 or 6 to 8 MPa pressure. For a typical mold forming area of 20 × 10 in or 500 × 250 mm, the drive system clamping load is 9 to 12 T or 32 to 107 Mkg_f. Platens and guide-rods must be designed to accommodate high bending forces. For forming pressures in excess of 100 lb_f/in^2 or 0.7 MPa, forming station designs begin to resemble those used in thermoplastic structural foam injection molding [22]. For forming pressures in excess of 200 lb_f/in^2 or 1.4 MPa, the presses begin to resemble those used in compression molding.

Vacuum System

The vacuum systems for both categories of forming equipment are quite similar. For stand-alone shuttle and rotary formers, the vacuum pump, surge tank and plumbing is usually an integral portion of the machine (Fig. 1.23). For installations of several forming presses, regardless of the sheet gage, a centrally located vacuum system is frequently used.

Even the least expensive vacuum forming press must have adequate means of rapidly drawing the sheet against the mold surface. One critical factor in efficient vacuum draw-down lies in an unencumbered, adequately sized line between the

© 1996 Carl Hanser Verlag. All rights reserved.
No unauthorized disclosure or reproduction; licensed to purchaser only.

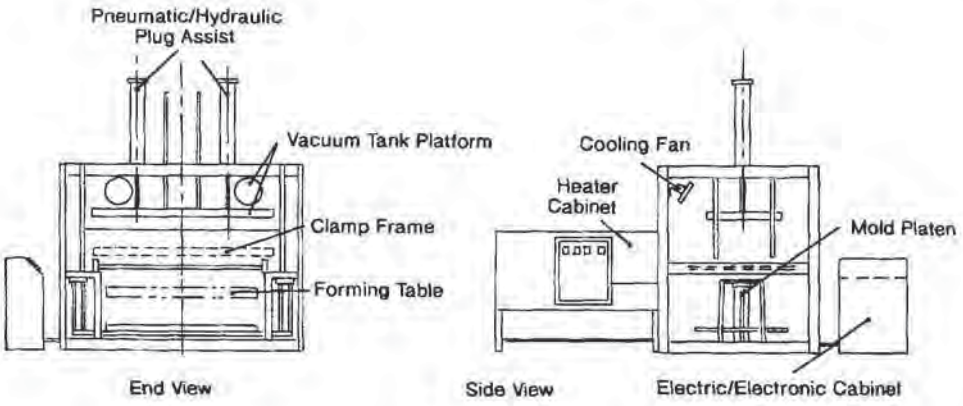

Figure 1.23 Single station cut sheet shuttle press—Drypoll/Zimco

vacuum surge tank and the mold cavity. Proper vacuum system design requires a vacuum pump capable of drawing down to 710 to 735 mm Hg vacuum[1] in the surge tank prior to the beginning of the forming cycle. The path between the surge tank and the cavity between the hot sheet and the mold should have as few constrictions as possible. Long pipes, flow constrictors, quick-disconnects, restrictive valves and large L/D vent holes should be eliminated. Fast-acting rotary ball valves are recommended for vacuum shut-off [23]. Section 6.5 details a method for determining pressure drops through each of the constrictions from the mold cavity to the vacuum pump inlet. A good estimate of the time required to evacuate a mold cavity is obtained from:

$$\theta = \frac{V}{S_o} \ln\left(\frac{p_i - p_o}{p_f - p_o}\right) \tag{1.1}$$

where θ is the pump-down time, V is the total volume of the system to be evacuated, p_i is the initial system pressure (absolute), p_f is the final system pressure, and p_o is the vacuum tank pressure. S_o is the volumetric evacuation rate. The evacuation rate of the vacuum pump is usually specified by the pump manufacturer, as S_p. The evacuation rate, S_o is given as:

$$\frac{1}{S_o} = \frac{1}{S_p} + \frac{1}{C} \tag{1.2}$$

where 1/C is the cumulative resistance of the system between the pump and the mold cavity. This resistance includes valves, piping, vent holes, vacuum box baffles and so on. A protocol for calculating the cumulative resistance is given in Section 6.5. The cumulative resistance is comprised, for the most part, of two resistances, the air flow resistance in the plumbing and the surge tank resistance. The resistance to air flow

[1] Pumps of this draw-down range may also be listed in vacuum draw-down units such as 25 to 50 torr, 28 to 29 in Hg or 0.5 to 1.0 lb_f/in^2 absolute.

© 1996 Carl Hanser Verlag. All rights reserved.
No unauthorized disclosure or reproduction; licensed to purchaser only.

between the vacuum or surge tank and the mold cavity, $1/C_p$, should not exceed the surge tank resistance, $1/C_t$. And this combined resistance should not exceed the pump resistance, $1/S_p$. This can be written as:

$$1/C \approx 1/C_p + 1/C_t \tag{1.3}$$

$$1/C_p \leq 1/C_t \tag{1.4}$$

$$1/S_p \leq 1/C \approx 1/C_p + 1/C_t \tag{1.5}$$

Therefore a good design volumetric evacuation speed is given as:

$$1/S_o \approx 2/S_p \approx 4/C_p \tag{1.6}$$

Examples 1.1 and 1.2 illustrate the relevance of vacuum pump capacity to surge tank size and pressure drop through plumbing. Other examples are found in Section 6.5.

Example 1.1 Pump-Down Time in Vacuum System

A vacuum pump manufacturer lists your vacuum pump capacity at 60 ft³/min, 0.0283 m³/s, or 1700 liter/min. Determine the expected evacuation rate of a typical pump and surge tank and the evacuation time to pump a 0.1 m³ mold cavity to 50 mm Hg if the pump pressure is 20 mm Hg.

Assume that the piping resistance equals the vacuum pump capacity, Equation 1.1. Therefore:

$$1/S_o = 2/S_p$$

or

$$S_o = 0.0283/2 = 0.01415 \text{ m}^3/\text{s}.$$

According to Equation 1.1, the pump-down time, θ, is:

$$\theta = \frac{0.1 \text{ m}^3}{0.01415 \text{ m}^3/\text{s}} \ln\left(\frac{760 - 20}{50 - 20}\right) = 22.7 \text{ s}.$$

Example 1.2 Pump-Down Time for Surge Tank

Consider pumping a surge tank of volume 1.0 m³ from 50 mm Hg to 20 mm Hg using the vacuum pump of Example 1.1. Determine the time to pump it down and compare this with the time to evacuate the mold cavity of Example 1.1.

According to Example 1.2, the vacuum pump rate is given as $S_p = 0.0283$ m³/s. The evacuation time is given in Equation 1.1:

$$\theta_r = \frac{1 \text{ m}^3}{0.0283 \text{ m}^3/\text{s}} \ln\left(\frac{50 - 10}{20 - 10}\right) = 49.0 \text{ s}$$

The time required to evacuate the mold cavity in Example 1.1 is 22.7 s. Therefore $\theta_r > \theta$ and the surge tank cannot recover in time. The vacuum in

© 1996 Carl Hanser Verlag. All rights reserved.
No unauthorized disclosure or reproduction; licensed to purchaser only.

the surge tank at the end of the forming cycle of 22.8 s is obtained from this equation as well:

$$p_f = p_o + (p_i - p_o) \exp[-\theta_r S_o/V]$$

or:

$$p_f = 10 + (40) \exp[-22.8 \cdot 0.0283/1] = 31 \text{ mm Hg}$$

Trial-and-error is used to match the pump-down time of the mold cavity with the surge tank recovery time.

The time θ_r, to recover the surge tank pressure to p_o value is determined from Equation 1.1. The surge tank volume is substituted as V and the final tank pressure at the end of draw-down is p_i, the initial pressure. The vacuum pump pressure is p_o, and the desired vacuum tank final pressure is p_f. Example 1.3 illustrates this. The total vacuum cycle time, θ_t, is given as the sum of θ and θ_r. For most cases, $\theta_r \leq \theta$ and the total cycle time is simply assumed to be equal to twice the draw-down time [24]. Vacuum pumps are either single or double staged. Two-stage vacuum pumps draw pressures down to 10 mm Hg, but evacuation capacity is usually half that for single-stage pumps. Typical pump capacities are given in Table 1.9 [24].

Example 1.3 Piping Resistance in Vacuum Systems

Consider piping resistance for a specific thermoformer to be given by [33]:

$$C_p = 22\ D^3/L_e$$

where D is the pipe diameter and L_e is the equivalent pipe length (see Chapter 5 for additional details). Determine the equivalent pipe length if the pipe diameter is 4 in = 100 mm and the vacuum system uses the vacuum system in Example 1.1. What is it if the pipe diameter is 6 in = 150 mm?

As noted in Equation 1.1, assume $1/S_p = 2/C_p$. Therefore:

$$S_o = C_p/2 = 11\ D^3/L_e$$

Rearranging, for D = 4:

$$L_e = 11\ D^3/S_o = 11 \cdot \frac{0.1^3}{0.0415} = 0.78 \text{ m} = 2.6 \text{ ft}$$

For D = 6:

$$L_e = 2.6 \text{ m} = 8.6 \text{ ft.}$$

Note that the equivalent length is proportional to the cube of the diameter of the vacuum line.

© 1996 Carl Hanser Verlag. All rights reserved.
No unauthorized disclosure or reproduction; licensed to purchaser only.

Table 1.9 Typical Vaccum Pump Specifications[1]

Pump specification			Theoretical pump capacity				
No of cylinders	Diameter (mm)	Stroke length (mm)	Single stage (m^3/min)	Two stage (m^3/min)	Pump speed (rpm)	Power required (kW)	Exit pipe diameter (mm)
1	76	70	0.255	–	800	0.56	19
2	76	70	0.510	0.255	800	0.74	25
2	102	70	0.906	0.453	800	1.48	32
2	127	80	1.70	0.850	750	2.2/3.7	38
2	140	102	2.80	1.40	900	3.7	52
3	140	102	4.22	2.80	900	5.6	52

[1] From [21: Table 10], with permission of Carl Hanser Verlag

Pressure System

Pneumatic action for air cylinders usually requires working air pressures of 90 lb_f/in^2 or 0.6 MPa. Air consumption depends on the size of the press and the type of forming being used. Typically maximum airflow range for both roll-fed and cut sheet presses is 35 to 250 ft^3/min, 1 to 7 m^3/min or 1000 to 7000 liter/min. Air is usually delivered at 100 to 200 lb_f/in^2 or 0.7 to 1.4 MPa. Air should be very dry with dew-point of $-40°F$ or $-40°C$. It should be absolutely oil-free, particularly if it is used as instrument air or for free blowing in prestretching, twin-sheet forming or pressure forming. Prestretching air is delivered to the mold cavity at very low pressures of 0.5 to 5 lb_f/in^2 absolute or 3.5 to 35 kPa. The air volumetric flow rate is controlled very carefully to $\pm 0.1\%$. Pressure forming air is delivered to the pressure box at 20 to 120 lb_f/in^2 or 0.14 to 0.83 MPa, also at very carefully controlled volumetric flow rates. Twin sheet forming air is delivered at pressures of 5 to 50 lb_f/in^2 or 35 to 350 kPa at very carefully controlled volumetric flow rates. Twin-sheet forming air is sometimes heated to 200°F or 95°C to prevent chilling around the blow pins that introduce the air to the mold cavity through the plastic sheet surface.

Pressure forming air must be carefully exhausted or bled from the pressure box prior to opening the mold. A two-tank system is used on occasion to handle spent air. Air from one tank is used to form the part, then exhausted to a second tank where it is recompressed with incoming air at higher pressure. The cycle then repeats. This system works best when forming at pressures above about 50 lb_f/in^2 or 0.35 MPa.

Process Control

Process repeatability is always of concern to thermoformers. The earliest roll-fed presses were equipped with automatic drop-down clock cycle timers. Accurate measurement and control of:

© 1996 Carl Hanser Verlag. All rights reserved.
No unauthorized disclosure or reproduction; licensed to purchaser only.

- Sheet temperature,
- Mold temperature,
- Prestretching pressure,
- Pre-inflation stretch height,
- Rate of stretching either by:
  - Plug assist, or
  - Pre-inflation,
- Forming pressure, and
- Sheet registry

are all desired. Now, control of:

- Rate of change of sheet temperature,
- Rate of bubble inflation,
- Time-dependent plug position, and
- Time-dependent draw-down

are sought. For example, as detailed in Chapter 9, repeatability of the crystalline level of CPET depends on accurate control of the rate of heating crystallizing sheet prior to forming [25,26]. Newer, more accurate processing techniques are replacing less reliable ones. For example:

- Microprocessor-driven servo motors are replacing cam-operated sequencing wheels.
- Newer presses may include such features as:
  - Programmable mold height adjustment,
  - Programmable daylight adjustment,
  - Multi-step, programmable mold closing speeds,
  - Programmable roll-fed chain width spacing, and
  - Programmable forming station sequencing including prestretching and post-forming sequences.
- Sheet gage and pattern registry monitors can now be added.

Safety is an ongoing concern. Thermoforming machines have many rotating and sliding elements and many pinch-points. Higher heater temperatures are used to increase throughput and to heat sheet more efficiently, Chapter 4. An emergency line shutdown should not only shut off heaters but shield the stationary sheet from the heaters. Heaters are now designed to automatically swing away or shift horizontally whenever the sheet stops moving. This reduces the chances of fire. Pressure boxes are pneumatic pressure vessels and so must have appropriate safety ratings and overpressure relief diaphragms. Pressure forming stations have pressure interlocks that prevent opening when internal air pressure exceeds a fixed, relatively low level. In many cases, increased production efficiency and substantially reduced labor costs more than offset the substantial costs of these process controls.

© 1996 Carl Hanser Verlag. All rights reserved.
No unauthorized disclosure or reproduction; licensed to purchaser only.

Trimming and Cut Parts Handling

All formed parts must be removed mechanically from the surrounding trim or web[1]. Trimming is detailed in Chapter 5. Cut sheet trimming is traditionally done at an off-line station. Trimming is done with pneumatic or hydromechanical steel-rule dies, routers, saws, punches, guillotines, water jets and/or punches. Semi-automatic microprocessor-controlled multi-axis trimming devices are used for many parts. Robots are used occasionally. Manual trimming is common when a few parts with complex trimming lines are fabricated. Band-saw cutting is common when the trimming line is planar. In-line trimming stations are commonly used in roll-fed forming operations. In-situ or in-the-mold trimming requires that the forming press be equipped with a separate pneumatic or mechanical press that drives the cutting knives through the formed sheet and against the mold anvil.

The separate in-line trim press is an alternative to in-mold or in-situ trimming. Typically, the press is a cam-action mechanical toggle-clamp platen press with steel-rule die cutters. If the trim press is integral with the former, the sheet with the formed parts intact is guided through the press bed by the integral pin-chain drive. If the unit is separate but in-line, proper sheet indexing must be provided. If the formed polymer shrinks appreciably or the parts show unusual distortion and warping, care must be taken to register the sheet to achieve pattern repeatability. Integral trim presses are much easier to align and register than separate units. They are recommended for roll-fed forming of CPET and PP polymers.

Certain other aspects are similar but not identical. For example, sheet handling and clamping during heating and forming is usually a function of sheet thickness and so is covered below. There is no standardization in mold bases as there is with injection molding. As a result, forming presses must have the flexibility to accept many mold configurations. This is true for both general categories of presses.

1.7 Heavy-Gage Thermoforming Machinery Specifics

Table 1.10 gives a check-list of important items to be considered in heavy-gage thermoforming machine design. The check-list focuses on cut-sheet thermoforming machinery requirements and desires. Heavy-gage thermoforming machines have been developed where the sheet is continuously fed from the extruder (Fig. 1.2). These machines incorporate certain features of roll-fed formers, such as web handling and

[1] The thermoforming industry has long been concerned about the use of the word "scrap" to describe the non-product portion of the sheet. Thermoforming economics dictate that the non-product should be reground, mixed with virgin resin, and reprocessed into useful product. Only rarely is the trim or web considered to be unsuitable for reprocessing. The two primary examples are in certain biomedical and medical products and in continuous-fiber reinforced high performance composites. Even in these cases, the web or trim is reground and reprocessed into other products. It is estimated that less than 1% of any extruded sheet surface is discarded as scrap.

© 1996 Carl Hanser Verlag. All rights reserved.
No unauthorized disclosure or reproduction; licensed to purchaser only.

Table 1.10 Check-List for Important Items for Heavy-Gage Forming Machines (TFS = To-and-fro shuttle; ILS = In-line shuttle; R = Rotary; OSP = Oven shuttle press; A = All heavy-gage machines)

Sheet handler

Vacuum must be applied individually to pick-and-place suction cups.
Vacuum pick-and-place should support full sheet weight on one or two suction cups.
Vacuum pick-up must allow up to two suction cups to engage and lift sheet before other suction cups are activated to provide vacuum break.
Smooth deceleration of table lifter as sheet enters clamp [R].
Manual placement in clamp should have center stop just below sheet to avoid drop-through [TFS, R].

Sheet clamp

Manual book mold requires lock-over clamps [TFS].
Pneumatic clamp should have barbs, teeth spaced every 1 in or 25 mm for tough sheet such as ABS, PS, every 0.5 in or 12 mm for soft sheet such as HDPE, PP, every 0.25 in or 6 mm for very soft sheet such as TPO or TPE [A].
Pneumatic clamp should have barbs on closing portion, flats on fixed portion [A].
Clamp pressure on cold sheet should be at least 50 lb_f/in^2 or 0.35 MPa to prevent extrusion during forming [A].
Clamp should hold at least 0.5 in or 12 mm sheet width for sheet less than 0.100 in or 2.5 mm in thickness [A].
Clamp should hold at least 2 in or 50 mm sheet width for sheet greater than 0.400 in or 10 mm in thickness [A].
Clamp frame, pneumatics must withstand at least 800°F or 425°C for 20 minutes for at least 10,000 cycles without sticking, binding, leaking air or oil [A].
Edge clamps must reliably open and close on sheet for at least 10,000 cycles without sticking or binding [ILS].
Pneumatics must be easy to replace quickly [A].
Hoses must be durable enough to withstand bending and elevated temperatures [A].
Rotary air hose connections must withstand vibration and heat [R].
Clamp frame must be rapidly adjustable for various sheet dimensions [A].
Shuttle rails or shuttle clamps must be self-lubricating or sealed to minimize contamination with sheet [TFS, ILS].
Rotary clamp frame arm must be capable of supporting maximum sheet weight in only one clamp without flexure [R].
Rotary clamp frame arm must not oscillate or bounce when rotation cycle ends or when automatic sheet loading is underway [R].
Rotation acceleration, constant speed and deceleration must be smooth and without oscillation or vibration [R].
Rotary clamp should be clamped in place with a drop pin or equivalent when the sheet is at a specific station [R].

Oven

Preheat oven recommended for hydroscopic polymers such as ABS, PS, PET, Celluloics [R].
Two-step oven recommended for hydroscopic polymers [ILS, TFS].
Oven baffles should close off sheet and clamp frame while in oven [TFS, R].
Oven must tightly clamp the sheet during the heating cycle so that the edge clamps can be opened and shuttled backwards [ILS].
Rapid disconnect for main electrical to top and bottom oven [A].
Rapid disconnects for individual heater elements [A].
Rapid disconnects for individual heater thermocouples [A].

(Continued)

© 1996 Carl Hanser Verlag. All rights reserved.
No unauthorized disclosure or reproduction; licensed to purchaser only.

Table 1.10 (Continued)

Open woven wire or chicken wire guards on top and bottom oven heaters [TFS, ILS, R].
Quartz plate between sheet and bottom heater [OSP].
Adequate places to fasten screens for pattern heating [TFS, ILS, R].
Air- or water-insulated ports in top and bottom oven surfaces for infrared pyrometer devices [A].
For very large area sheets, bottom oven should have drop-down side wall to allow the sagging sheet to exit without touching metal [A].
Shuttle rails must be self-lubricating or sealed to minimize contamination with sheet [OSP].
Photo-eye sensor/warning needed for excessive sheet sag [A].
Automatic oven shut-down, baffling or extraction when sheet time in oven exceeds upper limit [A].
Oven equipped with central system for dispensing CO_2 or other non-aggressive fire extinguishing material [A].
Easy adjustment of oven height above/below sheet plane to allow:
  Rapid change in height during sheet set-up,
  Rapid change during running [A].
Capability to lower bottom oven height during heating to accommodate sagging sheet [optional] [TFS, ILS, R].
Sufficient daylight between top and bottom oven to allow:
  Heater burn-out inspection and replacement,
  Individual heater temperature measurement by non-contact means such as infrared pyrometry [A].
Intermittent vacuum or air layer lift of sagging sheet [TFS, ILS, OSP].

Press

Smooth-acting, constant velocity press closure [A].
Acceleration/deceleration at end of stroke to minimize banging, chatter as mold enters sheet [A].
Clamping by:
  Platen locking devices,
  Mechanical/pneumatic assists,
  Servo-motor lockout,
  Pneumatic gland [A].
Self-lubricating or continuous-lubricating platen screws [A].
Enclosed or self-sealing overhead hydraulic/pneumatic lines to prevent oil vapor contamination of formed product [A].
Protected platen locking cogs or screws to minimize contamination from trim dust, chips, dirt, detritus [A].
Sites for laser leveling [A].
Rapid, easy-to-use platen alignment devices [A].
Rapid, easy-to-use horizontal plane positioning for platen on all ancillaries [A].
Configured to easily accept mold changeover [A].
Adequate daylight between platens to allow for:
  Inspection and maintenance with mold in place [A],
  Replacement of in-mold trim dies.
Adequate space around press to allow for:
  Adjustment of ancillaries,
  Proper placement of vacuum box and vacuum lines,
  Proper placement of water lines [A].
Upper platen frame robust enough to support ancillaries such as:
  Plug assist carrier,
  Trim-in-place die platen, if used,
  Pressure box [A].
Pneumatic interlocks to prevent:
  Premature air pressurization before pressure box fully engages mold,
  Premature opening of pressure box while still pressurized,

© 1996 Carl Hanser Verlag. All rights reserved.
No unauthorized disclosure or reproduction; licensed to purchaser only.

Table 1.10 (Continued)

Pressurization of an empty clamp frame [A].
Sufficient access space below bottom platen to allow for adequate mold travel adjustment [A].
Proper controls on all rate-dependent ancillaries such as:
Plug assist platens or individual cylinders,
Trim-in-place die platen or individual cylinders,
Pressure box [A].
Means for accessing overhead ancillaries for adjustment, removal, disengagement, repair, maintenance [A].

Plug assist
Relatively easy and rapid means for adjusting the travel length, and rate of travel of individual plugs [A].
Capability for internally heating/cooling individual aluminum plugs, including adequate space above the mold bed to allow for heating/cooling lines and thermocouples [A].
Relatively easy removal of individual plugs or at least methods for rendering individual plugs inoperable [A].

Trim-in-place[a]
Rapid means for determining sharpness of individual trim die sections [TFS, ILS].
Rapid means of removing individual trim die sections [TFS, ILS].
Rapid means of adjusting and aligning individual trim die sections for parallelism to the punch surface [TFS, ILS].

Pre-stretching
Pre-blow bubble height monitor with photoelectric eye connected to air pressure [A].
Bubble inflation rate control [A].
Bubble collapse sensor to deactivate air pressure [A].
Prestretching vacuum box mounts on upper or lower portion of press [A].
Prestretching vacuum box drop side to allow exit of prestretched sheet [R].

Load/unload
Clamp frame/formed part at operator [A].
Heavy, deep-drawn parts require break-away clamp frame, mechanical assist to remove [A].
Automated pickers/robots expensive, difficult to maintain, restricted to dedicated presses [R, ILS, OSP].

Vacuum box
Mold evacuation rate control [A].
Auxiliary dump tank for evacuation of large volume molds [A].

Condition monitors
Sheet temperature monitoring via infrared pyrometry:
Automatically through oven, both top and bottom [A],
Automatically at sheet exit from oven [TFS, IL S, R],
Hand-held as sheet exits oven [A].
Mold temperature monitoring with thermocouples in at least one portion of mold cavity [A].
For metal and ceramic heaters, individual thermocouples mounted on or embedded in many heaters on both top and bottom ovens [A].
Air pressure monitor on all pneumatic devices including:

[a] Trim-in-place is rarely used in heavy-gage thermoforming. When it is used, the trim dies are forged or machined and are mechanically or hydraulically driven

(Continued)

© 1996 Carl Hanser Verlag. All rights reserved.
No unauthorized disclosure or reproduction; licensed to purchaser only.

Table 1.10 (Continued)

Pressure box,
Plug assist cylinders,
Trim die if pneumatically driven [A].
Time-dependent vacuum monitor at:
Vacuum pump,
Surge tank
Vacuum box [A].
Time monitor on all phases of sheet transfer through the press [A].
Photoelectric cells on sheet in oven and as sheet exits oven [A].
Sheet presence sensor for quartz oven to shut off oven when no sheet is in clamp [R].
Process control
Times and sequences for all events [A].
Temperatures for all heaters or heater banks that are independently controlled [A].
Delay times for line stoppage [R].
Storage of all important event values and capability of resetting machine using stored data [A].
Automatic protocol for emergency shutdown for:
Fire,
Power overload, brownout and outage,
Light curtain interrupt,
Safety cage security breach [A].

in-line ovens. The simplest heavy-gage, cut-sheet thermoformer consists of a book-mold sheet clamp, stationary single-sided oven, a stationary mold/vacuum box and a simple vacuum system [27]. These thermoformers are used to form shallow draw products such as signs, transparent protective windows and disposable packaging.

Shuttle presses are most commonly used in custom thermoforming. While not as cycle time or energy efficient as rotary presses, they offer flexibility in forming as well as rapid mold change and valuable between-shot process parameter adjustment. The most common shuttle press is a single oven press, with the sheet being shuttled between the load/form/unload station and the stationary oven (Fig. 1.23). The oven is sometimes shuttled and the sheet in its clamp frame is stationary. This configuration is quite energy efficient if the oven lamps are quartz and are switched off when not over the sheet. Dual-oven single-press and dual-press, single-oven thermoformers are also used in special cases. Florian believes that these designs "... suffer from the definite misconception that [they are] saving energy..." [28]. In addition, increased labor costs and additional tooling costs usually obviate any improvement in time or energy efficiency. Dual-oven, single-press formers are used in sequential twin-sheet thermoforming, however (Fig. 1.24 and Chapter 9).

If production warrants improved cycle times or economics require increased energy efficiencies, rotary presses should always be considered (Fig. 1.25). Rotary presses have some limitations. The overall cycle time is governed by the slowest step in the process, be it loading and unloading, heating, or forming. If the heating step controls the process cycle time, the heater temperatures can be increased or a four-station rotary press used, with the fourth station being a preheater (Fig. 1.26). When the forming step controls the process time, as it does in the majority of cases,

© 1996 Carl Hanser Verlag. All rights reserved.
No unauthorized disclosure or reproduction; licensed to purchaser only.

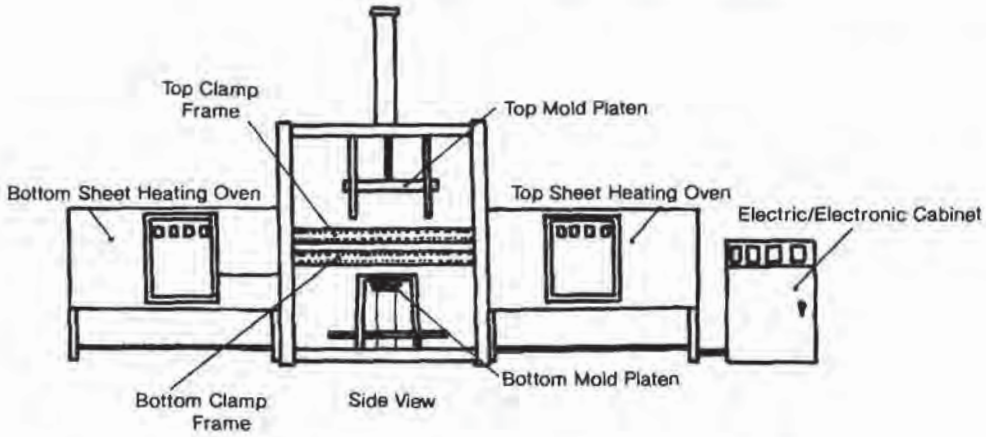

Figure 1.24 Dual heater simultaneous or sequential twin cut sheet shuttle press

heating efficiency suffers. The optimum forming conditions obtained on a shuttle thermoformer cannot be successfully translated to forming conditions on a rotary press. Rotary formers are also used to produce twin-sheet parts. As detailed in Chapter 9, there are several methods for dealing with the second sheet. Some are:

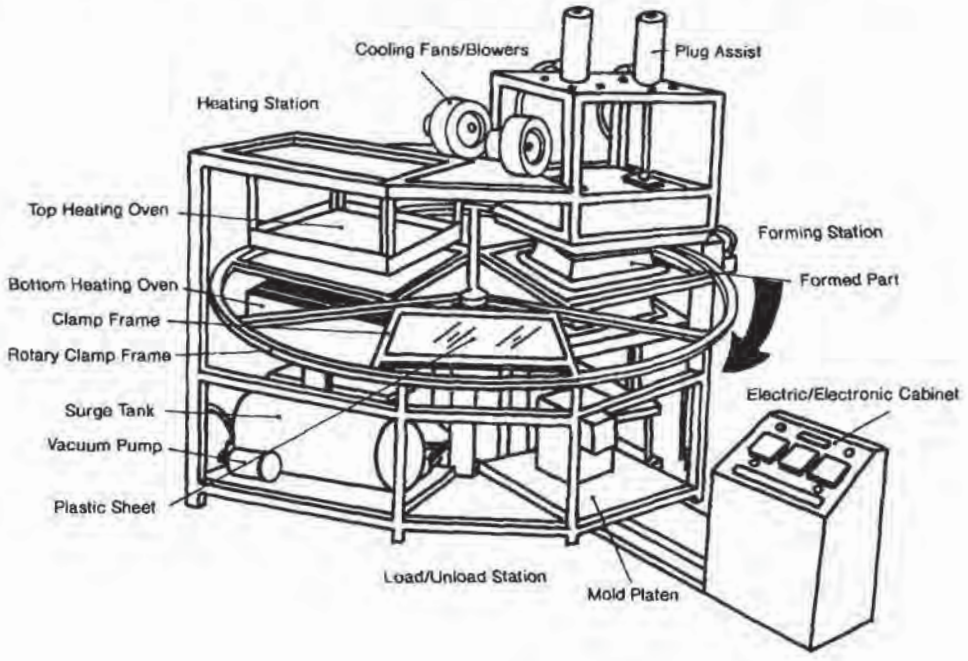

Figure 1.25 Cut sheet three-station rotary press

© 1996 Carl Hanser Verlag. All rights reserved.
No unauthorized disclosure or reproduction; licensed to purchaser only.

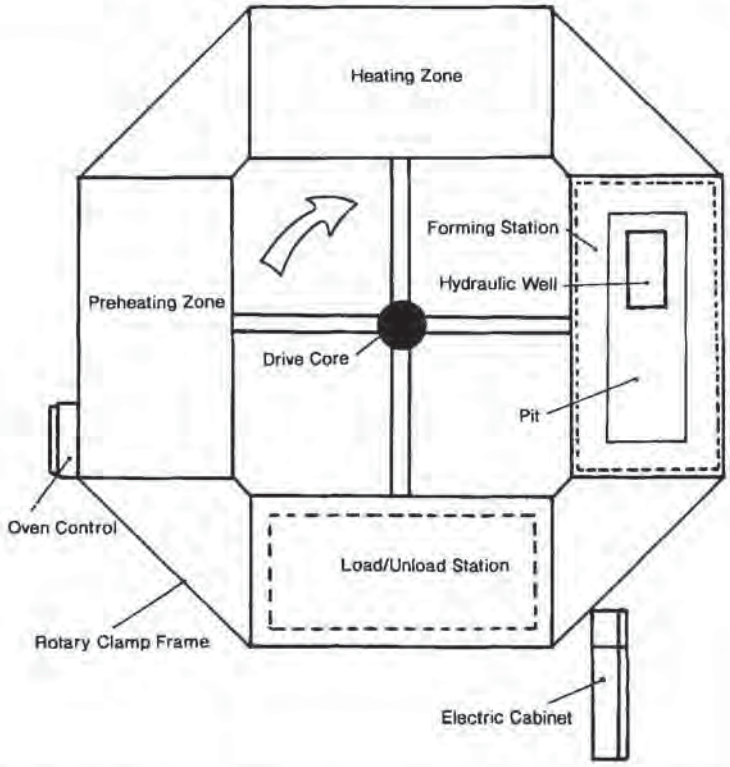

Figure 1.26 Top view of cut sheet four-station rotary press where the fourth station is a preheater oven

- The second sheet is heated and formed sequentially in the same former,
- The second sheet is simultaneously heated in a second rotary press and simultaneously formed with the first sheet in the first former, with overlapping sheet clamping frames, and
- The second sheet is clamped in a second tier rotary clamp, is simultaneously heated in a second tier oven on a single rotary press, and is simultaneously formed with the first sheet in a single rotary former.

Two shuttle formers can also be used in similar fashion.

Note in Table 1.10 that cut sheet is usually held in place with mechanical or pneumatic clamps. These clamps are toggle-locked and opened with air pressure. On shuttle presses, the clamp frame is indexed by motor-driven rack-and-pinion rails or by push-pull action of pneumatic or hydraulic pistons. The linear indexing of the rotary press carousel should be accurate to within 0.010 in or 0.25 mm. This requires a rotary drive motor accuracy and repeatability to within one arc minute. This is accomplished on large carousels with high-torque, low-rotation motors of about 1 rev/min, limit switches and electronic brakes. On smaller machines, indexing is also

© 1996 Carl Hanser Verlag. All rights reserved.
No unauthorized disclosure or reproduction; licensed to purchaser only.

done by driving the rotary table with a cam-arm-linked pneumatic cylinder. Positive position lock-in is achieved by dropping a tapered shot pin into a hardened bushing on the table. The pin is then pneumatically extracted prior to the next index sequence [29]. Ideally, the rotation cycle needs smooth acceleration and deceleration.

For heavy-gage forming, the mold is usually quite large, cumbersome and heavy. As a result, the mold is usually mounted to the press platen in the "down" position. Example 1.4 illustrates a method for determining the weight of a mold. There usually is no top "platen", per se. Ancillaries, such as plug assist cylinders or a pressure box, are therefore mounted over the mold on the top of the press framework. One exception to this is when a single press is used for twin-sheet forming. Another is when a vacuum box is used to prestretch the sheet. This box is normally mounted in the down position. As a result, the male mold is mounted in the "up" position and the press therefore has a top platen but no bottom platen. The sheet clamp frame usually travels as well, so that the formed part can be extracted from the vacuum box.

Example 1.4 Mold Weight

It is desired to thermoform a spa from 0.400 inch PMMA. The spa dimensions are 48 in × 60 in × 36 in deep. The mold outside dimensions are 76 in × 84 in by a bottom thickness of 12 in. What is the weight of the mold if it is made of aluminum? If a safety factor of 4 is used, what is the uniformly distributed static load on the forming press?

The density of aluminum is 167 lb/ft^3. The volume of the mold cavity is:

$$\text{Spa volume: } 48 \times 60 \times 36 = 103{,}680 \text{ in}^3 = 60 \text{ ft}^3$$

The volume of the mold before the mold cavity is formed is:

$$\text{Billet volume: } 76 \times 84 \times (36 + 12) = 306{,}432 \text{ in}^3 = 177.33 \text{ ft}^3$$

The mold volume: $177.33 - 60.0 = 107.33$ ft^3
Mold weight: 107.33×167 lb/ft^3 $= 29{,}600$ lb $= 14.8$ T $= 13{,}450$ kg
Loading level: $29{,}600/(76 \times 84) = 4.64$ lb/in^2 $= 670$ lb/ft^2
With a safety factor of four, the static load is $4 \times 4.64 = 18.6$ lb/in^2 $= 2{,}670$ lb/ft^2.

As discussed in detail in Chapter 3 on heating the sheet, for heavy-gage sheet, energy conduction from the sheet surface to its interior usually governs the rate of heating. As a result, heater energy efficiency is of secondary importance to energy distribution across the sheet surface. The local control and shaping of the energy source is called pattern heating or zoned heating. There are two primary ways of controlling local energy input to the sheet. In one, the heating source energy output, in kW/in^2 or kW/m^2 is uniform. Local control is accomplished with patterns or screen placed between the heater and the sheet surface. The heaters are usually wire or metal rods, heated metal or glass plates, heated screens, and direct or indirect gas burners. The second way uses many elements that are individually temperature or

© 1996 Carl Hanser Verlag. All rights reserved.
No unauthorized disclosure or reproduction; licensed to purchaser only.

energy controlled, including metal tapes and coils, ceramic tiles and halogen and quartz lamps. For very heavy-gage sheet, hot air convection ovens heat the sheet at a rate that allows adequate energy conduction into the sheet without sheet surface burning.

1.8 Thin-Gage Thermoforming Machinery Specifics

Table 1.11 gives a list of important items to be considered in thin-gage thermoforming machinery design. Typically, roll-fed thin-gage machinery designs are much more restrictive than those for heavy-gage. Thin-gage machines are designed to produce hundreds or thousands of parts per hour. Unlike heavy-gage forming, thin-gage forming appears as a continuous, seamless operation. It is not, even though sheet is supplied to the former from continuous rolls or directly from an extruder. For most roll-fed formers, the forming step is static, requiring the sheet to remain in contact

Table 1.11 Check-List for Important Items for Thin-Gage Forming Machines

Sheet takeoff or unwind station
- Roll stand capable of holding 1000 lb [454 kg] rolls.
- Roll stand capable of holding up to 6 ft [2 m] diameter rolls without vibration, instability.
- Roll stand capable of handling rolls wound on various core diameters.
- Roll core diameter should be standard such as 3 in or 75 mm, 6 in or 150 mm, or 8 in or 200 mm.
- Idler take-off to nip roll, or idler take-off to dancer.
- Passive tension brake, or roll speed governor.
- Roll weight overload warning.
- End-of-roll warning.
- Rapid roll changeover.

Pin-chain and Pin-rail
- Non-stick, no-scratch engagement shoes.
- Removable pins so that:
  - Pins can be sharpened,
  - Pins can be replaced if damaged, or
  - Pins designed for piercing specific polymers can be installed.
- Preheated pins for tough polymers.
- Self-lubricated chain links.
- Automatic parallel chain adjustment.
- Segmental chain guides for non-parallel chains.
- Manual method for adjusting chain non-parallelism during run.
- Lower pin guide to keep pin vertical.
- Lubrication that does not contaminate sheet.
- Pin-rail heating/cooling/temperature control.
- Chip vacuum at pin-sheet engagement.
- "Out-of-sheet" detector/warning light/horn.
- Servo-driven chain advancement, to achieve:

© 1996 Carl Hanser Verlag. All rights reserved.
No unauthorized disclosure or reproduction; licensed to purchaser only.

Table 1.11 (Continued)

Constant velocity during transfer, ft/s or mm/s,
Smooth and constant acceleration/deceleration rate, ft/s^2 or mm/s^2, at beginning and end of transfer time.

Oven
Preheat oven for hydroscopic polymers such as ABS, PS, PET, PMMA, Cellulosics.
Oven sides that extend to within 1 to 2 in or 25 to 50 mm of the sheet surface at the rail edge,
One to 2 in or 25 to 50 mm fiberglass insulation over entire inner surface of oven.
Rapid disconnect for main electrical to top and bottom oven.
Rapid disconnects for individual heater elements.
Rapid disconnects for individual heater thermocouples.
Open woven wire or chicken wire guards on top and bottom oven heaters.
Adequate places to fasten screens for pattern heating.
Air- or water-insulated ports in top and bottom oven surfaces for infrared pyrometer devices.
Internal baffles for ovens with more than one shot capacity, with baffles extending to within 1 to 2 in or 25 to 50 mm of the sheet surface.
Automatic heater isolation from the sheet when pin-chain rail shuts down, such as:
Pneumatically driven fly-open operation, or
Horizontal pneumatically driven heater retraction.
Photo-eye sensor/warning for excessive sheet sag.
Oven equipped with central system for dispensing CO_2 or other non-aggressive fire extinguishing material.
Adjustment of oven height above/below sheet plane to allow:
Rapid change during sheet set-up,
Rapid change during running.
Sufficient daylight between top and bottom oven to allow:
Heater burn-out inspection and replacement,
Individual heater temperature measurement by non-contact means such as infrared pyrometry.

Press
Smooth-acting, constant velocity press closure.
Acceleration/deceleration at end of stroke to minimize banging.
Clamping by:
Platen locking devices,
Mechanical/pneumatic assists,
Servo-motor lockout,
Pneumatic gland.
Self-lubricating or continuous-lubricating platen screws.
Enclosed or self-sealing overhead hydraulic oil lines to prevent oil vapor contamination of formed product.
Protected platen locking cogs or screws to minimize contamination from trim dust, chips, dirt, detritus.
Self-leveling press platens.
Configured to easily accept mold changeover.
Adequate daylight between platens to allow for:
Inspection and maintenance with mold in place,
Replacement of in-mold dies.
Adequate space around press to allow for:
Adjustment of ancillaries such as:
Plug assist platen,

(Continued)

© 1996 Carl Hanser Verlag. All rights reserved.
No unauthorized disclosure or reproduction; licensed to purchaser only.

Table 1.11 (Continued)

Cavity isolator platen,
Trim-in-place die platen,
Ejector ring platen.
Proper placement of vacuum lines from vacuum box,
Proper placement of water lines.
Clear identification various elements of the press.
Rapid, easy-to-use platen alignment devices.
Rapid, easy-to-use horizontal plane positioning for platen and all ancillaries.
Pneumatic interlocks to prevent:
Premature air pressurization before pressure box fully engages mold,
Premature opening of pressure box while still pressurized, and
Pressurization of an empty chamber.
Pneumatic interlocks to allow rapid venting of the pressure box before pressure box moves.
Proper controls on all rate-dependent ancillaries such as:
Plug assist platen,
Cavity isolator platen,
Trim-in-place die platen, and
Pressure box.
Means for lowering top platen to below pin-chain plane for:
Mold installation, and
Mold removal.

Plug assist
Rapid replacement of individual plugs.
Capability for internally heating/cooling aluminum plugs, including adequate space above the press to allow for heating/cooling lines and thermocouples.
Relatively easy removal of entire plug assist platen, or at least rendering it inoperative.
Relatively easy and rapid means for adjusting the travel length, and rate of travel of plug assist platen.

Ejector ring
Relatively easy means for adjusting travel of ring platen.

Cavity isolator
Relatively easy means for adjusting travel of isolator platen.

Trim-in-place
Rapid means for determining sharpness of individual trim die.
Rapid means of adjusting individual trim dies in:
Concentricity,
Parallelism to individual punch.
Rapid means of removing individual trim die.
Automatic trim dust removal.
Automatic part separation from trim web, by:
Individual cavity vacuum cups,
Shuttle that holds the ejected parts in plane as the mold falls away, then horizontally removes them to sorting table, or
Tipping or rotating mold that dumps parts onto sorting table.
Rapid means of clearing trim, chip, detritus from individual trim die during maintenance, inspection.
Air blow-back to ensure that all cavities are free of parts.

© 1996 Carl Hanser Verlag. All rights reserved.
No unauthorized disclosure or reproduction; licensed to purchaser only.

Table 1.11 (Continued)

Trim takeup station
Tension speed control, or
Slave to pin-chain drive.
Roll maximum diameter warining.
Condition monitors
Sheet temperature monitoring via infrared pyrometry either:
Automatically through the oven, both top and botton,
Automactically at sheet exit from oven,
Hand-held as sheet exits oven.
Mold temperature monitoring with thermocouples in at least one mold cavity.
For metal and ceramic heaters, individual thermocouples mounted on or embedded in many heaters on both top and bottom ovens.
Air pressure to all pneumatic devices including:
Pressure box,
Ejector ring platen,
Plug assist platen,
Trim die platen, particularly during cutting.
Time-dependent vacuum at:
Vacuum pump,
Surge tank,
Vacuum box,
At least one mold cavity.
Times on all phases of sheet transfer through the press.
Photoelectric cells on sheet in oven and as sheet exits oven.
Process control
Times and sequences for all events.
Temperatures for all heaters that are independently controlled.
Delay timers for events such as:
"Out-of-sheet",
Line stoppage,
Mold closure for "part in mold".
Storage of all important event values and capability of resetting machine using stored data.
Automatic protocol for emergency shutdown for:
Fire,
Power overload, brownout and outage,
Light curtain interrupt,
Safety cage security breach.

with a stationary mold for several seconds[1]. As a result, the sheet remains stationary in the oven for a like amount of time. Trimming of the part from the web or trim is also done while the sheet is stationary. The sheet is advanced from station to

[1] Special-purpose or dedicated forming machines are available that allow the sheet to move at a fixed constant velocity from the extruder roll-stack through a tempering oven and onto a rotary vacuum molding station. The molding station is a horizontal roll that contains multiple cavities. Evacuation is through traditional vent holes and the roll is evacuated through a rotating coupling. In-line trimming is usually done on a conventional platen-type trim press.

© 1996 Carl Hanser Verlag. All rights reserved.
No unauthorized disclosure or reproduction; licensed to purchaser only.

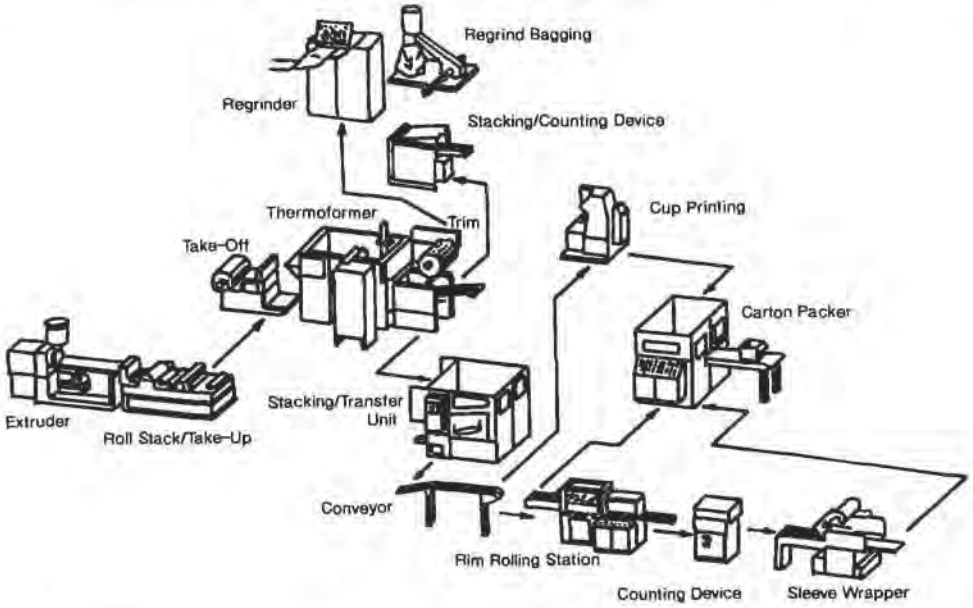

Figure 1.27 Thermoformed cup production scenario [30]

station in a jog or start-stop fashion. In certain areas, roll-fed thermoforming machines are portions of more complex systems such as the cup production schematic (Fig. 1.27) [30] or the form-fill-seal operation (Fig. 1.28) [31].

Sheet is usually transferred from the takeoff roll through the heater, forming press and trim die by means of a pair of endless chains containing regularly spaced pins or other impaling devices. The pin-chains are usually parallel although provisions can be made to allow the chains to diverge throughout their entire path or only

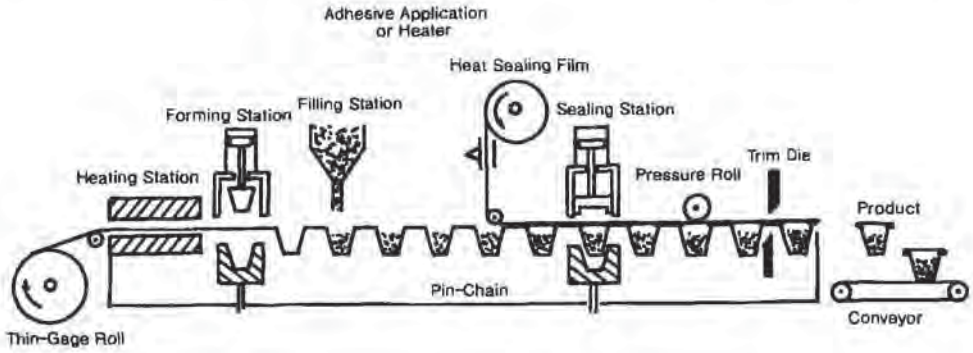

Figure 1.28 Thermoform, fill and seal production scenario [31]

© 1996 Carl Hanser Verlag. All rights reserved.
No unauthorized disclosure or reproduction; licensed to purchaser only.

in certain segments. Chain divergence is considered necessary when forming polymers with excessive sag, such as LDPE, PP and PET. Unlike heavy-gage forming machinery, thin-gage machinery sheet width is usually restricted to less than about 52 in or 1.3 m. For crystalline polymers or polymers that show excessive sag, sheet width is restricted to less than about 32 in or 0.76 m, unless sag bands are used. The sheet in the pin-chain region is usually shielded from the intense radiant heat to minimize sheet pull-out.

Electric radiant heat dominates the heating methods for thin-gage sheet. For decades, metal rod and wire heaters were the common means of heating thin-gage sheet. Ceramic or quartz heaters are used in most new machines. The newer heaters offer greater flexibility in controlling the amount of heat directed to certain portions of the sheet. The absorption of energy by the sheet depends on:

- The polymer classification, such as PVC, PE, PET or PS,
- The type and dosage of various adducts in the polymer, particularly colorants, pigments, and
- The thickness of the polymer sheet.

The last factor is most critical to the selection of proper equipment. As discussed in Chapter 2, most plastics are semi-transparent to incident infrared radiation. The total amount of energy absorbed is strongly dependent on the thickness of the polymer sheet. For very thin sheet or film, a substantial portion of incident radiant energy may be transmitted completely through the film. As a result, thin sheet and film heat very slowly when infrared heating is used. Direct contact heat transfer is recommended for thin films of thicknesses of less than about 0.005 in or 0.13 mm, for thin-gage sheet where the surface has been printed or metallized, or for thin-gage sheet that is laminated or contains embedded energy absorbers such as carbon or metal fibers. These aspects and others are discussed in detail in Chapter 3 on heating the sheet.

As noted above, sheet sag is a serious problem with certain polymers. Sag bands are standard fare for minimizing sag. In certain cases, sag bands cannot be fully utilized, because of mold configuration or the nature of the polymer. Special thermoformers are available that allow the sheet to be heated and formed *vertically*. The colder portion of the sheet supports the hotter portion of the sheet as it passes through the excessive sag thermal region. Alternatives to this approach, such as solid-phase pressure forming and compounding or reformulating the polymer to yield one with higher melt strength, are usually less expensive in the long haul.

The forming station of a typical thin-gage former is substantially more complex than that of a heavy-gage former. Owing to the thinner sheet, events must take place much more rapidly than those for a heavy-gage sheet. In addition:

- Molds are much smaller and are usually in multiples,
- Plugs must be ganged,
- Multiple molds require special hold-down plates called cavity isolators or hold-down grids, to minimize variations in wall thickness,
- Stripper plates are needed to uniformly strip the formed parts from the mold without racking, binding, scuffing or jamming.

© 1996 Carl Hanser Verlag. All rights reserved.
No unauthorized disclosure or reproduction; licensed to purchaser only.

Plugs dominate the prestretching process. Machines must have the capability of carrying the mold in the "up" or "down" position. This means that the presses should have two platens and both platens must travel. Presses with this capability are useful in pressure forming and matched die forming, as well. For these two technologies, the press clamping capability must be robust.

Thin-gage parts are removed from their web either while they reside on the mold or away from the forming press in an in-line stand-alone trimming press. Since the part is locked on the mold, trimming on the mold, or *trim-in-place*, affords the most dimensional control on the trimming location. If the part is completely cut from the web, it must be picked or removed from the press before the next sheet is indexed to the forming station. There are many ingenious ways to do this. Nevertheless, the picking method must be absolutely infallible. A part that is not picked or a part that is dropped before clearing the mold will cause havoc in the next forming step. Usually the trimming is not complete, with tabs remaining that hold the parts in the web until the sheet is clear of the mold. Mechanical or manual picking is then required. In-line stand-alone trimming is an economically viable alternative for polymers that do not show substantial distortion, shrinkage or "swimming" between the forming press and the trim press. Extensive efforts are made to correctly register the formed part in the trim press, as discussed in Chapter 5. Additional information is found in [34].

1.9 References

1. J. Harry DuBois, *Plastics History USA*, Cahners Books, Boston, 1972, pp. 38-51.
2. Anon., "Monoformer", Hayssen Mfg. Co., Sheyboygan WI., 1977.
3. A.H. Steinberg, "Stamped Reinforced Thermoplastic Sheet", Design. Engineering Seminar, 33rd SPI RP/C Conference, Washington DC, Feb 1978.
4. R.C. Progelhof and J.L. Throne, *Polymer Engineering Principles: Properties, Processes, and Tests for Design*, Hanser Publishers, Munich, 1993, Section 1.2 "Introduction to Polymer History".
5. W. McConnell, "The Oldest Infant", in P.F. Bruins, Ed., *Basic Principles of Thermoforming*, Gordon and Breach, New York, 1971, p. 3.
6. S. E. Farnham, *A Guide to Thermoformed Plastic Packaging*, Cahners Books, Boston, 1972, p. 8.
7. J.L. Throne, "Thermoforming: Polymer Sheet Fabrication Engineering, Part 1. Solid Sheet Forming", Plast. Rubber: Proc., *4* (1979), p. 129.
8. E.S. Childs, "Thermoforming-Trends and Prospects", in P.F. Bruins, Ed., *Basic Principles of Thermoforming*, Gordon and Breach, New York, 1971, p. 37.
9. M. Bakker, personal communication, 1 October 1985.
10. Anon., "Thermoforming", Modern Plastics, *62*:1 (Jan 1985), p. 59.
11. J.L. Throne, *Thermoforming*, Carl Hanser Verlag, Munich, 1986, Figure 1.1, p. 15.
12. E.S. Childs, "Thermoforming-Trends and Prospects", in P.F. Bruins, Ed., *Basic Principles of Thermoforming*, Gordon and Breach, New York, 1971, p. 38.
13. Anon., "Thermoforming Lustran ABS, Lustrex Polystyrene and Cadon Engineering Thermoplastics", Monsanto Bulletin #6541, Undated, p. 3.
14. E.S. Childs, "Thermoforming-Trends and Prospects", in P.F. Bruins, Ed., *Basic Principles of Thermoforming*, Gordon and Breach, New York, 1971, p. 40.

© 1996 Carl Hanser Verlag. All rights reserved.
No unauthorized disclosure or reproduction; licensed to purchaser only.

15. P.V. Alongi, "Thermoforming", Mod. Plast., *69*:13, (Dec 1992), pp. 577-579.
16. R. Wood., "Inline Thermoforming Offers Efficiencies for Packaging and Large Components", Plast. Mach. Equip., *19*:7 (Jul 1985), p. 18.
17. G.P. Kovach, "Thermoforming", in *Encyclopedia of Polymer Science and Technology*, Vol. 13, 1969, p. 832.
18. G. L. Beall, "Designers' Guide to Pressure Forming", Plast. Design. Forum, *10*:5 (May 1985), p. 42.
19. J.M. Wooldridge, "Polymer Process Modeling: Thermoforming of Simple Objects Via Finite Element Analysis", MS Thesis, U. Louisville, Louisville KY, 1985, p. 2.
20. Anon., Modern Plastics, *70*:12 (Nov 1993), pp. 489-515.
21. A. Höger, *Warmformen von Kunststoffen*, Carl Hanser Verlag, Munich, 1971, Chapter 4, "Maschinen zum Warmformen".
22. J.L. Throne, Thermoplastic Foams, Chapman & Hall, New York, 1995.
23. Wm. K. McConnell, Jr., Material Presented, Distributed at SPE Industrial Thermoforming Symposium & Workshop, 12-14 March 1985. Material Copyrighted by McConnell.
24. A. Höger, *Warmformen von Kunststoffen*, Carl Hanser Verlag, Munich, 1971, pp. 135-136.
25. J.L. Throne, "Thermoforming Crystallizing PET", SPE ANTEC Tech. Papers, *27* (1981), p. 598.
26. J.L. Throne, "Thermoforming Crystallizing Polyethylene Terephthalate (CPET)", Adv. Polym. Tech., *8* (1988), pp. 131-171.
27. J. Florian, *Practical Thermoforming: Principles and Applications*, Marcel Dekker, New York, 1987, pp. 190-191.
28. J. Florian, *Practical Thermoforming: Principles and Applications*, Marcel Dekker, New York, 1987, Florian pp. 199-201.
29. Anon., "Kostur... The Shape of Performance in Thermo Forming Production", Kostur Enterprises, Inc., Riviera Beach FL, 12 Dec 1983.
30. K.-H. Hartmann, "Wirtschaftliches Fertigen von warmgeformten Verpackungen", Kunststoffe, *78* (1988), pp. 398-401, Bild 2.
31. K.-H. Hartmann, "Wirtschaftliches Fertigen von warmgeformten Verpackungen", Kunststoffe, *78* (1988), pp. 398-401, Bild 5.
32. G.L. Beall, "A Brief History of the Mold Making and Mold Design Div. of SPE", Plast. Mach. Equip., *27*:6 (June 1993), pp. 38-40.
33. J.L. Throne, *Thermoforming*, Carl Hanser Verlag, Munich, 1987, p. 33.
34. G. Gruenwald, *Thermoforming: A Plastics Process*, Technomic Publishing Co., Inc., Lancaster PA, 1987, Chapter 6, "Trimming of Thermoformed Parts".
35. Anon., Polymer News, *16* (1991), p. 214.
36. Anon., Polymer News, *16* (1991), p. 87.
37. Anon., Polymer News, *12* (1987), pp. 50-51.
38. Anon., Polymer News, *12* (1987), pp. 215-216.
39. Anon., Polymer News, *13* (1988), pp. 20-21.
40. Anon., Polymer News, *13* (1988), pp. 152-153.
41. Anon., Polymer News, *16* (1991), p. 313.
42. Anon., Polymer News, *18* (1993), p. 148.
43. Anon., Polymer News, *16* (1991), p. 250.
44. Anon., Polymer News, *16* (1991), p. 340.
45. Anon., Polymer News, *11* (1986), pp. 214-215.
46. Anon., Polymer News, *18* (1993), p. 227.
47. Anon., Polymer News, *14* (1986), pp. 118-119.
48. Anon., Polymer News, *16* (1991), p. 86.
49. Anon., Polymer News, *16* (1991), pp. 25-26.
50. Anon., Polymer News, *16* (1991), p. 186.
51. Anon., Polymer News, *13* (1988), p. 151.
52. Anon., Polymer News, *15* (1990), p. 377.

© 1996 Carl Hanser Verlag. All rights reserved.
No unauthorized disclosure or reproduction; licensed to purchaser only.

2 Polymeric Materials

© 1996 Carl Hanser Verlag. All rights reserved.
No unauthorized disclosure or reproduction; licensed to purchaser only.

2.1 Introduction

If a polymer can be produced as a sheet, it can be thermoformed into a product [1,2]. Polymers are high molecular weight organic molecules that are produced by combining very pure carbon-based simple molecules under heat, pressure, and catalyst systems. There are more than 20 major classes of polymers available today [3] and many sub-classes, made by combining polymers with polymers, polymers with fillers and reinforcements, and polymers with additive and processing aids [4]. In order to achieve thermoformed parts having commercially interesting combinations of physical properties, it is necessary to understand the way in which basic polymer architecture affects material properties.

2.2 Network Nature of Polymers

There are two general categories of polymers—thermoplastics and thermosets. Commercially, the most important thermosetting polymers are intrinsically crosslinked resins such as epoxies, phenolics, and reacted unsaturated polyester resins. The polymers are formed from relatively simple chemically unsaturated molecules that are usually liquids at the reaction conditions. The unsaturation is seen as isolated, regularly-spaced double bonds regularly spaced along the carbon-carbon backbone, as -R-C = C-R-. The formation of three-dimensional ties is accomplished by opening the double bonds, -C = C-, with chemical aids or sometimes with heat and pressure. At some point during the formation of this three-dimensional network, the material usually becomes infusible and takes a permanent shape. Thermosets usually cannot be reused or returned to their original forms.

More than 80% of all polymers used in the world today are thermoplastics. These polymers are characterized by exceptionally long two-dimensional, nearly linear organic molecules, usually having saturated or single covalent bond carbon-carbon backbones, as -C-C-. In their final forms, thermoplastics are thermally and chemically stable at processing conditions. This means that they can be softened or melted, formed into useful articles, then resoftened or remelted and reused. Thermoforming economics depend on the thermal stability and resulting recyclability of polymers, and so nearly all commercially thermoformable polymers are thermoplastics.

The toughness of thermosets is due to the rigid three-dimensional network of relatively small building blocks. The toughness of thermoplastics is due mainly to the entanglements of the very long two-dimensional molecules and in certain cases, the formation of crystalline structures. For example, if the ethylene molecule, $CH_2 = CH_2$, is scaled in dimension 100 million times, each $-CH_2-$ unit would be about 10 mm or 3/8 in long. The single ethylene unit in a polyethylene backbone, $-CH_2-CH_2-$ is called a repeat unit. An olefin grease or oil has about 100 repeat units and on the same expanded scale would be about 2 m or 6 ft long, if the molecular chains are fully extended. Low-density polyethylene (LDPE) has about 1000 repeat

© 1996 Carl Hanser Verlag. All rights reserved.
No unauthorized disclosure or reproduction; licensed to purchaser only.

Table 2.1 Comparative Sizes of Polymer Molecules (Fully Extended Chains Scaled 100,000,000:1)

Polymer	End-to-end distance (Å)	Degree of polymerization	Chain or free segment length	
			Metric (m)	US (ft)
Epoxy adhesive	15.9	1	0.159	0.52
Melamine	35.4	5	0.354	1.17
Epoxy resin–medium MW	110.9	6.5	1.109	3.64
Phenolic	40.1	8	0.401	1.3
Alkyd-unsaturated polyester resin	94.4	19	0.944	3.10
Olefin grease	200	67	2.00	6.56
Epoxy resin–high MW	580.6	34	5.81	19.1
Polyethylene, low-density	2000	670	20.0	65.6
Polyethylene, UHMW	91,000	30,000	910	3000

units and would be about 20 m or 65 ft long, with fully extended chains and minimal branching. Ultra-high molecular weight polyethylene (UHMWPE), a nearly intractable polymer used for friction-and-wear applications, has about 100,000 repeat units, and the extended chains would be about 2 km or 1.2 miles in length. On the other hand, the chain lengths between crosslinking or tie points for thermosets are about 10 to 20 repeat units in length. On the same expanded scale, phenol-formaldehyde or phenolic resin would have chain lengths between tie points of about 25 mm or 1 in. More importantly, molecular diameter would be nearly 25 mm or 1 in, as well. Other comparisons are given in Table 2.1 [5].

Some thermoplastic polymers such as polyethylene are further toughened by crosslinking, with either irradiation or peroxide chemicals. Crosslinking is accomplished by removal of a small molecule such as hydrogen from the primary carbon-carbon backbone. Active sites on adjacent chains then react to form a tie point or crosslink. The number of tie points per thousand repeat units is usually quite small. Typically, crosslinked high-density polyethylene (HDPE) has about 0.5 to 1 tie points per thousand backbone carbons. Low-density polyethylene (LDPE) has about 5 to 10 per thousand backbone carbons. These few tie points serve only to partially immobilize the polymer above its traditional melting point. Thus, crosslinked thermoplastics remain very soft, thermoformable solids rather than becoming fluid above their melting points (Fig. 2.1). As expected, crosslinked LDPE, with its greater frequency of tie points, is considerably more difficult to stretch-form than crosslinked HDPE. The reprocessing, regrinding and re-extruding of crosslinked thermoplastics usually result in mechanical and thermal destruction of tie points or backbone carbon-carbon bonds. Furthermore, crosslinking does not allow melt processing and so small amounts of crosslinked polymer form intractable gels in uncrosslinked polymer extrudates.

Thermoforming requires biaxial stretching of polymer sheet. Although certain thermosetting polymers such as rubber soften above their glass transition tempera-

© 1996 Carl Hanser Verlag. All rights reserved.
No unauthorized disclosure or reproduction; licensed to purchaser only.

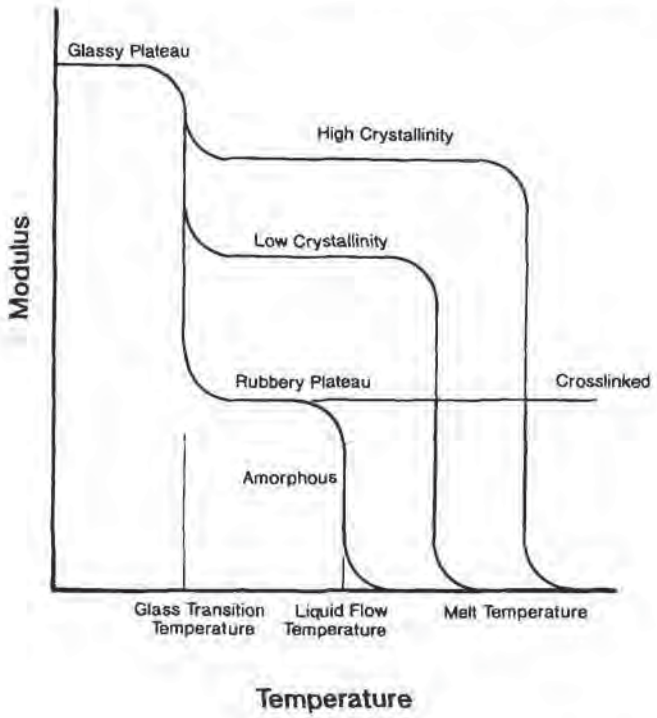

Figure 2.1 Schematic of temperature-dependent modulus for amorphous, crystalline and crosslinked polymers

tures, the tight three-dimensional network of most rigid thermosetting polymers restricts the gross deformation necessary in thermoforming[1]. However, partially crosslinked polyurethane has been simultaneously drawn, formed, and heat-stabilized to produce fully crosslinked thermoset shapes [7]. Once these molecules are immobilized, very little additional shaping is possible. Additional thermal energy input or regrind then leads to polymer degradation.

2.3 Addition and Condensation Polymerization

Thermoplastic polymers are produced from monomers in two general ways. Addition polymers are formed by continuous extension of a preexisting polymer chain by

[1] Low-density thermosetting and highly crosslinked thermoplastic foams are the exception to this. Foam cell architecture dominates the tensile and compression behavior of the polymer. Bending and stretching occur predominantly at cell strut or plate intersections rather than in the polymer itself [6].

© 1996 Carl Hanser Verlag. All rights reserved.
No unauthorized disclosure or reproduction; licensed to purchaser only.

attachment of a monomer containing a reactive double bond. The largest group of addition polymers are called generically *vinyl* polymers. Table 2.2 [8,9] summarizes the chemical structure of many common addition polymers, including many common thermoformable polymers such as HDPE, LDPE, polypropylene (PP), polyvinyl chloride (PVC), and polystyrene (PS). Condensation polymers are formed by reacting one, two, or more saturated comonomers with active end groups. Such end groups are amines, hydroxyls or carboxyls. The reaction usually results in evolution of a small by-product molecule such as water. This molecule must be removed continuously to continue the reaction. Thermoplastic polyester (PET), nylon (PA), polymethyl methacrylate (PMMA), and polycarbonate (PC) are examples of thermoformable condensation polymers. These and others are summarized in Table 2.3.

2.4 Aromatic and Aliphatic Polymers

Polyethylene and polypropylene are simple, nearly linear polymers consisting of -C-C- building blocks, with no double-bond unsaturation or ring structure. These are aliphatic polymers. Polystyrene has an unsaturated benzyl pendant group on every other backbone carbon, as is considered the simplest form of an aromatic polymer. Higher aromatic polymers such as polyethylene terephthalate and polycarbonate have ring structures such as benzyl groups within the backbone on regular intervals. Polymer properties such as stiffness and thermal stability are strong functions of the degree of aromaticity [10].

2.5 Molecular Weight and Molecular Weight Distribution

The molecular weight of a given polymer molecule is obtained by multiplying the molecular weight of its repeat unit by the number of repeat units, then addition in the molecular weight of the end groups. For example, the molecular weight of the ethylene repeat unit, $-CH_2-CH_2-$, is 28. For HDPE of 10,000 repeat units, the molecular weight is 280,30. In all commercial polymers, there is a distribution of polymer chain lengths (Fig. 2.2). The *number-average* polymer chain length is obtained by calculating the total weight of all polymer chains, w, then dividing by the total number of chains, n:

$$M_n = \frac{w}{n} = \frac{\Sigma N_i M_i}{\Sigma M_i} \tag{2.1}$$

The *weight-average* molecular weight is obtained by multiplying the weight of a chain of a given length, w, by the number of these chains, n, then dividing by the total weight of the chains, w:

$$M_w = \frac{nw}{w} = \frac{\Sigma N_i (N_i M_i)}{\Sigma N_i M_i} \tag{2.2}$$

© 1996 Carl Hanser Verlag. All rights reserved.
No unauthorized disclosure or reproduction; licensed to purchaser only.

Table 2.2 Chemical Structure of Vinyl-Type Thermoplastics

Common name	R_1	R_2	R_3	R_4	Subspecies	Glass transition temperature (°C)	Crystalline melt temperature (°C)
Polyethylene	H	H	H	H	LOPE (Branched)	−70	112
					HOPE (Linear)	−110	134 (137)[1]
Polyethylene	H	H	H	CH_3	Atactic	−15	A[2]
					Syndiotactic	−5	165(170)[1]
Polybutene-1	H	H	H	CH_2CH_3	(Isobutylene)	−70	A[2]
Polybutadiene	H	H	H	$HC{=}CH_2$	(Divinyl)	−55	A[2]
Polyvinyl chloride (PVC)	H	H	H	Cl		80	A[2] (212)[1]
Polyvinyl dichloride (PVDC)	H	H	Cl	Cl		−17	A[2]
Polyvinyl fluoride (PVF)	H	H	H	F		−20	A[2]
Polyvinyl difluoride (PVDF)	H	H	F	F		−35	A[2]
Polytetrafluoroethylene (PTFE)	F	F	F	F		125	326
Polysytrene (PS)	H	H	H	C_6H_5		94	A[2] (240)[3]
Polyvinyl alcohol (PVOH)	H	H	H	OH		85	A[2]
Polymethyl methacrylate (PMMA)	H	H	CH_3	$COCH_3$		100	A[2]
Polyvinyl acetate (PVAc)	H	H	H	$OOCCH_3$		30	A[2]
Polyacrylonitrile	H	H	H	CH		104	275[4] (327)[1]

[1] Melting temperature of pure crystal polymer
[2] Commercially amorphous polymer
[3] Isotactic melting point
[4] Highly oriented fiber

© 1996 Carl Hanser Verlag. All rights reserved.
No unauthorized disclosure or reproduction; licensed to purchaser only.

Table 2.3 Chemical Structure of Typical Condensation Thermoplastics

Common name	Repeat unit		Glass transition temperature (°C)	Crystalline melt temperature (°C)
Polyethylene terephthalate (PET)	$-(CH_2)_2-O-C(=O)-\Phi-C(=O)-O-$		70	260(267)[1]
Nylon 66 (PA-66)	$-N(H)-(CH_2)_6-N(H)-C(=O)-(CH_2)_4-C(=O)-$		48	240(265)[1]
Nylon 6 (PA-6) (polycaprolactum)	$-N(H)-(CH_2)_6-C(=O)-$		50	210
Polycarbonate (PC)	$-\Phi-C(CH_3)_2-\Phi-O-C(=O)-O-$		150	A[2]
Polyacetal (POM) (polyoxymethylene)	$-CH_2-O$		−60	180
Cellulose[3]	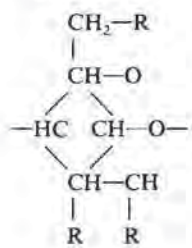	(R = OH) Cellulose	40	(?)[4]
		(R = NH_2) Cellulose nitrate	53	(?)
		(R = $OOCCH_3$) Cellulose triacetate	70,100(?)	280(?)(305)[1]
		(R = $OOCC_3H_7$) Cellulose tributyrate	120	180(?)(185)[1]

[1] Melting temperature of pure crystal polymer
[2] Commercially amorphous polymer
[3] Natural polymer
[4] Infusible, degrades before melting
Φ = Benzyl ring

© 1996 Carl Hanser Verlag. All rights reserved.
No unauthorized disclosure or reproduction; licensed to purchaser only.

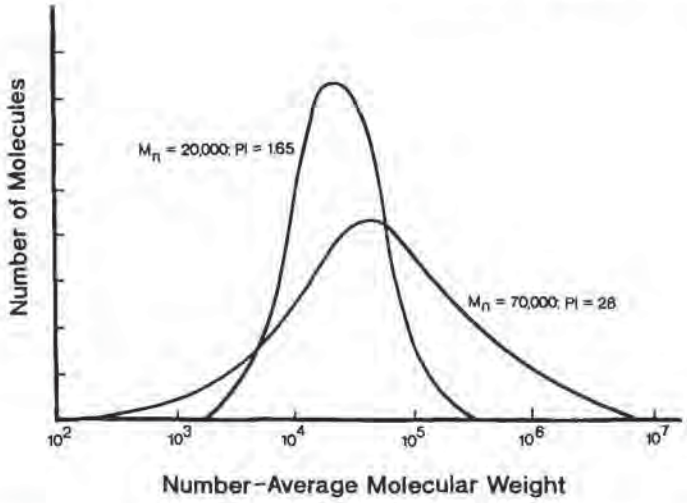

Figure 2.2 Typical molecular weight distributions for narrow and broad molecular weight polymers. Figure used by permission of copyright owner

The ratio of weight average to number average molecular weight is known as the *dispersity index*, DI:

$$DI = \frac{M_w}{M_n} \tag{2.3}$$

The dispersity index generally represents the shape of the chain length distribution curve. These three terms help to define the molecular characteristics of the polymer. Molecular weight distributions cannot be measured directly. Dilute solution viscosity measurements yield indirect information, as do end group analyses, turbidity and osmotic pressure measurements, and calculations based on infrared analyses [11]. Thus, whenever the phrase "molecular weight distribution" is used, it must be carefully defined.

2.6 Molecular Weight and Properties

A polymer that has a low molecular weight is easier to extrude into a sheet than one with a very high molecular weight. However, high molecular weight yields improved hot strength during forming and improved finished part properties. Figure 2.3 [12] illustrates this for polyethylene. At a low molecular weight of 1000, polyethylene is a waxy solid at room temperature and an oily liquid at temperatures of less than 212°F or 100°C. At a molecular weight of 100,000, it is a tough ductile plastic at room temperature and a highly elastic liquid above its 110°C or 230°F melt

© 1996 Carl Hanser Verlag. All rights reserved.
No unauthorized disclosure or reproduction; licensed to purchaser only.

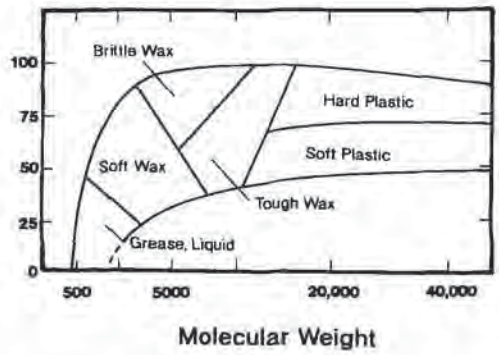

Figure 2.3 Relationship between polyethylene molecular weight, crystallinity and nature of polymer [12]. Figure used by permission of copyright owner

temperature. At a molecular weight of 1,000,000, as UHMWPE, it is an extremely tough crystalline solid at room temperature. The molecular chains are so long and entangled that it barely flows even at temperatures far above its melting point of 134°C or 273°F.

Polymethyl methacrylate (PMMA) is another example. At a molecular weight of 300, it is a viscous liquid at room temperature that is commonly used as a cell casting liquid to produce higher molecular weight PMMA. At a molecular weight of 30,000, PMMA is a glassy, brittle transparent solid at room temperature. It becomes a rubbery contiguous formable sheet when heated to temperatures of 150 to 200°C or 300 to 380°F or 50 to 100°C or 90 to 180°F above its softening point or glass transition temperature, $T_g = 105$°C or 220°F. Increasing the temperature further causes excessive chain mobility, manifested as sheet sag.

For some polymers, the molecular weight distribution can be significantly altered during polymerization or afterward in special depolymerization steps. Typically, broad molecular weight distribution polymers have very shear-sensitive viscosities over wide temperature ranges. These are usually easier to process than narrow molecular weight distribution polymers. Broad molecular weight distribution polymers are used in extrusion coating, laminating and heat sealing where high melt strength over a wide processing temperature range is sought. On the other hand, certain narrow molecular weight distribution polymers can be highly oriented and so yield very tough film and thin-gage sheet. Narrow molecular weight distribution polymers usually have better mechanical properties than broad molecular weight distribution polymers. It is difficult to generalize here, however, since other factors such as:

- Extent of chain entanglements,
- Extent of short-chain branching,
- Extent of long-chain branching,
- Polymer tacticity and isomerism,
- Pendant group size,

© 1996 Carl Hanser Verlag. All rights reserved.
No unauthorized disclosure or reproduction; licensed to purchaser only.

- Pendant group frequency, and
- Molecular level energy interactions such as;
  Van der Waals forces,
  Hydrogen bonding forces,
  Ionic bonding forces, and
  Dipole interaction,

act to mask and dominate the effect of molecular weight for any given homologous class of polymers.

2.7 Morphology and Properties

Polymer processing in general is concerned with the economic transition between the solid and fluid or semi-fluid states of polymers. It is easy to identify the liquidus phase of nonpolymeric crystalline substances such as metals and ceramics. An abrupt first-order thermodynamic transition from a rigid state to a waterlike fluid state occurs with a measurable absorption of energy, the latent heat of fusion. Crystalline metals and ceramics in the solid state have regular, ordered atomic structures that sharply diffract X-rays in known, repeatable fashions. It is difficult to envision long-chain, highly entangled polymers as having the high degree or thermodynamic order needed to form crystalline domains. Yet certain polymers such as nylons, polyethylene, polyethylene terephthalate and polypropylene readily crystallize when cooled from the melt. Although single polymer crystals are commonly formed in laboratories, polycrystalline structures are formed in commercial processes. Crystalline formation is a kinetic or rate-dependent process. Noncrystalline or *amorphous polymers* have molecular structures that are unordered. Disorder may be caused by:

- Bulk or stiffness or the polymer chain because of;
  Side chain branching frequency,
  Side chain branch length,
  Side chain branch bulk,
  Large pendant groups,
  Steric hindrance,
  Ladder-type backbone morphology, and
  Extensive aromaticity in backbone, and
- Rapid quenching of a potentially crystalline polymer from the melt.

Most crystallite regions in commercial crystallizable polymers are mixtures of spherulitic or sphere-like crystals, dendritic or tree-like crystals, and amorphous regions. The extent of crystallinity and to some extent, the size of the crystallites, for any polymer strongly effect such characteristics as:

- Its X-ray pattern,
- Its melting temperature,
- Its melting temperature range, and

© 1996 Carl Hanser Verlag. All rights reserved.
No unauthorized disclosure or reproduction; licensed to purchaser only.

- Nearly all commonly measured physical properties such as
  Tensile strength,
  Yield strength,
  Elongation at break,
  Impact strength, and
  Chemical resistance

For a crystallizable polymer, high molecular weight, narrow molecular weight distribution, low branching, and backbone linearity yield high crystallinity levels. Small amounts of nucleants such as:

- Pigments,
- Organic promoters,
- Catalyst residue,
- Fillers, and
- Reinforcing fibers,

enhance the rate of crystallization. Annealing and orientation also enhance crystallization while high shear processing and rapid cooling inhibit it.

Crystallization is a rate-dependent process, as shown in Table 2.4 [13,14]. The isothermal time to reach 50% of the ultimate crystallized fractional volume change is known as the *crystallization half-time*. The temperature-dependent semi-logarithmic half-time curves are characteristically cup-shaped, as seen for PET in Fig. 2.4 [15,16]. These curves are classically fit with the Avrami equation:

$$-\ln \phi = Kt^n \tag{2.4}$$

where ϕ is the volume fraction of uncrystallized material, given as:

$$\phi = 1 - \frac{\Delta\eta}{\Delta\eta_\infty} \tag{2.5}$$

Table 2.4 Isothermal Rates of Crystallization for Several Polymers at Tempertures 30°C or 54°F below Their Reported Melt Temperatures[1]

Polymer	Crystallization rate (μm/min)
Polyethylene	5000
Polyhexamethylene adipamide (PA 66 or nylon 66)	1200
Polyoxymethylene (POM or acetal)	400
Polycaprolactam (PA 6 or nylon 6)	150
Polychlorotrifluoroethylene (PCTFE)	30
Isotactic polypropylene (PP)	20
Polyethylene terephthalate (PET)	10
Isotactic polystyrene (iPS)	0.25
Polyvinyl chloride (PVC)	0.01

[1] Adapted from [13,14] with copyright permission

© 1996 Carl Hanser Verlag. All rights reserved.
No unauthorized disclosure or reproduction; licensed to purchaser only.

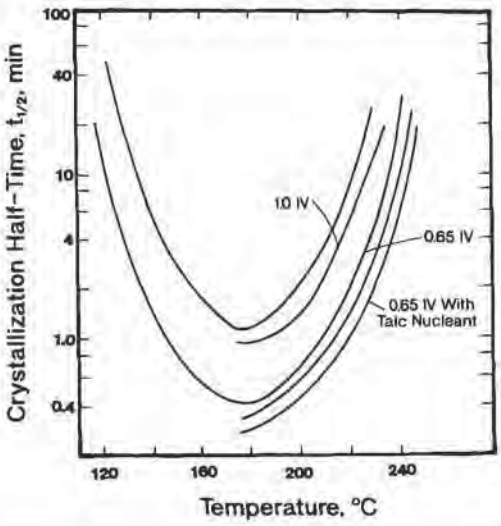

Figure 2.4. Crystallization half-time for various types of polyethylene terephthalate, PET [15,16]

where $\Delta\eta$ is the volumetric change determined by dilatometric methods. K and n are empirical coefficients. K is polymer specific and a strong function of temperature and possibly nucleant concentration, if any. The Avrami constant, n, is a measure of the nature of the crystallite formation. For moderate processing conditions, $n = 3$ for constant nucleation of spherical crystallites or sporadic plate-like growth [17]. As is apparent from Fig. 2.4, slow cooling enhances crystallization and quench cooling inhibits it. Reheating amorphous sheet of a crystalline polymer such as PET to temperatures where appreciable crystallization takes place leads to unwanted haze. It also leads to a method of fabricating crystalline structures from initially amorphous sheet, as described in detail in Chapter 9 [18]. Usually, thermoforming requires highly extensible sheet at relatively low stretching loads. Very few crystalline polymers can be vacuum thermoformed below their melt temperature. Polypropylene can be pressure thermoformed at or just below its melting temperature. The amount of pressure depends on the level of crystallinity and the size of and regularity of spherulites, as discussed in Chapter 9. Figure 2.5 shows a temperature-dependent modulus for polyisobutylene, a crystalline polymer [19].

X-ray patterns for polymers with crystalline levels less than about 30% are difficult to interpret. Amorphous polymers have no X-ray diffraction patterns, no melting point, and thus no latent heats of fusion. When an amorphous polymer is heated, the temperature range over which it changes from a rubbery solid to a flowable fluid can be as broad as 50 to 60°C or 80 to 125°F. Polystyrene and nearly all commercial PVCs are amorphous polymers. The temperature at which a polymer changes from a brittle, glass-like polymer to a rubbery one is the glass transition temperature, T_g. This is a second-order thermodynamic temperature where substantial chain segment mobility takes place along the backbone. Under stress, permanent

© 1996 Carl Hanser Verlag. All rights reserved.
No unauthorized disclosure or reproduction; licensed to purchaser only.

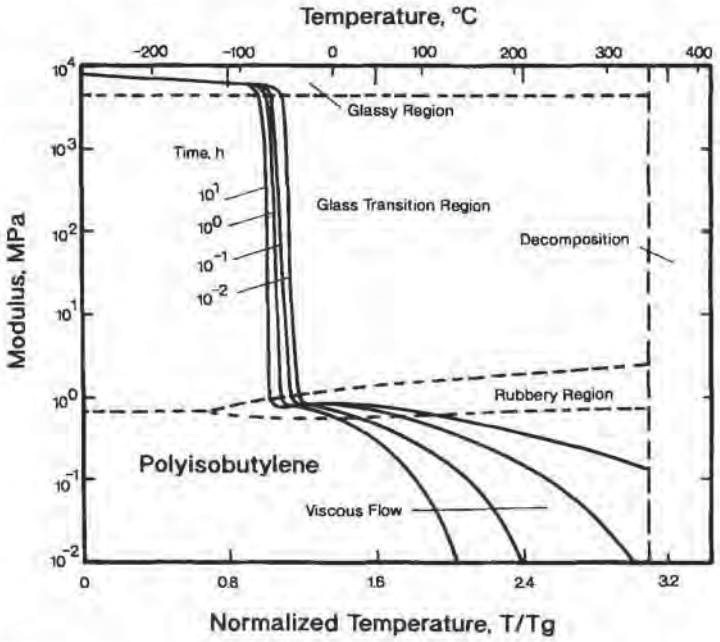

Figure 2.5 Temperature-dependent modulus of polyisobutylene, showing time-dependent glass transition region [19]

chain motion and intermolecular deformation are possible. Since polymers have broad distributions of molecular chain lengths, the glass transition temperature is in reality a temperature range of a few degrees (Fig. 2.6) [20]. Nevertheless a single value is usually given for a specific polymer. The glass transition temperature is the absolute lowest temperature at which the polymer can be formed. As processing temperatures increase above T_g, amorphous polymers become increasingly easier to process. Crystalline thermoplastics, cross-linked thermoplastics, and certain thermosetting polymers have glass transition temperatures, as well. For thermosets, chain mobility is restricted by the three-dimensional molecular network until the thermal degradation temperature is reached. In crystalline polymers, the morphological order in the crystalline regions restrict amorphous chain mobility until the melting temperature is reached (Fig. 2.7). For crystalline polymers, the ratio of melt temperature to glass transition temperature is 1.4 to 2.0 in °K. For polymer homologs, increasing molecular weight yields increasing crystallinity and melt temperature [21]. The glass transition temperature, T_g, is relatively unaffected by molecular weight. Figure 2.8 [22] shows a typical amorphous polymer phase diagram. Figure 2.9 [23] shows a similar phase diagram for a semicrystalline polymer. Glass transition temperatures for typical thermoformable polymers are given in Tables 2.2, 2.3 and 2.5.

© 1996 Carl Hanser Verlag. All rights reserved.
No unauthorized disclosure or reproduction; licensed to purchaser only.

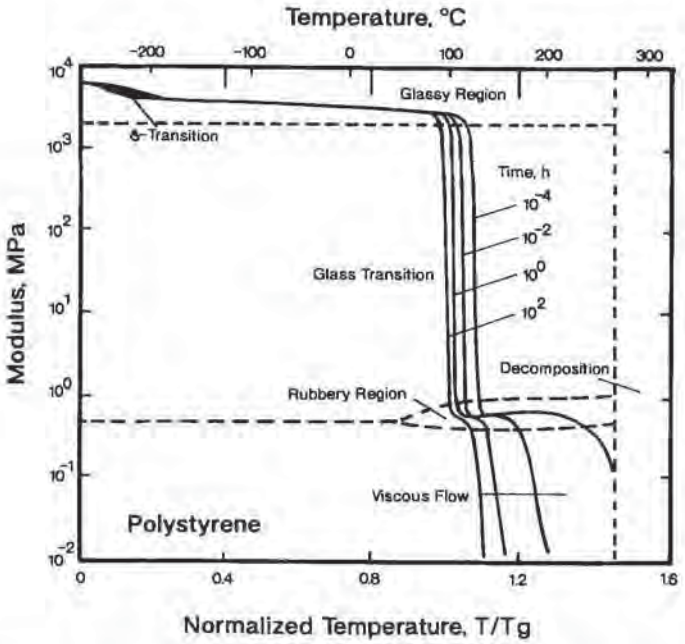

Figure 2.6 Temperature-dependent modulus of polystyrene, showing time-dependent glass transition region [20]

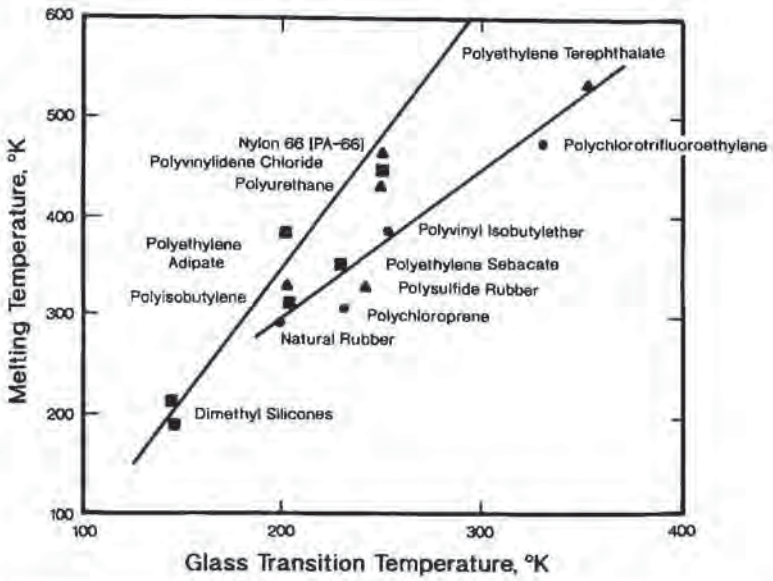

Figure 2.7 Relationship between glass transition temperature and melting temperature of several polymers [21]

© 1996 Carl Hanser Verlag. All rights reserved.
No unauthorized disclosure or reproduction; licensed to purchaser only.

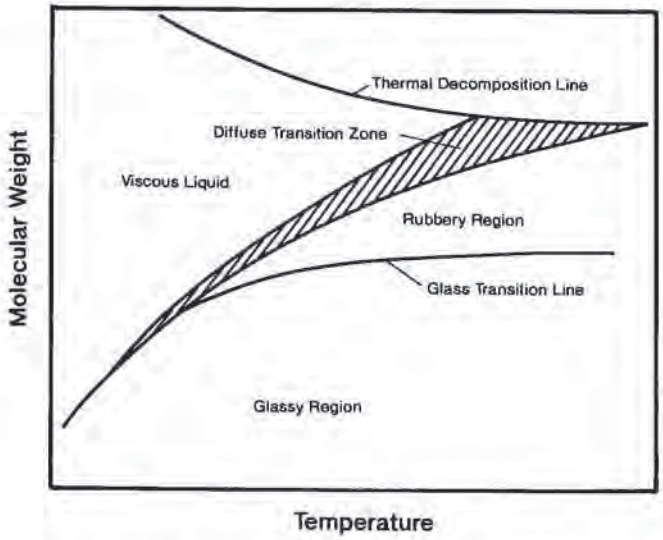

Figure 2.8 Amorphous polymer phase diagram [22]

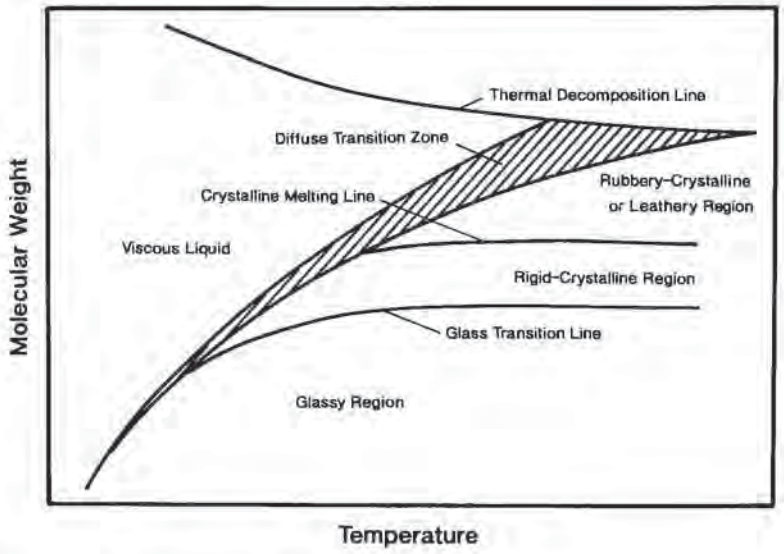

Figure 2.9 Crystalline polymer phase diagram [23]

© 1996 Carl Hanser Verlag. All rights reserved.
No unauthorized disclosure or reproduction; licensed to purchaser only.

Table 2.5 Characteristic Temperatures of Thermoformable Polymers

Polymer	Glass transition temperature		Melt temperature		Heat distortion temperature (0.46 N/mm²/66 psi)		Set and mold temperature		Lower forming temperature		Orienting temperature		Normal forming temperature		Upper forming temperature	
	(°C)	(°F)	(°C)	(°F)	(°C)	(°F)	(°C)	(°F)	(°C)	(°F)	(°C)	(°F)	(°C)	(°F)	(°C)	(°F)
Amorphous polymers																
Polystyrene	94	200	–	–	68–96	155–204	85	185	127	260	135	275	149	300	182	360
PMMA	100	212	–	–	74–113	165–235	85	185	149	300	163	325	177	350	193	380
PMMA/PVC alloy	105	221	–	–	81	177	79	175	143	290	154	310	171	340	182	360
ABS	88–120	190–248	–	–	77–113	170–235	82	180	127	260	137	280	146	295	182	360
Polycarbonate	150	300	–	–	138	280	132	270	168	335	177	350	191	375	204	400
Rigid PVC	77	170	–	–	57–82	135–180	66	150	104	220	118	245	138	280	154	310
Modified PPO	104–110	219–230	–	–	110	230	99	210	165	325	182	360	188	375	204	400
Polysulfone	190	374	–	–	181	358	163	325	191	375	213	415	246	475	302	575
Polyethersulfone (PES)	230	445	–	–	216	420	204	400	274	525	293	560	316	600	343	650
20% GR PES	225	437	–	–	216	420	210	410	279	535	293	560	316	600	357	675
Polyamide-imide	275	527	–	–	302	575	232	450	357	675	371	700	404	760	427	800
Crystalline polymers																
LOPE	–25	–13	115	239	40–44	104–112	66	150	116	240	129	265	132	270	168	335
EVA	–	–	107	225	62	114	77	170	127	260	138	280	146	295	182	360
HDPE	–110	–166	134	273	79–91	175–196	77	170	127	260	132	270	146	295	182	360
Cellulose acetate	70, 100	158, 212	230	445	52–93	125–200	71	160	127	260	141	285	154	310	182	360
Cellulose butyrate	120	248	140	284	54–108	130–227	79	175	127	260	138	280	146	295	182	360
Cellulose propionate	–	–	190	374	64–121	147–250	88	190	127	260	137	280	146	295	182	360
Polypropylene, homo-	5	41	168	334	107–121	225–250	88	190	132	270	138	280	154–163	310–325	166	330
Polypropylene, co-	–20	–4	150–175	302–347	85–104	185–220	88	190	143	290	177	350	185	365	193	380
40% GR PP	5	41	168	334	166	330	91	195	129	265	141	285	204	400	232	450
Polymethyl pentene	47	117	235	455	85	185	77	170	260	500	274	525	277	530	288	550
PVDC	0	32	160	320	68	155	66	150	163	325	177	350	182	360	199	390
Acrylonitrile	95	203	135	275	78	172	82	180	127	260	137	280	149	300	182	360
PET	70	158	255	490	49	120	77	170	121	250	138	280	149	300	166	330
PBT, neat	–80, 70	–112, 158	245	473	185	365	177	350	260	500	274	525	274	525	288	550
Nylon 6 (PA 6)	58	136	220	428	80	176	91	195	216	420	224	435	227	440	238	460
Nylon 66 (PA 66)	78	169	255	491	105	221	104	220	249	480	260	500	274	525	288	550
POM, copolymer	–55	–67	165	329	110–125	230–257	99	210	163	325	177	350	182	360	204	400
30% GR POM	–50	–58	166	331	163	325	104	220	163	325	177	350	182	360	204	400
PTFE	–53	–67	327	621	46	115	99	210	234	435	249	480	260	500	282	540
FEP	–55	–67	275	527	70	158	149	300	232	450	246	475	260	500	279	535
PEEK	100, 149	212, 300	334	633	140	284	160	320	399	750	413	775	418	785	427	800
Foams																
Polystyrene foam	70–85	158–185	–	–	55–65	131–149	50	122	88	190	96	205	104	220	113	235
Rigid PVC foam	70	158	–	–	65	149	66	150	110	230	124	255	143	290	171	340

© 1996 Carl Hanser Verlag. All rights reserved.
No unauthorized disclosure or reproduction; licensed to purchaser only.

Table 2.6 Biaxial Orientation Properties of Thermoformable Polymers[1]

Polymer	Orientation	Tensile strength		Elongation at break	Impact strength	
		(MPa)	(lb_f/ln^2)	(%)	(J/m)	(ft-lb/in)
Polystyrene	None	34.5–62	5000–9000	1–36	13.3–27	0.25–0.5
	Biaxial	48.3–83	7000–12,000	8–18	>160	>3
PMMA	None	51.7–70	7500–10,000	5–10	215	4
	Biaxial	55.2–75.8	8000–11,000	25–50	800	15
PP	None	31.4–41.4	4500–6000	100–600	530	10
	Blown	207	30,000	80	NA[2]	NA
	Tenter-frame	124–234	18,000–34,000	50–130	NA	NA
PET	None	48.3–70	7000–10,000	200–300	13.3–37	0.25–0.7
	Biaxial	207	30,000	100	NA	NA
HdPE	None	22.1–31.0	3200–4500	600–700	21.3–213	0.4–4.0
	Blown	34.5–35.9	5000–5200	450–500	NA	NA

[1] Adapted from [24–26]
[2] Not available

2.8 Molecular Orientation

In some polymers, sheets are biaxially oriented during the extrusion process to obtain improved properties in some polymers. Both crystalline and amorphous polymers can be oriented. For crystalline polymers, unique combinations of properties are achieved by carefully matching levels of mechanical stress to heating and cooling rates. The crystallites formed this way are formed from highly oriented molecules, yielding dramatic reductions in haze level, for example, and equally impressive increases in ultimate tensile strength, albeit at reduction in elongation at break. Thin-gage sheets of amorphous polymers such as PS and PMMA are biaxially oriented as well, to yield substantially increased ultimate elongation and ductility in the heated sheet and in the formed product. Some properties of oriented crystalline and amorphous polymers are given in Table 2.6 [24-26].

2.9 Chain Mobility and Polymer Stiffness

The intrinsic strength of a polymer depends on chain rigidity and ability of polymer-to-polymer intermolecular structure to withstand deformation or disentanglement under load. The ductility, hardness, resistance to impact and stiffness of a plastic product are related to the nature of the polymer molecular structure. Flexibility is a function of the degree of chain segment rotation about the -C-C-

© 1996 Carl Hanser Verlag. All rights reserved.
No unauthorized disclosure or reproduction; licensed to purchaser only.

Table 2.7 Effect of Steric Hindrance on Polyethylene Properties [27]

Effect	LDPE	HDPE
Branching: Chain ends per 1000 carbon atoms	25	2
Attainable crystallinity	~65%	~85%
Elastic modulus [MPa]	170	1380
Relative density [kg/m^3]	115	131
Crystalline melting point (°C)	115	131

backbone. If double bonds are included in the backbone, stiffness is increased. It is increased further if the occurrence of double bonds is regular, such as -C = C-C = C-. Aromaticity in a pendant group adds stiffness as with PS. Benzene ring inclusion in the backbone as with PC and PET further increases stiffness. If the backbone has only aromatic carbon-carbon bonds, the polymer becomes quite stiff, as with polycyclic diphenyls. Some of the stiffest polymers are the polyimides where backbone bonding occurs at four points on the aromatic ring rather than two. This forms a ladderlike or rodlike structure. Decreasing chain mobility implies increasing difficulty in thermoforming the polymer sheet.

The benzyl pendant group on PS stiffens the polymer chain, due to the difficulty in fitting the bulky pendant groups side by side along the backbone. This is called *steric hindrance*. Not all pendant groups cause stiffening, however. Long-chain branching on LDPE acts to separate main chains, increase free volume or the molecular-level voids in the solid. This reduces the bulk density of the polymer. The lowered density results in greater flexibility, lower tensile strength, lower T_g and T_m, and lower levels of crystallinity (Table 2.7) [27]. The methylene group on every other carbon of isotactic polypropylene represents the limiting case of short side-chain branching. The steric hindrance forces the polymer chain into a helix, stiffening the backbone and at the same time creating even greater free volume. As a result, PP has very low room temperature density and relatively high T_g and T_m.

Although not pendant groups, per se, halogen atoms such as chlorine on PVC and the carboxyl group on PMMA are much larger than, say, a hydrogen atom. These groups cause substantial steric hindrance and prevent or at least inhibit crystallization of the polymers. More important is the highly electronegative state of halogen atoms, such as the chlorine on PVC and the fluorine on PTFE or FEP. In very regular polymers, these tend to repel one another, thus stiffening the backbone into a rodlike configuration. Most halogen-substituted polymers without plasticizers are quite difficult to process into sheet. Polymers that have very high hydrogen bonding levels, such as PMMA, certain celluloses and nylons, also have increased stiffness. Secondary hydrogen bonds occur between main chain groups such as amines, -H-N···H-, and hydroxyls, -H-O···H-. In effect, these increase the effective diameter of the chain segment and reduce its mobility.

© 1996 Carl Hanser Verlag. All rights reserved.
No unauthorized disclosure or reproduction; licensed to purchaser only.

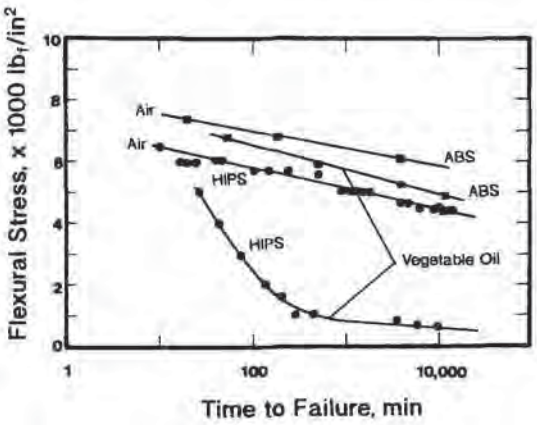

Figure 2.10 Effect of environment on flexural creep rupture of HIPS and ABS [28]

2.10 Stress-Crack Resistance

Environmental stress-crack resistance or ESCR is the ability of a strained polymer to withstand aggressive media. Many thermoformed products must withstand environments such as detergents, oils, greases and mild solvents. Solvent molecules tend to be quite small and so readily diffuse into the polymer, moved between adjacent polymer chains and act to separate them. When the polymer-solvent attraction forces exceed the polymer-polymer intermolecular attraction forces, the polymer chains are separated by the solvent. The polymer then dissolves, swells or crazes. Weak solvents act on the polymer chain only when it is strained. Unfortunately, most product stress crack failures occur because the strain polymer failed in a weak solvent over a long period of time (Fig. 2.10) [28]. Classic examples are rubber-impact-modified polystyrene shower stalls that craze when in contact with soap solutions for long times and refrigerator door and cabinet liners that craze or crack when in contact with certain foaming agents used in polyurethane insulation. Surface deglossing and microcrazing on PMMA and PVC are caused by exposure to very mildly aggressive environments. Migration and loss of small molecule plasticizers, erosion and acid rain also lead to microcrazing. UV-embrittlement is probably due to surface crosslinking.

2.11 Gas Permeation

Gas transmission through polymers depends on the extent of the free volume in the formed part on the relative order of magnitude of polymer-polymer and polymer-gas

© 1996 Carl Hanser Verlag. All rights reserved.
No unauthorized disclosure or reproduction; licensed to purchaser only.

molecule attraction forces. Gases that are chemically similar to the polymer repeat unit tend to migrate readily. Cellulosics transmit water but polyolefins do not. Olefins tend to transmit fluorocarbon gases but styrenics do not. The permeation of a gas through a given plastic is the product of its solubility in the plastic and its diffusivity through the plastic. Solubility is directly related to polymer-solvent affinity [29]. In semicrystalline polymers, the small molecule diffusion rate through amorphous or unordered polymer regions is many times higher than that through highly order crystalline regions. As expected, an increasing degree of crystallinity leads to a decrease in permeability of all small molecules. Orienting any polymer substantially increases the small molecule diffusion path. Orienting a crystalline polymer results in substantially reduced gas permeation. Polymers such as PET and nylon become more efficient gas barriers with increased orientation.

2.12 Copolymerization

Polymers made from a single set of monomers are called *homopolymers*. Frequently, specific end uses or processing conditions dictate properties that are unattainable by homopolymers. A common method of altering polymer properties is by co-reacting small amounts of reactive monomers with the primary polymer molecules. These copolymers can be added in the following fashions, by controlling the nature of the polymerization:

- Randomly along the polymer backbone, as random copolymerization. This results in:
  - Broadening of melt and glass transition temperatures,
  - Reduced stiffness or increased flexibility,
  - Reduction in melt viscosity and crystallinity, and
  - An increase in high temperature rubbery sheet strength and melt strength.
  - Classic examples include ethylene into polypropylene to reduce T_g and increase thermoformability and sodium methacrylate into polyethylene to produce an ionomeric polymer with reduced crystallinity, improved transparency and toughness.
- Fit into the polymer backbone as long-chain homopolymer segments, as block copolymerization. This results in main chain flexibility in otherwise brittle polymers. Classic examples include butadiene in polystyrene. The butadiene segments are not cosoluble with PS and so form a separate but chemically linked phase.
- As pendant groups, as branched or graft copolymerization. ABS or acrylonitrile-butadiene-styrene is a terpolymer with the acrylonitrile polymer grafted to the block butadiene-styrene copolymer backbone. The acrylonitrile adds improved solvent resistance and high forming temperature toughness to impact-modified polystyrene.

© 1996 Carl Hanser Verlag. All rights reserved.
No unauthorized disclosure or reproduction; licensed to purchaser only.

2.13 Blends

If two polymers are cosoluble, such as PS and polyphenylene oxide or PPO, or PVC and ABS, or polyvinyl acetate and PMMA, intensive shear melt mixing can yield a true thermodynamic single phase polymer mixture. The resulting polymer properties are nearly identical to those that are obtained through copolymerization. Note that physical blends of homologs such as polyethylenes or vinyls should yield true single phase blends, but may not. Insoluble blends yield macroscopic two-phase systems that might behave as if they are copolymers, as is the case of melt coblending butadiene rubber and polystyrene. However, many insoluble blends yield useless polymers.

2.14 Adducts

Nearly all thermoplastics are mixtures of polymers and adducts or nonpolymers added to modify the general characteristics of the polymers. Table 2.8 [29,30] is a short list of some adducts found in thermoplastics.

Plasticizers

Plasticizers are small molecules of a chemical nature similar to the polymer in which they are dissolved. Their role is to separate the main chains, thus reducing polymer-polymer intermolecular forces and allowing the polymer chains to move past one another during shearing. Plasticized polymers usually exhibit the following characteristics:

- Lower processing viscosities,
- Lower stiffness,

Table 2.8 Typical Nonpolymers Added to Polymers [29]

Antioxidants	Odor suppressants
Antistatic agents	Plasticizers
Bulk fillers	Processing aids
Colorants and pigments	Emulsifiers
Coupling agents	Internal lubricants
Crosslinking agents	Mold release agents
Fibrous reinforcements	Viscosity depressants
Flame retardants	External lubricants
Foaming agents	Anti-blocking agents
Heat stabilizers	Ultraviolet stabilizers

© 1996 Carl Hanser Verlag. All rights reserved.
No unauthorized disclosure or reproduction; licensed to purchaser only.

- Lower glass transition temperatures,
- Lower melt temperature,
- Lower continuous use temperature,
- Greater flexibility,
- Higher toughness,
- Greater tear strength, and
- Higher elongation at break.

These effects are controlled to a great degree by the thermodynamic compatibility of the polymer and plasticizer, and the plasticizer glass transition temperature. The glass transition temperature is also broadened by the plasticizer, with the greatest broadening occurring when the plasticizer is a poor solvent for the polymer. PVC is the most important polymer thermoformed as a plasticized sheet. PVC is nearly intractable in an unplasticized state. The effect of dioctyl phthalate (DOP) on the glass transition temperature of PVC is seen in Fig. 2.11 [31]. At 40% (wt) DOP, the glass transition temperature is lowered from 82°C or 180°F to −60°C or −80°F. The glass transition region is increased from about 10°C or 18°F to 30°C or 50°F. In order to ensure long-term property retention, plasticizers must have very low vapor pressure at room temperature and must be non-migrating.

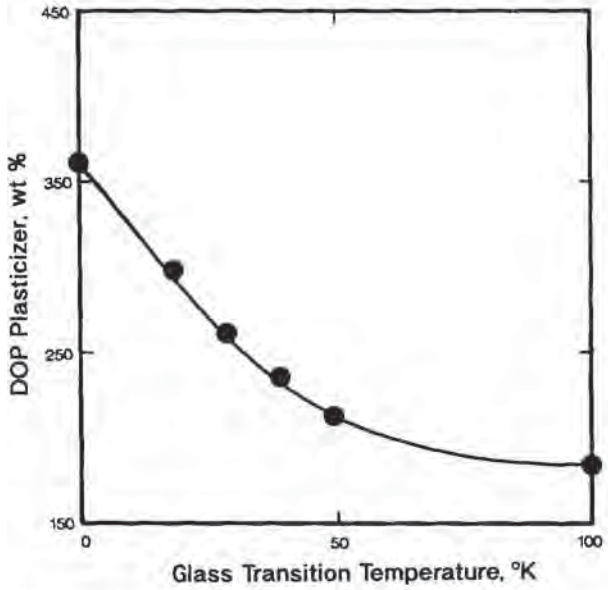

Figure 2.11 Effect of dioctyl phthalate [DOP] plasticizer concentration on glass transition temperature of polyvinyl chloride, PVC [31]

© 1996 Carl Hanser Verlag. All rights reserved.
No unauthorized disclosure or reproduction; licensed to purchaser only.

Other Additives

Plasticizers are one very specific category of additives. Many chemicals are added to polymers in order to change specific undesirable characteristics [3]. Surfactants and lubricants are aids used to improve processing quality and extruder production rate or throughput. Antioxidants are added to minimize polymer yellowing during processing and reprocessing. Tints are dyes added to change transparent plastic color from nonwhite to perceived "water-white". Organic dyes color transparent plastics but do not appreciably affect their long-wavelength radiant energy absorption spectra [32]. Organic and inorganic pigments color opaque plastics. The dosage level is usually less than 2% (wt). Titanium dioxide, TiO_2, is an opacifier in low dosage, as is carbon black. Carbon black is also used extensively as an ultraviolet light absorber, particularly in

Table 2.9 Common Fillers for Thermoformable Thermoplastics [33]

Silica products
- Minerals
  - Sand
  - Quartz
  - Novaculite
  - Tripoli
  - Diatomaceous earth
  - Dolomite
- Synthetic amorphous silica
  - Wet process silica
  - Fumed colloidal silica
  - Silica aerogel

Silicates
- Minerals
  - Kaolin or china clay
  - Mica
- Nepheline silicate
  - Talc
  - Wollastonite
  - Asbestos
- Synthetic products
  - Calcium silicate
  - Aluminum silicate

Glass
- Glass flakes
- Hollow glass spheres
- Cellular glass nodules
- Glass granules

Calcium carbonate
- Chalk
- Limestone
- Precipitated calcium carbonate

Metallic oxides
- Zinc oxide
- Alumina
- Magnesia
- Titania
- Beryllium oxide

Other inorganic compounds
- Barium sulfate
- Silicon carbide
- Tungsten carbide
- Molybdenum disulfide
- Barium ferrite

Metal powders
- Aluminum
- Bronze
- Lead
- Stainless steel
- Zinc

Carbon
- Carbon black
  - Channel black
  - Furnace black
- Ground petroleum coke
- Pyrolyzed products
- Exfoliated graphite

Cellulosic fillers
- Wood flour
- Shell flour
  - Peanut
  - Pecan
  - Walnut

Comminuted polymers

© 1996 Carl Hanser Verlag. All rights reserved.
No unauthorized disclosure or reproduction; licensed to purchaser only.

vinyls and polyolefins. Chemical and physical blowing agents are added to the polymer prior to extrusion to produce foamed sheet [6]. Chemical blowing agents are very fine powders of ultrapure thermodynamically unstable chemicals such as azodicarbonamide, $H_2N\text{-}CO\text{-}N = N\text{-}CO\text{-}NH_2$. Azodicarbonamide, azobisformamide or AZ decomposes to produce nitrogen. Sodium bicarbonate, $NaHCO_3$, with citric acid buffer, decomposes to produce CO_2 and H_2O vapor. It is used extensively to produce PS foam sheet. Frequently, hydrocarbons such as pentane and butane and halogenated hydrocarbons such as R123 and R142b are added to PS and polyethylene to produce low-density closed cell foams for shock mitigation and insulation applications.

Fillers and Reinforcing Fibers

Although fillers reduce overall resin costs slightly, they are usually not added solely for this reason. Common inorganic fillers such as talc, calcium carbonate and clay or kaolin increase sheet stiffness and processing temperature by interfering with polymer chain segment mobility. Table 2.9 [33] lists some common fillers used in thermoformable thermoplastics. Some increase in stiffness is beneficial. For example, 20% (wt) talc in PP broadens its thermoforming processing window enough to allow forming on conventional roll-fed equipment. Fillers also restrict bulk chain straightening and flexing under load. These restrictions reduce ultimate elongation, tensile strength, impact strength and fatigue strength of the neat polymer. Milled glass fibers, to 30% (wt) provide exceptional strength improvement in rubber-modified styrenics and mPPO, but processing is restricted to pressure forming. Even further improvements in polymer stiffness is obtained by adding reinforcing elements such as those listed in Table 2.10 [34]. Unfortunately, elements such as glass fibers, mica, or

Table 2.10 Typical Fibrous Elements in Polymers [34]

Cellulose fibers	*Fibrous glass*
α-cellulose	Filaments
Pulp preforms	Chopped strand
Cotton flock	Reinforcing mat
Jute	*Glass yarn*
Sisal	Glass ribbon
Rayon	*Whiskers*
Synthetic fibers	Boron
Polyamide, nylon, PA	Titanium dioxide
Polyester, PET, dacron™	*Metallic fibers*
Polyacrylonitrile, PAN, dynel™, orlon™	Aluminum
Polyvinyl alcohol, PVOH	Stainless steel
Other fibers	Copper
Carbon fibers	
Mineral fibers	
Asbestos	
Wollastonite	

© 1996 Carl Hanser Verlag. All rights reserved.
No unauthorized disclosure or reproduction; licensed to purchaser only.

graphite fibers so stiffen the polymer that matched-die forming at pressures near compression molding pressures and temperatures above the polymer melt temperature are required. Nevertheless, commercial parts are thermoformed from glass fiber-reinforced PP, PET and nylon and graphite fiber-reinforced polyimide. More details are given in Chapter 9.

2.15 Laminates

Certain end use applications need mechanical or barrier properties that no single polymer can provide. Polymers are therefore laminated, coated or coextruded into multilayer sheet. Examples include:

- UV and chemical barrier of PMMA on ABS,
- Fire retardant barrier of PVC on PMMA,
- Solid impact PS "cap sheets" on PS foam for stiffness and cut resistance,
- Thermoformable PET-EVOH-PET thin-gage sheet used to produce preforms for high barrier stretch blow-molded containers, and
- PVDC on PS for gas barrier insulating containers.

Other examples are described in Chapter 9. The control of multilayer thickness is of great concern to the sheet extruder. Mismatched viscosities lead to interlayer thickness variation. Temperatures must be matched to ensure good interlayer bonding. Plasticizers and additives must be nonmigratory and must be carefully monitored to prevent "blooming" at interfaces. Biaxial orientation during thermoforming will reveal poor interlayer adhesion. Orientation must be carefully monitored to minimize formation of microvoids in inherently weak inner layers. Multilayer structures must be carefully heated to prevent innerlayer interface overheating and delamination from mismatched thermal expansion coefficients.

2.16 Stress-Strain Behavior of Plastics

Thermoforming is a deformation process on a polymer in its rubbery solid state above T_g. For crystalline polymers, the deformation process occurs near the crystalline melting temperature, T_m. Technically, a nearly uniform force is applied to a two-dimensional membrane to biaxially stretch it. The amount of force required and the extent of stretching are directly related to the stress-strain behavior of the polymer at its process condition. Below, T_g, all polymers are brittle. The stress-strain curve is quite steep and linear and quite steep until fracture at a very low strain level (Fig. 2.12) [35]. In general, the tensile modulus values, or the slopes of the stress-strain curves, of nearly all unfilled or neat amorphous polymers below T_g are about 0.345 GPa or 500,000 lb_f/in^2 [36]. Within 20°C or 40°F above T_g, tensile

© 1996 Carl Hanser Verlag. All rights reserved.
No unauthorized disclosure or reproduction; licensed to purchaser only.

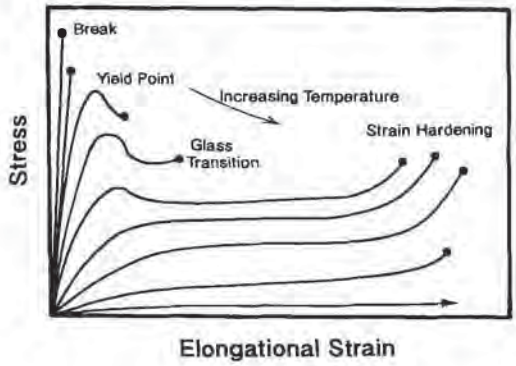

Figure 2.12 Temperature-dependent stress-strain schematic for an amorphous polymer

modulus values drop 3 to 4 decades, to 35 to 350 MPa or 50 to 500 lb_f/in^2. Ultimate tensile strengths also drop rapidly about the same orders of magnitude.

As the sheet temperature increases above T_g, all polymers become increasingly ductile (Fig. 2.12). Some polymers exhibit yielding at modest strain levels. The applied stress is then sustained over ever-increasing strain levels. There is strong indication that the minimum vacuum forming temperature is where the abrupt yield point vanishes. In crystalline polymers, the rubbery region is compromised to a great degree by the crystalline structure, as shown in schematic in Fig. 2.13 [37]. At high

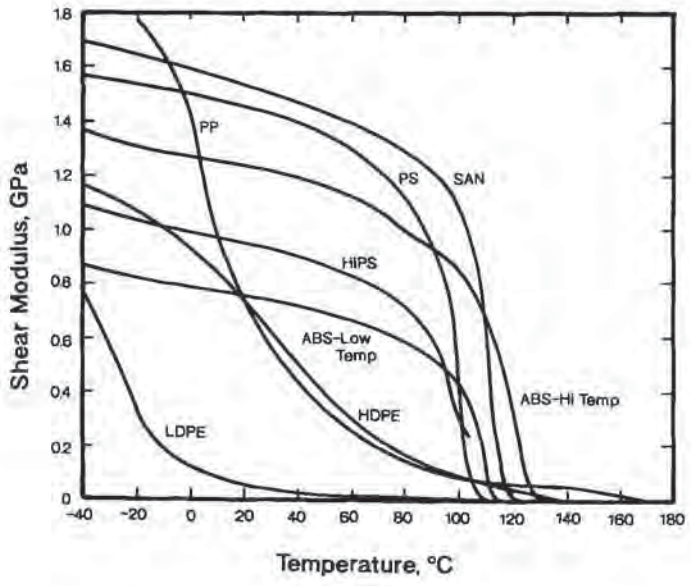

Figure 2.13 Temperature-dependent shear modulus for several thermoplastics [37]

© 1996 Carl Hanser Verlag. All rights reserved.
No unauthorized disclosure or reproduction; licensed to purchaser only.

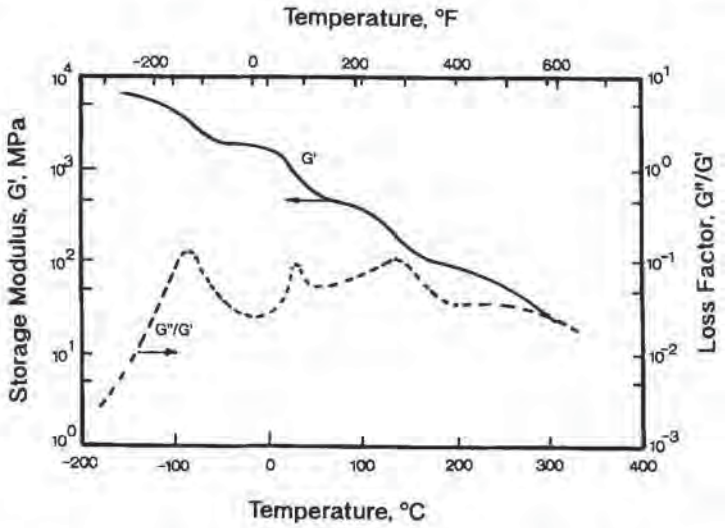

Figure 2.14 Temperature-dependent elastic modulus, G', and mechanical loss factor, G"/G' of polytetrafluoroethylene, PTFE [38]

levels of crystallinity, as with UHMWPE and PTFE, the modulus of the polymer above the glass transition temperature is only slightly less than that below the glass transition temperature (Fig. 2.14) [38]. An increasing level of crystallinity then has the effect of compressing the temperature effect on the stress-strain curves (Fig. 2.15). Further, for homologous crystalline polymer species, yield strength and ultimate tensile strength at a given temperature increase with increasing crystallinity (Fig. 2.16) [39].

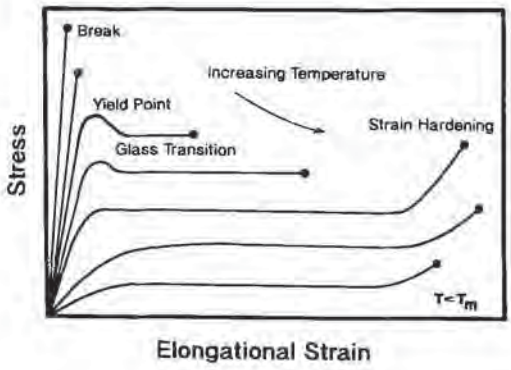

Figure 2.15 Temperature-dependent stress-strain schematic for a crystalline polymer

© 1996 Carl Hanser Verlag. All rights reserved.
No unauthorized disclosure or reproduction; licensed to purchaser only.

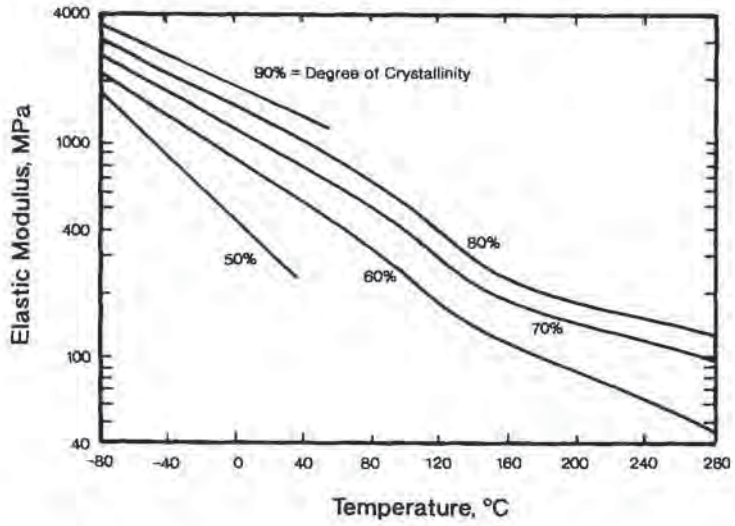

Figure 2.16 Effect of crystallinity level on temperature-dependent modulus of polytetrafluoroethylene, PTFE [39]

It is apparent that there is a direct relationship between the stress-strain behavior of a given polymer and the process of thermoforming it from sheet form to shaped product. As expected, the normal forming temperature of any polymer is closely related to T_g for amorphous polymers and T_m for crystalline polymers. Forming temperature ranges for many polymers are given in Table 2.5 [40]. The lower forming temperature represents the lowest temperature the polymer can be shaped without cracking or splitting or without using heroic forces. Typically, for amorphous materials, the lower forming temperature is about 20 to 30°C or 40 to 55°F above T_g and the normal forming temperature is about 70 to 100°C or 125 to 180°F above T_g. The "set temperature" is the temperature at which a part can be removed from the mold without significant distortion. The set temperature value is about equal to the polymer heat distortion temperature at 0.455 MPa or 66 lb_f/in^2 or about 10 to 20°C or 20 to 40°F below the polymer glass transition temperature, T_g. The orienting temperature is the temperature at which the polymer can be uniaxially stretched 375%. The upper forming temperature represents the temperature above which the polymer sags excessively, discolors, bubbles or smokes excessively. The upper forming temperature for a given polymer is usually about equal to the lowest injection temperature for that polymer. The crystalline polymer forming temperature range is usually quite narrow and the recommended forming temperature range is often within a few degrees of the polymer melt temperature. Certain crystalline polymers such as nylon (PA) and homopolymer polypropylene (PP) retain high degrees of order and therefore great strength up to abrupt melting points, then have very low melt viscosities and melt elasticities. As a result, these polymers have normal processing windows as narrow as 2 to 5°C or 5 to 10°F. It must be understood,

© 1996 Carl Hanser Verlag. All rights reserved.
No unauthorized disclosure or reproduction; licensed to purchaser only.

therefore, that the temperature ranges given in Table 2.5 represent extreme or ideal conditions. Practical forming ranges are usually much narrower. A more thorough analysis of the interaction of temperature-dependent stress-strain behavior, viscoelasticity, applied stress and extent of drawing is given in Chapter 4.

2.17 Thermal Properties

Heat capacity or specific heat and thermal conductivity are two important polymer physical properties used extensively in thermoforming.

Heat Capacity

Heat capacity at constant pressure, c_p, is a thermodynamic property, defined as the isobaric change in polymer enthalpy with temperature:

$$c_p = \left(\frac{\partial H}{\partial T}\right)_p \tag{2.6}$$

Heat capacity values for many polymers are obtained from enthalpic tables [41] or from graphs such as Fig. 2.17 [42,43]. The enthalpic curves for amorphous polymers are usually quite linear with temperature. Heat capacity values or the slopes of the

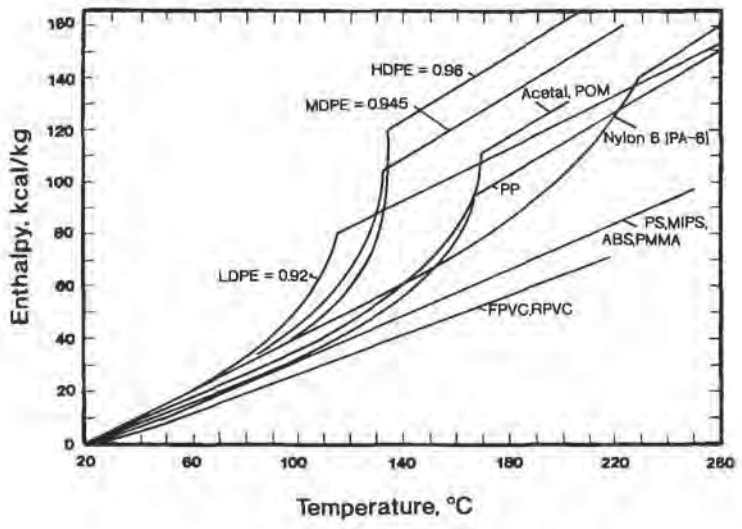

Figure 2.17 Enthalpies of several thermoplastics [42,43]

© 1996 Carl Hanser Verlag. All rights reserved.
No unauthorized disclosure or reproduction; licensed to purchaser only.

Table 2.11 Heat Capacities of Certain Thermoplastics in cal/g °C or Btu/lb °F

Polymer	Morphology[1]	C_p from enthalpy ($T_g < T < T_m$)	C_p from graph (50°C < T < 90°C)	C_p from DSC experiments	$\partial C_p/\partial T$ (per 100°C)
PS	A	0.68	0.45	0.50 @ 225°C	0.043
ABS	A	–	0.45	0.54 @ 225°C	0.074
PMMA	A	0.56	–	0.56 @ 225°C	0.048
PC	A	–	–	0.50 @ 225°C	0.033
PVC	A	0.65	0.39	–	–
PP	C	0.78	0.47	0.96 @ 125°C	0.132
HDPE	C	0.58	0.61	0.88 @ 80°C	0.597
EP-copoly	C	0.80	–	–	–
PTFE	C	0.25	–	–	–
PA-6	C	–	0.50	0.87 @ 180°C	0.502
PA-66	C	0.74	–	–	–
PET	C	–	0.45	–	0.09
mPPO	A	–	≈0.50	–	–

[1] A = commercially amorphous polymer, C = Commercially crystalline polymer

enthalpic cures are therefore only slightly dependent on temperature above the glass transition temperature, T_g. On the other hand, crystalline polymer enthalpic curves usually show dramatic changes near the melt temperatures of the polymer and exhibit discontinuities at the melt temperatures. As a result, it is difficult to give specific values for heat capacity of crystalline polymers. This is demonstrated in Table 2.11. Very accurate techniques for predicting heat capacities of simple organic molecules have been extended to polymers by assuming that:

- Energy is transmitted by translation of molecules or molecular segments,
- Each segment acts as a liquid harmonic oscillator, and
- The polymer is characterized as a semicrystalline solid [44].

The total molecular energy is the sum of its components:

- Translational,
- External rotational,
- Internal rotational,
- Vibrational, and
- Electronic.

From established tables of molecular energy contributions for each of the segmental groups of the polymer:

- Repeat units,
- End groups,
- Comonomeric elements,
- Pendant groups, and
- The like.

© 1996 Carl Hanser Verlag. All rights reserved.
No unauthorized disclosure or reproduction; licensed to purchaser only.

Relatively accurate but tedious calculations yield reasonable predictions of polymer heat capacity. Experimentally, the entire temperature-dependent heat capacity curve for any polymer can be obtained in a few minutes with less than a gram of polymer using standard differential scanning calorimetry, DSC. Basically a known weight of polymer is heated at a constant rate and its time-dependent temperature compared with a standard of known heat capacity. Characteristically within normal thermoforming heating ranges, neat amorphous polymers have heat capacity values of about 0.5 cal/g °C or 0.5 Btu/lb °F. Crystalline polymers have average values of about 0.9 cal/g °C or 0.9 Btu/lb °F. More details and examples are found in Chapter 3 on heating the sheet.

Thermal Conductivity

Energy transmission through polymer solids and quiescent liquids is by molecular interaction rather than the electron transfer characteristic of metals. Thus thermal conduction, a measure of the efficiency of energy transfer, is governed by the same energy elements that contribute to heat capacity. Theoretical predictions are based on a linear relationship between thermal conductivity, heat capacity and liquid sonic velocity. The accuracy of prediction is excellent for simple organic molecules. For polymers, processing effects on intermolecular free volume and molecular order in partially crystalline polymers cause the calculated results to deviate substantially from carefully measured experimental values. Further, energy tends to be preferentially transmitted along the molecule backbone rather than between molecular chains. Thus, the nature of the crystalline order and the type of pendant groups influences the values. Thermal conductivity is one of the most difficult transport properties to measure [45]. As a result, very few accurate values of thermal conductivity are available for polymers. Fortunately, thermal conductivity is not strongly temperature-dependent and so evaluation at one temperature is probably sufficient for use at other temperatures. And homologous series of polymers, such as polyolefins, styrenics and vinyls, tend to have similar values, Table 2.12. Typically, thermal conductivity values for amorphous polymer such as PS, PMMA and PVC tend to be in the range of 3 to 5×10^{-4} cal/g cm °C or 0.07 to 0.12 Btu/ft h °F. Owing to the higher degree of order for crystalline polymers, values tend to be about twice those of amorphous values. The exceptions are low-crystallinity celluloses and PP, where the effect of crystalline order is obviated by the high free volume caused by steric hindrance. Typically, metals have thermal conductivity values that are hundreds of times greater than those for polymers. Additional information on thermal conductivity is found in Chapter 3.

Thermal Diffusivity

Thermal conductivity is a measure of the *extent* of energy transmission through the solid polymer. Thermal diffusivity is a measure of the *rate* at which energy is transferred:

© 1996 Carl Hanser Verlag. All rights reserved.
No unauthorized disclosure or reproduction; licensed to purchaser only.

Table 2.12 Thermal Properties of Thermoformable Polymers and Certain Mold Materials at 25°C

Polymer	Density		Thermal conductivity		Heat capacity		Thermal diffusivity		Thermal expansion coefficient	
	(kg/m^3)	(lb/ft^3)	(cal/s cm °C) $\times 10^{-4}$	(Btu/ft h °F)	(cal/g °C)	(Btu/lb °F)	(cm^2/s) $\times 10^{-4}$	(ft^2/h) $\times 10^{-4}$	($°C^{-1}$) $\times 10^{-6}$	($°F^{-1}$) $\times 10^{-6}$
Amorphous polymers										
Polystyrene	1050	65.5	4.3	0.105	0.54	0.54	7.66	29.7	70	39
PMMA	1200	74.9	4.3	0.105	0.615	0.615	5.9	22.8	70	39
PMMA/PVC alloy	1300	81.1	3.3	0.080	0.6	0.6	4.2	16.4	79–142	44–79
ABS	1050	65.5	2–3	0.048–0.073	0.4	0.4	4.8–7.1	18.6–27.5	60–130	33–72
Polycarbonate	1200	74.9	5.0	0.121	0.49	0.49	8.5	33.0	60–70	33–39
Rigid PVC	1350	84.2	3.45–4.1	0.083–0.100	0.365	0.365	7–8.4	27.1–32.5	70–80	39–45
Modified PPO	1070	66.8	5.5	0.133	0.585	0.585	8.8	34.0	60	33
Polysulfone	1240	77.4	6.74	0.163	0.54	0.54	10.1	39.0	54	32
Polyethersulfone (PES)	1370	85.5	4.3	0.105	0.46	0.46	6.9	26.7	55	31
20% GR PES	1520	94.8	7.8	0.190	0.67	0.67	7.7	29.9	23–32	13–18
Polyamide-imide	1400	87.4	14.4	0.348	0.565	0.565	18.2	70.5	36	20
Crystalline polymers										
LDPE	920	57.4	7.57–9.6	0.183–0.233	0.88–1.05	0.88–1.05	7.85–11.9	30.4–46.1	250	140
EVA	940	58.7	8.27	0.200	0.95	0.95	9.26	35.9	160–200	90–110
HDPE	960	59.9	9.0–12.1	0.217–0.292	0.88–1.15	0.88–1.15	8.1–14.3	31.5-55.4	200	110
Cellulose acetate	1300	81.1	5.2	0.125	0.67	0.67	5.9	23.0	120	67
Cellulose butyrate	1180	73.6	5.0	0.121	0.67	0.67	6.33	24.5	120	67
Cellulose propionate	1210	75.5	5.0	0.121	0.71	0.71	5.8	22.6	110–130	61–72
Poypropylene, homo-	900	56.2	4.1–4.2	0.100–0.125	0.83	0.83	5.5–6.92	21.4–26.8	150	83
Polypropylene, co-	910	56.8	5.0	0.121	0.81	0.81	6.8	26.3	120	67
40% GR PP	1220	76.1	8.4–8.8	0.203–0.213	0.77	0.77	8.9–9.3	34.6–36.2	27–32	15–18
Polymethyl pentene	830	51.8	4.1	0.100	0.91	0.91	5.5	21.2	117	65
PVDC	1670	104.2	3.0	0.073	0.45	0.45	4.0	15.6	190	106
Acrylonitrile	1150	71.8	6.2	0.150	0.6	0.6	9.0	34.8	66	37
PET	1370	85.5	5.7	0.138	0.44	0.44	9.5	36.8	70	39
PBT, neat	1310	81.7	5.0	0.121	0.54	0.54	7.1	27.4	60	33

(Continued)

© 1996 Carl Hanser Verlag. All rights reserved.
No unauthorized disclosure or reproduction; licensed to purchaser only.

Table 2.12 (Continued)

Polymer	Density		Thermal conductivity		Heat capacity		Thermal diffusivity		Thermal expansion coefficient	
	(kg/m^3)	(lb/ft^3)	(cal/s cm °C) $\times 10^{-4}$	(Btu/ft h °F)	(cal/g °C)	(Btu/lb °F)	(cm^2/s) $\times 10^{-4}$	(ft^2/h) $\times 10^{-4}$	($°C^{-1}$) $\times 10^{-6}$	($°F^{-1}$) $\times 10^{-6}$
Nylon 6 (PA 6)	1130	70.5	6.9	0.167	0.71	0.71	8.6	33.3	80	44
Nylon 66 (PA 66)	1140	71.1	5.5	0.133	0.71	0.71	6.8	26.3	80	44
POM, copolymer	1415	88.3	5.9–7.2	0.142–0.175	0.61	0.61	6.8–8.4	26.4–32.5	90–110	50–61
30% CR POM	1530	95.5	10.1	0.244	0.615	0.615	10.7	41.5	40–50	22–28
PTFE	2170	135.4	5.9	0.142	0.42	0.42	8.4	25.0	100	56
FEP	2200	137.3	6.0	0.145	0.465	0.465	5.86	22.7	80	45
PEEK	1320	82.4	5.9	0.142	0.565	0.565	7.9	30.5	47	23
Foams										
Polystyrene foam	64	4.0	0.57–0.69	0.0139–0.0167	0.5	0.5	17.9–21.5	69.5–83.5	150–200	83–111
Rigid PVC foam	64	4.0	0.57–0.69	0.0139–0.0167	0.4	0.4	22.4-26.9	86.9–104.4	140–180	78–100
Mold materials										
Alumina	2680	167.2	3000	72.5	0.23	0.23	4865	18,850	19	11
Copper/bronze	8800	549	4500.	109	0.09	0.09	5690	22,000	18	10
Nickel	8900	555	2200	53.2	0.112	0.112	2210	8560	13	7.2
Steel	7900	493	880	21.3	0.11	0.11	1010	3930	11	6.1
Maple	450	28.1	3.0	0.073	0.25	0.25	26.8	104	60	33
Plaster	900–1100	56–69	7.2	0.174	0.26	0.26	25–31	97–120	10	5.6
Al-epoxy	1700	106	20–40	0.484–0.967	0.3	0.3	39–78	152–304	45	25
Zinc alloy	6700	418	2500	60.4	0.10	0.10	3730	14,450	27	15
Syntactic foam—plugs	560	35	2.9	0.07	0.50	0.5	10	40	31	17

© 1996 Carl Hanser Verlag. All rights reserved.
No unauthorized disclosure or reproduction; licensed to purchaser only.

$$\alpha = \frac{k}{\rho c_p}$$

$$\frac{cm^2}{s} = \frac{cal/g\ cm\ s\ °C}{(g/cm^3)(cal/g\ °C)} \qquad (2.7)$$

$$\frac{ft^2}{h} = \frac{Btu/ft\ h\ °F}{(lb/ft^3)(Btu/lb\ °F)}$$

This combination of physical properties arises naturally from considerations of transient heat conduction, as detailed in Chapter 3 on sheet heating and Chapter 5 on cooling. Values for all polymers are typically 5 to 10×10^{-4} cm^2/s or 20 to 40×10^{-4} ft^2/h. Polyolefins show the greatest range in values. Metals have values that are hundreds of times larger than polymers, as seen in Table 2.12.

Thermal Expansion Coefficient

As polymers heat, chain mobility increases and molecules tend to move away from one another, increasing free volume. Factors that inhibit chain mobility tend to minimize thermal expansion. Thermal expansion is reduced with:

Increasing crystallinity,
Orientation,
Steric hindrance,
Hydrogen bonding,
Crosslinking,
Rigid fillers, and
Molecular polarity as with PVC.

Thermal expansion is enhanced with:

Plasticizers,
Lubricants,
Processing aids,
Solvents, and
Dissolved gases.

Flexible polymers tend to have thermal expansion coefficient values of about 100×10^{-6} $°C^{-1}$ or 50×10^{-6} $°F^{-1}$. Rigid polymers have values of about 50×10^{-6} $°C^{-1}$ or 25×10^{-6} $°F^{-1}$. In contrast, metals have values of 10 to 20×10^{-6} $°C^{-1}$ or 5 to 10×10^{-6} $°F^{-1}$.

2.18 Infrared Spectra

Certain polymeric molecular elements and chain segment motions are sympathetic to specific energy levels. The presence of these elements is detected by measuring the

© 1996 Carl Hanser Verlag. All rights reserved.
No unauthorized disclosure or reproduction; licensed to purchaser only.

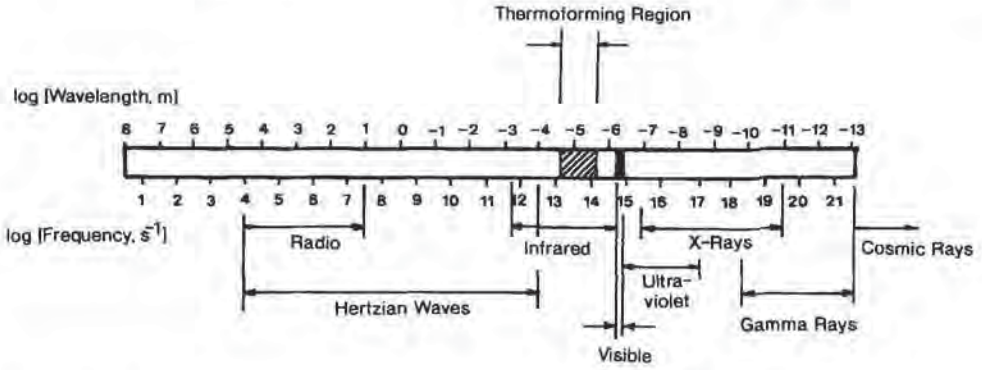

Figure 2.18 Electromatic radiation scheme showing relative locations of visible light, ultraviolet and infrared radiation and the normal thermoforming region [46]

intensity and wavelength location of absorbed infrared electromagnetic radiation. The infrared region is a small portion of the total electromagnetic radiation spectrum (Fig. 2.18) [46]. The visible light radiation wavelength range is 0.38 μm to 0.71 μm. The ultraviolet or UV light wavelength range is 0.006 μm to 0.38 μm. The infrared or IR wavelength range is 0.71 μm to 100 μm. The near-infrared portion of the IR spectrum is 0.71 μm to 5 μm. The far-infrared portion of the IR spectrum is 5 μm to 100 μm, with the longer wavelength portion overlapping the Hertzian wave range. Thermal radiation important in heat transfer is limited to the wavelength range of 0.1 to 20 μm [47]. As discussed in Chapter 3, thermoformer radiant heaters emit energy in the infrared region, with the peak wavelength dependent on the radiant heater temperature. The efficiency of absorption of that radiation by semitransparent polymers depends on the matching of the radiant source peak wavelength to the primary absorption wavelengths of the polymer. Each functional group on the polymer molecule may have more than one absorption wavelength. Most polymers have carbon-hydrogen bonds. The -C-H unit stretching IR band is 3 μm to 3.7 μm. The bending band is 6.7 μm to 7.7 μm, and the rocking band is 11 μm to 17 μm. The combination of functional group absorption bands is called the *IR spectrum* for that polymer. Polymers yield unique IR spectra. Since the intensity of an absorption band is directly related to the concentration of the functional group absorbing the radiation, IR is used for quantitative analysis of plastics. Absolute measures of the following can be obtained from IR analysis:

- Copolymer concentrations,
- Blend concentrations,
- Amounts and types of processing aids,
- Amounts and types of dyes,
- Amounts and types of plasticizers, and
- Amounts and types of solvents.

© 1996 Carl Hanser Verlag. All rights reserved.
No unauthorized disclosure or reproduction; licensed to purchaser only.

Table 2.13 Characteristic Infrared Absorption Bands for Organics

Specific vibrational mode	Wavelength range (μm)	Wavenumber range (cm^{-1})
-OH stretch	2.7–3.3	3030–3700
-NH stretch	2.7–3.3	3030–3700
-CH stretch	3.0–3.7	2700–3300
-C≡X stretch	4.2–4.78	2090–2380
-C=O stretch	5.4–6.1	1640–1850
-C=N stretch	5.9–6.4	1560–1695
-C=C stretch	5.9–6.4	1560–1695
-NH bend	6.1–6.75	1480–1640
-CH bend	6.75–7.7	1300–1480
-OH bend	6.85–8.3	1205–1460
-C-O stretch	7.7–11.1	910–1300
-C-N stretch	7.7–11.1	910–1300
-C-C stretch	8.3–12.5	800–1200
-CH rock	11.1–16.7	600–900
-NH rock	11.1–14.2	700–900

Further, the nature of the polymerization is determined by determining the types and amounts of end groups. And the extent of thermal and oxidative degradation are determined by subtracting the IR spectrum of the virgin polymer from that of the processed one, then measuring the intensity of the -C = O stretching band, 5.4 μm to 6.1 μm or that of the -C = C stretching band, 5.9 μm to 6.4 μm. Characteristic IR absorption bands are given in Table 2.13.

The IR spectra for a few common transparent or translucent thermoformable polymers are given in Figs. 2.19 to 2.32 [48]. The strong absorption band at 3.2 μm to 3.7 μm is -C-H stretching and is found on all carbon-hydrogen based polymers. PTFE has no hydrogen and so shows no absorption in that band (Fig. 2.32). On the other hand, PTFE shows strong absorption in the 8.2 μm to 8.7 μm IR band, for -C-F stretching. The PVC spectrum shows a strong absorption region at about 8.1 μm for -C-Cl stretching. The 2.8 μm to 3.0 μm for cellulose acetate is the -O-H

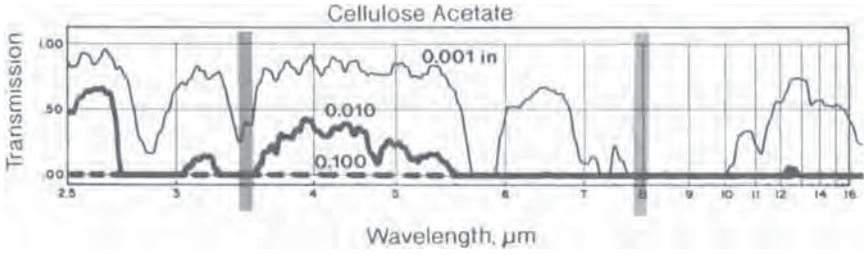

Figure 2.19 Infrared transmission spectrum for cellulose acetate [48]

© 1996 Carl Hanser Verlag. All rights reserved.
No unauthorized disclosure or reproduction; licensed to purchaser only.

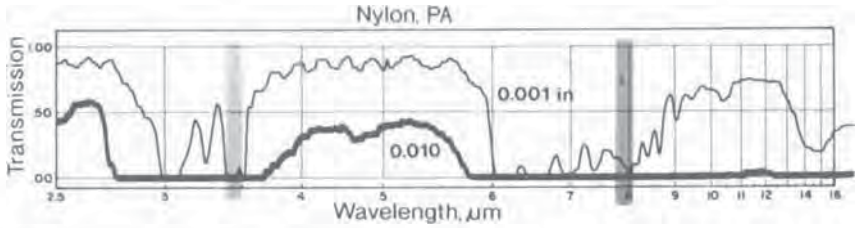

Figure 2.20 Infrared transmission spectrum for nylon, PA [48]

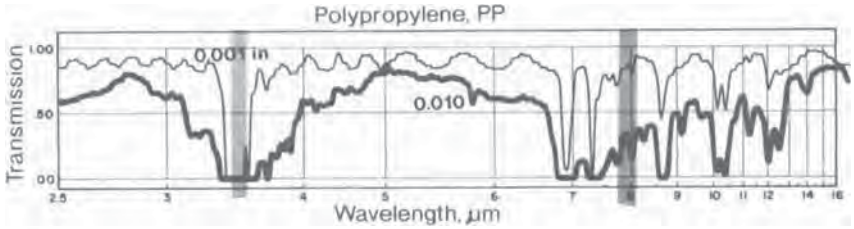

Figure 2.21 Infrared transmission spectrum for polypropylene, PP [48]

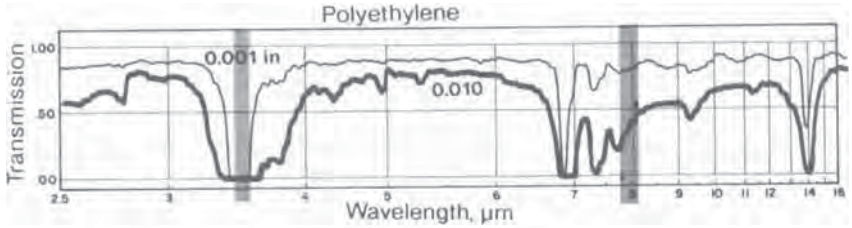

Figure 2.22 Infrared transmission spectrum for polyethylene [48]

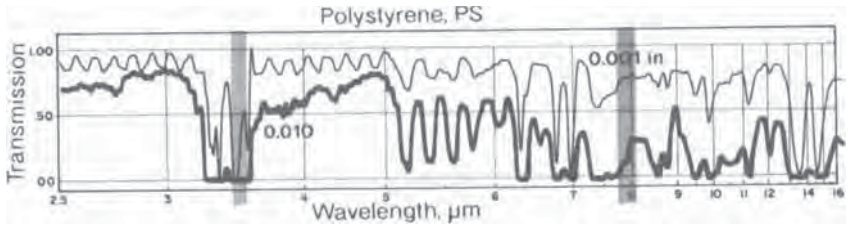

Figure 2.23 Infrared transmission spectrum for polystyrene, PS [48]

© 1996 Carl Hanser Verlag. All rights reserved.
No unauthorized disclosure or reproduction; licensed to purchaser only.

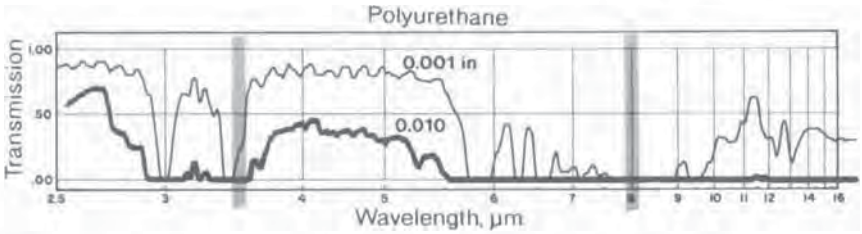

Figure 2.24 Infrared transmission spectrum for thermoplastic polyurethane [48]

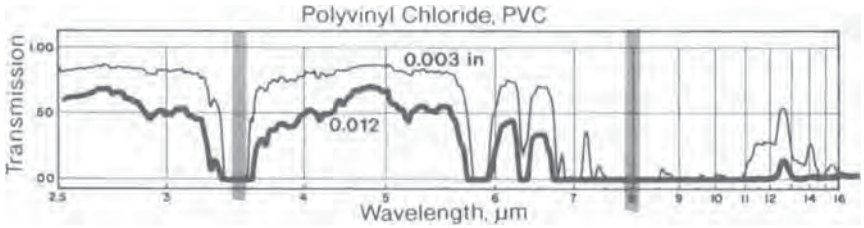

Figure 2.25 Infrared transmission spectrum for polyvinyl chloride, PVC [48]

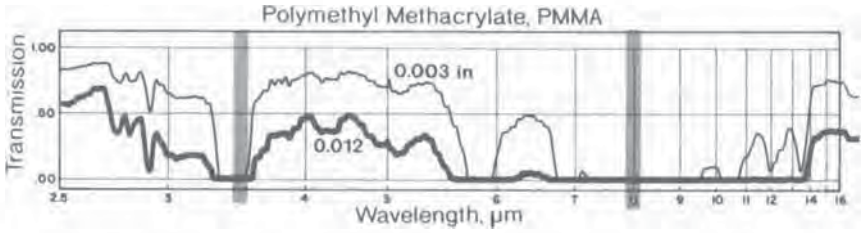

Figure 2.26 Infrared transmission spectrum for polymethyl methacrylate, PMMA [48]

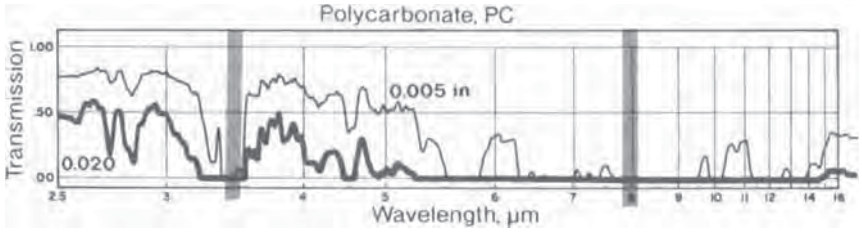

Figure 2.27 Infrared transmission spectrum for polycarbonate, PC [48]

© 1996 Carl Hanser Verlag. All rights reserved.
No unauthorized disclosure or reproduction; licensed to purchaser only.

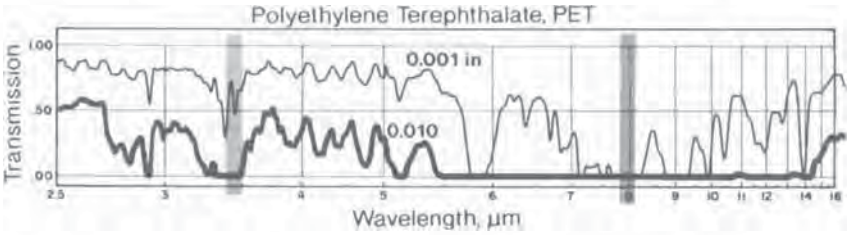

Figure 2.28 Infrared transmission spectrum for polyethylene terephthalate, PET [48]

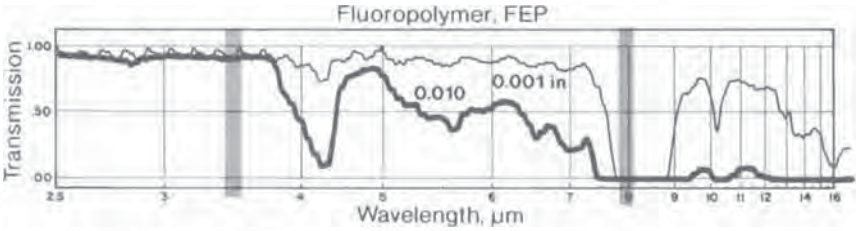

Figure 2.29 Infrared transmission spectrum for fluoropolymer, FEP [48]

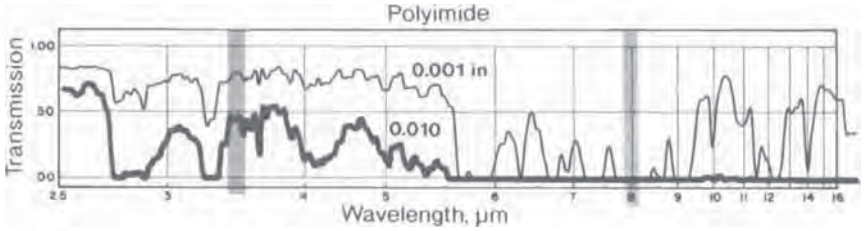

Figure 2.30 Infrared transmission spectrum for polyimide [48]

stretching mode. In polycarbonate, the -C = O stretching mode is shown as an absorption band of 5.4 μm to 6.1 μm. In certain polymers such as polyamides, polyethylenes and PET, orientation and crystallinity are revealed in specific IR absorption bands. The crystalline portion of nylon 66 absorbs at 10.7 μm and 11.7 μm and the amorphous portion absorbs at 8.8 μm [49]. The extent of crystallinity is determined by comparing the intensities of these bands.

Weak and strong IR absorption bands for common thermoplastics are given in Table 2.14. Absorptivity and transmissivity are related as:

$$\alpha + \tau = 1 \tag{2.8}$$

The typical radiation units are cm^{-1}. The larger the value becomes, the greater the radiation effect becomes. Transmissivity values greater than 1 cm^{-1} imply high

© 1996 Carl Hanser Verlag. All rights reserved.
No unauthorized disclosure or reproduction; licensed to purchaser only.

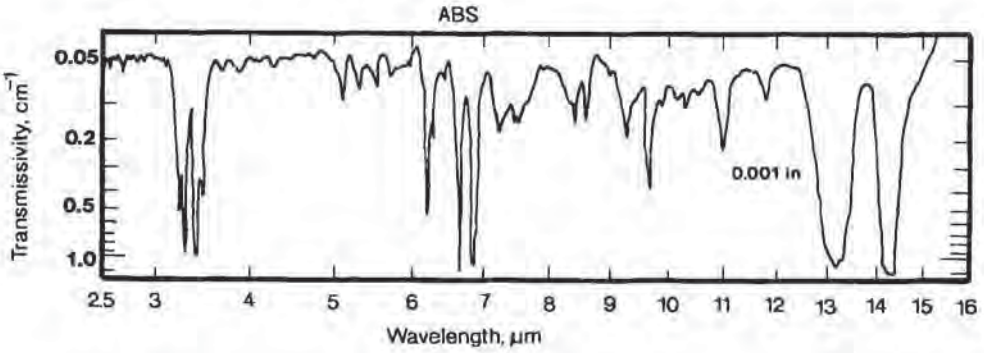

Figure 2.31 Infrared transmission spectrum for ABS [48]

absorption and infrared opacity and absorptivity values less than 0.1 cm^{-1} imply high infrared transparency. The effect of thickness is predicted with Beer's law:

$$I(\lambda) = I_o(\lambda)\, e^{-\alpha(\lambda)x} \tag{2.9}$$

where I_o is the incident wavelength-dependent radiation, α is the absorptivity and x is the thickness of the plastic sheet. Figures 2.19-2.30 show the effect of sheet thickness on IR transmission. As is apparent, as the sheet increases in thickness, the amount of IR energy absorbed increases but the general shape of the IR spectra remains the same. For very thin films of less than 1 μm, surface molecular orientation may distort the absolute values of the IR spectra and therefore the energy absorption characteristics of the films..

The primary effect of organic colorant on polymer should be in the visible wavelength range [0.38 μm to 0.71 μm]. Solid inorganic particles such as TiO_2, carbon black, and talc act as opacifiers by increasing surface absorption of visible light and minimizing the amount of visible light that is transmitted into or through

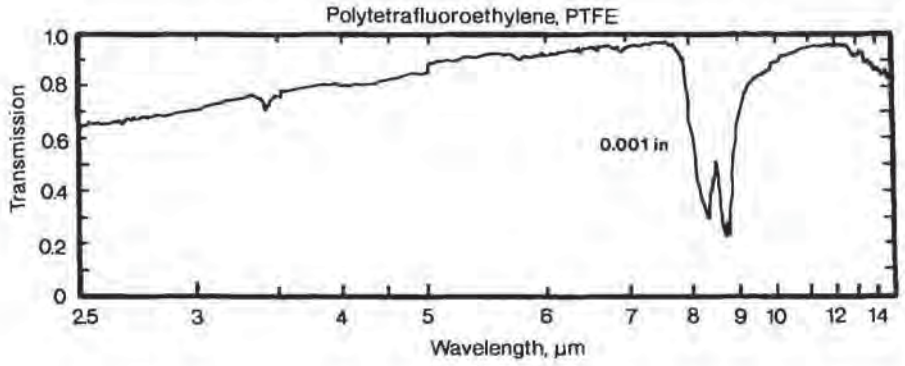

Figure 2.32 Infrared transmission spectrum for polytetrafluoroethylene, PTFE

© 1996 Carl Hanser Verlag. All rights reserved.
No unauthorized disclosure or reproduction; licensed to purchaser only.

Table 2.14 Characteristic Polymer Infrared Absorption Bands in Wavelength (Values in Parentheses Represent Weak Absorption Bands)

Polymer	Primary (μm)	Secondary (μm)
HDPE	3.2–3.9	(7.0–8.0)
LDPE	3.2–3.9	6.7–7.1
		7.0–8.0
PP	3.2–3.6	6.6–7.0
		7.1–7.3
		(8.4–8.7)
		(9.8–10.1)
PS	3.2–3.6	6.4–7.3
ABS	2.8–3.6	6.4–7.3
PVC	3.2–3.6	(1.65–1.8)
		2.2–2.5
		5.7–6.0
		6.8–11.0
PMMA	3.2–3.6	1.4–2.2
		1.1–1.25
		5.7–6.0
		6.2–9.5
PA 6	3.0–3.2	19.–2.8
		(6.0–7.8)
Cellulose acetate	5.5–6.0	2.7–2.9
	7.8–10.0	
PET	3.3–3.6	5.9–6.0
		7.0–9.2
FEP	7.4–9.0	(4.2–4.4)
PEI	2.7–3.0	5.8–6.0
		(6.9–9.2)
PC	3.2–3.6	5.5–6.2
		6.6–7.7
		7.8–9.5

the polymer. Thus, effective opacifiers should have particle sizes in the 0.1 to 10 μm range. Opacifiers with particle sizes of 3 to 12 μm will also act to block incident infrared radiation and thus change the absorption characteristics of the polymer. The effect of colorant dosage on the polymer IR spectrum is shown in Fig. 2.33 [50]. The general effect is to gradually increase the IR absorptivity with increasing dosage. The nature of the colorant also affects the polymer IR spectrum (Fig. 2.34) [51]. Organic dyes and tints are designed to affect the polymer electromagnetic radiation spectrum in the visible wavelength range (Fig. 2.35), and are usually used in small quantities. Although the spectra of these organics overlay those of the polymers, the small dosages usually do not materially affect the energy absorption efficiencies of the polymers. As discussed in Chapter 3, a sound measure of the amount of energy absorbed by a plastic is obtained by integrating the wavelength-dependent absorption curve over the wavelength range of the incident radiation. This is shown in

© 1996 Carl Hanser Verlag. All rights reserved.
No unauthorized disclosure or reproduction; licensed to purchaser only.

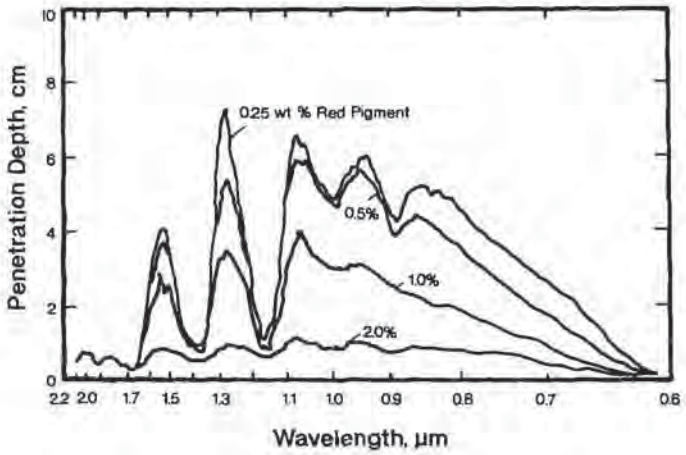

Figure 2.33 Effect of colorant dosage on absorption characteristics of polymethyl methacrylate, PMMA [50]

Fig. 2.36 [52] for several colorants. Simply put, IR spectra offer substantial information about relative processing effects such as:

- The effect of increasing heater temperature on sheet heating rate,
- The effect of sheet downgaging on energy absorption, and thus on cycle time, sheet surface temperature, and discoloration,
- The effect of increasing sheet thickness on sheet surface temperature,
- The effect of thin cap-sheeting or film on heating rate of sheet,
- The effect of changing pigment type and dosage, and
- The effect of printing on sheet heating characteristics.

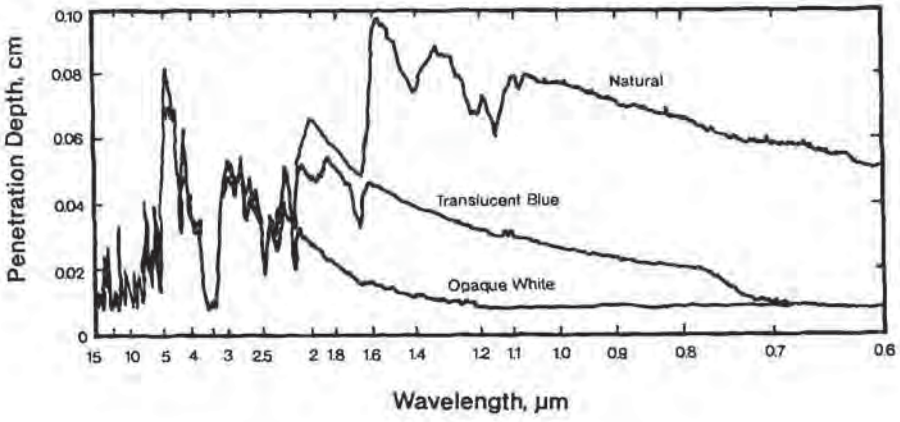

Figure 2.34 Effect of pigment type on absorption characteristics of polystyrene, PS [51]

© 1996 Carl Hanser Verlag. All rights reserved.
No unauthorized disclosure or reproduction; licensed to purchaser only.

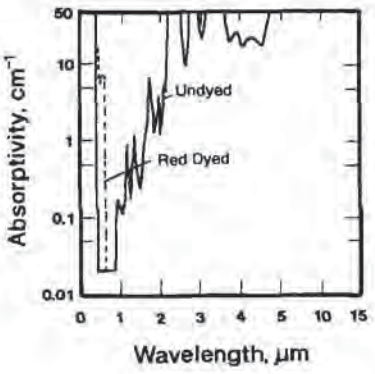

Figure 2.35 Absorptivity of natural and red dyed polymethyl methacrylate, PMMA

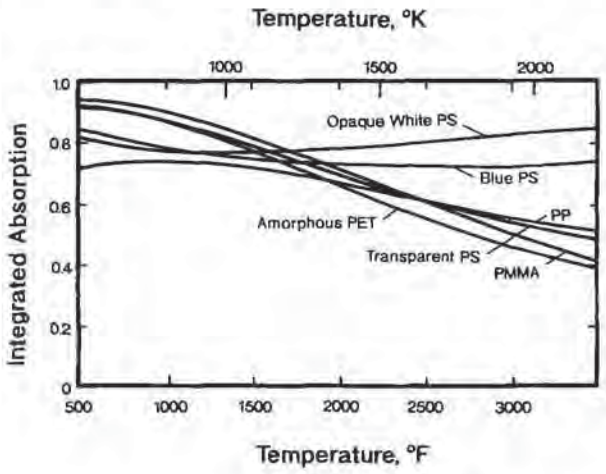

Figure 2.36 Heater temperature-dependent total absorption for several natural and pigmented thermoplastics [52]

2.19 Summary

Although it was stated at the beginning of this chapter that "If a polymer can be produced as a sheet, it can be thermoformed into a product", this does not mean that all polymers thermoform with equal effort. Typically, amorphous polymers have broader forming windows than crystalline ones. Again, the forming temperatures given in Table 2.5 represent extremes and ideal conditions. Actual forming temperature ranges are usually only a few degrees. Table 2.15 gives some general forming characteristics for many of the polymers listed in Tables 2.5 and 2.12. Special, more expensive polymeric homologs are being developed to circumvent the forming inadequacies of certain polymeric classes.

© 1996 Carl Hanser Verlag. All rights reserved.
No unauthorized disclosure or reproduction; licensed to purchaser only.

Table 2.15 Thermoforming Processing Characteristics of Some Formable Polymers. (These characteristics are generic unless otherwise noted)

Polymer	Process temperature range		Char. maximum draw ratio	Major draw limitation	Comments
	(°C)	(°F)			
PS	150–190	300–375	8:1	Tears at high temperatures	Some yellowing at higher temperatures, long oven times. Trim dust is tenacious. Parts are brittle in 3D corners at deep draw. Sheet is easily marked off in plug assist.
HIPS	163–204	325–400	8:1	Elongation is limited at high rubber content.	Yellowing at higher temperatures. Tends to be difficult to form into sharp 3D corners. Needs to be held on mold longer than PS or ABS. This is particularly true for high rubber content. Sheet is easily marked off in plug assist.
ABS	150–204	300–400	10:1	Elongation at high temperature.	Moisture causes pits, bubbles, blisters. Discolors at higher temperatures, long oven times. Can be splitty at low temperatures.
mPPO	163–218	325–425	6:1	Stiff at moderate temperature.	Thermoforms like HIPS but stiffer. Odor can be objectionable. Can yellow at high forming temperature. Sharp corners difficult to form at modern temperatures. Heavy gage must be trimmed cold. Trim dust can be tenacious. Ideal candidate for pressure forming.
OPS	127–160	260–320	5:1	Very stiff at low temperature. Can lose orientation at high temperature.	Must be very carefully heated to maintain orientation. Birefringence can be used to monitor orientation. Sheet best heated by direct contact. Sharp corners difficult. Very tough, splitty to trim cold. Superior surface gloss, opticals, impact strength.

(Continued)

© 1996 Carl Hanser Verlag. All rights reserved.
No unauthorized disclosure or reproduction; licensed to purchaser only.

Table 2.15 (Continued)

Polymer	Process temperature range		Char. maximum draw ratio	Major draw limitation	Comments
	(°C)	(°F)			
PMMA	150–204	300–400	12:1	Elongation at high temperature for lightly crosslinked PMMA.	Sheet can scorch, blister at high energy input. Surface can change from glossy to matte at high energy input. Highly stretched sheet can be brittle in 3D corners. Sheet is easily scratched during handling, trimming. Sheet frequently thermoforming with protective film in place. Trim dust can be tenacious, statically charged.
PMMA/PVC	150–190	300–375	8:1	Elongation at high temperature.	Sheet can blister, scorch, yellow at high energy input. Sheet can be brittle during trimming. Sheet can be pressure formed with good results.
FPVC	107–150	225–300	10:1	General weakness at higher temperatures.	Upper temperature limit is discoloration. Plasticizer odor objectionable. Rubbery sheet requires longer mold times to set. Embossings wash at high temperature or draw ratios > 5:1.
RPVC	121–177	250–350	6:1	General weakness at higher temperatures.	Upper temperature limit is discoloration. Long oven times cause yellowing. Decomposition product is HCl. Difficult to prestretch as heavy gage. Thin gage transparency not as good as PS, ABS. Tends to be tougher in 3D corners than PS, PMMA. Virgin transparent has bluish tint to balance yellowish regrind color.
LDPE	127–177	260–350	6:1	Melt elasticity low at forming temperatures.	Usually processed above its melt temperature of 115°C. Can exhibit excessive sag very quickly. Sag bands recommended for thin gage. Increased haze at higher temperatures.

© 1996 Carl Hanser Verlag. All rights reserved.
No unauthorized disclosure or reproduction; licensed to purchaser only.

HDPE	138–193	280–380	8:1	Melt elasticity.	Usually processed above its melt temperature of 135°C. Can exhibit excessive sag. Black sheet heats much faster than white. Thin gage sheet can excessively sag very quickly. Increased haze at higher temperatures.
PP	143–166	290–330	6:1	Excessive sag and narrow forming window.	Very difficult to control sag with straight homopolymer. Very narrow forming temperature range. Sag bands should be slip-coated to prevent sticking. Draw frequently shows necking. Sheet easily marked by plug. Thin gage can have high residual stress, can pull out of pins during heating. High energy input increases haze. Sheet does not draw well into sharp corners when cold. Best parts are pressure-formed. Trim blades must be sharp to avoid forming whiskers, angel hair. Parts formed at higher temperature onto cold mold are frequently brittle. Can be pressure-formed in thin gage below melt temperature.
EP Copoly.	132–177	270–350	8:1	Sags, necks at high forming temperature.	Forms like HDPE in thin gage. Good elongation at lower forming temperature range. Can be very difficult to trim when very cold.
OPP	143–166	290–330	5:1	Rapidly loses orientation, sages at upper temperature.	Very low haze, excellent surface gloss, high impact strength. Must be heated very carefully to maintain orientation. Thin-gage sheet heated best with direct contact.
EVA	135–177	275–350	8:1	Tears at high temperature.	Not normally used alone. As a tie layer, usually draws well with little resistance.

(Continued)

© 1996 Carl Hanser Verlag. All rights reserved.
No unauthorized disclosure or reproduction; licensed to purchaser only.

Table 2.15 (Continued)

Polymer	Process temperature range		Char. maximum draw ratio	Major draw limitation	Comments
	(°C)	(°F)			
PP—20% talc	149–204	300–400	5:1	Elongation low at moderate-to-high temperature.	Stiff at forming temperature. Elongation limited by filler loading. Deep draw restricted. Matte surface may not be acceptable. Sharp corners difficult to form without plug assist. Plug assist useful primarily at low forming temperature. Pressure forming desired heavy-gage sheet.
PP—40% GR	149–232	300–450	4:1	Very stiff at all forming temperatures.	Best pressure-formed. Deep draws cause splits, polymer-rich areas in corners. Plug assist not always effective owing to low melt strength of base polymer.
PC	177–232	350–450	8:1	Stiffness even at upper forming temperature.	Tends to be stiff at all forming temperatures. Can discolor at high temperature. Moisture causes pinholes, pock marks, bubbles, brittleness. Transparent sheet harder to heat than acrylic. Sharp corners hard to form at low forming temperature. Very tough to trim cold. Routering recommended.
APET	127–166	260–330	6:1	Sags, necks, anneals, orients rapidly at high temperature.	Slowly crystallizing polymer. Rate increases with decreasing molecular weight. Low molecular weight heat sets rapidly. Residual stress problem in thin gage. Necking difficult to avoid in deep drawn parts. Plug assist enhances necking. Bubble prestretching enhances orientation, reduces maximum draw ratio. Hard to form sharp corners on hot mold. Trimming is difficult cold, can cause whiskers or angel hair.

© 1996 Carl Hanser Verlag. All rights reserved.
No unauthorized disclosure or reproduction; licensed to purchaser only.

					Trim registry difficult owing to high polymer movement. Very thin gage sheet and film best heated by direct contact.
CPET	185–199	365–390	5:1	Very stiff if sheet too hot. Sheet tears if too cold.	Requires careful oven temperature control. Mold must be heated to 180°C or 360°F or so. Excessive draw-down leads to brittle corners. Crystallinity in 20% range gives optimum properties. Difficult to control crystallinity in very thin sheet. Normal gage range of 1 mm or 0.040 in or more.
TPE/TPO (Depends on polymer)	135–177	275–350	6:1	Spring-back.	Many versions of thermoplastic elastomers. Those with high natural rubber content more difficult to maintain part shape. Very cold molds required. Hard to maintain long-term dimensions. Pre-stretch must remain on during forming to minimize spring-back.
PS Foam	93–121	200–250	4:1	Cell collapse at high temperature, very stiff at low temperature.	Thin laminating film improves surface appearance, increases maximum draw, stiffens final product. Parts mostly restricted to shallow draw. Matched die molding usually required for low temperature forming, preferred to control sheet thickness expansion from oven. Trim dust is statically charged, very tenacious. Sharp corners not desired owing to splittiness, poor impact of foam.

(Continued)

© 1996 Carl Hanser Verlag. All rights reserved.
No unauthorized disclosure or reproduction; licensed to purchaser only.

Table 2.15 (Continued)

Polymer	Process temperature range		Char. maximum draw ratio	Major draw limitation	Comments
	(°C)	(°F)			
PP foam	149–166	300–330	4:1	Cell collapse, stickiness, mushiness can occur very rapidly.	Matched die molding preferred. Compression molding sometimes recommended. Processing window very narrow. Cell collapse catastrophic. Crosslinked PP preferred. Deep draw difficult without prestretching. Material elasticity at lowest temperature prevents sharp corners.
XLPE foam	149–204	300–400	4:1	Cell collapse, mold stick at high temperature.	Sheet tends to be rubbery-elastic, like TPE. Some spring-back. Cell rupture at high energy input. Difficult to get deep draw even with aggressive plugging. Foam very soft at low density. Best for shallow draw.
PET foam	185–199	365–390	4:1 (?)	Hot mold and other CPET forming limitations.	Early results show 400 to 900 kg/m³ PET form like unfoamed CPET. Foam sheet crystallinity <20% in 2.5 mm or 0.100 in thicknesses or less. Formed sheet crystallinity ~ 20% as with CPET. Sheet thickness typically > 1 mm or 0.040 inch).

© 1996 Carl Hanser Verlag. All rights reserved.
No unauthorized disclosure or reproduction; licensed to purchaser only.

2.20 References

1. J. Frados, Ed., *Plastics Engineering Handbook*, 4th Ed., Van Nostrand Reinhold Co., New York, 1976, p. 274.
2. J.L. Throne, "Polymer Properties", in M. Bakker, Ed., *Encyclopedia of Packaging Technology*, John Wiley & Sons, New York, 1986.
3. J.-M. Charrier, *Polymeric Materials and Processing: Plastics, Elastomers and Composites*, Hanser Publishers, Munich, 1991.
4. R. Gächter and H. Müller, Eds., *Plastics Additives Handbook: Stabilizers, Processing Aids, Plasticizers, Fillers, Reinforcements, Colorants for Thermoplastics*, 2nd Ed., Carl Hanser Verlag, Munich, 1985.
5. H.R. Simonds, *Source Book of the New Plastics*, Vol. II, Van Nostrand Reinhold Co., New York, 1961, p. 21.
6. J.L. Throne, *Thermoplastic Foams*, Sherwood Publishers, Hinckley OH, 1996.
7. J.L. Throne, "Thermoforming—A Look Forward", SPE ANTEC Tech. Papers, *29* (1983), p. 464.
8. R.D. Deanin, *Polymer Structure, Properties, and Applications*, Cahners Books, Boston, 1972, p. 154.
9. J.L. Throne, *Plastics Process Engineering*, Marcel Dekker, New York, 1979, p. 65.
10. R.C. Progelhof and J.L. Throne, *Polymer Engineering Principles: Properties, Processes, Tests for Design*, Hanser Publishers, Munich, 1993, Chapter 1.
11. R.C. Progelhof and J.L. Throne, *Polymer Engineering Principles: Properties, Processes, Tests for Design*, Hanser Publishers, Munich, 1993, Table 2.4, pp. 90-91.
12. T. Alfrey and E.F. Gurnee, *Organic Polymers*, Prentice-Hall, New York, 1967, p. 51.
13. R.C. Progelhof and J.L. Throne, *Polymer Engineering Principles: Properties, Processes, Tests for Design*, Hanser Publishers, Munich, 1993, p. 129.
14. A. Ziabicki, *Fundamentals of Fibre Formation: The Science of Fibre Spinning and Drawing*, John Wiley & Sons, New York, 1976, p. 112.
15. J.L. Throne, "Thermoforming Crystallizing Polyethylene Terephthalate (CPET)", Adv. Polym. Tech., *8* (1988), pp. 131-171.
16. J.L. Throne, "Thermoforming Crystallizing PET", SPE ANTEC Tech. Papers, *27* (1981), p. 598.
17. J.A. Brydson, *Plastics Materials*, Iliffe, London, 1966, p. 58.
18. R.E. Dempsey et al., US Patent 4,127,631, Assigned to Amoco Chemicals Corp., Chicago IL, 28 Nov 1978.
19. H. Saechtling, *International Plastics Handbook for the Technologist, Engineer and User*, 2nd Ed., Hanser Publishers, Munich, 1987, Figure 82, p. 166.
20. L.J. Gibson and M.F. Ashby, *Cellular Solids: Structure & Properties*, Pergamon Press, Oxford, 1988, Figure 3.2, p. 47.
21. J.A. Brydson, *Plastics Materials*, Iliffe, London, 1966, p. 34.
22. R.C. Progelhof and J.L. Throne, *Polymer Engineering Principles: Properties, Processes, Tests for Design*, Hanser Publishers, Munich, 1993, Figure 2.45, p. 135.
23. R.C. Progelhof and J.L. Throne, *Polymer Engineering Principles: Properties, Processes, Tests for Design*, Hanser Publishers, Munich, 1993, Figure 2.46, p. 136.
24. L.E. Nielsen, *Mechanical Properties of Polymers*, Reinhold, New York, 1962, p. 244.
25. R.D. Deanin, *Polymer Structure, Properties, and Applications*, Cahners Books, Boston, 1972, p. 88.
26. J.L. Throne, "Polymer Properties", in M. Bakker, Ed., *Encyclopedia of Packaging Technology*, John Wiley & Sons, New York, 1986, p. 533.
27. R.M. Ogorkiewicz, Ed., *Thermoplastics: Properties and Design*, Wiley-Interscience, Ltd., London, 1974, p. 28.
28. J.B. Howard, "Fracture—Long Term Testing", in N.M. Bikales, Ed., *Mechanical Properties of Polymers*, Wiley-Interscience, New York, 1971, p. 73.

© 1996 Carl Hanser Verlag. All rights reserved.
No unauthorized disclosure or reproduction; licensed to purchaser only.

29. R.L. Baldwin and K.E. Van Holde, Fortschr. Hochpolym. Forsch., *1* (1960), p. 451. See also J.L. Throne, *Plastics Process Engineering*, Marcel Dekker, New York, 1979, p. 765.
30. R.C. Progelhof and J.L. Throne, *Polymer Engineering Principles: Properties, Processes, Tests for Design*, Hanser Publishers, Munich, 1993, p. 12.
31. R.C. Progelhof and J.L. Throne, *Polymer Engineering Principles: Properties, Processes, Tests for Design*, Hanser Publishers, Munich, 1993, Figure 2.47, p 142.
32. F. Brinken and H. Potente, "Some Considerations of Thermodynamics in Thermoforming", SPE ANTEC Tech. Papers, *29* (1983), p. 467.
33. R.C. Progelhof and J.L. Throne, *Polymer Engineering Principles: Properties, Processes, Tests for Design*, Hanser Publishers, Munich, 1993, Table 1.4.
34. R.C. Progelhof and J.L. Throne, *Polymer Engineering Principles: Properties, Processes, Tests for Design*, Hanser Publishers, Munich, 1993, Table 1.3, p. 13.
35. J.L. Throne, "Polystyrene Foam Sheet Expansion During Heating", SPE ANTEC Tech. Papers, *29* (1983), p. 1328.
36. J.A. Brydson, *Plastics Materials*, Iliffe, London, 1966, p. 58.
37. H. Domininghaus, *Plastics for Engineers: Materials, Properties, Applications*, Hanser Publishers, Munich, 1993, Figure 133, p. 208.
38. H. Domininghaus, *Plastics for Engineers: Materials, Properties, Applications*, Hanser Publishers, Munich, 1993, Figure 246, p. 316.
39. H. Domininghaus, *Plastics for Engineers: Materials, Properties, Applications*, Hanser Publishers, Munich, 1993, Figure 241, p. 311.
40. Material adapted from W.K. McConnell, Jr., handout material, "Thermoforming Technology for Industrial Applications", SPE Seminar, 12-14 March 1985, Arlington TX.
41. J.L. Throne, *Plastics Process Engineering*, Marcel Dekker, New York, 1979, pp. 714-735. Taken from an extensive series of tables published by R.G. Griskey in Modern Plastics, 1966-1967.
42. H. Voigt, "Lehrgang für Thermoformung", Paul Kiefel Thermoformmaschinen GmbH, Freilassing, Germany, undated.
43. Z. Tadmor and C.G. Gogos, *Principles of Polymer Processing*, John Wiley & Sons, Inc., New York, 1979, pp. 697-703.
44. B.C. Sakiadis and J. Coates, AIChE J., *2* (1956), p. 88. See also J.L. Throne, *Plastics Process Engineering*, Marcel Dekker, New York, 1979, p. 737.
45. R.C. Progelhof, J.L. Throne and R.R. Ruetsch, "Methods for Predicting the Thermal Conductivity of Composite Systems: A Review", Polym. Eng. Sci., *16* (1976), p. 615.
46. J.P. Holman, *Heat Transfer*, 4th Ed., McGraw-Hill Book Company, New York, 1976, Figure 8-1, p. 274.
47. F. Kreith, *Principles of Heat Transfer*, 2nd Ed., International Textbook Co., Scranton, 1965, p. 199.
48. Anon., "Plastic Film Measurement", Technical Note TN100, IRCON, Inc., Niles IL, 1993, Figures 2-5.
49. I. Kossler, "Infrared-Absorption Spectroscopy", N.M. Bikales, Ed., *Characterization of Polymers*, Wiley-Interscience, New York, 1971, p. 125.
50. D. Weinand, "Modellbildung zum Aufheizen und Verstrecken beim Thermoformen", Doktor-Ingenieurs Dissertation, Rheinisch-Westfälische Technische Hochschule, Aachen, Germany, 16 Juli 1987, Bild 3.10.
51. D. Weinand, "Modellbildung zum Aufheizen und Verstrecken beim Thermoformen", Doktor-Ingenieurs Dissertation, Rheinisch-Westfälische Technische Hochschule, Aachen, Germany, 16 Juli 1987, Bild 3.9.
52. D. Weinand, "Modellbildung zum Aufheizen und Verstrecken beim Thermoformen", Doktor-Ingenieurs Dissertation, Rheinisch-Westfälische Technische Hochschule, Aachen, Germany, 16 Juli 1987, Bild 2.14.

© 1996 Carl Hanser Verlag. All rights reserved.
No unauthorized disclosure or reproduction; licensed to purchaser only.

3 Heating the Sheet

© 1996 Carl Hanser Verlag. All rights reserved.
No unauthorized disclosure or reproduction; licensed to purchaser only.

3.1 Introduction

The thermoforming process is neatly segmented into four steps:

- Heating the sheet,
- Stretching the sheet,
- Cooling the sheet on the mold surface, and
- Trimming the part from its surroundings.

During the forming and trimming steps, the sheet dimensions are changing but the sheet is essentially at constant temperature. During the heating and cooling steps, the sheet dimensions are essentially constant, but the sheet temperature is changing. Thus the heat transfer process and the mechanical deformation process are best treated separately.

This chapter focuses on the ways in which sheet is heated to the stretching or forming temperature. Chapter 4 concentrates on the technical details of sheet stretching. Chapter 5 considers the process of cooling and the trimming step. The material in these chapters is quite technical. However, newer thermoforming technologies mandate a thorough understanding of the basic concepts underlying the general process. And many of the troubleshooting solutions to processing problems are apparent once these concepts are understood. Roll-fed formers have used infrared heating for years owing to its efficiency in heating thin-gage sheet. Heavy-gage cut sheet formers have used forced convection hot air ovens for heating, in order to minimize sheet surface degradation. There are technical and management reasons behind these decisions. In certain instances, these are not necessarily the optimum choices. Pattern or zone heating is used extensively to produce more uniform part wall thicknesses and so parts designers should be aware of some of the details of this technique. Again, what is important is an adequate understanding of the interaction between the plastic sheet, initially at room temperature but being heated to its proper forming temperature, and the chosen heating medium.

The material in this chapter begins with a review of the basic types of heating methods. Then thin-gage heating, particularly infrared heating, and forced convection hot air heating of heavy-gage material are considered in detail. Equilibration time is discussed. This is the time it takes for the sheet to achieve a uniform temperature across its cross-section, once the heating source is removed. Computer-aided models are also outlined. And finally, guidelines for determining heating cycle times for both thin-gage and heavy-gage sheet are presented.

3.2 Energy Absorption by Sheet

Thermoforming is an energy intensive plastics process. Economics require the most efficient use of energy. The amount of energy needed to heat a unit mass of sheet

© 1996 Carl Hanser Verlag. All rights reserved.
No unauthorized disclosure or reproduction; licensed to purchaser only.

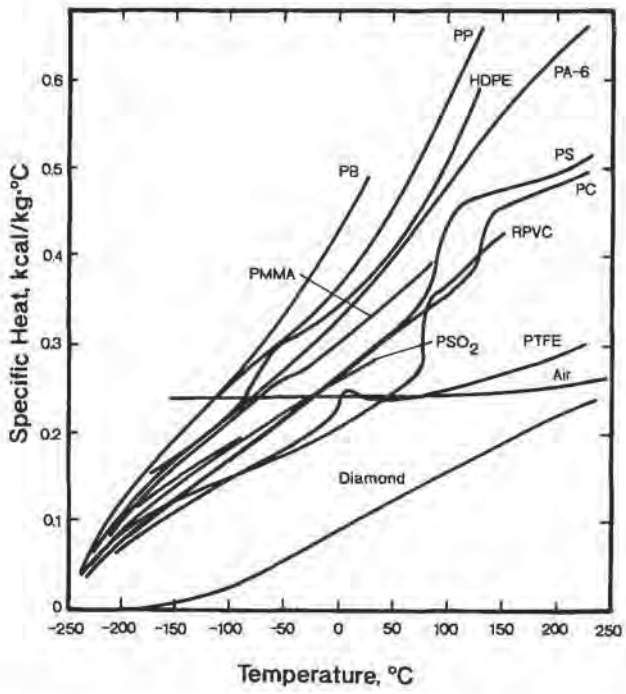

Figure 3.1 Temperature-dependent heat capacities or specific heats of several thermoplastics

from room temperature, RT, to the forming condition, T_f, is *enthalpy increase*, Δh, and is obtained from:

$$Q \text{ or } \Delta h = \int_{RT}^{T_f} c_p(T)\, dT \qquad [cal/g] \equiv [cal/g\ °C] \cdot [°C] \qquad (3.1)$$

$$[Btu/lb] \equiv [Btu/lb°F] \cdot [°F]$$

$c_p(T)$ is the temperature-dependent heat capacity (Table 2.5 and Fig. 3.1) [1]. The forming temperature is assumed to be the average sheet temperature at the normal forming temperature:

$$T_f \equiv \left(\frac{1}{L}\right) \int_0^L T(x)\, dx \qquad (3.2)$$

T(x) is the temperature at position x across the sheet half-thickness, $0 < x < L$. If the temperature dependency of heat capacity is unknown, an average value will give a reasonable estimate. If the heat capacity of a specific polymer is unknown, a value of a homologous polymer can be used as a first approximation. The change in enthalpy is a much better method of determining the amount of energy uptake by the sheet. Figure 2.17 provides enthalpy values for several thermoformable polymers. H is the enthalpy at a given temperature, as [cal/g], [kcal/kg], or [Btu/lb]. The energies needed to heat typical polymers to forming temperatures are given in Table 3.1.

© 1996 Carl Hanser Verlag. All rights reserved.
No unauthorized disclosure or reproduction; licensed to purchaser only.

Table 3.1 Thin-Gage Heating Efficiencies (Heater Temperature, $T_\infty = 760°C$; Heater Output, $Q/A = 40\ kW/m^2$)

Polymer	Normal forming temperature (°C)	Enthalpy (cal/g)	Density (g/cm^3)	$C_{p,ave}$ [1] (cal/g°C)	Heating rate (s/mm)	Energy absorbed (kW/m^2)	Efficiency (%)	Maximum effective heating transfer coefficient ($kW/m^2 \cdot °C$)	($Btu/ft^2 \cdot h \cdot °F$)
LOPE	129	71.7	0.92	0.498	25	11.5	27.6	0.0182	3.21
PMMA	177	104.1	1.2	0.559	27	19.44	48.6	0.0333	5.87
PVC	138	55.9	1.4	0.265	21	15.88	39.7	0.0255	4.50
PS	146	65.0	1.05	0.341	13–15	19.03–21.97	47.6–54.9	0.0310–0.0358	5.46–6.30
PTFE/FEP[2]	288	66.9	2.2	0.342	13	25.86	64.7	0.0548	9.65
PA 66[2]	224	105.0	1.2	0.479	27	19.84	49.6	0.0370	6.52

[1] Used only for effective heat transfer coefficient calculation
[2] Values from Fig. 3.26

© 1996 Carl Hanser Verlag. All rights reserved.
No unauthorized disclosure or reproduction; licensed to purchaser only.

Some of these values are based on assumed values for heat capacity and some are approximate. Example 3.1 compares energy uptake for ABS and HDPE, representing amorphous and crystalline polymers, respectively. As detailed in Chapter 2, additional energy is required to melt a crystalline polymer such as HDPE. If the energy input to both sheet is the same, it requires substantially longer to heat HDPE than ABS. Example 3.2 illustrates this point.

Example 3.1 Energy Absorbed by Plastic Sheet

Calculate the amount of energy required to heat ABS and HDPE to their respective normal forming temperatures. If the energy input is the same to each sheet, calculate the relative times to heat each sheet to the forming temperature.

From Table 2.5, the normal forming temperature of both of these polymers is 295°F or 146°C. The amount of energy required to heat the plastic from room temperature (say 77°F or 25°C) to the forming temperature is obtained from Fig. 2.17.

HDPE: 128 kcal/kg @ 146°C − 8 kcal/kg @ 25°C = 120 kcal/kg
ABS: 51 kcal/kg @ 146°C − 7 kcal/kg @ 25°C = 45 kcal/kg

The densities of these polymers are obtained from Table 2.12.

HDPE: 960 kg/m^3
ABS: 1050 kg/m^3

The energy required per unit volume is given as:

HDPE: 120 kcal/kg · 960 kg/m^3 = 0.115 × 10^6 kcal/m^3
ABS: 45 kcal/kg · 1050 kg/m^3 = 0.0473 × 10^6 kcal/m^3

Relative to the heating time for ABS, HDPE takes 0.115/0.0473 = 2.43 times longer to heat to the normal forming temperature.

Example 3.2 Time to Heat Plastic Sheet

Consider the two polymers of Example 3.1. If the plastic is 0.100 inch thick (2.5 mm) and the sheet receives 12.9 W/in^2 (2 W/cm^2) heating energy[1]*, determine the time required to heat the sheet to the forming temperature. Assume that the sheet heats uniformly throughout its thickness. 1 W = 3.413 Btu/h.*

The energy required to raise each polymer to the forming temperature is given as:

HDPE: 120 kcal/kg · 1.8 = 216 Btu/lb
ABS: 45 kcal/kg · 1.8 = 81 Btu/lb

[1] Correctly, this example assumes that the net energy interchange between the heater and the sheet is constant with time. See the section on basic concepts in radiation heat transfer for additional details on this constant heat flux assumption.

© 1996 Carl Hanser Verlag. All rights reserved.
No unauthorized disclosure or reproduction; licensed to purchaser only.

$$\text{HDPE: } 216\,\frac{\text{Btu}}{\text{lb}} \cdot 0.96 \cdot 62.4\,\frac{\text{lb}}{\text{ft}^3} \cdot 0.1\text{ in} \cdot \frac{1}{1728}\,\frac{\text{ft}^3}{\text{in}^3} = 0.749\,\frac{\text{Btu}}{\text{in}^2}$$

$$\text{ABS: } 45\,\frac{\text{Btu}}{\text{lb}} \cdot 1.05 \cdot 62.4\,\frac{\text{lb}}{\text{ft}^3} \cdot 0.1\text{ in} \cdot \frac{1}{1728}\,\frac{\text{ft}^3}{\text{in}^3} = 0.307\,\frac{\text{Btu}}{\text{in}^2}$$

Energy input per unit time x time = Total energy uptake

$$\text{HDPE: } 12.9\,\frac{\text{W}}{\text{in}^2} \times \text{t (time in h)} \cdot 3.413\,\frac{\text{Btu}}{\text{W} \cdot \text{h}} = 0.749\,\frac{\text{Btu}}{\text{in}^2}$$

$$\text{HDPE: } 12.9\,\frac{\text{W}}{\text{in}^2} \times \text{t (time in h)} \cdot 3.413\,\frac{\text{Btu}}{\text{W} \cdot \text{h}} = 0.307\,\frac{\text{Btu}}{\text{in}^2}$$

Solving for time:

$$\text{HDPE: } t = \frac{0.749}{3.413 \cdot 12.9} = 0.017\text{ h} = 61.2\text{ s}$$

$$\text{ABS: } t = \frac{0.307}{3.413 \cdot 12.9} = 0.00697\text{ h} = 25.1\text{ s}$$

There are many ways of heating sheet to the forming temperature. No heating process is 100% efficient. Regardless of the nature of the polymers, all heating systems must input more specific energy than the amount indicated in Table 3.1. Economics dictate a balance between the efficiency of net energy interchange between the source of heat and the sheet and the net rate of heating to the forming conditions. Where the heating rate controls the cycle time, process optimization usually calls for lowered energy efficiencies. To a large degree, sheet thickness dictates the type of heating that is most effective. Thin sheets are heated quite efficiently with radiant heaters. Thick sheets are best heated in forced convection hot air ovens.

3.3 Heat Transfer Modes

There are three ways of exchanging energy between objects of different temperatures:

Conduction

Conduction is solid phase contact heat transfer. Conduction is the primary way energy moves through plastic sheet and metal molds. Three thermal properties are important in conduction:

- Density,
- Specific heat, heat capacity or enthalpy, and
- Thermal conductivity.

These properties have been reviewed in Chapter 2. In addition, thermal diffusivity is important in time-dependent heat conduction. Thermal diffusivity was also reviewed in Chapter 2.

© 1996 Carl Hanser Verlag. All rights reserved.
No unauthorized disclosure or reproduction; licensed to purchaser only.

Convection

Convection is fluid phase contact heat transfer. Throughout the thermoforming process, the sheet contacts ambient air. Energy is transferred when the air temperature differs from the sheet temperature. Energy transfer depends on the extent of air movement. As expected, energy transfer is low in quiescent air and relatively high when the air is actively moved across the plastic surface. The proportionality between thermal driving force or temperature differential and the amount of heat transferred is called the *convective heat transfer coefficient*. Convection is important when water mist or fog is used to cool the free surface of a formed part[1]. Otherwise, the effect of convection on overall heat transfer is secondary to conduction and radiation.

Radiation

Radiation is electromagnetic energy *interchange* between an energy *source* or hot element and an energy *sink* or cold element. Radiation pervades nature. Electromagnetic energy is usually characterized by the wavelength of the energy. As seen in Fig. 3.2 [2], X-rays and gamma rays are characterized by very short wavelengths. Ultraviolet rays have wavelengths less than 0.4 μm. Visible light wavelength range is 0.4 to 0.7 μm. Near infrared wavelength range is 0.7 to about 2 μm. Far infrared wavelength range is from about 2 μm to 8 μm. Longer wavelength electromagnetic energy includes microwave, short wave radio frequency, long radio frequency and ultrasonic frequency.

Heated metal or ceramic surfaces are used throughout thermoforming to radiantly heat plastic sheet. The majority of energy transfer takes place in the 2 μm to 8 μm wavelength range, or the *far infrared region*. There are several aspects of radiant heat transfer that require careful attention. For example, the efficiency of energy transfer depends on the relative abilities of the source and sink to transfer

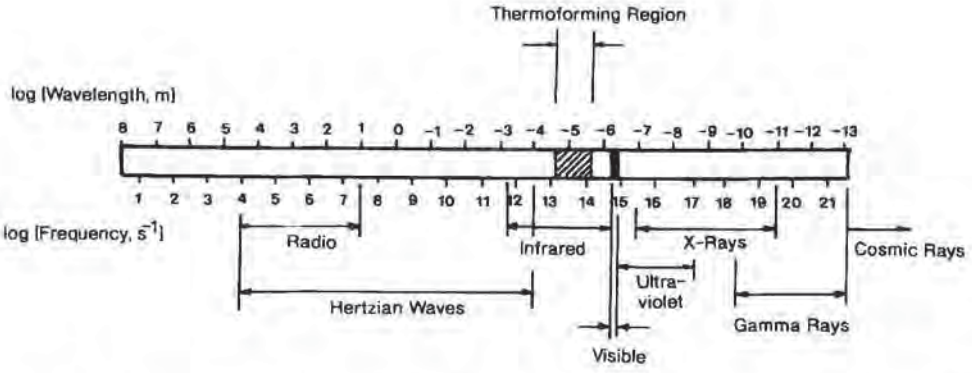

Figure 3.2 Electromagnetic radiation spectrum, showing radio waves, atomic energy, visible light, ultraviolet and infrared domains. Thermoforming region is also shown [2]

[1] Cooling the formed part against the mold is the subject of Chapter 5.

© 1996 Carl Hanser Verlag. All rights reserved.
No unauthorized disclosure or reproduction; licensed to purchaser only.

energy efficiently. Absorptivity and emissivity are terms used to describe this efficiency. For most thermoforming applications, the energy interchange is between the heater surface and the plastic sheet surface. In some cases, energy is transmitted into or through the polymer. In addition, even though the sheet is sandwiched between the heaters, the interchanging elements are not infinite in extent. As a result, the efficiency of energy interchange depends on geometric factors as well as material properties.

Efficient heating and cooling of thermoplastic sheet depends on the balance between the rate of energy input to the sheet surface and the rate of energy conduction from the sheet surface to the centerline. There are two classic cases of time-dependent conduction that illustrate this.

Step Change in Surface Temperature

Consider contact or trapped sheet forming (Fig. 1.5). When the sheet is placed against the isothermal hot plate, its surface temperature immediately increases to the plate temperature (Fig. 3.3). As time increases, energy is conducted to the interior of the sheet. If the sheet is held against the hot surface long enough, the sheet temperature will eventually equal the hot surface temperature everywhere throughout the sheet. If the sheet is heated on both sides as shown in Fig. 3.4, the temperature profile through the sheet will be symmetric about the centerline.

Constant Energy Input to the Sheet Surface

The amount of energy the heaters interchange with the sheet surface per unit area is called *heat flux* (kW/m^2 or $Btu/h \cdot ft^2$). If the energy input is constant, the time-dependent temperature profile of Fig. 3.5 is obtained. This case illustrates some basic concepts in radiation heat transfer to plastic sheet. If the energy input is equal on both sides of the sheet, the time-dependent temperature profile through the sheet is symmetric about the centerline (Fig. 3.6). The temperature profile is again symmetric about the centerline when the sheet is heated on both sides. Unlike the previous case, the sheet surface temperature continues to increase with time. Unlike the previous case, the sheet temperature never reaches a constant value.

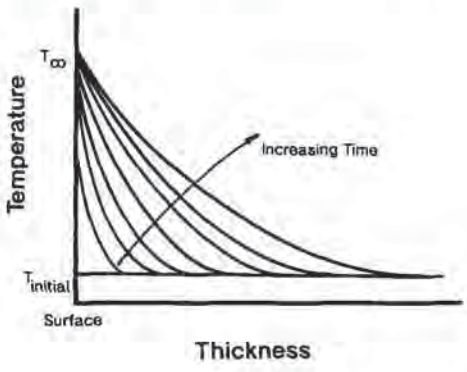

Figure 3.3 Time-dependent temperature profile for conduction into polymer sheet, constant surface temperature indicative of contact heating

© 1996 Carl Hanser Verlag. All rights reserved.
No unauthorized disclosure or reproduction; licensed to purchaser only.

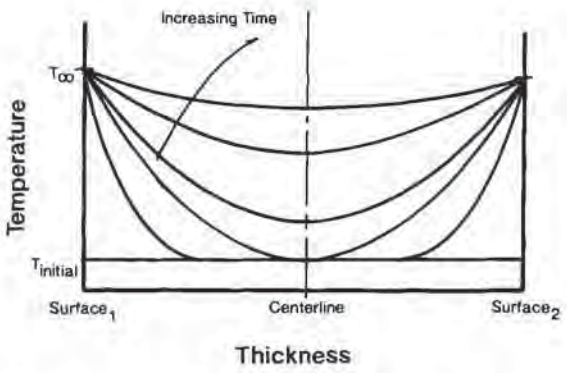

Figure 3.4 Time-dependent temperature profile for two-sided conduction into polymer sheet, constant surface temperature indicative of contact heating

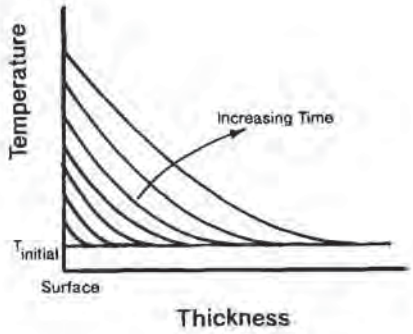

Figure 3.5 Time-dependent temperature profile for conduction into polymer sheet, constant surface heat flux, indicative of radiation heating

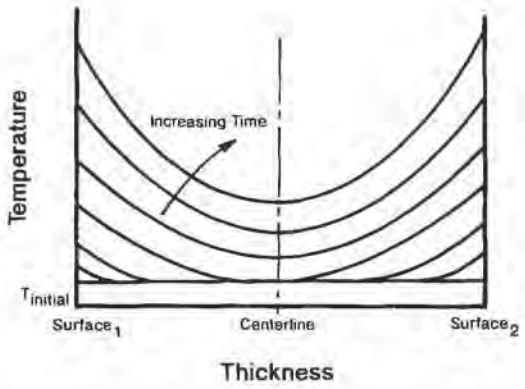

Figure 3.6 Time-dependent temperature profile for two-sided conduction into polymer sheet, constant surface heat flux, indicative of radiation heating

© 1996 Carl Hanser Verlag. All rights reserved.
No unauthorized disclosure or reproduction; licensed to purchaser only.

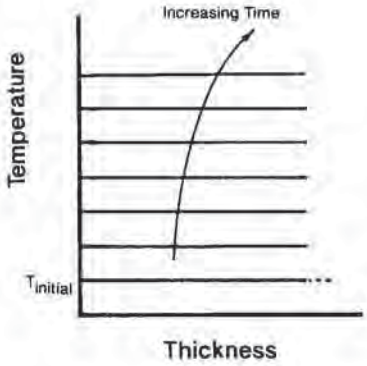

Figure 3.7 Time-dependent temperature profile for conduction into polymer sheet, very low heat flux, very high polymer thermal conductivity or very thin sheet

It is apparent from these two cases that there is an interrelationship or coupling between the energy input to the sheet surface and energy conducted to interior of the sheet. Consider this coupling in concept.

Figure 3.7 is an extreme example of very low heat flux to the sheet surface coupled with very high thermal conductivity or diffusivity or very thin sheet (or both). The temperature profile through the sheet is essentially flat and the centerline temperature essentially equals the surface temperature.

If the energy input to the sheet surface is very high and the polymer thermal conductivity or diffusivity is very low or the sheet is very thick, the sheet surface temperature will appear to reach a fixed temperature nearly instantaneously, as shown in Fig. 3.8 or Fig. 3.3.

Figure 3.9 shows a more typical coupling between sheet surface and internal temperatures.

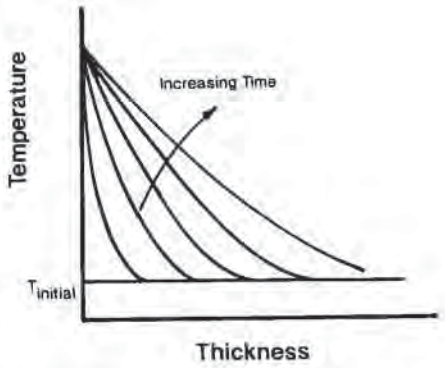

Figure 3.8 Time-dependent profile for conduction into polymer sheet, very high energy input to the surface, low polymer thermal conductivity or very thick sheet

© 1996 Carl Hanser Verlag. All rights reserved.
No unauthorized disclosure or reproduction; licensed to purchaser only.

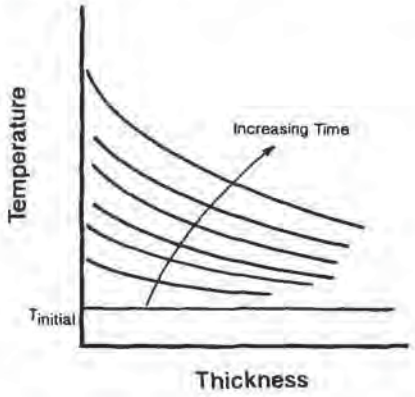

Figure 3.9 Time-dependent profile for conduction into polymer sheet for typical energy flux, polymer properties and nominal sheet thickness ranges

3.4 Incorporating Formability and Time-Dependent Heating

Formability is a key aspect of thermoforming. As seen in Table 2.5, all thermoformable polymers have *forming windows*, defined by the lower, normal and upper forming temperatures (LFT, NFT and UFT). As noted, the lower and upper forming temperatures form the absolute boundaries on formability. Whether a specific polymer can be formed into a specific shape at temperatures near these boundaries depends on:

- The sheet characteristics such as:
  - Intrinsic orientation,
  - Hot strength,
  - Sag tendencies,
  - Thermal sensitivity of the polymer,
  - Sheet geometry and
  - Thickness,
- Uniformity of heating,
- Depth of draw,
- General mold geometry, and
- Other mechanical aspects such as:
  - Transfer time,
  - Ambient air temperature,
  - Plugging geometry,
  - Plug rate,
  - Plug temperature, etc.

Despite these limitations, the upper and lower forming temperatures are useful in defining the nature of the temperature within the sheet. The upper forming temperature relates to the sheet surface. For example, if the upper forming temperature is set because the polymer is prone to blistering or color change above this temperature, the sheet surface temperature must never exceed this value during forming. If the

© 1996 Carl Hanser Verlag. All rights reserved.
No unauthorized disclosure or reproduction; licensed to purchaser only.

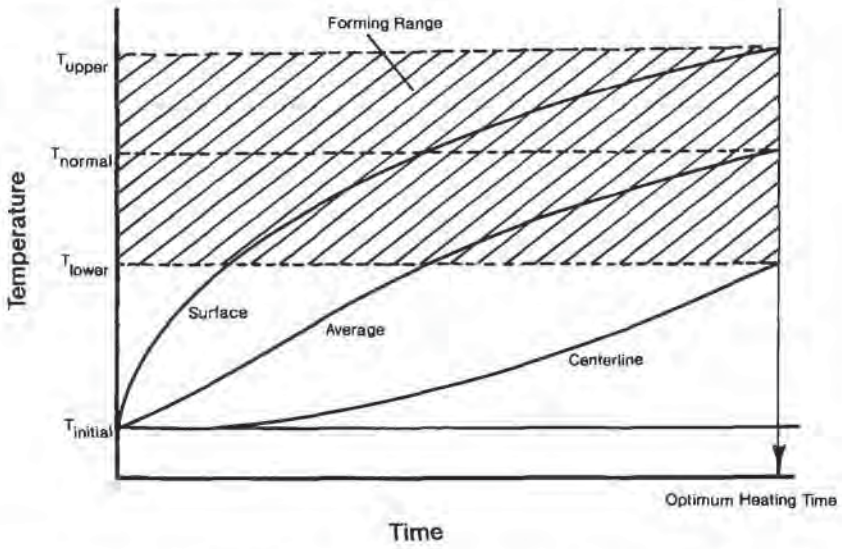

Figure 3.10 Ideal relationship between polymer forming temperature range [shaded area] and time-dependent sheet surface, average and centerline temperatures

lower forming temperature is set because the polymer is too stiff to be formed or because it forms microcracks below this temperature, the centerline temperature must exceed this temperature before the sheet can be formed. The forming temperature range is shown as a time-independent band in Fig. 3.10. Figure 3.10 also shows the superimposition of the time-dependent local temperatures from Fig. 3.8 for the ideal case where the surface temperature reaches the upper forming temperature at the same time the centerline temperature reaches the lower forming temperature. And the average sheet temperature just equals the normal forming temperature at the same time[1].

As an example of the interplay between the sheet characteristics and the time-dependent energy input to the sheet, consider the following examples:

Thin-Gage Sheet

As noted, when the sheet is very thin, energy input to the sheet controls. If the sheet of Fig. 3.10 is dramatically reduced in thickness, the temperature profiles of 3.11 are obtained. Although this profile is entirely acceptable, it is apparent that the rate of heating can be increased substantially without affecting the formability of the polymer (Fig. 3.12).

[1] The shapes of the temperature curves for sheet surface, average and centerline are representative of profiles for sheet heated by radiant or radiant/convective means. The actual shapes depend on the nature of energy input to the sheet surface and the conductive and geometric characteristics of the sheet. See Section 3.15 on predicting temperature profiles for more details.

© 1996 Carl Hanser Verlag. All rights reserved.
No unauthorized disclosure or reproduction; licensed to purchaser only.

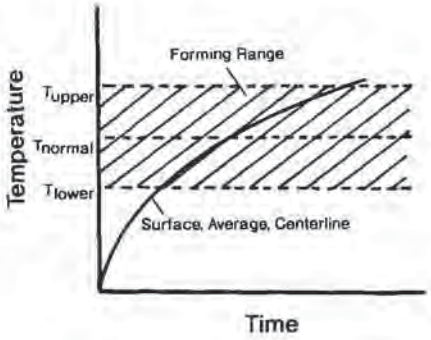

Figure 3.11 Relationship between polymer forming temperature range [shaded area] and timed-dependent sheet surface, average and centerline temperatures for very thin sheet

Heavy-Gage Sheet

When the sheet is very thick, conduction from the sheet surface to the centerline controls. If the sheet of Fig. 3.10 is dramatically increased in thickness, the

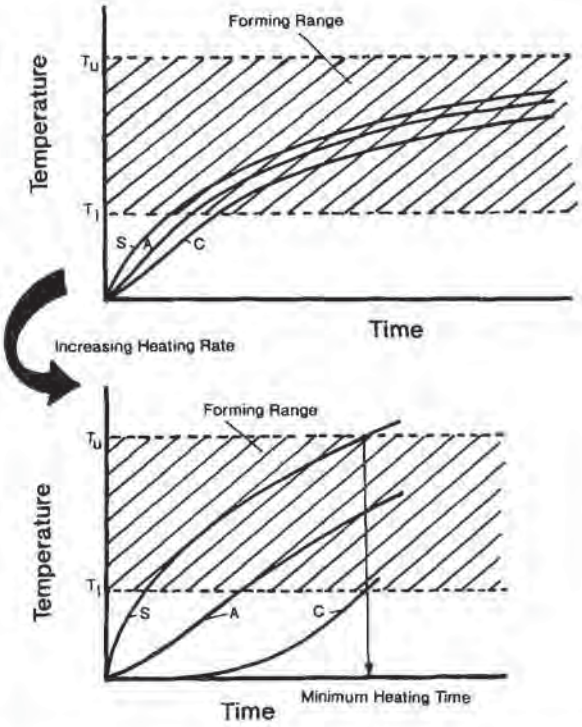

Figure 3.12 Effect of increasing energy input rate on the relationship between polymer forming temperature range [shaded area] and time-dependent sheet surface, average and centerline temperatures for very thin sheet

© 1996 Carl Hanser Verlag. All rights reserved.
No unauthorized disclosure or reproduction; licensed to purchaser only.

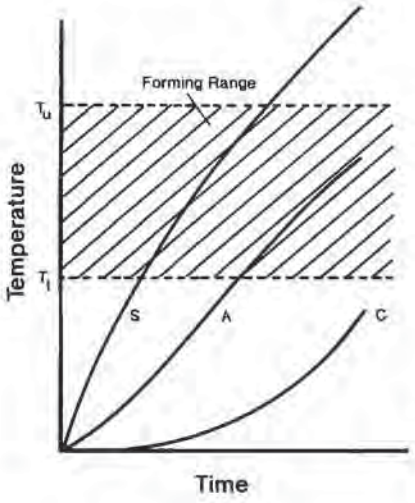

Figure 3.13 Relationship between polymer forming temperature range [shaded area] and time-dependent sheet surface, average and centerline temperatures for very heavy gage sheet

temperature profiles of Fig. 3.13 are obtained. To get the temperatures back into the forming window, the rate of heating must be decreased (Fig. 3.14).

Changing Polymer Characteristics Without Changing Sheet Thickness

If the new polymer has a broader forming window than the old polymer, the rate of heating can be increased without affecting the formability characteristics. If the new polymer has a narrower forming window, the heating rate must be decreased as seen in schematic in Fig. 3.15. If the new polymer has a higher thermal conductivity than the old polymer, as is the case when filled polymers are used, the rate of heating can be increased without affecting the formability characteristics. If the new polymer has a lower thermal conductivity, as may be the case when foamed polymers are used, the heating rate must be decreased.

Changing Other Aspects of the Forming Process

If the new mold requires greater depth of draw than the old one, the sheet may need to be formed at higher temperatures than before. As a result, the forming window may need to be narrowed or the lower forming temperature value increased. The result is that the rate of energy input may need to be reduced and the time to the forming condition extended. If the sheet requires prestretching, time between exiting the oven and completing the stretching may be longer than with straight forming. As a result, the sheet may need to be heated to higher temperatures than before. The rate of heating may need to be reduced and the time to the forming condition extended to increase the average temperature without exceeding the upper forming temperature. Example 3.3 illustrates the interaction of forming temperatures with heating cycle times for ABS and HDPE.

© 1996 Carl Hanser Verlag. All rights reserved.
No unauthorized disclosure or reproduction; licensed to purchaser only.

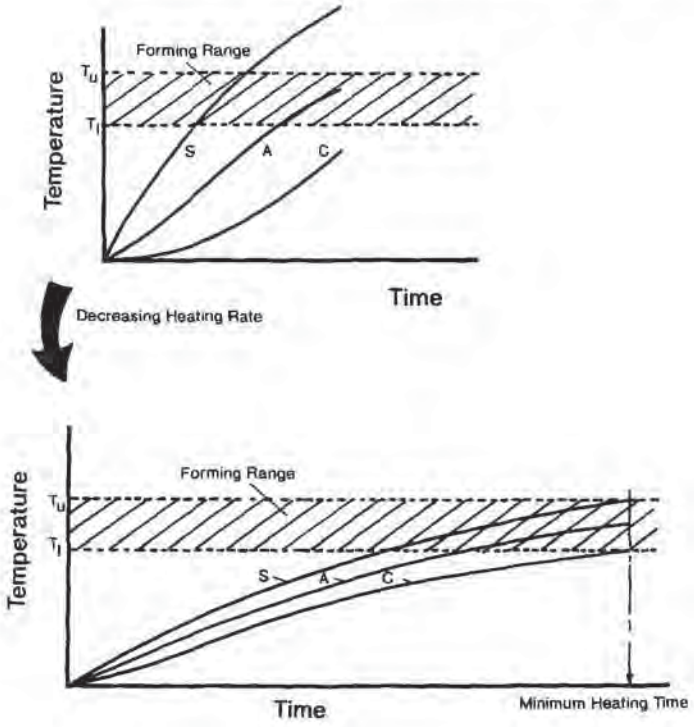

Figure 3.14 Effect of decreasing energy input rate on the relationship between polymer forming temperature range [shaded area] and time-dependent sheet surface, average and centerline temperatures for very heavy gage sheet

Example 3.3 Minimum and Maximum Forming Times

Consider the two polymers of Examples 3.1 and 3.2. Determine the times required to reach lower and upper forming temperatures.

The upper and lower forming temperatures are obtained from Table 2.5 for ABS and HDPE. As is apparent, the lower forming temperature for both is 260°F (127°C) and the upper forming temperature is 360°F (182°C). The enthalpy increases to these temperatures are obtained from Fig. 3.1, as before:

HDPE: LFT: 62 kcal/kg = 112 Btu/lb UFT: 142 kcal/kg = 256 Btu/lb
ABS: LFT: 36 kcal/kg = 65 Btu/lb UFT: 60 kcal/kg = 108 Btu/lb

Since all other factors are equal, the times are obtained by ratio with the values of Example 3.2. The values are tabulated here:

© 1996 Carl Hanser Verlag. All rights reserved.
No unauthorized disclosure or reproduction; licensed to purchaser only.

Polymer	Time (s) to reach		
	Lower forming temperature	Normal forming temperature	Upper forming temperature
HDPE	31.7	61.2	72.5
ABS	20.1	25.1	33.5

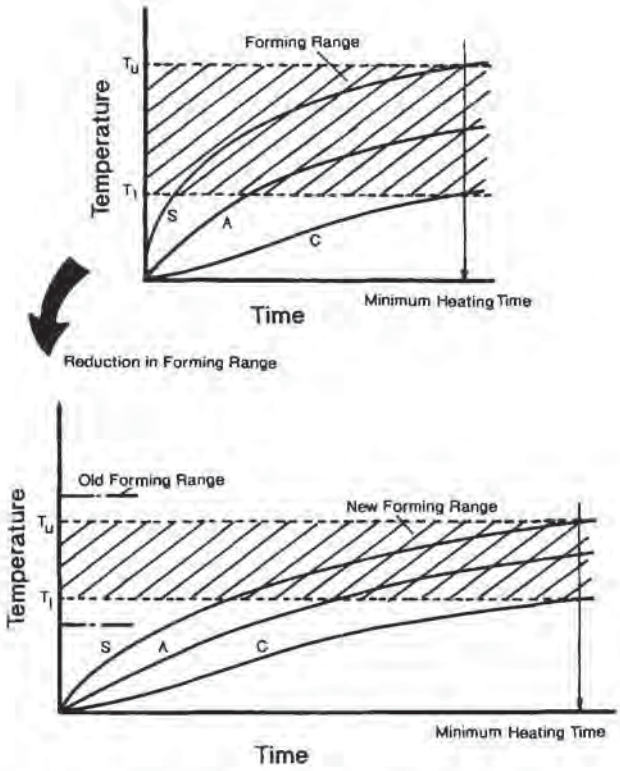

Figure 3.15 Effect of decreasing forming window on the relationship between polymer forming temperature range [shaded area] and time-dependent sheet surface, average and centerline temperatures

These various interactions and the general concepts of coupling of energy input to the sheet surface and conduction into the sheet interior are bundled into a predicting method in as described in Section 3.15. The various elements of this protocol are discussed below and the details of the protocol follow these discussions.

© 1996 Carl Hanser Verlag. All rights reserved.
No unauthorized disclosure or reproduction; licensed to purchaser only.

3.5 Conduction

As noted, conduction is *solid phase energy transfer* on an atomic or molecular level. Owing to high vibrational and rotational mobility of electrons and regular crystallographic structure, metals achieve high levels of conduction energy transfer. Organic materials, on the other hand, have relatively immobile atomic structures and so are poor thermal and electrical conductors. Polymers have even less molecular mobility and in addition, have high free volumes, allowing chain segments to move without contacting other segments. Polymers are therefore very poor thermal and electrical conductors. This was noted in Chapter 2.

Classically, thermoformable sheet is considered as a two-dimensional planar surface with lateral dimensions far greater than its thickness dimension. In the bulk of the analyses that follow, the sheet is assumed to be planar to incident energy. One-dimensional *steady-state heat conduction* across the sheet thickness is given as:

$$\frac{Q}{A} = -k\left(\frac{\Delta T}{\Delta x}\right) \tag{3.3}$$

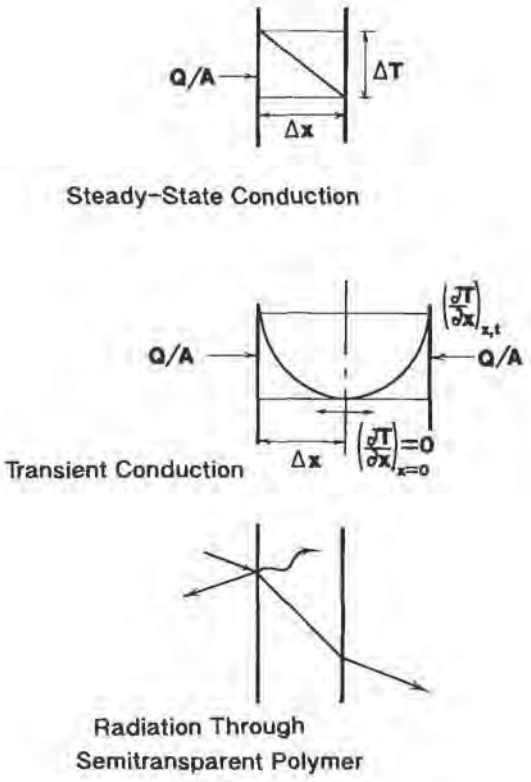

Figure 3.16 Classical temperature profiles through plastics

© 1996 Carl Hanser Verlag. All rights reserved.
No unauthorized disclosure or reproduction; licensed to purchaser only.

where Q/A is the heat flux, k the polymer thermal conductivity, ΔT is the temperature difference and Δx is the sheet thickness (Fig. 3.16). $\Delta T/\Delta x$ is the thermal gradient across the sheet thickness. The dimensions of these terms are:

k	cal/cm · s · °C	Btu/ft · h · °F
Δx	cm	ft
ΔT	°C	°F
Q/A	cal/cm² · s or kW/m²	Btu/ft² · h

Example 3.4 shows the importance of material thermal conductivity in conduction heat transfer. It is apparent that energy conduction through plastic sheet is an important effect.

Example 3.4 Relative Steady-State Temperature Differential

Compare the steady-state temperature difference for 0.3 cm (0.01 ft) thick polystyrene and aluminum for a thermal heat flux of 0.21 cal/cm² · s [8.8 kW/m²].

The thermal conductivity for polystyrene $= 5.8 \times 10^{-4}$ cal/cm · s · °C. That for aluminum is 5.8×10^{-1} cal/cm · s · °C. The temperature difference for polystyrene is:

$$\Delta T = \frac{(Q/A)}{k} = 0.21 \frac{\text{cal}}{\text{cm}^2 \cdot \text{s}} \cdot \frac{1}{5.8 \times 10^{-4}} \frac{\text{cm} \cdot \text{s} \cdot °\text{C}}{\text{cal}} \cdot 0.3 \text{ cm} = 103°\text{C}$$

For aluminum, the temperature difference is:

$$\Delta T = \frac{(Q/A)}{k} = 0.21 \frac{\text{cal}}{\text{cm}^2 \cdot \text{s}} \cdot \frac{1}{5.8 \times 10^{-1}} \frac{\text{cm} \cdot \text{s} \cdot °\text{C}}{\text{cal}} \cdot 0.3 \text{ cm} = 0.10°\text{C}$$

As noted, conduction of energy from the sheet surface to its interior controls the heating rate. The *rate* at which energy transfer occurs is called *transient one-dimensional heat conduction*. The time-dependent net energy increase or decrease equals the change in heat flux within the plastic sheet [3,4]:

$$\text{Net enthalpy change per unit time} = \frac{\partial H}{\partial \theta} \approx \rho c_p \frac{\partial T}{\partial \theta} = \frac{\partial}{\partial x}\left(k \frac{\partial T}{\partial x}\right) = \frac{\partial}{\partial x}\left(\frac{Q}{A}\right) \qquad (3.4)$$

The polymer temperature is now a function of time and position across the sheet thickness, $T(\theta,x)$. Three boundary conditions are needed to solve this equation in most applications:

The Initial Condition

The initial temperature throughout the sheet, $T(\theta = 0, x = L)$ is needed, where L is the half-sheet thickness for equal two-sided heat flux energy input to the sheet surface. Usually the initial sheet temperature is not dependent of thickness for equal two-sided heat flux energy input to the sheet surface. Thus:

$$T(0,L) = T_0 \qquad (3.5)$$

© 1996 Carl Hanser Verlag. All rights reserved.
No unauthorized disclosure or reproduction; licensed to purchaser only.

A Symmetry Condition

When the sheet is heated uniformly from both sides, the centerline forms a plane of symmetry (Fig. 3.5). The energy conducted from one side just equals that conducted from the other side. Thus the heat flux at the symmetry plane is zero, $Q/A = 0$. The condition at the centerline is described as:

$$\left.\frac{\partial T}{\partial x}\right|_{\theta, x = 0} = 0 \tag{3.6}$$

The Surface Condition

The condition at the sheet surface in contact with the heating environment is also required. There are three characteristic conditions:

Conduction, where the sheet directly contacts the heating source. For this condition:

$$T(\theta, x = L) = T_L(\theta) \tag{3.7}$$

Depending on the nature of the heating source, $T_L(\theta)$ can be time-dependent or constant.

Convection, where the sheet contacts a fluid environment. For this condition:

$$\left.\frac{Q}{A}\right|_{\theta, x = L} = -k \left.\frac{\partial T}{\partial x}\right|_{\theta, x = L} = h[T(\theta) - T_\infty(\theta)] \tag{3.8}$$

The term h is the convective heat transfer coefficient. $T(\theta)$ is the sheet surface temperature and $T_\infty(\theta)$ is the temperature of the environment. These temperatures can be time-dependent.

Radiation, where there is energy interchange between the plastic sheet at absolute temperature $T^*(\theta)$ and the heating source at absolute temperature $T^*_\infty(\theta)$. The general form for this boundary condition is:

$$\left.\frac{Q}{A}\right|_{\theta, x = L} = f[T^*(\theta), T^*_\infty(\theta)] = G[T^{*4} - T^{*4}_\infty] \tag{3.9}$$

The function $f[\cdots]$ is highly nonlinear in absolute temperature. The third equality is one representation showing the typical radiation fourth-power relationship, with G including geometry and radiation characteristics of both the heating source and the sheet. Quantification of the term G is given in the radiation section below. Numerical solution of the one-dimensional transient heat conduction equation with the nonlinear radiant heat flux boundary condition is difficult. As discussed below, certain approximations are made to simplify the arithmetic. These approximations also allow more direct comparison of radiation and convetion effects.

Of course, combinations of these boundary conditions are significant as well. Figure 3.16 illustrates some of the characteristics of the temperature profiles through plastics for these various modes of energy transfer.

© 1996 Carl Hanser Verlag. All rights reserved.
No unauthorized disclosure or reproduction; licensed to purchaser only.

3.6 Convection Heat Transfer Coefficient

The convection heat transfer coefficient, h, is defined in Equation 3.8 as a proportionality constant[1]. When the energy source is a fluid, energy is transferred between the bulk moving fluid at temperature T_∞ and the solid surface at temperature T across a thin near-stagnant fluid layer. The heat transfer coefficient is a measure of the resistance to heat transfer across this layer. As the bulk fluid motion increases, the resistance to heat transfer decreases and the value of h increases. Representative ranges for heat transfer coefficients are given in Table 3.2. As is apparent, air is a poor convective heat transfer medium, water is more efficient than air and condensing steam is an excellent heat transfer medium. Example 3.5 shows the linearity between fluid temperature and energy transmitted to the plastic sheet.

Table 3.2 Range in Values for Convection Heat Transfer Coefficient

	Conventional heat transfer coefficient	
Fluid	(10^{-3} W/cm^2 · s · °C)	(Btu/ft^2 · h · °F)
Quiescent air	0.5–1	0.8–2
Air moved with fans	1–3	2–5
Air moved with blowers	3–10	5–20
Air and water mist	30–60	50–100
Fog	30–60	50–100
Water spray	30–90	50–150
Oil in pipes	30–180	50–300
Water in pipes	60–600	100–1,000
Steam in pipes, condensing	600–3,000	1,000–15,000

Example 3.5 Convection Heat Transfer to Plastic Sheet

For a sheet at temperature $T_0 = 100°F$ in hot air at temperature $T_\infty = 200°F$, the heat flux, Q/A, is 200 Btu/ft^2 · h. What is the heat flux when the air temperature, $T_\infty = 300°F$?

The solution uses a ratio of heat flux to temperature difference:

$$\frac{(Q/A)_{300}}{(Q/A)_{200}} = \left(\frac{T_\infty - T_0}{T_\infty - T_0}\right) = \frac{(300-100)}{(200-100)} = 2$$

Or:

$$(Q/A)_{300} = 2 \times 200 = 400 \text{ Btu/ft}^2 \cdot \text{h}.$$

[1] The convection heat transfer coefficient is also important in mold cooling analysis, as detailed in Chapter 5.

© 1996 Carl Hanser Verlag. All rights reserved.
No unauthorized disclosure or reproduction; licensed to purchaser only.

The Biot Number

An important interrelationship between conduction and convection is useful here in determining the relative importance of convection energy. The Biot number, a dimensionless group, is defined as:

$$Bi = \frac{hL}{k} \tag{3.10}$$

where Bi is the Biot number and L is a characteristic sheet dimension, typically the half-thickness. The range on the Biot number is zero to infinity, $0 < Bi < \infty$. Consider the following cases:

- Small Biot number occurs when the sheet thickness is very small, the convection heat transfer coefficient is very small, the sheet thermal conductivity is very large or combinations of these are in effect. Convection controls energy transfer into the sheet. For these conditions, $Bi < 0.1$ or so.
- Large Biot number occurs when the sheet thickness is very great, the convection heat transfer coefficient is great, the sheet thermal conductivity is small or combinations of these are in effect. Conduction into the plastic controls energy transfer into the sheet. For these conditions, $Bi > 1$ or so.

Example 3.6 illustrates the use of this dimensionless group. As expected, the Biot number value for very heavy gage sheet is usually very large. Similarly that for very thin sheet is very small. Usually if the energy transfer between the environment and the sheet surface controls, that is, if Bi is very small, a more efficient means of heating should be sought.

Example 3.6 The Biot Number in Convection Heating

Consider a 0.240 inch (=2L) sheet heated in a high-velocity forced air convection oven where $h = 10$ Btu/ft² · h · F. The thermal conductivity, $k = 0.1$ Btu/ft · h · F. What is the Biot number? Does convection or conduction heat transfer control?

Then consider a 0.024 inch (=2L) sheet heated in natural convection air where $h = 2$ Btu/ft² · h · F. The thermal conductivity, $k = 0.2$ Btu/ft · h · F. Does convection or conduction heat transfer control the heating rate of this sheet?

For the first case, from Equation 3.10,

$$Bi = \frac{hL}{k} = \frac{10}{0.1} \cdot \frac{0.12}{12} = 1$$

Since Bi is large, conduction probably controls the heating rate.

For the second case:

$$Bi = \frac{hL}{k} = \frac{2}{0.2} \cdot \frac{0.012}{12} = 0.01$$

Since Bi is small, convection controls the heating rate.

© 1996 Carl Hanser Verlag. All rights reserved.
No unauthorized disclosure or reproduction; licensed to purchaser only.

Effective Radiation Heat Transfer Coefficient

As noted, the radiant heat flux boundary condition, Equation 3.9, is nonlinear. Example 3.7 shows this strong nonlinearity. In certain instances, the nonlinear radiation condition can be approximated by a *pseudo-convection* condition:

$$Q/A = f(T,T_\infty) \approx h_r(T - T_\infty) \tag{3.11}$$

where h_r is a pseudo-convection heat transfer coefficient or *radiation heat transfer coefficient*. Methods for obtaining values of h_r and ways of combining the value of the radiation heat transfer coefficient with the convection heat transfer coefficient value are detailed below. This approximation is best for high radiant heater temperatures or where $T_\infty > T$. Thin-gage roll-fed sheet formed into products such as cookie trays, blister packs and live plant containers are examples where this approximation is useful[1].

Example 3.7 Radiation Heat Transfer to Plastic Sheet

For a sheet at temperature $T_0 = 100°F$ being heated radiantly from a hot plate at temperature $T_\infty = 200°F$, the heat flux, Q/A, is 200 Btu/ft² · h. What is the heat flux when the plate temperature, $T_\infty = 300°F$? The absolute sheet temperature, $T_0 = 100 + 460 = 560°R$. The absolute plate temperature is either $T_\infty = 200 + 460 = 660°R$ or $T_\infty = 300 + 460 = 760°R$.

The solution uses a ratio of heat flux to temperature difference:

$$\frac{(Q/A)_{300}}{(Q/A)_{200}} = \left(\frac{T_\infty^{*4} - T_0^4}{T_\infty^{*4} - T_0^4}\right) = \frac{(760^4 - 560^4)}{(660^4 - 560^4)} = 2.6$$

Or:

$$(Q/A)_{300} = 2.6 \times 200 = 520 \text{ Btu/ft}^2 \cdot \text{h}.$$

[1] In even more specific cases, the difference between the heater temperature, T_∞, and the sheet surface temperature is so large that the difference in the fourth powers of their absolute temperatures is essentially independent of time. In that case, the heat flux, Q/A, to the sheet surface is assumed to be constant. The resulting equation is:

$$\frac{Q}{A} = f(T,T_\infty) \approx f(T_\infty \text{ only}) \tag{3.12}$$

As seen in Equation 3.9, the temperature gradient at the sheet surface is then constant:

$$-k\frac{\partial T}{\partial x} \approx f(T_\infty \text{ only}) \tag{3.13}$$

The constant heat flux condition represents one of the two ideal cases described earlier. This condition is approximated when roll-forming very thin-gage sheet exposed to very high radiant heater temperatures.

© 1996 Carl Hanser Verlag. All rights reserved.
No unauthorized disclosure or reproduction; licensed to purchaser only.

Constant Heat Flux

In certain instances, $T_\infty \gg T$ and the heat flux can be considered constant, for at least a short portion of the heating cycle:

$$Q/A \approx f(T,T_\infty) \approx f(T_\infty) \tag{3.14}$$

The determination of radiant heater output efficiency is a practical use for the concept of *constant heat flux*. This technique is detailed below.

For very thin sheets that are truly opaque to incident radiation, the *lumped-parameter approximation* is important. If the energy transfer *through* the sheet is secondary to the energy transfer *to* the sheet, the partial differential equation, Equation 3.4, is replaced with a simple ordinary differential equation based on a simple time-dependent heat balance. The lumped-parameter approximation is discussed later in this chapter.

Plastic sheet can be heated to forming conditions by conduction and/or hot air convection energy transfer. In *trapped sheet forming* [5], the sheet contacts a heated, porous blow plate only on one side (Fig. 3.17). The energy is conducted through the sheet and convected to the ambient air on the free surface. Trapped sheet forming is used in thin-gage form-fill-seal operations, when the plastic sheet is very thin, 0.13 mm or 0.005 in or less, when the sheet requires very high forming temperature, and/or when the plastic thermally degrades. The arithmetic for predicting sheet temperature is given below. Thick PMMA and PC sheet is held vertically on rails in large forced convection hot air ovens prior to being *drape-formed* into aircraft canopies [6] and whirlpool spas. Slow convection heating allows very thick sheets to

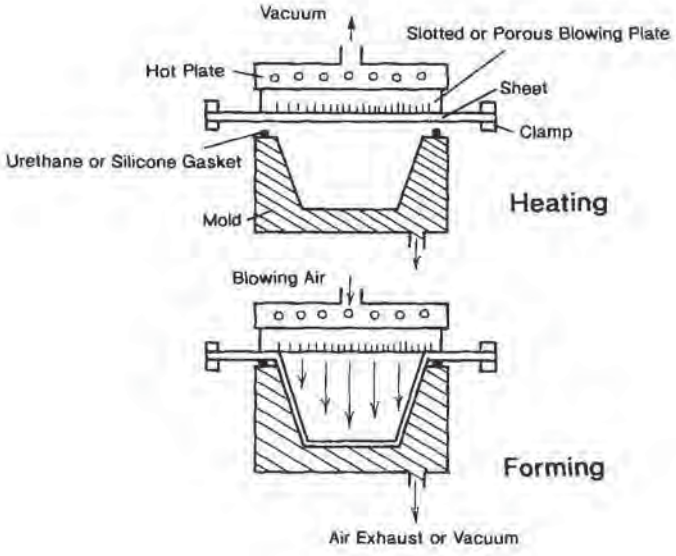

Figure 3.17 Trapped sheet forming, an example of conduction heating of plastic sheet [5]

© 1996 Carl Hanser Verlag. All rights reserved.
No unauthorized disclosure or reproduction; licensed to purchaser only.

thoroughly dry, anneal and stress relieve prior to forming. This gentle treatment minimizes distortion, spring-back and impact crazing. Contact heating accounts for about 15% of the surface area of sheet formed. Convection heating accounts for about 5% with radiant heating representing the remaining 80%.

3.7 Radiation Heating

Radiation is electromagnetic energy transfer between a hot source and a cold sink *that it sees*. Radiation energy transfer does not depend on the distance separating the source and the sink. It is the most energy efficient way of heating planar surfaces but misuse can lead to surface scorching or burn, very uneven temperature distribution through the thickness of the sheet, and energy waste. Most roll-fed and many shuttle thermoformers now heat with radiant sources. Common heating sources are:

- Nichrome spiral wires,
- Steel rod heaters,
- Steel or Nichrome tapes,
- Halogen tube heaters,
- Ceramic plates with embedded resistance wires,
- Ceramic bricks with embedded resistance wires,
- Quartz tube heaters,
- Steel plates that reradiate combustion energy from gas flames,
- Steel wire grids that reradiate combustion energy from gas flames, and
- Direct gas combustion.

Primary radiant heat transfer is correctly a *net energy interchange* between an energy source and energy sink(s). It is apparent that the hot source radiates energy toward the sink, but the sink also radiates energy, albeit weakly, toward the hot source. The primary radiant energy impinging on any surface is either absorbed, reflected or transmitted (Fig. 3.16). If the incident radiant energy is either reflected or absorbed on the surface, the sink is opaque. Other radiation characteristics of materials are given in Table 3.3.

The thermal radiation wavelength range is normally from about 0.1 μm to 20 μm. The ultraviolet or UV region is 0.1 μm to 0.38 μm. The visible light region is 0.38 μm to 0.7 μm. Near-infrared is 0.7 μm to about 3 μm and far-infrared is about 3 μm to 20 μm. The important wavelength range for most radiant thermoforming processes is a portion of the far-infrared range from about 3 μm to about 20 μm. As reference, the sun at an effective surface temperature of about 5500°C [10,000°F] emits more than 90% of its radiation in the wavelength range of 0.1 μm (UV) to 3 μm, or the near-infrared region.

The efficiency of radiant energy interchange depends on several attributes of the source and sink relationship. Some of these are:

© 1996 Carl Hanser Verlag. All rights reserved.
No unauthorized disclosure or reproduction; licensed to purchaser only.

Table 3.3 Radiation Characteristics of Bodies

Nature	Definition
Surface reflection, diffuse	Incident radiation reflected evenly in hemisphere
Surface reflection, specular	Incident radiation reflected preferentially in a given steradian segment of hemisphere
Opaque	Unreflected incident radiant energy absorbed on surface, no transmission
Transparent	All unreflected incident radiant energy transmitted through and out of material
Transparent with internal reflection—light-piping	All unreflected incident radiant energy transmitted through material, partially reflected back from second surface—sometimes specular
Translucent	Properly, semitransparent
Semitransparent	Nonreflected incident radiant energy partially absorbed volumetrically, partially transmitted through sheet
Black body—ideal	All radiant energy totally absorbed at all wavelengths, no energy reflected, no energy transmitted Also, a radiant source that emits the maximum amount of energy at all wavelengths
White body—ideal	In contrast to black body, no radiant energy absorbed at any wavelength, can be either ideally transparent or perfectly reflecting
Gray body—ideal	A fixed fraction of radiant energy absorbed, independent of wavelength

- The efficiencies of the sink and the source in absorbing and emitting radiation,
- The wavelength dependencies of these efficiencies,
- The geometry of the sink and the source and their relative proximities, and
- The absolute temperatures of the sink and the source.

The objective of the sections that follow is to quantify the proportionality constant G in Equation 3.9. An understanding of basic elements of radiation energy interchange is needed to achieve this objective.

Black Body Radiation

The *maximum* total energy emitted by any source at all wavelengths at a given absolute temperature T^* is that emitted by a *black body*:

$$E_b = \sigma T^{*4} \tag{3.15}$$

T^* is the source temperature in $K = °C + 273$ or $°R = °F + 460$. σ is the Stefan-Boltzmann constant having the following units:

$$[\sigma] = 0.5674 \times 10^{-10} \frac{kW}{m^2 \cdot K}$$

$$= 0.1714 \times 10^{-8} \frac{Btu}{ft^2 \cdot h \cdot °R}$$

© 1996 Carl Hanser Verlag. All rights reserved.
No unauthorized disclosure or reproduction; licensed to purchaser only.

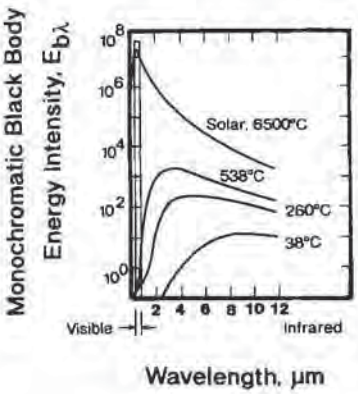

Figure 3.18 Temperature- and wavelength-dependent monochromatic black body energy intensity

E_b is the total energy emitted for all wavelengths, in kW/m^2 or $Btu/ft^2 \cdot h$. All thermoforming radiant sources are referenced to the amount of energy emitted by a black body source.

The wavelength-dependent radiant energy emitted by a black body at temperature T* is given as:

$$E_b = C_1 \cdot \frac{\lambda^{-5}}{[\exp(C_2/\lambda T^*) - 1]} \tag{3.16}$$

where λ is the monochromatic wavelength in μm. The values for C_1 and C_2 are given as:

$$[C_1] = 3.743 \times 10^5 \frac{kW \cdot \mu m^4}{m^2} = 1.187 \times 10^8 \frac{Btu \cdot \mu m^4}{ft^2 \cdot h}$$

$$[C_2] = 1.439 \times 10^4 \, K \cdot \mu m = 2.59 \times 10^4 \, °R \cdot \mu m$$

The wavelength-dependent energy emitted by a black body source at temperature T* is given in Fig. 3.18. The wavelength at which the maximum energy is emitted is given as:

$$\lambda_{max} = a/T^* \tag{3.17}$$

The specific energy emitted at this wavelength is:

$$E_{b,\lambda,max} = C_3 \cdot T^{*5} \tag{3.18}$$

Appropriate values for a and C_3 are:

$$[a] = 2897.6 \, \mu m \cdot K = 5215.6 \, \mu m \cdot °R$$

$$[C_3] = 1.287 \times 10^{-14} \frac{kW}{m^2 \cdot K^5 \cdot \mu m} = 2.161 \times 10^{-13} \frac{Btu}{ft^2 \cdot h \cdot °R^5 \cdot \mu m}$$

Example 3.8 illustrates the energy output from a black body. Nearly 20% of the total emitted energy occurs within 0.5 μm of the peak wavelength value (Equation 3.17). Typical radiant heater temperatures ranges from 400°F to 1500°F or 200°C to 815°C. The total energy emitted by a black body source, the wavelength at maximum energy

© 1996 Carl Hanser Verlag. All rights reserved.
No unauthorized disclosure or reproduction; licensed to purchaser only.

emission and the energy emitted at that wavelength are given in Table 3.4 for several temperatures in this range.

Example 3.8 Energy Output from a Black Body

A black body is at 800°C. Determine the total amount of energy emitted and the amount emitted at the wavelength of maximum energy emission.

The total amount of energy is obtained from Equation 3.15:

$$E_{b,0-\infty} = 0.5674 \times 10^{-10} \cdot (800 + 273)^4 = \frac{75.2\ \text{kW}}{\text{m}^2} = \frac{23{,}880\ \text{Btu}}{\text{ft}^2 \cdot \text{h}}$$

The wavelength of maximum energy emission is given as:

$$\lambda_{max} = 2897.6/(800 + 273) = 2.7\ \mu\text{m}$$

$$E_{b,\lambda,max} = 1.287 \times 10^{-14} \cdot (800 + 273)^5 = \frac{18.3\ \text{kW}}{\text{m}^2 \cdot \mu\text{m}} = \frac{5.817\ \text{Btu}}{\text{ft}^2 \cdot \text{h} \cdot \mu\text{m}}$$

Approximately (5.82/75.2) = 7.7% of the total radiant energy emitted over the entire wavelength spectrum is emitted at exactly 2.7 μm.

Most plastics absorb radiant energy preferentially in specific wavelength ranges as discussed in Chapter 2 and as seen in Table 3.5. To maximize the energy absorbed by the plastic, thermoformer heater temperatures should be set to those correspond-

Table 3.4 Wavelength of Maximum Energy Transmission Black Body Radiation

Temperature		Wavelength	Specific energy at peak wavelength[1]	
(°F)	(°C)	(μm)	(kW/m² · μm)	(Btu/ft² · h · μm)
400	204	6.06	0.32	102
500	260	5.43	0.55	176
600	316	4.92	0.91	289
700	371	4.50	1.43	454
800	427	4.14	2.16	686
900	482	3.84	3.16	1005
1000	538	3.57	4.52	1435
1100	593	3.34	6.28	2000
1200	649	3.14	8.57	2720
1300	704	2.96	11.5	3650
1400	760	2.80	15.1	4810
1500	816	2.66	19.7	6250
1600	871	2.53	25.2	8020
1700	927	2.41	32.0	10,200
1800	982	2.31	40.1	12,700
1900	1038	2.21	49.8	15,800
2000	1093	2.11	61.3	19,500

[1] $E_{b,\lambda,max} = C_3 T^{*5}$ where $C_3 = 1.287 \times 10^{-14}\ \text{kW/m}^2 \cdot \text{k}^5 \cdot \mu\text{m} = 2.161 \times 10^{-13}\ \text{Btu/ft}^2 \cdot \text{R}^5 \cdot \mu\text{m}$

© 1996 Carl Hanser Verlag. All rights reserved.
No unauthorized disclosure or reproduction; licensed to purchaser only.

Table 3.5 Ideal Radiant Heater Temperature Ranges for Several Thermoformable Plastics

Plastic	Ideal wavelength (μm)	Temperature range (°C)	(°F)
LDPE	3.2–3.9	470–630	877–1170
HDPE	3.2–3.7	510–630	950–1170
PS	3.2–3.7	510–630	950–1170
	(6.4–7.4)	120–180	245–355
PVC	3.2–3.6	530–630	990–1170
	(5.7–6.0)	210–235	410–455
PMMA	3.2–3.6	530–630	990–1170
PA-6	3.0–3.2	630–690	1170–1280
PET	3.3–3.6	605–630	1120–1170
	(7.0–9.2	42–140	107–285
Cellulose acetate	5.5–6.0	210–255	410–490
	7.8–10.0	15–100	60–210

ing to these wavelength ranges. The practical upper limit for thermoformer heater temperature is about 1650°F or 900°C. Above this temperature, special materials of construction are needed for the heaters, special reflectors are required, and the high energy level to the polymer sheet makes its temperature control very difficult.

The fraction of energy emitted by a black body source at a given temperature over a given wavelength range is obtained by subtracting values from Fig. 3.19 or Table 3.6 [7]. Examples 3.9 and 3.10 illustrate the usefulness of this approach.

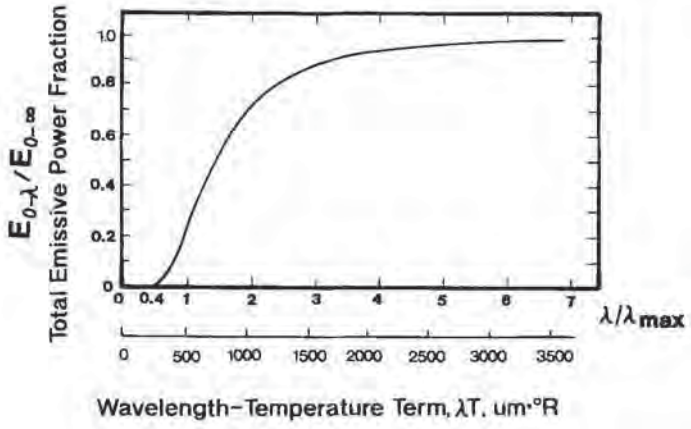

Figure 3.19 Fraction of total emissive power, $E_{0-\lambda}/E_{0-\infty}$, at or below wavelength

© 1996 Carl Hanser Verlag. All rights reserved.
No unauthorized disclosure or reproduction; licensed to purchaser only.

Table 3.6 Radiation Functions [7]

λT^*	$\frac{E_{\lambda,b}}{\sigma T^{*5}} \times 10^5$	$\frac{E_{b,0-\lambda T^*}}{\sigma T^{*4}}$	λT^*	$\frac{E_{\lambda,b}}{\sigma T^{*5}} \times 10^5$	$\frac{E_{b,0-\lambda T^*}}{\sigma T^{*4}}$
0	0	0	8200	8.293	0.5727
1000	0.000394	0	8400	7.954	0.5890
1200	0.001184	0	8600	7.624	0.6045
1400	0.01194	0	8800	7.304	0.6195
1600	0.0618	0.0001	9000	6.995	0.6337
1800	0.2070	0.0003	9200	6.697	0.6474
2000	0.5151	0.0009	9400	6.411	0.6606
2200	1.0384	0.0025	9600	6.136	0.6731
2400	1.791	0.0053	9800	5.872	0.6851
2600	2.753	0.0098	10000	5.619	0.6966
2800	3.872	0.0164	10200	5.378	0.7076
3000	5.081	0.0254	10400	5.146	0.7181
3200	6.312	0.0368	10600	4.925	0.7282
3400	7.506	0.0506	10800	4.714	0.7378
3600	8.613	0.0667	11000	4.512	0.7474
3800	9.601	0.0850	11200	4.320	0.7559
4000	10.450	0.1051	11400	4.137	0.7643
4200	11.151	0.1267	11600	3.962	0.7724
4400	11.704	0.1496	11800	3.795	0.7802
4600	12.114	0.1734	12000	3.637	0.7876
4800	12.392	0.1979	12200	3.485	0.7947
5000	12.556	0.2229	12400	3.341	0.8015
5200	12.607	0.2481	12600	3.203	0.8081
5400	12.571	0.2733	12800	3.071	0.8144
5600	12.458	0.2983	13000	2.947	0.8204
5800	12.282	0.3230	13200	2.827	0.8262
6000	12.053	0.3474	13400	2.714	0.8317
6200	11.783	0.3712	13600	2.605	0.8370
6400	11.480	0.3945	13800	2.502	0.8421
6600	11.152	0.4171	14000	2.416	0.8470
6800	10.808	0.4391	14200	2.309	0.8517
7000	10.451	0.4604	14400	2.219	0.8563
7200	10.089	0.4809	14600	2.134	0.8606
7400	9.723	0.5007	14800	2.052	0.8648
7600	9.357	0.5199	15000	1.972	0.8688
7800	8.997	0.5381			
8000	8.642	0.5558			

Example 3.9 Energy Emitted in a Narrow Wavelength Range

Consider an 800°C = 1472°F black body emitter. Determine the fraction of total energy emitted in the wavelength range of 2 μm to 4 μm. Repeat this for a 700°C = 1292°F source.

© 1996 Carl Hanser Verlag. All rights reserved.
No unauthorized disclosure or reproduction; licensed to purchaser only.

The term $\lambda T^* = 2 \cdot (1472 + 460) = 3864$. From Table 3.6, the fraction of energy emitted between 0 and 2 μm is given as:

$$E_{b,0-2} = 9.14\%$$

For λT^* at 4 μm, the fraction of energy emitted between 0 and 4 μm is:

$$E_{b,0-4} = 53.14\%$$

Thus the amount of energy emitted between 2 μm and 4 μm is $(53.1 - 9.1) = 44\%$ of the total amount.

For a 700°C source, the energy fractions at 2 μm and 4 μm are, respectively:

$$E_{b,0-2} = 5.9\%$$

$$E_{b,0-4} = 45.3\%$$

And the amount of energy emitted between 2 μm and 4 μm is $(45.3 - 5.9) = 39.4\%$ of the total.

Example 3.10 Energy Emitted in The Thermoforming Wavelength Range

Consider an 800°F ceramic heater. Assume it emits as a black body. Determine the fraction of total energy emitted in the normal thermoforming wavelength range of 3.5 μm to 9 μm.

The term $\lambda T^* = 3.5 \cdot (800 + 460) = 4410$. From Table 3.6, the fraction of energy emitted between 0 and 3.5 μm is given as:

$$E_{b,0-3.5} = 15.1\%$$

For λT^* at 9 μm, the fraction of energy emitted between 0 and 9 μm is:

$$E_{b,0-9} = 76.2\%$$

Thus the amount of energy emitted in the 3.5 μm to 9 μm thermoforming wavelength range is $(76.2 - 15.1) = 61.1\%$ of the total amount.

Gray Body—Emissivity

No practical material emits at black body energy levels. Many materials, including nearly all polymers, emit at 80% to 95% of the maximum level, however. A *gray body* is one that emits energy at a fixed fraction of the total black body energy level:

$$E_g = \epsilon \cdot \sigma T^{*4} \tag{3.19}$$

where ϵ is *emissivity*, $0 < \epsilon < 1$. If the fraction of energy emitted by the material is wavelength-dependent, $\epsilon = \epsilon(\lambda)$. Emissivities are usually wavelength-dependent for real surfaces (Fig. 3.20). The total energy is obtained from integration:

$$E_{g,\,total} = \sigma T^{*4} \cdot \int_0^\infty \epsilon(\lambda)\, d\lambda \tag{3.20}$$

© 1996 Carl Hanser Verlag. All rights reserved.
No unauthorized disclosure or reproduction; licensed to purchaser only.

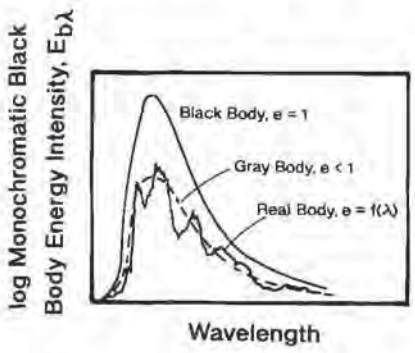

Figure 3.20 Comparison of wavelength-dependent monochromatic energy intensity for black, gray and real bodies

As an approximation, emissivity can be considered constant over specific ranges in wavelength. The individual energies in each of these range segments are then summed to obtain the total energy:

$$E_{g,total} = \frac{\sigma T^{*4}}{(\lambda_N - \lambda_1)} \cdot \sum_{j=1}^{N-1} \epsilon_j(\lambda_{j+1} - \lambda_j) \tag{3.21}$$

The individual black body energies are obtained from Fig. 3.19. In Table 3.7 [8] are given some wavelength-dependent emissivities and absorptivities for materials found in many thermoforming operations. For many materials, however, only an average value is known. Usually polished or very smooth surfaces emit at much lower energy levels, $0 < \epsilon < 0.3$, than pitted, oxidized, rusted, matte or irregular surfaces, $0.8 < \epsilon < 0.95$. The emissivity of a plastic sheet should be determined at its temperature whereas its energy absorption efficiency or *absorptivity*, α, should be determined at the emitter temperature. Strictly speaking, $\alpha \neq \epsilon$, but practically α and ϵ are assumed equal.

All surfaces radiate energy. The maximum amount of energy absorbed by the plastic sheet is determined from a net radiant energy balance between the gray-body source, emitter or heater and the gray-body sink, the polymer sheet:

$$\frac{Q}{A} = \sigma F_g(T_x^{*4} - T_s^{*4}) \tag{3.22}$$

T_x^* is the absolute heater temperature and T_s^* is the sheet temperature, in K or °R. Again σ is the Stefan-Boltzmann constant. F_g is a factor that corrects black-body energy for the gray-body nature of the emitter or heater, ϵ_h, and the source or sheet, ϵ_s. For planar heaters and flat sheet, F_g, the *gray body correction factor*, is:

$$F_g = \left[\frac{1}{\epsilon_h} + \frac{1}{\epsilon_s} - 1\right]^{-1} \tag{3.23}$$

$F_g = 1$ when both surfaces are black bodies. Examples 3.11 and 3.12 illustrate the relative effect of F_g on the energy interchange efficiency. About 21% of the energy interchange occurs in the absorption wavelength regions of 3.2-3.7 μm and 6.4-7.4 μm that are ideal for styrenics such as PS, HIPS and ABS. Other examples of gray-body correction factors are given below.

© 1996 Carl Hanser Verlag. All rights reserved.
No unauthorized disclosure or reproduction; licensed to purchaser only.

Table 3.7 Emissivities and Absorptivities for Various Materials Used in Thermoforming[1]

Material	Emission values at various temperatures and peak wavelength				Absorption values
	38°C (100°F) 9.3 μm	260°C (500°F) 5.4 μm	538°C (1000°F) 3.6 μm	1371°C (2500°F) 1.8 μm	
Aluminum					
Polished	0.04	0.05	0.08	0.19	0.26
Oxidized	0.11	0.12	0.18	–	–
Anodized	0.94	0.42	0.60	0.34	–
Chromium					
Polished	0.08	0.17	0.26	0.40	–
Iron, steel					
Polished	0.06	0.08	0.13	0.25	0.45
Cast, oxidized	0.63	0.66	0.76	–	–
Galvanized					
New	0.23	–	–	0.42	0.66
Dirty	0.28	–	–	0.90	0.89
Steel plate	0.94	0.97	0.98	–	–
Oxide	0.96	–	0.85	–	0.74
Steel tube, oxidized	–	0.80	–	–	–
Stainless steel					
Polished	0.15	0.18	0.22	–	–
Weathered	0.85	0.85	0.85	–	–
Tungsten filament	0.03	–	–	0.18	–
Paper, white	0.95	–	0.82	0.25	0.27
Plaster	0.91	–	–	–	–
Enameled steel, white	–	–	–	0.65	–
Paints					
Black lacquer	0.96	0.98	–	–	0.97–0.99
Oil, all colours	0.94	0.90	–	–	–
White, ZnO	0.95	–	0.91	–	0.12–0.26
Water	0.96	–	–	–	–
Wood	0.93	–	–	–	–
Glass	0.90	–	–	–	–

[1] From [40] with permission of copyright owner; absorption values for solar radiation from [41]

Example 3.11 Gray-Body Correction Factor—I

Consider an 800°C = 1472°F heating source with an emissivity of $\epsilon_x = 0.95$ interchanging energy with ABS at 20°C = 68°F. The ABS is semi-matte finish with $\epsilon_s = 0.85$. Determine the energy interchange and compare it with the black-body energy interchange value.

© 1996 Carl Hanser Verlag. All rights reserved.
No unauthorized disclosure or reproduction; licensed to purchaser only.

From Equation 3.23, $F_g = 0.814$. The black-body energy interchange is obtained from Equation 3.22, with $F_g = 1$.

$$E_{b,total} = 0.5674 \times 100 \times [1.073^4 - 0.293^4] = 74.8 \text{ kW/m}^2$$

The gray-body energy interchange is:

$$E_{g,total} = 0.814 \cdot 74.8 = 60.9 \text{ kW/m}^2.$$

The gray-body energy interchange is 81.4% efficient.

Example 3.12 Gray-Body Correction Factor—II

Using the information of Example 3.9, determine the energy interchange when the sheet temperature is 150°C = 302°F. Then determine the amount of energy absorption in the preferential absorption wavelength ranges of 3.2 μm to 3.7 μm and 6.4 μm to 7.4 μm.

From Equation 3.23, $F_g = 0.814$. The black-body energy interchange is obtained from Equation 3.22 with $F_g = 1$.

$$E_{b,total} = 0.5674 \times 100 \times [1.073^4 - 0.423^4] = 73.4 \text{ kW/m}^2$$

The gray-body energy interchange is:

$$E_{g,total} = 0.814 \cdot 73.4 = 59.7 \text{ kW/m}^2.$$

The gray-body energy interchange at this temperature is about 98% as efficient as that when the sheet is at room temperature.

The energy interchange between the source and the sink follows the details of Example 3.9. Consider the heater first. $\lambda T^* = 3.2 \cdot (1472 + 460) = 6182$ and $3.7 \cdot (1472 + 460) = 7148$. Then $\lambda T^* = 6.4 \cdot (1472 + 460) = 12{,}365$ and $7.4 \cdot (1472 + 460) = 14{,}297$. From Table 3.6, the following black-body energies are obtained:

$$E_{b,0-3.2} = 36.9\% \quad E_{b,0-3.7} = 47.6\% \quad E_{b,0-6.4} = 80.0\% \quad E_{b,0.7.4} = 84.5\%$$

The percentage of total black-body energy emitted in these wavelength ranges is:

$$E_{b,ranges} = (84.5 - 80.0) + (47.6\text{-}36.9) = 15.2\%$$

The actual amount of black-body energy emitted in these wavelengths is:

$$E_{b,heater} = 0.152 \cdot 56.74 \cdot 1.073^4 = 11.43 \text{ kW/m}^2$$

Consider the sheet. $\lambda T^* = 3.2 \cdot (302 + 460) = 2438$ and $3.7 \cdot (302 + 460) = 2819$. Then $\lambda T^* = 6.4 \cdot (302 + 640) = 4877$ and $7.4 \cdot (302 + 460) = 5639$. From Table 3.6, the following black body-energies are obtained:

$$E_{b,0-3.2} = 6.1\% \quad E_{b,0-3.7} = 17.3\% \quad E_{b,0-6.4} = 20.8\% \quad E_{b,0.7.4} = 30.3\%$$

The percentage of total black-body energy emitted in these wavelength ranges is:

$$E_{b,ranges} = (30.3 - 20.8) + (17.3 - 6.1) = 20.7\%.$$

© 1996 Carl Hanser Verlag. All rights reserved.
No unauthorized disclosure or reproduction; licensed to purchaser only.

The black-body energy emitted in these wavelengths is:

$$E_{b,sheet} = 0.207 \cdot 56.74 \cdot 0.423^4 = 0.38 \text{ kW/m}^2$$

The total black-body energy interchange is then:

$$E_{b,heater} - E_{b,sheet} = 11.43 - 0.38 = 11.05 \text{ kW/m}^2$$

The total gray-body energy interchange in these wavelength ranges is:

$$E_{g,inter} = F_g \cdot 11.05 = 9.0 \text{ kW/m}^2$$

The total efficiency in these wavelength ranges, based on total black-body emitter energy is:

$$\frac{E_{g,inter}}{E_{b,0-\infty}} = \frac{100 \cdot 9.0}{75.2} = 12\%$$

In addition to a correction factor for the nonblack nature of the source and sink, a correction factor is usually needed to compensate for the relative sheet and heater geometries. The radiation correction factor or "view factor", F, is unity when both the heater and sheet surfaces are considered as infinite planar surfaces. The view factor is unity when the sheet can be considered as completely enclosed by the heater. The nonplanar nature of heater surfaces and the energy losses at the sheet edge usually yield values of the view factor, F, that are less than unity. These cases are described below.

When gray-body and geometry effects are included, the general net radiant energy balance between the source and the sink is written as:

$$\frac{Q}{A} = \{\sigma F F_g\} \cdot (T_\infty^{*4} - T_s^{*4}) \tag{3.24}$$

Radiant Heater Efficiency—Constant Heat Flux Application

Consider a square aluminum plate, L units on a side by t units thick (Fig. 3.21). The aluminum plate weight is known, $m = \rho \cdot L^2 t = (2.7 \text{ g/cm}^3) \cdot L^2 t$. Its heat capacity from Table 2.5 is $c_p = 0.224$ cal/g °C [Btu/lb °F]. The plate is mounted on a thermally insulated rod such as a broom handle. A thermocouple is embedded in the center of the plate and its output is monitored on a strip chart recorder. The plate is sprayed with matte black oven paint to increase emissivity to approximately unity ($\epsilon \approx 1$). The room temperature plate is put in the radiant oven and its temperature measured for several seconds over a 20°C (or so) temperature range near room temperature. A heat balance on the plate is:

$$mc_p \frac{dT}{d\theta} = A\left(\frac{Q}{A}\right) \approx A\{\sigma F F_g\} T_\infty^{*4} \tag{3.25}$$

The second approximation is assumed since $T_\infty \gg T$. A is the plate area, $A = 2L^2$. The areas of the plate edges are ignored. $T = T_0$ when $\theta = 0$. This equation is integrated to yield:

© 1996 Carl Hanser Verlag. All rights reserved.
No unauthorized disclosure or reproduction; licensed to purchaser only.

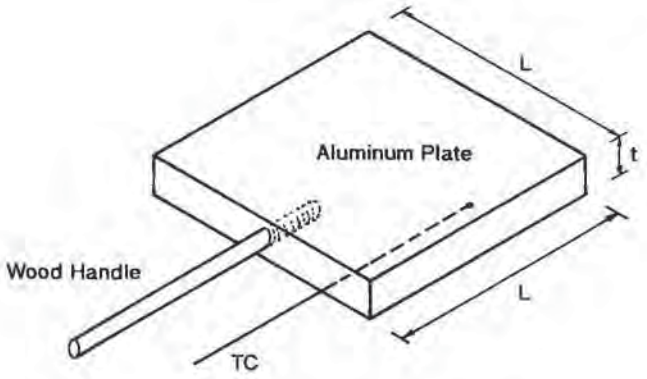

Figure 3.21 Aluminum plate used to determine heat flux from local heaters

$$T = T_0 + \left[\frac{\{\sigma F F_g\} T_\infty^{*\,4}}{(mc_p/A)}\right]\theta = T_0 + \left[\frac{\{\sigma F F_g\} T_\infty^{*\,4}}{(\rho t c_p/2)}\right]\theta \tag{3.26}$$

For very short times, $\theta < 10$ s, the plate temperature increases linearly with time, with the slope of the temperature curve containing information about the efficiency of the radiant heating source. Example 3.13 illustrates the use of this equation in determining the energy output of radiant heaters. Heaters are rated in 'watt density' or Watts per unit area of heater surface. The units of watt density are W/cm^2 or W/in^2. This is a direct measure of the consumption of electric power. The efficiency of conversion of electricity to heat is illustrated in Example 3.13 as well. The application of the concept of constant heat flux illustrates a practical way of measuring and monitoring radiant heater performance.

Example 3.13 Radiant Heater Efficiency

Consider a 6-in × 6-in aluminum plate, 0.125 in thick. It is heated on both sides from 100 to 125°F in 9.43 s by exposure to ceramic heaters having a measured temperature of 600°F. Determine the radiant heater efficiency. Determine the efficiency of energy conversion if the heaters are rated as 8 W/in^2 at 600°F.

The plate mass is given as:

$$m = \rho \cdot L^2 t = 0.439 \text{ lb} = 199 \text{ g}.$$

The increase in energy in the plate is:

$$q = m \cdot c_p \cdot dT = 199 \text{ g} \cdot \frac{0.224 \text{ cal}}{\text{g} \cdot °\text{C}} \cdot \frac{(125 - 100)}{1.8} °\text{C} = 619 \text{ cal}$$

The rate of increase is:

$$q/\theta = 619/9.43 \text{ s} = 65.7 \text{ cal/s}$$

© 1996 Carl Hanser Verlag. All rights reserved.
No unauthorized disclosure or reproduction; licensed to purchaser only.

The heat flux to the plate is:

$$\frac{q/\theta}{A} = 65.7 \frac{cal}{s} \cdot \frac{1}{2 \cdot 15.2^2\ cm^2} = 0.142 \frac{cal}{cm^2 \cdot s} = 0.595 \frac{W}{cm^2} = 1885 \frac{Btu}{ft^2 \cdot h} = 3.83 \frac{W}{in^2}$$

The ideal heat flux from this source temperature is obtained from:

$$\frac{Q}{A} = \sigma T_{\infty}^{*4} = 0.164 \frac{cal}{cm^2 \cdot s} = 0.685 \frac{W}{cm^2} = 2172 \frac{Btu}{ft^2 \cdot h} = 4.42 \frac{W}{in^2}$$

The radiant heater efficiency is given as:

$$\text{Efficiency} = 100 \cdot \frac{3.83}{4.42} = 87\%$$

The energy conversion efficiency is given by the ratio of the energy actually emitted by the heater to the rated heater efficiency. For the heater rating of 8 W/in², the energy conversion efficiency is:

$$\text{Energy Conversion Efficiency} = 100 \cdot \frac{3.83}{8} = 47.9\%$$

3.8 Real Heaters—Efficiencies

As noted earlier, only a fraction of the energy supplied by utility companies to the thermoforming machine is converted to radiant energy to heat the sheet (Fig. 3.22) [9]. Efficiencies of actual radiant heating sources are given in Table 3.8. The efficiencies of various types of heating sources for various polymers are given in Table 3.9. These values represent net efficiencies. The energy conversion from power source to radiant thermal energy at the heater surface is relatively efficient (Example 3.13). Quartz heaters are more efficient at higher temperatures (Fig. 3.23). About 50% of the electrical power input is converted to radiant energy at 316°C or 600°F. Essentially all is converted at 900°C or 1650°F. As seen in Table 3.8, tubular and spiral wire heaters have similar efficiencies at about 50% when new. Gas combustion efficiency at 900°C or 1650°F for one type of surface infrared burner is reported to be 82% to 84% [10], with an average heat flux at this temperature of 236.5 kW/m² or 75,000 Btu/ft² · h. The ideal black body energy emitted at this temperature is 107.4 kW/m² or 33,970 Btu/ft² · h.

Other types of surface burners show efficiencies somewhat lower than this. Note in Table 3.8 that the effective surface heat fluxes for most gas-fired burners operating at very high temperatures are substantially greater than the values predicted by black body radiation. Convective energy transfer is apparently a major factor with these burners. Since all radiant heaters operate in an air environment, convection losses from heater surfaces reduce heater efficiency, sometimes by as much as 30% to 50%.

© 1996 Carl Hanser Verlag. All rights reserved.
No unauthorized disclosure or reproduction; licensed to purchaser only.

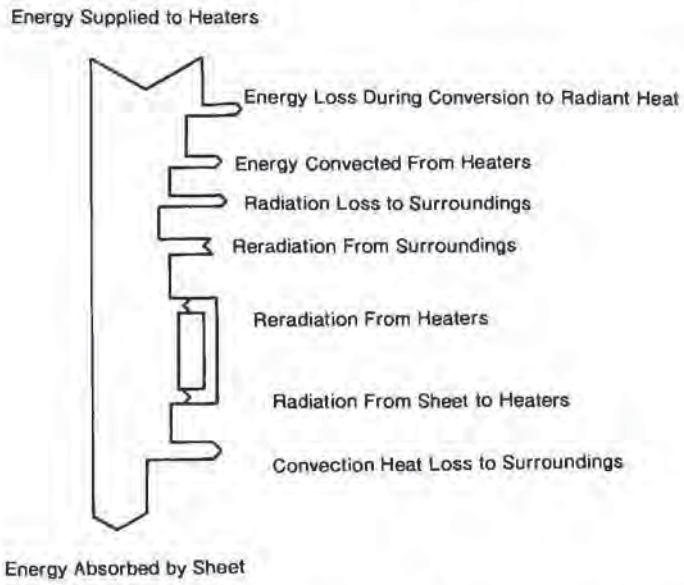

Figure 3.22 Schematic of heat transfer energy distribution in thermoforming operation [9]. Figure used by permission of Society of Plastics Engineers, Inc.

An estimate of the convection heat loss is detailed below. Heaters radiant energy to *all visible surfaces*, including:

- Plastic sheet,
- Reflectors,
- Other heaters,
- Rails,
- Sheet clamping devices,
- Heater guards,
- Objects outside the oven edges,
- Oven sidewalls, and
- Shields and baffles.

As much as 20% to 30% of the energy emitted by radiant heaters is lost to the environment in this way. Further, a fraction of net radiant energy absorbed by the plastic sheet is convected to the cooler air environment from the hot sheet itself. Thus, only about 20% to 50% of the power supplied by the utility is converted into increasing the enthalpy of the sheet. The actual efficiency depends on:

- Matching source temperature with plastic radiation absorption range,
- Minimizing all thermal sinks other than the plastic sheet, and
- Controlling the convective energy losses from heater and sheet surfaces.

© 1996 Carl Hanser Verlag. All rights reserved.
No unauthorized disclosure or reproduction; licensed to purchaser only.

Table 3.8 Efficiencies of Commercial Radiant Heating Sources[1]

Radiant source	Maximum energy		Maximum temperature		Black body energy		Maximum efficienty	Response time		Comments
								Heating	Cooling	
	(kW/m²)	(Btu/ft² · h)	(°C)	(°F)	(kW/m²)	(Btu/ft² · h)	(%)			
Bulb:										
R-40 reflector	16.1	5120	2200	4000	2140	678,000	<1	3s	10s	Spot output, color sensitive
G-30 bulb	6.4	2030	2200	4000	2140	678,000	<1	3s	10s	Needs reflector, color sensitive
Ceramic spot	1.4	1535	870	1600	97.3	30,900	1.4	5–10 min	5–10 min	Spot output
Quartz lamp	310	98295	2200	4000	2140	678,000	14.5	3s	10s	Needs reflector, color sensitive, seals may need cooling, must be kept clean
Tube:										
Metal sheated	46.5	14745	870	1600	97.3	30,900	48	5 min	5 min	Needs reflector, surface exposed, airflow causes large heat loses, resists shock, vibration
Quartz tube	77.5	24575	980	1800	141	44,700	55	1 min	20s	Needs reflector
Strip:										
Quartz faced	58.1	18430	760	1400	64.7	20,500	90	2–4 min	2–4 min	
Panel:										
Coated glass	14.1	4555	315	600	6.8	2,200	1	5 min	5 min	Very even heating, low temperature leads to airflow losses
Fiberglass	12.9	4095	595	1100	32.0	10,200	40	5 min	5 min	Even heating, can be zoned
Metal sheath	31	9830	595	1100	32.0	10,200	97	5 min	5 min	See comments on metal sheathed tube
Ceramic faced	31	9830	760	1400	64.7	20,500	48	5–10 min	5–10 min	Available with soft or hard face

[Refs. on p. 194]

© 1996 Carl Hanser Verlag. All rights reserved.
No unauthorized disclosure or reproduction; licensed to purchaser only.

Quartz or hard ceramic	62	19660	980	1800	141	44,700	44	5–20 min	5–20 min		Thermally shock sensitive
Exposed foil	59.2	18770	815	1500	79.7	25,300	74	4s	10s		Shock hazard, convective heat losses can be high
GaS-IR impingment:											
Ceramic plate	1890	600000	1260	2300	314	99,400	3–5[1]	1–3 min	2–4 min		Efficiency decrease increased output
Gas-IR surface burn:											
Ceramic plate	252	80000	930	1700	117.7	37,300	20–55[3]	2–3 min	2–3 min		Same as above
Screen	126	4000	870	1600	97.7	30,900	20–55[3]	1 min	1 min		Same as above, screen maintenance can be a problem
Ceramic fiber	148	47000	900	1650	107.7	34,000	33–65[2,3]	4–8s	4–8s		Emitter can be damaged by force or fluids
Catalytic	15.8	5000	370	700	9.8	3,100	20–55[3]	30 min	30 min		Low temperature, emitter can be damaged by force or fluids

[1] Adapted from [42], with copyright permission
[2] Greater than 100%
[3] Listed efficiency, but greater than 100% of black body efficiency for given temperature

© 1996 Carl Hanser Verlag. All rights reserved.
No unauthorized disclosure or reproduction; licensed to purchaser only.

Radiative Heat Transfer Coefficient

Convective energy losses are determined with an energy balance around all solid surfaces, including the heater and plastic sheet. The effect of radiation heat transfer must be included as well. This is done by examining the surface boundary condition for the transient one-dimensional heat conduction (Equation 3.9):

$$\frac{Q}{A} = -k \left.\frac{\partial T}{\partial x}\right|_{(\theta,L)} = f[T, T_\infty, F, F_g, \epsilon_h, \epsilon_s] \tag{3.27}$$

For radiation absorption (only) on a solid surface, $x = L$, the proper form for $f[\cdots]$ is:

$$f[T, T_\infty, F, F_g, \epsilon_h, \epsilon_s] = \{\sigma F F_g\}[T_\infty^{*4} - T^{*4}] \tag{3.28}$$

As noted, the radiation boundary condition is nonlinear, unlike the convection boundary condition that is linear with temperature, $f[\cdots] = h(T_\infty - T)$. For certain cases, the radiation nonlinearity can be dealt with by letting $T^* = a \cdot T_\infty^*$, where a is a proportionality. Then $f[\cdots]$ becomes:

$$f[T, T_\infty, F, F_g, \epsilon_h, \epsilon_s] \approx h_r(T_\infty - T) \tag{3.29}$$

where h_r, a *radiation heat transfer coefficient*, is given as:

$$h_r = \{\sigma F F_g\} T_\infty^{*3}(a + 1)(a^2 + 1) = F F_g \cdot R \tag{3.30}$$

where R is the radiation factor (Fig. 3.24). Note that the proportionality a is *not* constant but varies with the absolute value of the sheet temperature. If a is very small, or $T_\infty^* \gg T^*$ throughout the heating cycle, R is approximately constant. Further if a does not vary much throughout the heating cycle, values of R are determined at the beginning and end of the heating cycle and an average value or R

Table 3.9 Radiant Heater Efficiencies for Several Polymers[1]

Polymer	Heater type			
	Ceramic 510°C (950°F) 4.0 μm	Metal rod 550°C (1022°F) 3.8 μm	Quartz 680°C (1256°F) 3.0 μm	Quartz 760°C (1400°F) 2.8 μm
LDPE	13%	15%	17%	20%
HPDE	13%	15%	17%	20%
PS	13%	15%	17%	20%
PVC	5%	5%	22%	25%
PMMA	0%	2%	50%	65%
PA-6	30%	28%	24%	28%
Cellulose acetate	18%	28%	48%	56%
For the typical gray body thermoforming wavelength range, 1.4 to 3.6 μm	28%	33%	70%	77%

[1] Adapted from [33]

© 1996 Carl Hanser Verlag. All rights reserved.
No unauthorized disclosure or reproduction; licensed to purchaser only.

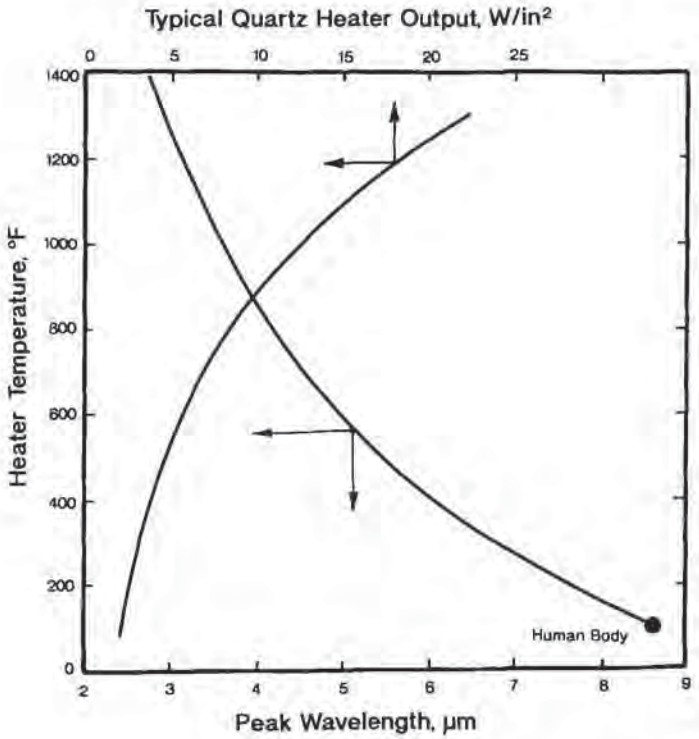

Figure 3.23 Temperature-dependent peak wavelength and quartz heater output

is used. Example 3.16 illustrates the use of the radiation factor. As is apparent, the value of R increases with increasing heater temperature and increasing sheet temperature. In the example, a 200°F increase in heater temperature results in a 29% increase in the rate of heating. Similarly increasing the sheet temperature to the forming temperature results in a 20% to 30% increase in heating rate. Typically, the average value for R is accurate to within 15% to 20% of the actual value. To obtain a value for the radiation heat transfer coefficient, h_r, the average value of R must be corrected for the gray-body interchange factor, F_g and the view factor, F. As a result, the actual value for the radiation heat transfer coefficient, h_r, can be substantially less than the value for R. Typical values for h_r are 1 to 10 times those for moving air convection heat transfer coefficients in Table 3.2. The use of the artificial radiation heat transfer coefficient should be restricted to problems where rapid solutions and approximate answers are acceptable.

Convection and the Heat Transfer Coefficient

Air trapped between the heater banks and the plastic sheet surfaces is very slow moving or quiescent. It therefore attains a nearly isothermal temperature having a

© 1996 Carl Hanser Verlag. All rights reserved.
No unauthorized disclosure or reproduction; licensed to purchaser only.

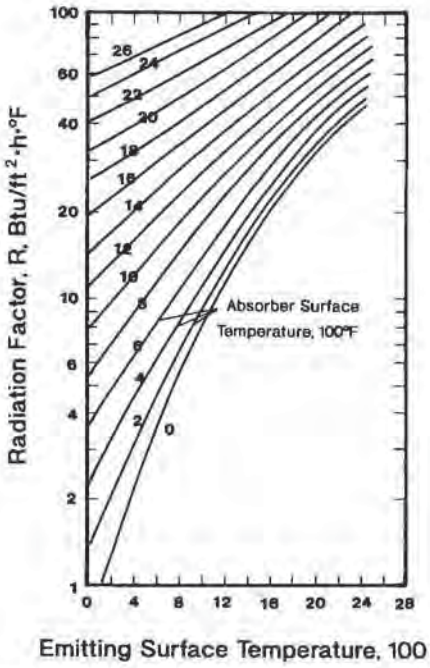

Figure 3.24 Source and sink temperature-dependent radiation heat transfer coefficient

value somewhere between that of the sheet surface value and that of the radiant source. The nature of energy transfer is by rising, buoyant warm air and settling cool air. This is *natural convection*. The natural convection heat transfer coefficient is obtained from:

$$h = K\left(\frac{\Delta T}{G}\right)^{1/4} \tag{3.31}$$

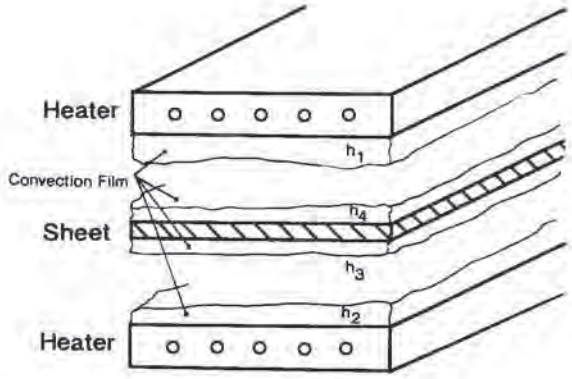

Figure 3.25 Location of various convection heat transfer coefficients between sheet and top and bottom heaters

© 1996 Carl Hanser Verlag. All rights reserved.
No unauthorized disclosure or reproduction; licensed to purchaser only.

Table 3.10 Convection Heat Transfer Coefficients for Natural Convection from Flat Plates and Rods $h = K\left(\frac{\Delta T}{G}\right)^{1/4}$

Geometry/attitude	K_{metric} (h in kW/m² · °C) (ΔT in °C) (G, D, L in m)	$K_{English}$ (h in Btu/ft² · h · °F) (ΔT in °F) (G, D, L, in ft)
Heat plate (G = L)		
Facing upward	0.00149	0. 263
Facing downward	0.000746	0.131
Rod (G = D)	0.001533	0.27
	0.002839[1]	0.50[1]

[1] From reference [43]

G is the length of the plate heater or the diameter of a rod heater. σT is the temperature difference between the hot surface and the air. The proportionality constant K depends on the heater geometry G and whether the heater faces up or down (Table 3.10). Example 3.14 illustrates the method of calculation for the convection heat transfer coefficient. The range of 0.5 to 2 Btu/ft² · h · °F or 2.8×10^{-3} to 11.3×10^{-3} kW/m² · °C is typical of natural convection heat transfer coefficients for quiescent air (Table 3.2). The range is a factor of 10 or so less than the typical range for forced air convection heat transfer coefficients and 20 times less than those for radiation heat transfer coefficients. Note that if the air is hotter than the plastic sheet, energy is convected to the sheet. If the sheet is hotter than the air, as in Example 3.15, energy is convected from the sheet. A combined convection and radiation heat transfer coefficient is written as:

$$h_{effective} = h + h_r \tag{3.32}$$

Example 3.14 The Radiation Factor

Consider heating a plastic sheet initially at 80°F to 400°F using a heating source at 800°F. Determine the initial and final values of the radiation factor. Obtain an average value. Increase heater temperature to 1000°F and recalculate values.

From Fig. 3.24, at 800°F, the initial value of $R_i = 6.0$ Btu/ft² · h · °F. The final value of $R_f = 8.1$. The average value of $R_a = 7.05$ Btu/ft² · h · °F.

From Fig. 3.24, at 1000°F, $R_i = 8.15$, $R_f = 10.05$ and $R_a = 9.1$ Btu/ft² · h · °F.

Example 3.15 Convection Heat Transfer Coefficient

Consider 200°F air trapped between a 300°F sheet and a 800°F heater. The sheet is sandwiched between two heaters. Determine the heat transfer coefficients between the air and the sheet and the air and the heaters. G = 1.

© 1996 Carl Hanser Verlag. All rights reserved.
No unauthorized disclosure or reproduction; licensed to purchaser only.

There are actually *four* heat transfer coefficients to consider, as shown in Fig. 3.25:

h_1 (heater, facing down) $= 0.131 \cdot (800 - 200)^{1/4} = 0.65$ Btu/ft$^2 \cdot$ h $\cdot$ °F
h_2 (heater, facing up) $= 0.263 \cdot (800 - 200)^{1/4} = 1.30$ Btu/ft$^2 \cdot$ h $\cdot$ °F
h_3 (sheet, facing down) $= 0.131 \cdot (300 - 200)^{1/4} = 0.41$ Btu/ft$^2 \cdot$ h $\cdot$ °F
h_4 (sheet, facing up) $= 0.263 \cdot (300 - 200)^{1/4} = 0.83$ Btu/ft$^2 \cdot$ h $\cdot$ °F

The range is 0.4 to 1.3 Btu/ft$^2 \cdot$ h $\cdot$ °F.

Example 3.16 shows how the effective heat transfer coefficient changes in value as the sheet is heated. In this idealized case, the radiation contribution to the overall heat transfer coefficient overwhelms the convection contribution. In practical thermoforming, the radiation contribution is diminished by values of F and F_g that are less than unity. Nevertheless, in most cases, radiation heat transfer dominates the overall heat transfer coefficient.

Example 3.16 Combined Heat Transfer Coefficient

Given the conditions of Examples 3.14 and 3.15, determine the effective heat transfer coefficient. Assume that $F = F_g = 1$.

The initial sheet temperature is 80°F with a 200°F air temperature and a radiant heater temperature of 800°F. The final sheet temperature is 400°F with a 200°F air temperature and the same radiant heater temperature.

From Example 3.14, the radiation heat transfer coefficients are $R_i = 6.0$ Btu/ft$^2 \cdot$ h $\cdot$ °F and $R_f = 8.1$. There are four initial convection heat transfer coefficients and four final ones. Only the values between the sheet and the air are important here:

$h_{1,i}$ (heater, facing down) $= 0.131 \cdot (800 - 200)^{1/4} = 0.65$ Btu/ft$^2 \cdot$ h $\cdot$ °F
$h_{2,i}$ (heater, facing up) $= 0.263 \cdot (800 - 200)^{1/4} = 1.30$ Btu/ft$^2 \cdot$ h $\cdot$ °F
$h_{3,i}$ (sheet, facing down) $= 0.131 \cdot (200 - 80)^{1/4} = 0.43$ Btu/ft$^2 \cdot$ h $\cdot$ °F
$h_{4,i}$ (sheet, facing up) $= 0.263 \cdot (200 - 80)^{1/4} = 0.87$ Btu/ft$^2 \cdot$ h $\cdot$ °F

$h_{1,f}$ (heater, facing down) $= 0.131 \cdot (800 - 200)^{1/4} = 0.65$ Btu/ft$^2 \cdot$ h $\cdot$ °F
$h_{2,f}$ (heater, facing up) $= 0.263 \cdot (800 - 200)^{1/4} = 1.30$ Btu/ft$^2 \cdot$ h $\cdot$ °F
$h_{3,f}$ (sheet, facing down) $= 0.131 \cdot (200 - 400)^{1/4} = -0.49$ Btu/ft$^2 \cdot$ h $\cdot$ °F
$h_{4,f}$ (sheet, facing up) $= 0.263 \cdot (200 - 400)^{1/4} = -0.99$ Btu/ft$^2 \cdot$ h $\cdot$ °F

Note that the signs on the convection coefficients indicate the way in which energy is being transferred.

The initial and final effective heat transfer coefficients, $h_{e,i}$ and $h_{e,f}$, are:

$h_{e,i}$ (sheet, facing up) $= R_i + h_{4,i} = 6.0 + 0.87 = 6.87$ Btu/ft$^2 \cdot$ h $\cdot$ °F
$h_{e,i}$ (sheet, facing down) $= R_i + h_{3,i} = 6.0 + 0.43 = 6.43$ Btu/ft$^2 \cdot$ h $\cdot$ °F
$h_{e,f}$ (sheet, facing up) $= R_f + h_{4,f} = 8.1 - 0.49 = 7.61$ Btu/ft$^2 \cdot$ h $\cdot$ °F
$h_{e,f}$ (sheet, facing down) $= R_f + h_{3,f} = 8.1 - 0.99 = 7.11$ Btu/ft$^2 \cdot$ h $\cdot$ °F

An effective heat transfer coefficient can also be obtained from an overall heat balance on a given plastic sheet. Effective values in Table 3.11 are obtained from

© 1996 Carl Hanser Verlag. All rights reserved.
No unauthorized disclosure or reproduction; licensed to purchaser only.

Table 3.11 Rod Heater Reflector Efficiencies—Effective Heat Transfer Coefficients[1]

Material	Emissivity	Heater temperature (°C)	Reflector temperature (°C)	Convection heat transfer ($kW/m^2 \cdot °C$)
Gold, new	0.92	690	320	0.0244
Gold, aged	–	683	323	0.0176
Stainless steel, new	0.60	686	304	0.0125
Stainless steel, aged	–	668	352	0.0142
Aluminum, new	0.30	719	274	0.0199
Aluminum, aged	–	693	287	0.0199

[1] Adapted from [11], with permission

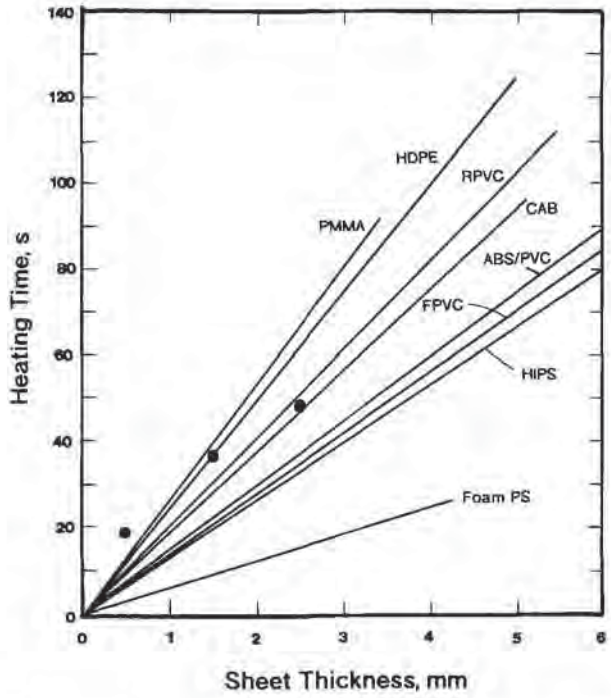

Figure 3.26 Two-sided quartz heating of sheet. Heat flux = 40 kW/m^2 or 12,700 $Btu/ft^2 \cdot h \cdot °F$, peak wavelength = 2.8 μm, heater temperature = 760°C or 1400°F. Solid points obtained at heat flux = 43 kW/mm^2 or 12,700 $Btu/ft^2 \cdot h \cdot °F$, peak wavelength = 3.7 μm, heater temperature = 510°C or 950°F

thin-gage heating rate data of Fig. 3.26 and typical forming conditions. Values range from about 4.5 to 9.7 $Btu/ft^2 \cdot h \cdot °F$ or 0.0255 to 0.0548 $kW/m^2 \cdot °C$. If the convection contribution is essentially constant at about 1 $Btu/ft^2 \cdot h \cdot °F$ or 0.005 $kW/m^2 \cdot °C$, the radiation contribution is about 4 to 9 times that of the convection

© 1996 Carl Hanser Verlag. All rights reserved.
No unauthorized disclosure or reproduction; licensed to purchaser only.

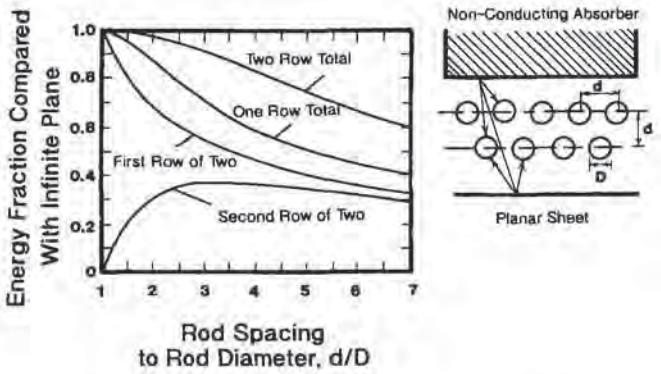

Figure 3.27 Radiation between metal rod heaters and planar sheet [41]. Figure used by permission of McGraw-Hill Book Co., Inc.

contribution[1]. Further, if the average black-body net radiant interchange yields an effective radiation heat transfer coefficient of about 10 to 15 Btu/ft^2 · h · °F or 0.05 to 0.075 kW/m^2 · °C, the radiant interchange efficiency is about 40% to 60%. This efficiency is the product of the gray-body factor, F_g, and the view factor, F. This efficiency agrees reasonably well with values that are discussed below. These effective heat transfer coefficient values are typical of experimental data obtained in other ways [11].

Rod Heaters

Rod heaters, with or without reflectors, are used to heat sheet in many thermoformers. The energy emitted from rod heaters is related to that emitted by a heated plane. Figure 3.27 assumes that the surface behind the rod heaters is nonconducting. Example 3.17 illustrates how to determine the relative energy efficiency of rod heaters. As is apparent, the closer the heaters are to one another, the more efficient the energy transfer becomes. The gray-body correction factor F_g for gray surface radiation between a plane and a tube bank is:

$$F_g = \epsilon_\infty \cdot \epsilon_s \tag{3.33}$$

Example 3.17 Rod Heater Efficiency

Consider a single row of rod heaters 0.5 in or 12.7 mm in diameter, spaced 3 in or 76 mm apart. Determine the relative energy efficiency as compared with a flat plate. Change the spacing to 1.5 in or 38 mm and recompute.

[1] Note that this assumes that the convection energy transfer is from the air to the sheet, with the air temperature hotter than the sheet temperature. Obviously if the convection contribution is negative, the radiation effect is 6 to 11 times greater.

© 1996 Carl Hanser Verlag. All rights reserved.
No unauthorized disclosure or reproduction; licensed to purchaser only.

Fig. 3.27 requires the determination of R, the ratio of center-to-center distance to the diameter.

$$R = 3/0.5 = 6$$

From Curve B of Fig. 3.27, F = 0.46 or the heating is 46% as efficient as from a flat plate.

For R = 1.5/0.5 = 3, F = 0.73 or 73% as efficient.

Example 3.18 compares the gray-body correction factors for rod and plate heaters. Usually the gray-body correction factor values are quite comparable. However, the rod heater efficiency is low when compared with the flat plate, as also shown in Example 3.18. Radiant energy loss from the back of rod heaters is minimized by reflectors. New aluminum and gold-fired porcelain enamel give the greatest reflector efficiencies. However efficiencies deteriorate with age. Stainless steel appears to provide the best long-term efficiency (Table 3.11). The effective heat transfer coefficient from the top of the reflector is essentially independent of reflector material and reflector temperature (Fig. 3.28). The range in heat transfer coefficient is about 2 to 4 Btu/ft^2 · h · °F or 0.01 to 0.02 kW/m^2 · °C. Essentially all of this is reradiation from the reflectors.

Example 3.18 Gray-Body Correction Factor for Rod Heater

Compare the values for F_g for flat plates and rod heaters if $\epsilon_\infty = 0.9$ and $\epsilon_s = 0.85$. Then determine the relative gray-body efficiencies.

From Equation 3.33, $F_{g,rod} = 0.9 \cdot 0.85 = 0.765$
From Equation 3.23, $F_{g,plate} = [1/0.85 + 1/0.9 - 1]^{-1} = 0.777$
The two factors are essentially the same.
From Example 3.17, at 1.5-in spacing of 0.50-in diameter rods, the rod efficiency is 0.73. As a result,

$$\text{Rod efficiency} = 0.73 \cdot 0.765 = 0.558$$
$$\text{Plate efficiency} = 1 \cdot 0.777 = 0.777$$

Or the hot plate transfers nearly 40% more energy than the rod heaters.

3.9 Long-Term Radiant Heater Efficiencies

Radiant heater efficiency decreases with time as seen in Table 3.12. The values represent overall efficiencies or effective energy conversion for several commercial heaters. Efficiency is thought to decrease exponentially with time as a first-order system response:

$$\eta = \eta_0 \, e^{-a\theta} \tag{3.34}$$

© 1996 Carl Hanser Verlag. All rights reserved.
No unauthorized disclosure or reproduction; licensed to purchaser only.

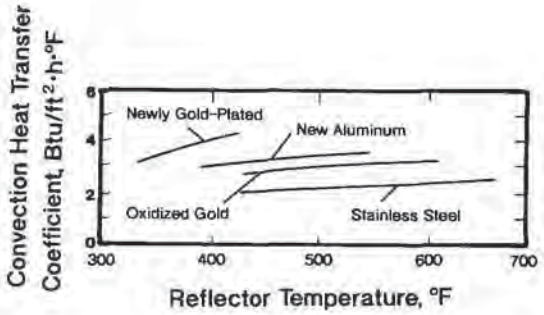

Figure 3.28 Convection heat transfer coefficients for metal rod heaters with reflectors

where a is the time constant of the heater, in month^{-1}. The expected efficiencies of heaters at various times are shown in Table 3.12[1].

Since heater efficiency is directly related to the radiant heat transfer coefficient, any decrease in heater efficiency at constant heater temperature increases the time to achieve sheet forming temperature. Since heater efficiency loss is gradual, cycle times can lengthen imperceptibly over weeks. Usually power input or heater temperature is gradually increased to compensate for the decrease in efficiency. An increase in heater temperature results in a reduction in the peak wavelength and this effect might result in heating in the less efficient regions of the infrared spectrum. Since efficient sheet heating is a key to optimum economic performance, all heater manufacturers now recommend strict, scheduled periodic replacement of all elements, regardless of their apparent performance.

3.10 Edge Losses—View Factor

Net radiant energy interchange between ideal infinite parallel heat sources and sinks does not depend on the distance between them. This is not the case for finite dimensions of heaters and sheets. The spacing between the plane of the heater and that of the sheet surface affects the efficiency of energy transfer. So long as the sheet width dimension is much larger than the sheet-to-heater spacing dimension, radiation losses to machinery elements are small. The relative amount of energy actually received by the sheet depends on the ability of the heater to "see" the sheet. In simple terms:

What the heater sees is what it heats

[1] These values assume that the heaters are still functioning at these times.

© 1996 Carl Hanser Verlag. All rights reserved.
No unauthorized disclosure or reproduction; licensed to purchaser only.

Table 3.12 Commercial Radiant Heater Overall Efficiencies[1]

Heater type	η_0, efficiency		Average life (h)	Time constant a ($month^{-1}$)	Efficiency at end of life	Expected efficiency[3]		
	new	after 6 months[2]				12 mo	18 mo	24 mo
Coiled wire, nichrome	16–18	8–10	1500	0.0926–0.1155	11–13	4–4.5	2–2.3	1–1.1
Tubular rod[4]	42	21	3000	0.1155	19	10.5	5.3	2.6
Ceramic panel	62	55	12,000–15,000	0.02	31–36	49	43	38
Quartz heater	55	48	8,000–10,000	0.0227	33–36	42	37	32
Gas-fired IR panel	40–45	25	5,000–6,000	0.0926–0.104	11–12	13	7	4

[1] Adapted from [6], with copyright permission
[2] One month = 440 h, assumed for time constant only
[3] After 6 months use, 4–8% efficiency can be gained by replacing all reflectors
[4] Sanding, polishing increases efficiency by 10–15%

© 1996 Carl Hanser Verlag. All rights reserved.
No unauthorized disclosure or reproduction; licensed to purchaser only.

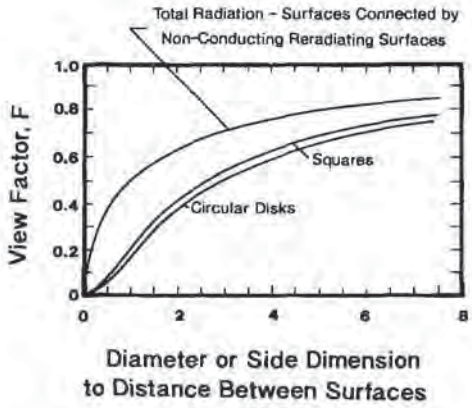

Figure 3.29 Radiation view factor for radiant interchange between parallel surfaces

The radiant energy interchange between black bodies of equal finite dimension connected by reradiating walls is given as Fig. 3.29. The factor F is called a radiation factor or "view factor" and typically has a value less than one. Furthermore, F varies across the sheet surface. Example 3.19 illustrates the effect of sheet-to-heater spacing on the view factor. To obtain the proper net energy interchange value between gray surfaces, this view factor must then be multiplied by the gray-body correction factor, F_g. Example 3.19 includes the relative effect. The energy that is not transmitted to the sheet is lost to the surroundings and is called "edge losses". In Example 3.19, edge losses amount to 36% for the wide spacing and 23% for the narrow spacing. The edge loss is reduced if the side walls reradiate or reflect. Although spacing is used to control the heating characteristics of the sheet without changing the heater temperature, it is now recognized that this is an inefficient use of energy. Heater spacing is usually governed by sheet sag and minimization of sheet "striping" or local overheating beneath rod and quartz heaters.

Example 3.19 View Factor and Edge Losses

Consider a 600 mm × 600 mm sheet being heated with a 600 × 600 mm plate heater. Ignore edges. What is the view factor F, from Fig. 3.29, for sheet-to-heater spacing for 150 mm? For 75 mm? What are the equivalent values if the sides reradiate?

Then consider a gray-body correction factor for $\epsilon_\infty = 0.9$ and $\epsilon_s = 0.85$.

R = side/spacing = 600/150 = 4. From Fig. 3.29, F = 0.64. For R = 600/75 = 8, F = 0.77.

For reradiating sides, $F_{R=4} = 0.765$. $F_{R=8} = 0.86$. An oven with reradiating sides is 19% more efficient at R = 4 than one that has no reradiating sides. It is 12% more efficient at R = 8.

© 1996 Carl Hanser Verlag. All rights reserved.
No unauthorized disclosure or reproduction; licensed to purchaser only.

The gray-body correction factor, $F_g = [1/0.9 + 1/0.85 - 1]^{-1} = 0.777$. The adjusted efficiencies, $\eta = FF_g$, are now:

$$\eta_{R=4} = 100 \cdot 0.64 \cdot 0.777 = 49.7\% \qquad \eta_{R=8} = 100 \cdot 0.77 \cdot 0.777 = 59.8\%$$

Local Energy Input

The view factor obtained from Fig. 3.29 yields an *average* radiant energy transfer efficiency. The specific local energy transfer rate is also important. As seen in Fig. 3.30 [12] for uniform energy output from the radiant heaters, the edges of the sheet receive substantially less energy than the center. This is because the heaters in the center see substantially more sheet than those at the edges. In other words, the heaters at the edge radiate to a greater amount of non-sheet than those in the center. Figure 3.31 illustrates this. An accurate estimate of the energy of Fig. 3.30 is

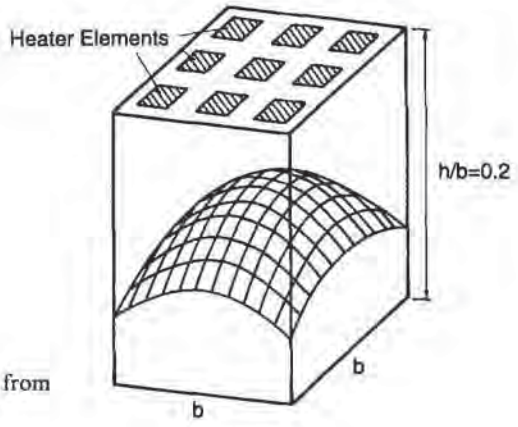

Figure 3.30 Energy received by finite sheet from uniform energy output by heaters [12]

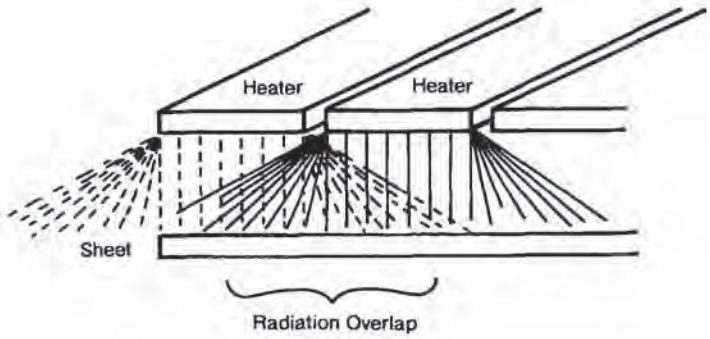

Figure 3.31 Schematic of radiation overlap from heaters to sheet

© 1996 Carl Hanser Verlag. All rights reserved.
No unauthorized disclosure or reproduction; licensed to purchaser only.

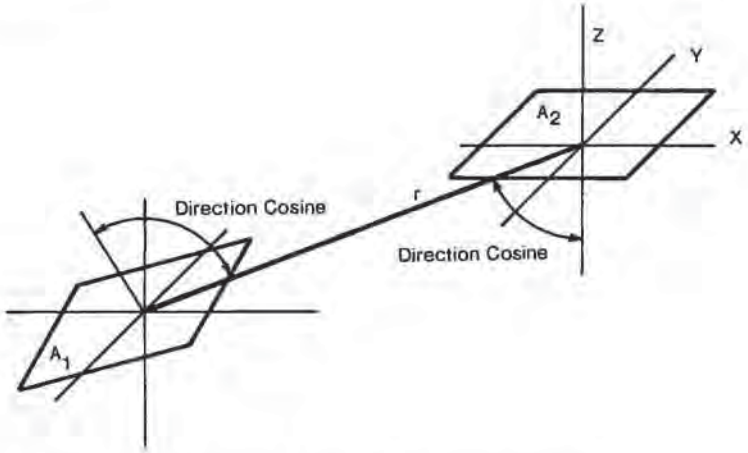

Figure 3.32 Radiation ray tracing between finite parallel plane elements [13]

obtained from radiant heat transfer theory. Consider energy interchange between two differential surface elements (Fig. 3.32) [13]. The intensity of the energy emitted from surface element dA_1 is constant in a hemisphere of radius r from the surface. Any element that intersects this hemisphere receives an amount of energy proportional to its projected area *relative to the area of the hemisphere*. The projected area depends on the attitude of that element to the source plane. In differential form, the total energy interchange between these elements is:

$$q_{1\leftrightarrow 2} = \sigma F_g(T^{*4}_{heater} - T^{*4}_{sheet}) \int_{A_2}\int_{A_1} \frac{\cos\phi_1 \cos\phi_2}{\pi r^2}\, dA_1\, dA_2 \qquad (3.35)$$

The double-integral term on the right side represents the view factor, F. The terms, cos ϕ, are direction cosines and r is the solid angle radius between the elements. Figure 3.29 is obtained through proper integration of the double integral of Equation 3.35.

Quartz and ceramic heating elements are discrete and isothermal 'bricks'. As a result, the differential form of the view factor that yields the double integral can be replaced with the difference form:

$$q_{1\leftrightarrow 2} = \sigma F_g(T^{*4}_{heater} - T^{*4}_{sheet}) \left[\sum_{A_1}\sum_{A_2} \frac{\cos\phi_1 \cos\phi_2}{\pi r^2}\, \Delta A_1\, \Delta A_2\right] \qquad (3.36)$$

where the "1" element is the heater and the "2" element the sheet[1]. Consider a grid of heater and sheet elements in the X-Y direction separated by a distance z in the Z direction. For parallel surfaces z units apart:

[1] This assumes that the sheet is made of elements as well. In fact, the sheet should be considered as an infinite number of infinitesimal elements and the double integral replaced with a integrodifferential form. This is not done in this discussion.

© 1996 Carl Hanser Verlag. All rights reserved.
No unauthorized disclosure or reproduction; licensed to purchaser only.

$$\cos \phi_1 = \cos \phi_2 = \frac{z}{r} \tag{3.37}$$

The spherical radius between any two heater and sheet element is given as:

$$r = \sqrt{x^2 + y^2 + z^2} \tag{3.38}$$

The amount of energy emitted *from* a single heater element *to all* plastic elements is:

$$q_{1 \rightarrow \Sigma 2} = \sigma F_g \left[\sum_{A_2} \frac{z^2}{\pi (x^2 + y^2 + z^2)^2} (T^{*4}_{\text{heater}} - T^{*4}_{\text{sheet}}) \Delta A_1 \, \Delta A_2 \right] \tag{3.39}$$

T_h is the single heater element temperature and T_s represents one of the many sheet surface element temperatures. Likewise, the amount of energy received *by* a single plastic element *from all* heater elements is:

$$q_{\Sigma 1 \rightarrow 2} = \sigma F_g \left[\sum_{A_1} \frac{z^2}{\pi (x^2 + y^2 + z^2)^2} (T^{*4}_{\text{heater}} - T^{*4}_{\text{sheet}}) \Delta A_1 \, \Delta A_2 \right] \tag{3.40}$$

Note that the individual element temperatures are now incorporated within the summation. Individual heater element and sheet element temperatures vary and this expression accommodates these variations. Furthermore note that the summation in Equation 3.39 implies that the [XY] position of the heater element is fixed and the [XY] position of each sheet element is computed *relative to* that [XY] position. Although Equations 3.35 through 3.40 appear formidable, they are rapidly solved on a computer. Figure 3.33 gives the computer solution for energy input to a sheet containing 49 elements from a heater bank containing 49 elements. The energy

11 60. 9%	12 74. 0%	13 76. 8%	14 77. 3%	15 76. 8%	16 74. 0%	17 60. 9%
21 74. 0%	22 90. 8%	23 94. 4%	24 95. 1%	25 94. 4%	26 90. 8%	27 74. 0%
31 76. 8%	32 94. 4%	33 98. 4%	34 99. 2%	35 98. 4%	36 94. 4%	37 76. 8%
41 77. 3%	42 95. 1%	43 99. 2%	44 100%	45 99. 2%	46 95. 1%	47 77. 3%
51 76. 8%	52 94. 4%	53 98. 4%	54 99. 2%	55 98. 4%	56 94. 4%	57 76. 8%
61 74. 0%	62 90. 8%	63 94. 4%	64 95. 1%	65 94. 4%	66 90. 8%	67 74. 0%
71 60. 9%	72 74. 0%	73 76. 8%	74 77. 3%	75 76. 8%	76 74. 0%	77 60. 9%

Figure 3.33 Local heat flux distribution from 7 × 7 uniform 540°F heaters. Values based on 100% at element [4,4]. Relative heater-to-sheet spacing, Z = 1 [14]

© 1996 Carl Hanser Verlag. All rights reserved.
No unauthorized disclosure or reproduction; licensed to purchaser only.

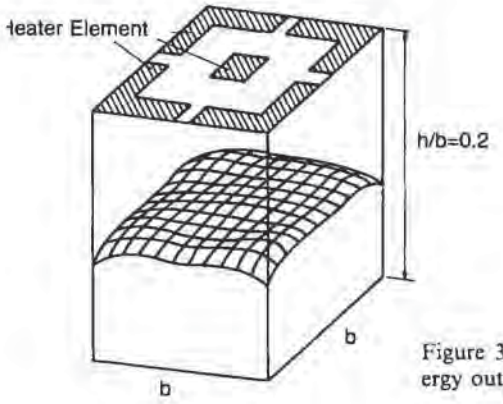

Figure 3.34 Energy received by finite sheet from zonal energy output by heaters [15]

output is the same from each heater element. The elemental values represent the amount of energy received by a given sheet element relative to that received by the center sheet element [14]. As is apparent, the values of Fig. 3.33 support the proposed scheme of Fig. 3.30. The energy flux from each heater element can be varied to achieve near-uniform energy input to the plastic sheet. Figure 3.34 is one proposed scheme of an optimized heating system where the energy flux is the same to each element [15]. Figure 3.35 is the computer solution obtained by varying the individual heater element temperatures. As is apparent from Equation 3.40 and earlier discussion, small changes in absolute heater element temperatures yield

11 185% 706F	12 130% 608F	13 135% 618F	14 135% 618F	15 135% 618F	16 130% 608F	17 185% 706F
21 130% 608F	22 80% 486F	23 90% 514F	24 90% 514F	25 90% 514F	26 80% 486F	27 130% 608F
31 135% 618F	32 90% 514F	33 95% 527F	34 90% 514F	35 95% 527F	36 90% 514F	37 135% 618F
41 135% 618F	42 90% 514F	43 90% 514F	44 92.5% 521F	45 90% 514F	46 90% 514F	47 135% 618F
51 135% 618F	52 90% 514F	53 95% 527F	54 90% 514F	55 95% 527F	56 90% 514F	57 135% 618F
61 130% 608F	62 80% 486F	63 90% 514F	64 90% 514F	65 90% 514F	66 80% 486F	67 130% 608F
71 185% 706F	72 130% 608F	73 135% 618F	74 135% 618F	75 135% 618F	76 130% 608F	77 185% 706F

Figure 3.35 Uniform heat flux everywhere [±1.5%]. Relative heater temperature in °F. Relative heater-to-sheet spacing, Z = 1

© 1996 Carl Hanser Verlag. All rights reserved.
No unauthorized disclosure or reproduction; licensed to purchaser only.

substantial changes in emitted energy. This is apparent in Fig. 3.35 for the 7×7 heater by 7×7 sheet configuration. The heater temperature profile predicted in Fig. 3.35 mirrors current forming practice, with corner heaters running hotter than edge heaters and center heaters running substantially cooler than peripheral heaters.

Pattern Heating

Pattern heating is the placing of welded wire screens between the sheet and the heater in strategic locations to partially block the radiant energy. Radiant screens are frequently used to achieve uniform wall thickness in odd-shaped parts [16-18] when the heater output is fixed, as with plate and rod heaters. Fine welded stainless steel wire mesh is cut to an approximate shape of the blocking region and is placed between the heater plane and the sheet surface (Fig. 3.36). The screens are frequently laid on the wire screen protecting the lower heaters from sheet drop. They are wired in position below the upper heaters. If f_s is the fraction of open area in the screen and T^*_{sc} is its absolute temperature, the energy interchanged between the heater and the sheet beneath the screen is given as:

$$\frac{Q}{A} = \{\sigma F_{\infty - s} F_{g,\infty - s}\} \cdot f_s \cdot [T^{*4}_{\infty} - T^{*4}_{s}] \tag{3.41}$$

The energy interchanged between the heater and the screen is:

$$\frac{Q}{A} = \{\sigma F_{\infty - sc} F_{g,\infty - sc}\} \cdot (1 - f_s) \cdot [T^{*4}_{\infty} - T^{*4}_{sc}] \tag{3.42}$$

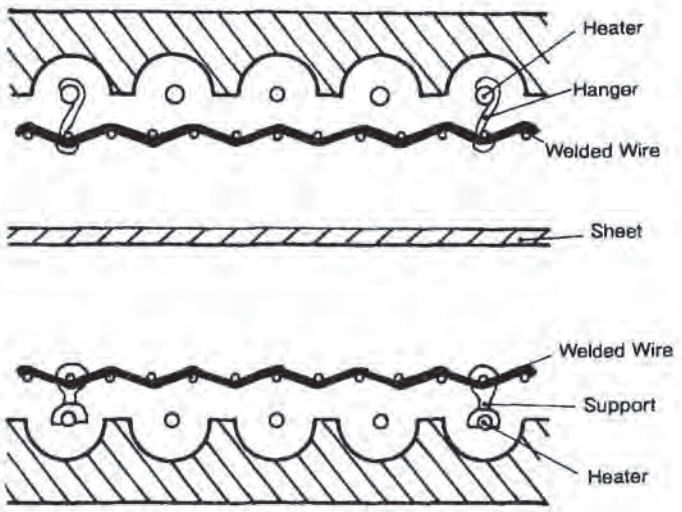

Figure 3.36 Examples of attaching welded wire screen for pattern heating on rod heaters

© 1996 Carl Hanser Verlag. All rights reserved.
No unauthorized disclosure or reproduction; licensed to purchaser only.

And that interchanged between the screen and the sheet is:

$$\frac{Q}{A} = \{\sigma F_{sc-s} F_{g,sc-s}\} \cdot f_s \cdot [T_{sc}^{*4} - T_s^{*4}] \tag{3.43}$$

Note that there are three view factors and three gray-body correction factors. The sheet-to-heater distance, the sheet-to-screen distance and the screen-to-heater distance have different values and the respective view factors will therefore be different. Furthermore, the emissivities of the screen, sheet and heater are different. Example 3.20 illustrates the extent of reduction in energy interchange. The fraction of open area in the screen is the primary method of controlling energy interchange in pattern heating. Multiple screens are used if necessary (Fig. 3.37).

Example 3.20 Pattern Heating—Efficiencies

Consider a screen having a 0.030-in wire with a square 0.060-in center-to-center distance. The screen is positioned halfway between a 30 × 30 in sheet and a 30 × 30 in heater, spaced 6 inches apart. The heater emissivity is 0.9, the sheet emissivity is 0.85 and the stainless steel screen emissivity is 0.3. The heater temperature is 800°C, the emitter temperature is 500°C and the sheet temperature is 200°C. Determine the efficiency of heat transfer relative to the unscreened sheet.

The area of a single square is $0.060 \times 0.060 = 0.36 \times 10^{-2}$ in^2. The projected area of the wire in the square is $2 \times 0.06 \times 0.015 + 2 \times (0.06 - 2 \cdot 0.015) \times 0.15 = 0.027 \times 10^{-2}$ in^2. Thus, the wire covers 75% of the surface area. $f_s = 0.25$.

For the heater-to-screen interchange, $F_g = 0.9 \cdot 0.3 = 0.27$. The view factor is obtained from Fig. 3.27 for $R = 0.060/0.030 = 2$, and is $F = 0.86$. Thus the heater-to-screen efficiency is:

$$\eta_{sc-x} = FF_g(1 - f_s) = 0.27 \cdot 0.86 \cdot 0.75 = 0.174$$

For the screen-to-sheet interchange, $F_g = 0.3 \cdot 0.85 = 0.255$. The view factor is obtained from Fig. 3.29 and is $F = 0.86$. The screen-to-sheet efficiency is:

$$\eta_{sc-s} = FF_g(1 - f_s) = 0.255 \cdot 0.86 \cdot 0.75 = 0.164$$

For the heater-to-sheet interchange, $F_g = [1/0.9 + 1/0.85 - 1]^{-1} = 0.777$. The view factor is obtained from Fig. 3.29 for $R = 30/6 = 5$ and is $F = 0.7$. The heater-to-sheet efficiency is:

$$\eta_{x-s} = FF_g \cdot f_s = 0.777 \cdot 0.7 \cdot 0.25 = 0.136$$

The energy interchange equation is:

$$\frac{Q}{A} = \{\sigma FF_g\} f_s [T_{source}^{*4} - T_{sink}^{*4}]$$

For the heater-to-screen interchange:

$$\frac{Q}{A} = 56.74 \cdot 0.174 \cdot [1.073^4 - 0.773^4] = 9.56 \text{ kW/m}^2$$

© 1996 Carl Hanser Verlag. All rights reserved.
No unauthorized disclosure or reproduction; licensed to purchaser only.

For the screen-to-sheet interchange:

$$\frac{Q}{A} = 56.74 \cdot 0.164 \cdot [0.773^4 - 0.473^4] = 2.86 \text{ kW/m}^2$$

For the heater-to-sheet interchange:

$$\frac{Q}{A} = 56.74 \cdot 0.136 \cdot [1.073^4 - 0.473^4] = 9.84 \text{ kW/m}^2$$

The total energy transfer is:

$$\frac{Q}{A} = 9.56 + 2.86 + 9.84 = 22.26 \text{ kW/m}^2$$

This compares with the unscreened energy transfer:

$$\frac{Q}{A} = 56.74 \cdot 0.70 \cdot 0.777 \cdot [1.073^4 - 0.473^4] = 31.57 \text{ kW/m}^2$$

The screen provides a 29.5% reduction in the amount of radiant energy interchange between the heater and the sheet.

Zone, Zoned or Zonal Heating

With the advent of discrete heating elements, the effect of shielding or screening certain areas of the sheet has been, for the most part, replaced with local heating element energy output control. The earliest heating stations employed manually set proportional controllers on every heating element. Computer-aided controllers are now used. In certain circumstances, the energy output from every heating element is controllable. For very large ovens and very many heating elements, individual control is impractical. Regional banks of heating elements have a single controller and thermocouple. Thus, for an oven with 100×100 elements, top and bottom, requiring 20,000 controlling elements, the oven may have 40 *zones*, top and bottom. In certain circumstances, individual elements may be transferred from one zone to another electronically. In other cases, hard rewiring is necessary. Usually, zonal conditions are displayed on a CRT screen. As noted in the equipment section, most ceramic and metal plate heaters use PID-based controls and thermocouple temperature is the indicating readout variable. Quartz heaters operate on percentage of the time on and percentage is the indicating readout variable. Technically, of course, these variables are simply measures of intrinsic energy output of the heater or bank of heaters. Zone heating or zonal heating is used to change local energy input to the sheet in much the same way as pattern heating. With pattern heating, the pattern must be some distance from the sheet surface to minimize a sharp edge effect, *shadowing* or *spotlighting* where the pattern ends. In zone heating, the heaters are some distance from the sheet surface to begin with. As a result, energy change in a local heater or heater bank not only affects the sheet directly below it but also changes the energy input to the sheet elements in the vicinity. This is seen in the

© 1996 Carl Hanser Verlag. All rights reserved.
No unauthorized disclosure or reproduction; licensed to purchaser only.

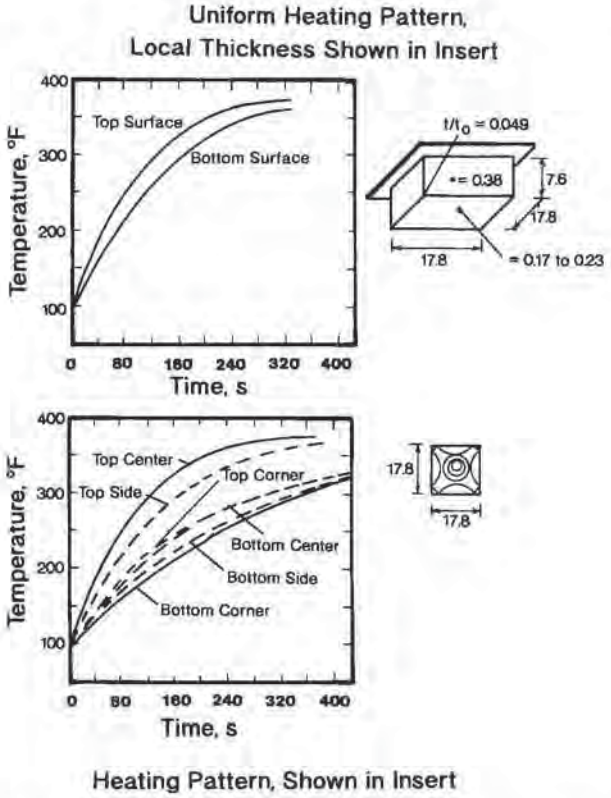

Figure 3.37 Effect of patterning on thermoforming part wall thickness and temperature for polystyrene, PS [16,17]. Initial sheet thickness = 2.1 mm. In lower figure, up to four layers of tissue paper are used as screening. In lower figure, thickness ratio, t/t_0 = 0.29 to 0.32 over entire part. Figure used by permission of Krieger Co.

computer-generated energy input scheme of Fig. 3.38 [14]. Increasing a specific heater element energy output 14% results in a 6% increase in energy input to the immediate sheet element neighbors and lesser amounts elsewhere even though energy outputs from neighboring heater elements have not changed. If this is an undesirable effect or the effect sought requires greater focus, the bank of heaters making up the specific zone must be reduced in number.

Heater to Sheet Distance

As stated earlier, radiation does not depend on fluid or solid medium. Relative heater-to-sheet spacing does affect radiant energy interchange however. This was demonstrated in Fig. 3.29 and is apparent in Equation 3.40. Figure 3.39 shows the effect of a 50% increase in heater-to-sheet spacing *relative to* the optimum energy

© 1996 Carl Hanser Verlag. All rights reserved.
No unauthorized disclosure or reproduction; licensed to purchaser only.

11 0 0.1%	12 0 0.2%	13 0.2% 0.4%	14 0.8% 1.6%	15 3.1% 6.2%	16 7.0% 14.1%	17 3.1% 6.3%
21 0 0.1%	22 0 0.2%	23 0.2% 0.5%	24 1.1% 2.2%	25 6.9% 14.0%	26 28.2% 56.4%	27 7.0% 14.1%
31 0 0	32 0 0.1%	33 0.2% 0.4%	34 0.7% 1.5%	35 3.1% 6.3%	36 6.9% 14.0%	37 3.1% 6.2%
41 0 0	42 0 0.1%	43 0.1% 0.3%	44 0.4% 0.7%	45 0.7% 1.5%	46 1.1% 2.2%	47 0.8% 1.6%
51 0 0	52 0 0.1%	53 0 0.1%	54 0.1% 0.3%	55 0.2% 0.4%	56 0.2% 0.5%	57 0.2% 0.4%
61 0 0	62 0 0	63 0 0.1%	64 0 0.1%	65 0 0.1%	66 0.1% 0.2%	67 0.1% 0.2%
71 0 0	72 0 0	73 0 0	74 0 0	75 0 0	76 0 0.1%	77 0 0.1%

Figure 3.38 Spotlighting effect from two-fold and four-fold increases in heater output at [2,6]. Percentage represents local increase in heat absorption [14]

11 73%	12 83%	13 85%	14 85%	15 85%	16 83%	17 73%
21 85%	22 95%	23 97%	24 98%	25 97%	26 95%	27 83%
31 85%	32 97%	33 99%	34 99.5%	35 99%	36 97%	37 85%
41 85%	42 98%	43 99.5%	44 100%	45 99.5%	46 98%	47 85%
51 85%	52 97%	53 99%	54 99.5%	55 99%	56 97%	57 85%
61 83%	62 95%	63 97%	64 98%	65 97%	66 95%	67 83%
71 73%	72 83%	73 85%	74 85%	75 85%	76 83%	77 73%

Figure 3.39 Effect of heater-to-sheet spacing on energy received by sheet elements. Local percentage of initial energy input for $Z = 1.5$ as given in Figure 3.35 for $Z = 1$ [14]

© 1996 Carl Hanser Verlag. All rights reserved.
No unauthorized disclosure or reproduction; licensed to purchaser only.

input profile of Fig. 3.35 [14]. As expected, energy input to edges and corners are most affected. But the overall energy input to the sheet also substantially decreases. The energy output from each of the heaters must be changed to compensate for the change in gap distance. Again, the arithmetic in Equation 3.40 is a most useful aid in this process.

3.11 Thin-Gage Sheet—Approximate Heating Rates

For thin-gage sheet, especially roll-fed film for packaging and blister-pack applications, the time-dependent heating model can be significantly simplified. The net enthalpic change in the sheet is simply equated to the rate at which energy in the sheet is interchanged with its environment. As a first approximation, the temperature gradient through the plastic film thickness is assumed to be zero. There are two general approaches to this *lumped-parameter approximation*—constant environmental temperature and constant heat flux to the sheet surface.

Constant Environmental Temperature Approximation

Consider T_∞ to be the constant environmental temperature. The lumped-parameter approximation then becomes:

$$d(VH) = V \cdot \rho c_p \, dT = hA(T_\infty - T) \, d\theta \tag{3.44}$$

V is the sheet volume, $V = At$, A is the sheet surface area and t is its thickness. T is the sheet temperature. T_∞ can be the radiant heater temperature, with h being the approximate radiation heat transfer coefficient. Or T_∞ can be air temperature with h being the convection heat transfer coefficient. This ordinary differential equation is written as:

$$\frac{dT}{(T_\infty - T)} = \left(\frac{h}{t\rho c_p}\right) d\theta \tag{3.45}$$

If $t_0 = T(\theta = 0)$, and T_∞ is constant:

$$\ln\left(\frac{T_\infty - T}{T_\infty - T_0}\right) = \frac{-h\theta}{t\rho c_p} \tag{3.46}$$

or:

$$\left(\frac{T_\infty - T}{T_\infty - T_0}\right) = \exp\left[\frac{-h\theta}{t\rho c_p}\right] \tag{3.47}$$

This is a first-order response of a system to a change in boundary conditions. This lumped-parameter transient heat transfer model is valid only where conduction through the sheet thickness is less significant than energy transmission from the environment to the sheet surface. There are two dimensionless groups that define the

© 1996 Carl Hanser Verlag. All rights reserved.
No unauthorized disclosure or reproduction; licensed to purchaser only.

Table 3.13 Lumped-Parameter Maximum Sheet Thickness

Moving air heat transfer coefficient, Table 3.2:
0.0014 cal/cm² · s · °C
1 Btu/ft² · h · °F
Plastics thermal conductivity, Table 3.12:
4.1 to 8.3 × 10⁻⁴ cal/cm · s · °C
0.1 to 0.2 Btu/ft² · h · °F/ft
Maximum thickness for Bi = 0.1:
0.025 to 0.5 cm
0.010 to 0.100 in
10 to 100 mils

limits of the lumped-parameter model. One is the Biot number, $Bi = ht/k$, which is the ratio of internal to external heat transfer. The second is the Fourier number, $Fo = k\theta/\rho c_p L^2 = \alpha\theta/L^2$, where α is the thermal diffusivity, $\alpha = k/\rho c_p$, and L is the half-thickness of the sheet when heated equally from both sides[1]. The lumped-parameter model should be applied *only* when $Bi < 0.1$, or when the internal resistance is low. For air moving over plastic sheet, the sheet thickness should be less than about 0.010 in or 0.3 mm or so, Table 3.13 [19], but can be more than this for higher thermal conductivity and higher air velocity. Figure 3.40 [20] expands the limits of Table 3.13 by demonstrating the relative sensitivity of the sheet thickness to the assumed temperature difference from the sheet surface to its centerline. Example 3.21 explores the use of this figure in determining the appropriateness of the lumped-parameter model for convectively heating one side and both sides of a thin-gage sheet. Practical heating times for various thin-gage polymers over a wide range in sheet thickness are given in Fig. 3.26 [21]. The linear relationship is apparent. The energy source temperature and the sheet temperature at forming time is not given for these data. A radiant heater at $T_\infty = 760°C$ or 1400°F produces an energy spectrum with a peak wavelength of about 2.8 μm. The energy source output at this temperature is 40 kW/m². This energy input produces a near-linear heating rate. A lower source temperature, $T_\infty = 510°C$ or 950°F, does not produce a forming time that is linear with sheet thickness.

[1] Note throughout the discussion on sheet heating that the half-thickness of the sheet is used if the sheet is heated equally on both sides. **If** the sheet is heated on only one side, as is the case with trapped sheet heating, contact heating, or single-side radiant heating, *and* **if** the free surface can be considered as *insulated* or without appreciable energy transfer to the surroundings, **then** the proper value for L is the total sheet thickness. **If** the sheet is unevenly heated on both sides **or if** one side of the sheet is heated in one fashion, such as contact heating and the other side is heated in another fashion, such as forced convection heating, **then** the proper value for L is the total sheet thickness. More importantly, models describing non-symmetric heating or one-side heating with an insulated free surface *cannot* be applied. The proper model requires appropriate boundary conditions on each surface of the sheet.

© 1996 Carl Hanser Verlag. All rights reserved.
No unauthorized disclosure or reproduction; licensed to purchaser only.

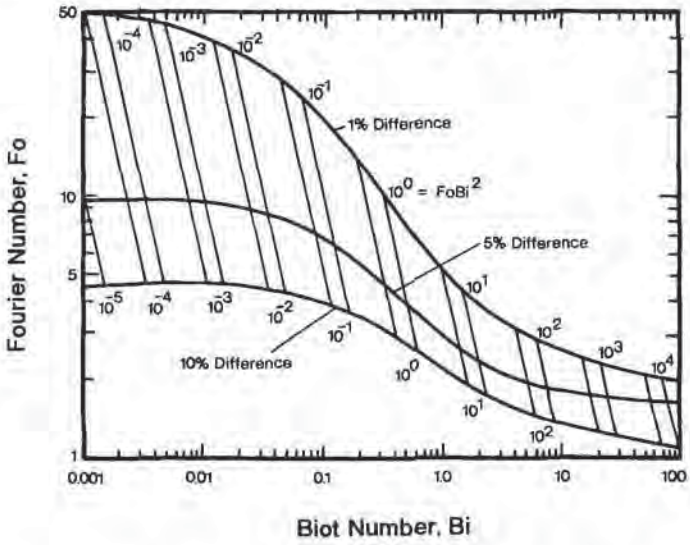

Figure 3.40 Sensitivity of sheet thickness to temperature difference between sheet surface and centerline [20]. Dimensionless time, Fourier number = $\alpha\theta/L^2$ and relative surface resistance, Biot number = hL/k

Example 3.21 The Limits on the Lumped-Parameter Model

A 0.020-in (0.5 cm) PET sheet is radiantly heated equally on both sides, from room temperature, 80°F to its forming temperature, 380°F. The combined convection and radiation heat transfer coefficient is 10 Btu/ft² · h · °F. The thermal diffusivity of the sheet is 0.002 ft²/h and its thermal conductivity is 0.08 Btu/ft · h · °F. Determine the heating time for a 1% difference in temperature between the sheet surface and center. Repeat for a 10% difference. What is the heating time for one-sided heating and a 1% or 10% temperature difference? Comment on the relative times.

For Fig. 3.40, values for Bi and Fo are required.

$$\mathrm{Bi} = \mathrm{hL/k} = 10\,\frac{\mathrm{Btu}}{\mathrm{ft^2 \cdot h \cdot °F}} \cdot \frac{0.01}{12}\,\mathrm{ft} \cdot \frac{1}{0.08}\,\frac{\mathrm{ft \cdot h \cdot °F}}{\mathrm{Btu}} = 1.04$$

$$\mathrm{Fo} = \alpha\theta/L^2 = 0.002\,\frac{\mathrm{ft^2}}{\mathrm{h}} \cdot \frac{\theta}{3600}\,(\mathrm{s}) \cdot \frac{144}{0.0001}\,\mathrm{ft^{-2}} = 0.8\theta\,(\mathrm{s})$$

From Fig. 3.40, Fo = 5.2 at 1% ΔT. Therefore $\theta = 5.2/0.8 = 6.5$s.

From Fig. 3.40, Fo = 2.1 at 10% ΔT. Therefore $\theta = 2.1/0.8 = 2.6$s.

In other words, to keep the centerline essentially at the surface temperature, the heating rate must be adjusted to achieve the forming temperature in about 6.5 seconds. At the forming temperature of 380°F, the centerline temperature will be $0.99 \cdot (380 - 80) + 80 = 377$°F, or 3°F below the surface temperature. If the heating rate is faster than this, the centerline temperature

© 1996 Carl Hanser Verlag. All rights reserved.
No unauthorized disclosure or reproduction; licensed to purchaser only.

will lag the surface temperature by more than 1%. If the heating rate is such that the sheet reaches the forming temperature in about 2.6 seconds, the centerline temperature will lag the surface temperature by about 10%. At the forming temperature of 380°F, the centerline temperature will be $0.90 \cdot (280 - 80) + 80 = 350°F$, or 30°F below the surface temperature.

For one-sided heating, L = 0.020 in.

$$Bi = hL/k = 10 \frac{Btu}{ft^2 \cdot h \cdot °F} \cdot \frac{0.02}{12} ft \cdot \frac{1}{0.08} \frac{ft \cdot h \cdot °F}{Btu} = 2.08$$

$$Fo = \alpha\theta/L^2 = 0.002 \frac{ft^2}{h} \cdot \frac{\theta}{3600} (s) \cdot \frac{144}{0.0004} ft^{-2} = 0.2\theta\ (s)$$

From Fig. 3.40, Fo = 4.05 at 1% ΔT. Therefore $\theta = 4.05/0.2 = 20.25$s.

From Fig. 3.40, Fo = 1.8 at 10% ΔT. Therefore $\theta = 1.8/0.2 = 9.0$s.

It takes $20.25/6.5 = 3.1$ times longer to heat the one-sided sheet to 1% temperature difference and 3.5 times longer to heat it to 10% temperature difference.

Constant Heat Flux Approximation

If the heat flux to a thin sheet is constant, Q/A = constant, then:

$$\frac{Q}{A} = \text{constant} = t\rho c_p \frac{dT}{d\theta} \tag{3.48}$$

Rearranging:

$$dT = \frac{Q}{A} \frac{1}{t\rho c_p} d\theta \tag{3.49}$$

Integrating this yields:

$$T - T_0 = \frac{Q}{A} \frac{\theta}{t\rho c_p} \tag{3.50}$$

For a given set of processing conditions, the constant heat flux approximation indicates that the time to heat a very thin sheet of plastic to a given forming temperature is proportional to the sheet thickness. The data of Fig. 3.26 indicate this linearity, even though no values for forming temperature or heat flux are given.

Thin-Gage Approximations—Comments

The heating efficiencies for several polymers can be determined by using the normal forming temperatures from Tables 3.1 or 2.5. For a given polymer, the enthalpic change between room temperature and the normal forming temperature is determined from Fig. 2.17. The individual heating rate is determined from the slope of the curve of Fig. 3.26, for example. The net energy increase is then calculated. As seen in

© 1996 Carl Hanser Verlag. All rights reserved.
No unauthorized disclosure or reproduction; licensed to purchaser only.

Table 3.1, most thin-gage polymers absorb 40% to 60% of the energy supplied by the heating source. The relatively low efficiency of LDPE is unexplained. PP heating efficiency is also reported to be low [22]. This indicates that the 760°C source temperature used in the calculation may be improper for efficient heating of olefin materials. This is discussed below.

This analysis is restricted to one very specific processing area—thin-gage polymers—and to very stringent conditions—lumped-parameter with linear approximation of the logarithmic function. But it serves to illustrate that only a fraction of the energy emitted by the source, about half in the cases examined, is actually taken up by the polymer sheet. The rest is lost to the environment or passes completely through the sheet unabsorbed.

3.12 Heavy-Gage Sheet—Internal Temperature Control

For thin-gage sheet and film, energy transmission to the sheet controls the heating cycle time. Radiant heating is far more efficient than convection heating and so is preferred for thin-gage thermoforming. For heavy-gage sheet however, energy absorbed on the sheet surface must be conducted through the thermally insulating plastic to its centerline[1]. For very thick sheets, the overall heating cycle time is controlled by the sheet centerline temperature and so the overall heating rate must be controlled to prevent surface overheating. As with the thin-gage discussion earlier, there are two general cases to be considered—constant environmental temperature, T_∞ = constant, and constant heat flux to the sheet surface, Q/A = constant.

Constant Environmental Temperature

Usually hot air is used as a heating medium for very heavy sheet. As a result, the T_∞ = constant case prevails. As with all transient heating problems, the centerline temperature lags the surface temperature. This is seen by reviewing the graphical solution to the one-dimensional time-dependent heat conduction equation with a convection boundary condition (Figs. 3.41 and 3.42) [23,24]. Figure 3.41 gives the conditions at the sheet centerline. Figure 3.42 gives the equivalent conditions at the sheet surface. Similar figures for intermediate points throughout the thickness of the sheet are found in standard handbooks [25]. As with the thin-gage approximation, the dimensionless temperature dependency, Y, for heavy-gage sheet is a function of two dimensionless groups, the Biot number and the Fourier number:

[1] Again, symmetric heating is assumed throughout this discussion. The general arithmetic described herein must be modified if the sheet is heated in an unsymmetric fashion or if it is heated only on one side.

© 1996 Carl Hanser Verlag. All rights reserved.
No unauthorized disclosure or reproduction; licensed to purchaser only.

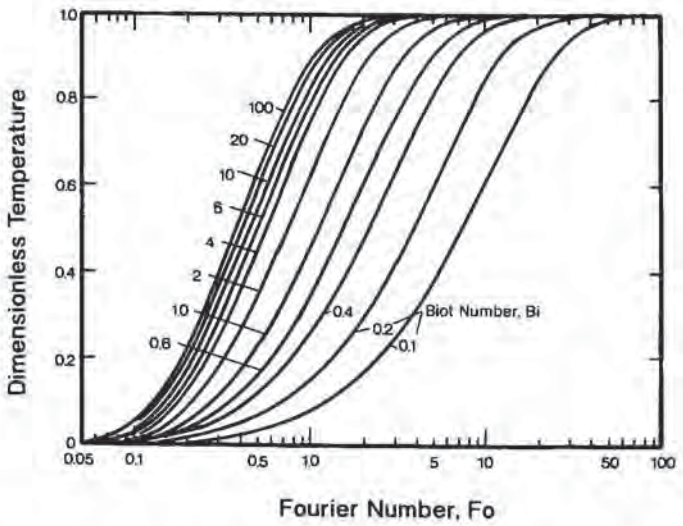

Figure 3.41 Time-dependent temperature profile at center of plastic sheet with relative surface resistance as parameter [23,24]. Biot number, $Bi = hL/k$, Fourier number, $Fo = \alpha\theta/L^2$. Dimensionless temperature $= (T - T_{initial})/(T_{heater} - T_{initial})$

- The Biot number, $Bi = hL/k$. It represents the convective boundary condition and is the ratio of external to internal resistance at the environment-sheet interface.

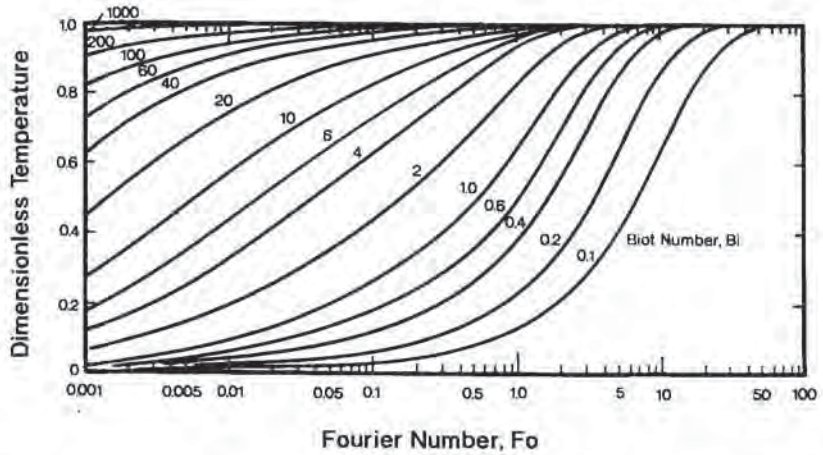

Figure 3.42 Time-dependent temperature profile at plastic sheet surface with relative surface resistance as parameter [23,24]. Biot number, $Bi = hL/k$, Fourier number, $Fo = \alpha\theta/L^2$. Dimensionless temperature $= (T - T_{initial})/(T_{heater} - T_{initial})$

© 1996 Carl Hanser Verlag. All rights reserved.
No unauthorized disclosure or reproduction; licensed to purchaser only.

- The Fourier number, $Fo = \alpha\theta/L^2$. It represents a dimensionless time for conduction of energy.
- Y is the dimensionless temperature, $Y = (T - T_0)/(T_\infty - T_0)$. $Y(\theta = 0) = 0$. $Y(\theta = \infty) = 1$.

Examples 3.22 and 3.23 show how these figures are used with heavy-gage sheet. As noted, forced air convection heating yields a lower energy input per unit time than does radiation heating. This lowered energy input enables the centerline temperature to reach the lower limit on the forming window before the sheet surface temperature exceeds the upper forming temperature.

Example 3.22 Transient Heating with Convective Boundary Conditions—I

Consider a 0.250-in or 6.4 mm sheet placed in a hot air forced convection oven with an air temperature, $T_\infty = 500°F = 260°C$. The thermal diffusivity of the sheet is 0.002 ft²/h and its thermal conductivity is 0.08 Btu/ft · h · °F. The convection heat transfer coefficient is 2 Btu/ft² · h · °F. Determine the time to heat the centerline from 80°F to 320°F, the lower forming temperature. What is the surface temperature at this time? Increase the oven temperature to 600°F and repeat the exercise.

The Biot and Fourier numbers are needed for Figs. 3.41 and 3.42.

$$Bi = hL/k = \frac{2\ \text{Btu}}{\text{ft}^2 \cdot \text{h} \cdot °\text{F}} \cdot \frac{0.250}{2.12}\ \text{ft} \cdot \frac{1}{0.08} \frac{\text{ft} \cdot \text{h} \cdot °\text{F}}{\text{Btu}} = 0.26$$

$$Fo = 0.002 \frac{\text{ft}^2}{\text{h}} \cdot \frac{\theta}{3600}\ (\text{s}) \cdot \frac{144}{(0.250/2)^2\ \text{ft}^2} = 0.005\theta\ (\text{s})$$

For the condition at the centerline:

$$Y = \frac{(320 - 80)}{(500 - 80)} = 0.57$$

From Fig. 3.41, Fo = 3.6. Therefore $\theta = 3.6/0.005 = 720$ seconds = 12 minutes.

From Fig. 3.42, for the sheet surface at this Fourier number, Y = 0.626. Therefore:

$$T_s = 80 + 0.626 \cdot (500 - 80) = 343°F$$

The surface is 343 − 320 = 23°F hotter than the centerline.

For the 600°F oven temperature, Y = 0.46, and from Fig. 3.41, Fo = 2.78. The time to heat the centerline to this temperature, $\theta = 2.78/0.005 = 556$ s = 9.3 minutes. From Fig. 3.42, the dimensionless surface temperature at Fo = 2.78 is Y = 0.52. The surface temperature is now 350°F or 30°F above the centerline temperature.

© 1996 Carl Hanser Verlag. All rights reserved.
No unauthorized disclosure or reproduction; licensed to purchaser only.

Example 3.23 Transient Heating with Convective Boundary Conditions—II

Consider the sheet of Example 3.22. What is the centerline temperature when the sheet surface reaches the upper forming temperature of 380°F? Use an oven temperature of 600°F.

For a surface temperature of 380°F:

$$Y = \frac{(380 - 80)}{(600 - 80)} = 0.58$$

The Fourier number at this value of Y from Fig. 3.42 is Fo = 3.15. The centerline temperature from Fig. 3.41 for this value of Fo is Y = 0.53. The centerline temperature is $0.53 \cdot (600 - 80) + 80 = 355$°F or 25°F below the surface temperature.

The average sheet temperature is usually obtained by interpolation for x/L values between zero and one. Table 3.14 shows interpolated values for two cases. The second case also includes an empirical equation that accurately predicts the internal sheet temperatures. The average temperature can also be approximated by:

$$T_{average,approx} \approx (1/3)T_{surface} + (2/3)T_{centerline} \tag{3.51}$$

The approximate average temperature for the first case of Table 3.14 is 221°C, or within 2%. The approximate average temperature for the second is 161°C or within 3%.

Table 3.14 Convective and Conduction Heat Transfer Through Heavy-Gage Plastic Sheet

At $T_\infty = 800$°C Fo = 0.34, θ = 67.6 s Bi = 1.04			At $T_\infty = 760$°C Fo = 0.5, θ = 89 s Bi = 0.52		
x/L	Y	Temperature (°C)	Y	Temperature (°C)	Temperature[1] (°C)
0	0.833	150	0.865	120	120
0.2	0.82	160	0.84	138	131
0.4	0.78	192	0.82	153	147
0.6	0.74	223	0.80	168	169
0.8	0.65	293	0.75	205	200
1.0	0.56	363	0.70	242	242
$T_{average}$		=225°C	$T_{average}$	=169°C	=166°C

[1] Calculated from $T = 151.65 \cdot e^{-0.51x} + 90.35$ where $0 < x < 3.2$ cm

© 1996 Carl Hanser Verlag. All rights reserved.
No unauthorized disclosure or reproduction; licensed to purchaser only.

The Constant Heat Flux Case

For sheet that is not very heavy or for sheet having a large forming window, the energy input to the sheet surface is supplied by forced convection hot air ovens and radiant heater ovens where indirect radiation is used. For these ovens, the concept of constant heat flux may be applied. In Equation 3.27, the heat flux to the sheet surface was given as:

$$\frac{Q}{A} = f(T, T_\infty, G, F) \tag{3.52}$$

where G is a geometric factor that might include radiation view factor and F is a gray-body factor. The heat flux to the sheet surface can be considered constant if:

- The time of exposure to the heat flux is short,
- The environmental temperature, $T_\infty \gg T$, or
- The environmental temperature changes with heating rate such that Q/A is constant.

Figure 3.43 [26] shows the graphical representation for the effect of constant heat flux input to the sheet surface on surface and internal temperatures in a non-thin sheet. The arithmetic again depends on the dimensionless group, Fourier number, $Fo = \alpha\theta / L^2$ and on a dimensionless temperature, Q*, given as:

$$Q^* = (T - T_0) \cdot \left[\frac{k}{(Q/A)L}\right] \tag{3.53}$$

The dimensionless distance, x/L, is zero at the surface and one at the centerline. Examples 3.24 and 3.25 illustrate the use of this graphic for determining the heating cycle time in a moderately heavy-gage sheet. Note that the time-temperature curves are linear beyond $Fo = \frac{1}{2}$. The following equation describes these curves:

$$Q^* = Fo + \left(\frac{x}{L}\right)^2 - \left(\frac{x}{L}\right) + \frac{1}{3}: \qquad Fo \geqslant \tfrac{1}{2} \tag{3.54}$$

Example 3.24 Heating Rate of Thick Sheets in Constant Heat Flux—I

A 0.250-in sheet of PET is heated at the rate of 3000 Btu/ft² · h[1]*. Determine its surface temperature when its centerline temperature is 320°F. The thermal diffusivity of the sheet is 0.002 ft²/h and its thermal conductivity is 0.08 Btu/ft · h · °F.*

For Fig. 3.43, the Fourier number is:

$$Fo = \alpha\theta = 0.002 \frac{ft^2}{h} \cdot \frac{\theta}{3600}(s) \cdot \frac{144}{(0.250/2)^2\ ft^2} = 0.005\theta\ (s)$$

[1] Compare this value with the heat flux, $h(T_\infty - T_2)$ for Example 3.22. For $T_\infty = 500°F$, $T = 80°F$, and $h = 2$ Btu/ft² · h · °F, $Q/A = 840$ Btu/ft² · h.

© 1996 Carl Hanser Verlag. All rights reserved.
No unauthorized disclosure or reproduction; licensed to purchaser only.

The dimensionless temperature Q* is:

$$Q^* = (320 - 80) \cdot \left[\frac{0.08 \cdot 12}{3000 \cdot 0.125}\right] = (320 - 80) \cdot 0.00256 = 0.614$$

From Fig. 3.43, Fo = 0.756. $\theta = 0.756/0.005 = 151$ seconds or 2.5 minutes. The dimensionless sheet surface temperature at this time is given as Q* = 1.12. Thus $T_{surface} = 1.12/0.00256 + 80 = 518°F$. Thus for this example, the temperature difference between the surface and the centerline is nearly 200°F. At this heating rate, the sheet surface may scorch or discolor before the centerline temperature reaches the minimum forming temperature value.

Example 3.25 Heating Rate of Thick Sheets in Constant Heat Flux—II

Consider the data of Example 3.24. Assume that the constant heat flux is 840 Btu/ft² · h. Using Equation 3.54, determine the surface temperature when the centerline temperature is 320°F. Compare the results with the constant ambient air case of Example 3.22.

The Fourier number remains 0.005θ (s). The dimensionless temperature, Q* is:

$$Q^* = (320 - 80) \cdot \left[\frac{0.08 \cdot 12}{840 \cdot 0.125}\right] = (320 - 80) \cdot 0.00914 = 2.19$$

This value is beyond the curves in Fig. 3.43. As a result, Equation 3.54 is used:

$$Q^* = Fo + \left(\frac{x}{L}\right)^2 - \left(\frac{x}{L}\right) + \frac{1}{3}; \qquad Fo \geq \tfrac{1}{2}$$

For x/L = 1, Fo = 2.19 − 1 + 1 − 1/3 = 1.86. Thus $\theta = 1.86/0.005 = 371$ seconds or 6.2 minutes.

At this Fourier number, the dimensionless temperature Q* at x/L = 0 is given as Q* = 2.19 + 1/3 = 2.52. The temperature at the surface is 2.52/0.00914 + 80 = 356°F.

In Example 3.22 for constant 500°F ambient air and a convection heat transfer coefficient, $h = 2$ Btu/ft² · h · °F, the sheet heated to the 320°F centerline temperature in 12 minutes. The surface temperature was 343°F at that time.

When comparing constant heat flux and constant ambient temperature, the discussion of Section 3.12 must be kept in mind. For constant heat flux, the sheet surface temperature increases linearly with time beyond Fo = ½, as seen in Fig. 3.43. There is no upper limit to the surface temperature for this concept. For constant ambient temperature, the sheet surface temperature asymptotically approaches the ambient temperature.

© 1996 Carl Hanser Verlag. All rights reserved.
No unauthorized disclosure or reproduction; licensed to purchaser only.

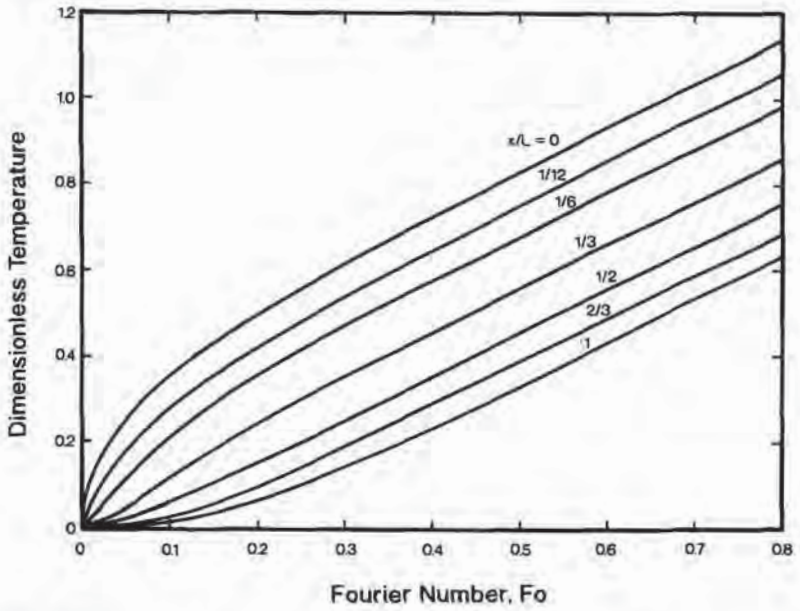

Figure 3.43 Time-dependent temperature profile through plastic sheet with constant heat flux to the sheet surface [26]. Fourier number, $Fo = \alpha\theta/L^2$. Dimensionless temperature $= (T - T_{initial})/(T_{heater} - T_{initial})$

The Thickness Effect

If conduction controls, the effect of sheet thickness on time-dependent temperature is quite dramatic. First note that for the boundary condition, the dimensionless group, $Bi = hL/k$, doubling the sheet thickness doubles the value of the Biot number. The dimensionless time is given as the Fourier number, $Fo = \alpha\theta/L^2$. Doubling the thickness increases the Fourier number by a factor of four. Reviewing Fig. 3.42, if the Biot number doubles and the Fourier number is constant, the effect is a dramatic increase in surface temperature[1]. If the Fourier number increases by four at constant Biot number, there is a dramatic increase in surface temperature[2]. If the Biot number doubles and the Fourier number increases by four, the result is an even more dramatic increase in surface temperature. Example 3.26 focuses on the relative effect of thickness on temperature. The conduction heat transfer axiom appears applicable here:

All other things equal, heating times increase in proportion to the *square* of the sheet thickness.

[1] This has the effect of doubling the heat transfer coefficient. The energy input to the surface doubles.

[2] This has the same effect as increasing the cycle time by a factor of four. The same energy input results in an increased surface temperature.

© 1996 Carl Hanser Verlag. All rights reserved.
No unauthorized disclosure or reproduction; licensed to purchaser only.

Table 3.15 is an experimental corroboration of this axiom for PMMA and a *PVC/PMMA* blend.

Example 3.26 Thickness Effect—Heavy-Gage Sheet

Consider a sheet having a Biot number of 0.2 and a Fourier number of 5.0 at the end of the heating cycle. If the initial sheet temperature is 80°F and the centerline temperature at the end of the heating cycle is 380°F, determine the surface temperature. Now increase the sheet thickness by 20%, keeping the heating cycle the same and recalculate the sheet surface temperature. What is the percentage increase in cycle time needed to get the centerline back to 380°F?

From Fig. 3.42, Y = 0.592. Therefore the heater temperature is:

$$Y = \frac{(380 - 80)}{(T_\infty - 80)} = 0.592$$

$T_\infty = 587°F$ from this expression. From Fig. 3.41, Y = 0.64. The surface temperature is:

$$Y = \frac{(T - 80)}{(587 - 80)} = 0.64$$

or $T_{surface} = 404°F$.

For a 20% increase in sheet thickness, Bi = 0.24 and Fo = 3.47. From Fig. 3.42, Y = 0.50. The ambient temperature remains at 587°F. Therefore the new centerline temperature is:

$$T_{centerline} = 0.5 \cdot (587 - 80) + 80 = 334°F$$

The surface temperature is given from Fig. 3.41 as Y = 0.60, or $T_{surface} = 0.6 \cdot (587 - 80) + 80 = 384°F$.

From Fig. 3.42, the Fourier number when Bi = 0.24 and Y = 0.592 is Fo = 4.0. The cycle time increase is $100 \cdot (4.0 - 3.47)/3.47 = 15\%$. The sheet surface temperature at this Fourier number from Fig. 3.41 is Y = 0.64 and the surface temperature, $T_{surface} = 0.64 \cdot (587 - 80) + 80 = 404°F$. There is essentially no effect on the thermal driving force into the sheet. The major effect is increased cycle time.

Summary

Thus if Bi < 0.1, the sheet heating process is probably controlled by the rate at which energy is delivered to the sheet surface. Increasing the rate of energy input will result in reduced heating cycle times. On the other hand, if Bi > 1, the heating process is probably controlled by the rate at which heat is conducted to the interior of the sheet. Increasing the rate of energy input may result in surface melting, scorching, yellowing or blistering. Although the range in values for plastic thermal conductivity

© 1996 Carl Hanser Verlag. All rights reserved.
No unauthorized disclosure or reproduction; licensed to purchaser only.

Table 3.15 Thermoforming Heating Cycle Times for Heavy-Gage PVC/PMMA and PMMA Sheet[1]

Sheet thickness (cm)	X/X_0	$(X/X_0)^2$	PVC/PMMA		PMMA	
			time (s)	$[\theta/\theta_0]$	time (s)	$[\theta/\theta_0]$
0.102	1.0	1.0	15	1.0	13	1.0
0.152	1.49	2.22	35	2.33	29	2.23
0.203	1.99	3.96	61	4.07	51	3.92
0.236	2.31	5.35	82	5.47	–	–
0.254	2.49	6.20	–	–	80	6.15
0.318	3.12	9.72	150	10.0	126	9.69
0.475	4.66	21.7	324	21.6	276	21.2
0.635	6.23	38.8	594	39.6	495	38.1
0.953	9.34	87.3	–	–	1122	86.3

[1] Adapted from [44], with copyright permission. Sheet heated on both sides. Note: Heating time controlled by conduction through plastic is proportional to square of sheet thickness. Compare columns 3, 5, and 7

is relatively narrow, usually no more than a factor of two or so, the effective heat transfer coefficient value range is more than 20. Thus the range in sheet thicknesses where *neither* conduction *nor* convection dominate the heating rate is quite broad. Further, this range spans most of the common sheet thermoforming thicknesses. As a result, care must be taken in applying any of the above approximations. Case-by-case analysis is always recommended.

3.13 Equilibration

When the sheet has reached its forming temperature, it is removed from the heating environment. Immediately the surface temperature begins to decrease. The centerline temperature continues to increase, albeit at a rate slower than before. A schematic of the time-dependent temperature gradient through the sheet is shown as Fig. 3.44. The sheet temperature approaches the average value. This effect is known as *equilibration*. The relationship between equilibration time, sheet temperature and the forming window is shown in Fig. 3.45. The time to equilibration is sometimes called the *soaking time*. Equilibration time values are strongly dependent on the sheet thickness and the sheet temperature profile through the sheet at the time the sheet exits the oven. The shape of the temperature profile through the sheet depends on the method of heating. The exponential form for the temperature profile is the best representation of the shape when the sheet is convectively heated. A more linear form is best when the sheet is heated at constant flux. These cases are detailed below.

© 1996 Carl Hanser Verlag. All rights reserved.
No unauthorized disclosure or reproduction; licensed to purchaser only.

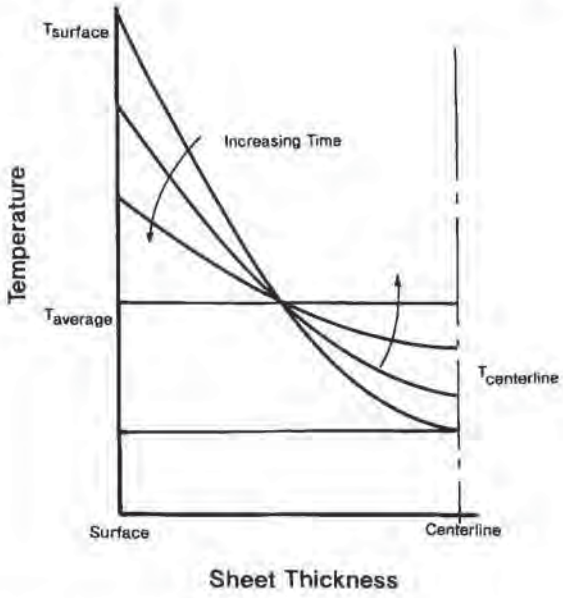

Figure 3.44 Schematic of time-dependent temperature profile through plastic sheet during equilibration

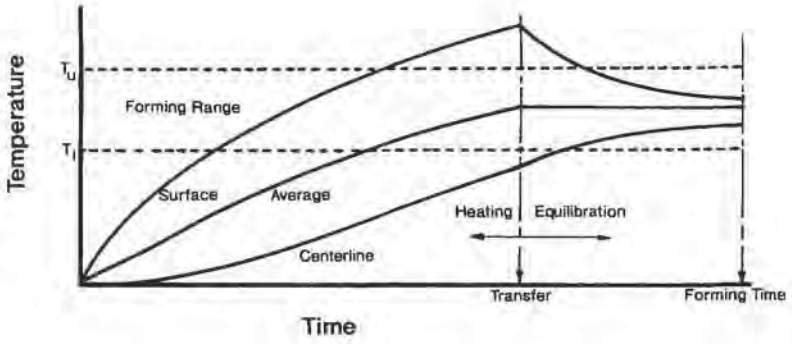

Figure 3.45 Relationship between polymer forming temperature range [dashed area] and time-dependent sheet surface, average and centerline temperatures for heating and equilibration of polymer sheet

Convection Heating

When convection heat transfer controls the energy input to the sheet, approximate equilibration times are obtained either from Fig. 3.46 or from:

$$Fo_{equil} = \alpha\theta/L^2 = \pi^{-2} \cdot \ln\left[\frac{4000 \cdot bL \cdot [1 - e^{-bL}]}{(bL)^2 + \pi^2}\right] \qquad (3.55)$$

© 1996 Carl Hanser Verlag. All rights reserved.
No unauthorized disclosure or reproduction; licensed to purchaser only.

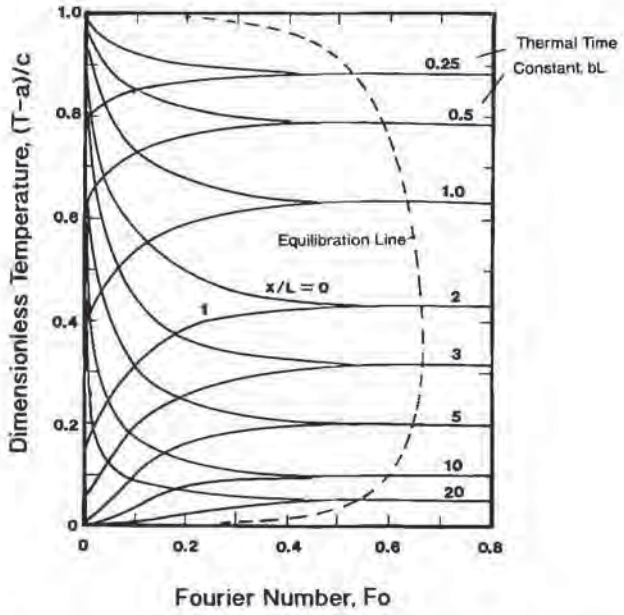

Figure 3.46 Adiabatic time-dependent equilibration temperature through sheet thickness [27]. Initial sheet temperature profile, $T(x) = a \cdot e^{bx} + c$, where a, b, c are curve-fit parameters. Fourier number, $Fo = \alpha\theta/L^2$. Figure used by permission of McGraw-Hill Book Co.

This equation and the curves of Fig. 3.46 are determined by assuming that the sheet has a temperature profile $T(x) = a \cdot \exp(bx) + c$ at the instant the heat source is removed. This empirical profile has been used previously with good success to calculate the local temperature for heavy-gage sheet in Table 3.14. Theoretically, this empirical profile does not exactly mirror typical heat conduction temperature profiles, but practically it yields useful approximate information. Example 3.27 illustrates the method of calculating equilibration times. Note in Fig. 3.46 that the dimensionless equilibrium time Fo_{eq} is essentially constant over a wide range of values of bL ($0.5 < bL < 10$). As a first approximation, Fo_{eq} can be considered constant with a value of about 0.6. This means that the equilibration time is approximately proportional to the square of the sheet thickness, in a manner similar to conduction-controlled heating of heavy-gage sheet.

Example 3.27 Equilibration Time—I

A polystyrene sheet $2L = 0.240$ in thick is exited from the heater when its surface temperature is 350°F and its centerline temperature is 300°F. From calculations, the sheet temperature at $x = L/2$ is 320°F. Determine the time needed to cool the sheet to a uniform temperature. The sheet thermal diffusivity is $0.002\ ft^2/h$.

© 1996 Carl Hanser Verlag. All rights reserved.
No unauthorized disclosure or reproduction; licensed to purchaser only.

In order to use Equation 3.55 to calculate Fo_{equil}, the temperature profile through the sheet must be emulated by $T(x) = a \cdot e^{bx} + c$. From trial and error, the following values for a, b, and c are:

$$a = 29.1°F$$

$$c = 270.9°F$$

$$b = 100\ ft^{-1}$$

$$T(0.5L) = 318.9°F \text{ (compared with } 320°F \text{ calculated)}$$

From Equation 3.55, $Fo_{equil} = 0.552$. The equilibration time is given as:

$$\theta = Fo \cdot \frac{L^2}{\alpha} = \frac{0.552}{0.002} \cdot (0.01)^2 \cdot 3600 = 99.4\ s$$

Constant Heat Flux

For constant heat flux for dimensionless time, $Fo > \frac{1}{2}$, the temperature profile is best given by Equation 3.54. The equilibration curves are shown in Fig. 3.47 [27], where the equilibration times begin at specific values of Fo. Example 3.28 compares times for constant heat flux with those for step change in surface temperature.

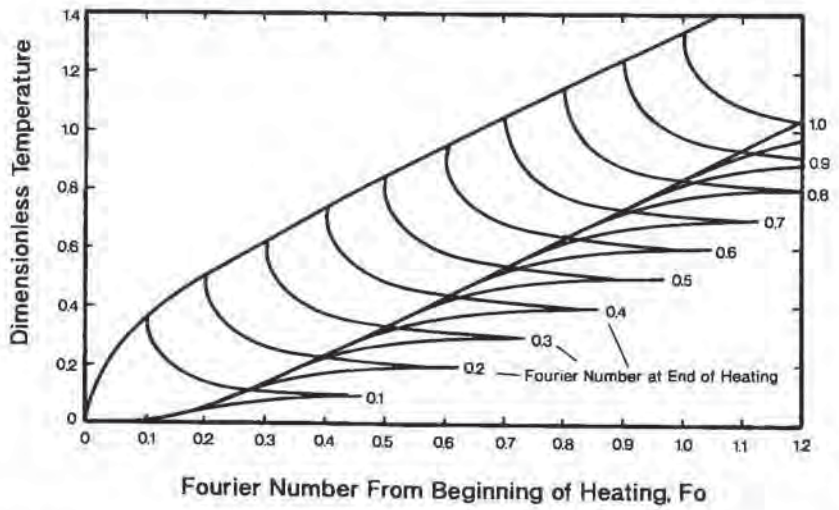

Figure 3.47 Time-dependent temperature profile through plastic sheet with constant heat flux to the sheet surface [27], showing equilibration. See Figure 3.43. Fourier number, $Fo = \alpha\theta/L^2$. Dimensionless temperature $= (T - T_{initial})/(T_{heater} - T_{initial})$

© 1996 Carl Hanser Verlag. All rights reserved.
No unauthorized disclosure or reproduction; licensed to purchaser only.

Example 3.28 Equilibration Time—II

Consider constant flux energy input to the sheet. Assume that the energy input is 1700 Btu/ft² · h. Determine the surface temperature when the centerline temperature reaches 300°F. Then determine the time required to get the surface and centerline temperatures to within 5°F. Finally determine the time required to get full equilibration.

The dimensionless heat flux, Q*, is given as:

$$Q^* = (300 - 80) \cdot \left[\frac{0.08}{1700 \cdot 0.01}\right] = 1.035$$

From Equation 3.54, the Fourier number at x/L = 1 is:

$$Fo = 1.035 - 1 + 1 - 1/3 = 0.702$$

The sheet surface temperature, when x/L = 0, is given as:

$$Q^* = (T_{surf} - 80) \cdot \left[\frac{0.08}{1700 \cdot 0.01}\right] = 1.368$$

Or

$$T_{surf} = 370°F.$$

From Fig. 3.47, the Fourier number when ΔQ^* less than 5% of the average value for Q* is Fo = 0.333. Fo ≥ 0.5 when $\Delta Q^* = 0$. As a result, the time to reach 5% of average and the full equilibration time are given as:

$$\theta_{5\%} = Fo \cdot \frac{L^2}{\alpha} = \frac{0.333}{0.002} \cdot (0.01)^2 \cdot 3600 = 59.9 \text{ s}$$

$$\theta_0 = Fo \cdot \frac{L^2}{\alpha} = \frac{0.500}{0.002} \cdot (0.01)^2 \cdot 3600 = 90 \text{ s}$$

Computed Equilibration Times

In Section 3.5, the finite difference form for the one-dimensional heat conduction equation was presented, together with appropriate boundary conditions. The simplest way of determining the temperature profile through the sheet during equilibration is to simply "switch off" the surface energy boundary condition. For the effective convective boundary condition, this is written in terms of Equations 3.8 and 3.11 as:

$$\frac{Q}{A} = h_{eff} \cdot \beta(T_\infty - T) \tag{3.56}$$

where h_{eff} is the combined convection and effective radiation heat transfer coefficients, $h_{eff} = h + h_r$ and β is the switching factor. So long as the sheet is in the heating portion of the cycle, $\beta = 1$. When the sheet is removed from the oven and

© 1996 Carl Hanser Verlag. All rights reserved.
No unauthorized disclosure or reproduction; licensed to purchaser only.

transferred to the forming press, $\beta = 0$. In a practical sense however, heat transfer between the sheet surface and its environment does not cease when the sheet is removed from the oven. Instead, the environmental temperature T_∞ simply becomes the cool air temperature surrounding the forming press. The effective heat transfer coefficient, h_{eff}, becomes just the convection heat transfer coefficient between the environmental air and the hotter sheet[1]. Computer models of this arithmetic are usually designed to accommodate sheet surface cooling during equilibration.

For heavy-gage sheet, the calculated times needed to achieve temperature differences across the sheet of ten degrees (10°C) or less are usually longer than the practical time to transfer the sheet to the forming station and begin the forming process. This means that at the time of forming, the sheet temperature and hence the sheet strength varies across the sheet cross-section. As seen in Chapter 4, particularly Fig. 4.5, the sheet strength is quite nonlinear with temperature. As detailed in Chapter 4, temperature dependency is modeled with either the W-L-F equation or an Arrhenius equation.

The W-L-F Equation

The W-L-F equation is given as:

$$\log_{10} a_T = -\frac{C_{1g}}{C_{2g}} \frac{(T - T_g)}{C_{2g} + T - T_g} \tag{3.57}$$

where a_T, the shift factor, is the effect of temperature on polymer response to applied load, C_{1g} and C_{2g} are experimentally determined constants, and T_g is the glass transition temperature of the polymer. Table 3.16 gives W-L-F coefficients for several thermoformable polymers. As a first approximation, $C_{1g} = 17.44$ and $C_{2g} = 51.6$ are adequate "universal constants" [28]. The W-L-F equation is suitable in the temperature range of $T_g < T < T_g + 100°C$.

Table 3.16 Williams-Landel-Ferry or WLF Constants for Several Polymers—Universal Constants Also Given [45]

Polymer	C_1	C_2	T_g (K)
Polyisobutylene (PIB)	16.6	104	202
Natural rubber	16.7	53.6	202
Polyurethane elastomer	15.6	32.6	238
Polystyrene (PS)	14.5	50.5	373
Polyethyl methacrylate (PEMA)	17.6	65.6	335
Polycarbonate (PC)	16.14	56	423
Universal constant	17.44	51.6	–

[1] Technically, the sheet surface also interchanges radiant energy with its surroundings. The linear form for the radiant heat transfer coefficient, Equation 3.29, works well here. Example 3.29 illustrates the relative values for the convective and radiative heat transfer coefficients during the equilibration step.

© 1996 Carl Hanser Verlag. All rights reserved.
No unauthorized disclosure or reproduction; licensed to purchaser only.

The Arrhenius Equation

For polymers being processed at temperatures in excess of $T_g + 100°C$, the Arrhenius equation is used:

$$\log_{10} a_T = \frac{\Delta H_a}{R}\left(\frac{1}{T} - \frac{1}{T_0}\right) \tag{3.58}$$

ΔH_a is the viscoelastic activation energy of the polymer, R is the universal gas constant and T_0 is the reference temperature where $T_0 \neq T_g$.

Relating Shift Factors to Sheet Stiffness

The shift factor allows average properties to be determined when the sheet has a nonuniform temperature profile. The stiffness of a beam in flexure, for example, is determined by integrating the local modulus across the beam thickness:

$$S = \frac{\int_0^b E(y;T)y^2\,dy}{\int_0^b y^2\,dy} \tag{3.59}$$

where E(y;T) is the temperature-dependent local modulus and b is the sheet half-thickness[1]. When E(T) is referenced to the reference temperature T_0 through a_T, the expression becomes:

$$S = \frac{\int_0^b E_0(T_0)a_T y^2\,dy}{\int_0^b y^2\,dy} = \frac{E_0(T_0)\int_0^b a_T(y)y^2\,dy}{\int_0^b y^2\,dy} \tag{3.60}$$

The relative effect of the nonuniform temperature on the sheet stiffness is obtained by integration, once T(y) is known, either from graphics, Figs. 3.46 or 3.47, or from computation. Similar equations can be derived for tensile and compressive strengths of a nonisothermal sheet.

3.14 Infrared-Transparent Polymers

Many thermoformable polymers such as PET, PMMA, PS, PC and PVC, may be transparent in visible light but not transparent in incident radiative interchange. As noted in Chapter 2, the visible light wavelength range is 0.38 μm to 0.7 μm. Less than 1% of the total black body radiation is emitted in the visible region for radiant heater temperatures less than 800°C or 1472°F. For some polymers such as PS, PMMA and PET, however, the transparent region extends into the infrared region. For these

[1] This again assumes that the sheet has been heated uniformly and centerline symmetry is valid.

© 1996 Carl Hanser Verlag. All rights reserved.
No unauthorized disclosure or reproduction; licensed to purchaser only.

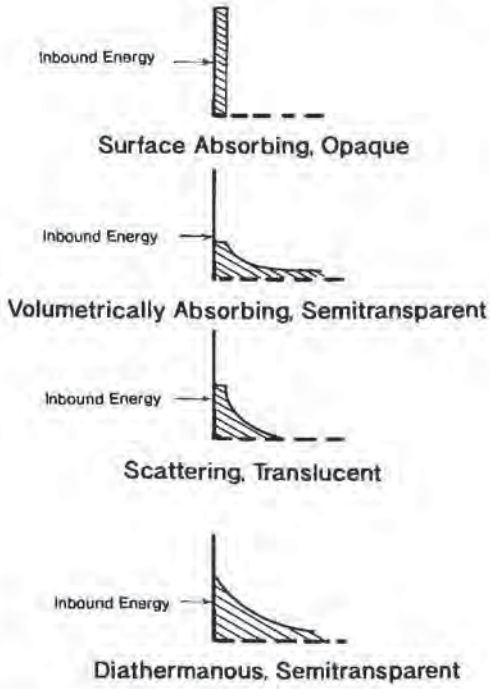

Figure 3.48 Schematic of radiation energy absorption within a semitransparent sheet

polymers, energy is absorbed volumetrically in the short wavelength far-infrared region (Fig. 3.48). Correctly, these polymers are *semi-transparent* to incident radiation. The exact determination of the effect of volumetric energy absorption on temperature profiles in semi-transparent sheet has been made using opposing heat flux energy balances [29,30]. Expressions for wavelength-dependent reflectance, r, transmittance, t, and absorptance, a, are obtained. Surface or interfacial reflectance is obtained from:

$$r = \frac{(n-1)^2}{(n+1)^2} \tag{3.61}$$

Example 3.29 Energy Loss for Equilibrating Sheet

Consider a 350°F sheet in 80°F stagnant air. Determine the energy loss from the sheet surface. Air heat transfer coefficient is 2 Btu/ft² · h · °F. $F_g = 0.7$ and $F = 1.0$.

Radiation effect is given from Equation 3.24:

$$\frac{Q}{A} = \{\sigma F F_g\}[0.45^4 - 0.30^4] = 56.74 \cdot 0.7 \cdot 1.0 \cdot [0.041 - 0.0081] = 1.31 \text{ kW/m}^2$$

© 1996 Carl Hanser Verlag. All rights reserved.
No unauthorized disclosure or reproduction; licensed to purchaser only.

The air convection coefficient is given as:

$$\frac{Q}{A} = 2 \cdot (350 - 80) = 540 \frac{Btu}{ft^2 \cdot h \cdot °F} \cdot \frac{1}{317.1} (kW/m^2) = 1.70 \ kW/m^2$$

The total heat interchange is:

$$\left.\frac{Q}{A}\right|_{total} = 1.31 + 1.70 = 3.01 \ kW/m^2$$

Approximately 56% of the heat loss is due to air motion and the rest to radiation from the sheet to its environment.

where n is the index of refraction of the polymer. Reflectance for most transparent polymers is quite small. Example 3.30 illustrates this for PET. Even with a very large index of refraction of n = 1.65, only 6% of the incident energy is reflected. Transmittance, t, is given as:

$$t = t_o(1 - r)^2 \cdot e^{-\mu x} \tag{3.62}$$

Example 3.30 Interfacial Reflectance

PET has a refractive index of 1.65 when the value for air is n = 1. Determine the extent of interfacial reflectance.

From Equation 3.61:

$$r = \frac{(1.65 - 1)^2}{(1.65 + 1)^2} = 0.06$$

Or 6% of the incident radiation is reflected.

where t_o is the wavelength-specific transmittance at the polymer surface and μ is the wavelength-dependent Beer's Law absorption coefficient. Examples of wavelength-dependent absorption coefficients are given for several polymers in Chapter 2. Absorption curves are usually not mathematically modeled. Some infrared analyzers produce integrated absorptivity values. Figure 3.49 [31] shows integrated absorptivity for various thicknesses of PMMA. Another approach is to partition the absorption curve, as seen in Table 3.17 for PMMA. An infinite value for the Beer absorption coefficient implies that all the incident energy is absorbed on the sheet surface. Example 3.31 shows the relationship between absorption and volumetric energy uptake. Typically, volumetric absorption accounts for no more than about 10% to 15% of the total net radiant energy interchange.

Example 3.31 Short Wavelength Absorption in PMMA

For PMMA, the average absorpiton coefficient in the 0.4 μm to 2.2 μm visible-near-infrared wavelength range is 0.8 cm^{-1}. For a 1.25 cm sheet, determine the amount of energy absorbed in this wavelength range. Let reflectance, r = 0.06. If the emitter temperature is 800°C or 1472°F, determine the amount of volumetric energy absorption in this wavelength range.

© 1996 Carl Hanser Verlag. All rights reserved.
No unauthorized disclosure or reproduction; licensed to purchaser only.

The amount of energy transmitted in this wavelength is given from Equation 3.62 as:

$$t/t_0 = (1 - r)^2 \cdot e^{-\mu x} = 0.94^2 \cdot e^{-1} = 0.325$$

The amount of energy absorbed is given as:

$$a = 1 - r - t/t_0 = 1 - 0.06 - 0.325 = 0.615$$

Or 61.5% of the incident energy in the subject wavelength range is absorbed. The total amount of energy emitted is determined by following Example 3.10 and using Table 3.6.

For the wavelength range of $0 < \lambda < 0.4\ \mu m$, $\lambda T^* = 0.04 \cdot (1472 + 460) = 772.8$. The amount of energy emitted in this region is 0.00030.

For the wavelength range of $0 < \lambda < 2.2\ \mu m$, $\lambda T^* = 2.2 \cdot (1472 + 460) = 4250$. The amount of energy emitted in this region is 0.1159. The net amount of energy emitted is:

$$100 \cdot (0.1159 - 0.0003) = 11.56\%$$

The maximum amount of energy absorbed in this wavelength range is therefore:

$$11.56\% \cdot 0.615 = 7.1\%$$

As seen in Figs. 2.19 to 2.30, values for μ, the Beer absorption coefficient, are usually independent of sheet thickness for unpigmented polymers [32]. Average values for pigmented polymers tend to decrease with increasing sheet thickness (Fig. 3.50) [33]. Organic dyes increase the absorption coefficient values *primarily in the*

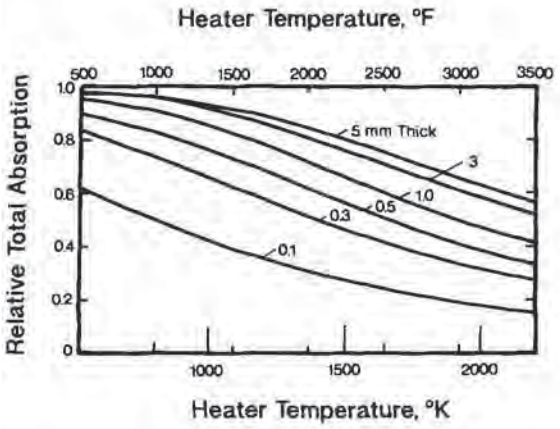

Figure 3.49 PMMA sheet thickness-dependent total absorption of radiant energy as a function of heater temperature [31]

© 1996 Carl Hanser Verlag. All rights reserved.
No unauthorized disclosure or reproduction; licensed to purchaser only.

Table 3.17 Absorption Coefficient Values—Step-Function Approximation for PMMA[1]

Wavelength [μm]	Absorption coefficient μ (cm^{-1})
0–0.4	∞
0.4–0.9	0.02
0.9–1.65	0.45
1.65–2.2	2.0
2.2–∞	∞

[1] Adapted from [17]

visible wavelength range. Inorganic pigment particle sizes are usually in the 0.1 μm to 10 μm range. These particles interfere with visible light transmission and act to increase scattering within the polymer (Fig. 3.51 and Fig. 2.34). This general effect increases the absorption coefficient values across the entire wavelength spectrum in proportion to the particle concentration. Very fine particles such as talc and TiO_2 cause less scattering, as seen by comparing absorption coefficients of unpigmented PET with carbon- and TiO_2-pigmented PET (Fig. 3.51). At heater temperatures of 1000 K, 727°C or 1340°F or less, the average absorption for 1 mm thick PS sheet is essentially independent of pigment type or color [34]. At much higher heater temperatures, absorption increases with pigments. Nevertheless, there is strong practical evidence that black sheet heats faster than white or natural sheet, *regardless of the particle size or type of polymer*. A typical ranking of absorption with color is [35]:

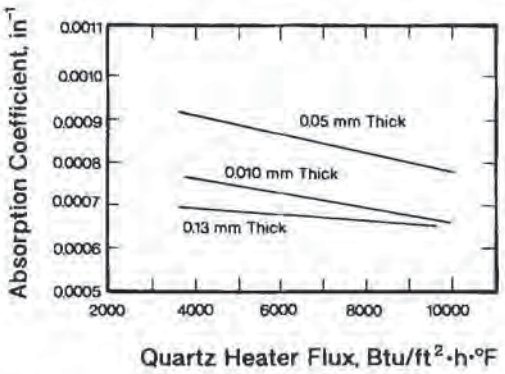

Figure 3.50 Absorption coefficient for various thicknesses of PET with quartz heaters [33]. Figure used by permission of Society of Plastics Engineers, Inc.

© 1996 Carl Hanser Verlag. All rights reserved.
No unauthorized disclosure or reproduction; licensed to purchaser only.

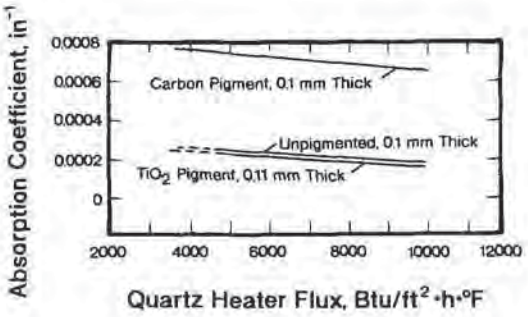

Figure 3.51 Absorption coefficient for pigmented PET with quartz heaters [33]. Figure used by permission of Society of Plastics Engineers, Inc.

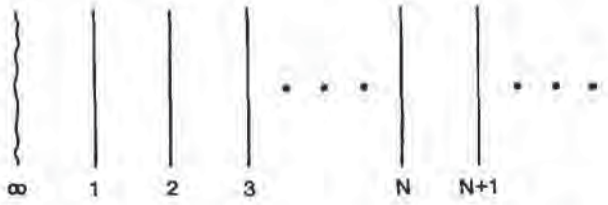

Figure 3.52 Nodal characteristics of one-dimensional finite difference method

Black (most absorbing)
Red
Green
Blue
Yellow
Ecru
White
Natural (least absorbing)

Internal reflectance is considered to be the primary variable in this ranking [36].

The general effect of volumetric energy absorption is the flattening of the temperature profile within the sheet. For thin-gage sheet, low energy absorption implies low heating efficiency[1]. Pigments increase energy absorption and improve heating rates of thin-gage sheet[2]. At a given energy input rate, pigments increase sheet surface temperature in an otherwise transparent polymer. Most optically

[1] For very thin sheets, energy transmission completely *through* the sheet may control the rate at which the sheet is heated. It is apparent from Fig. 3.49 that increasing heater temperature may actually *reduce* the efficiency of energy uptake.

[2] Care must be taken when heating very thin unpigmented sheet that contains printing. Energy may be preferentially absorbed by the printed section of the sheet, leading to uneven heating and serious local sheet distortion.

© 1996 Carl Hanser Verlag. All rights reserved.
No unauthorized disclosure or reproduction; licensed to purchaser only.

transparent polymers are opaque to incident far-infrared radiation and so the effect of volumetric absorption is secondary.

3.15 Computer-Aided Prediction of Sheet Temperature

In the 1980s, a software program, TF1, was developed to aid engineers in determining formability conditions for several types of plastics [37][1]. The program is based on the solution of the one-dimensional transient heat conduction equation, Equation 3.4:

$$\rho c_p \left(\frac{\partial T}{\partial \theta}\right) = k\left(\frac{\partial^2 T}{\partial x^2}\right) \tag{3.63}$$

subject to the initial condition, Equation 3.5, the symmetry condition, Equation 3.6, and the combined convection surface condition:

$$-k\left.\frac{\partial T}{\partial x}\right|_{\theta, X = L} = (h + h_r)(T - T_\infty) \tag{3.64}$$

where h is the convection heat transfer coefficient and h_r is the radiation contribution, written as the effective radiation heat transfer coefficient, Equation 3.30. As has been discussed, h_r includes geometric and radiative efficiencies as well as sink and source temperatures. The numerical solution uses finite difference methods [38]. The explicit method uses a time step defined as:

$$\delta\theta = \frac{Fo \cdot \delta x^2}{\alpha} \tag{3.65}$$

where α is the thermal diffusivity, $\alpha = k/\rho c_p$. Fo is the Fourier number. For mathematical stability of the explicit finite difference equations, $Fo \leqslant \frac{1}{2}$. Figure 3.54 shows the general nodal characteristics of the method. The temperatures of interior elements $(2 < n > N - 1)$ are given as:

$$T_n(\theta + \delta\theta) = Fo\left[T_{n-1}(\theta) + T_{n+1}(\theta) - \left(2 - \frac{1}{Fo}\right)T_n(\theta)\right] \tag{3.66}$$

The Nth element is at the centerline or plane of symmetry. Therefore, $T_{N-1} \equiv T_{N+1}$. The equation for the Nth element is:

[1] There are several limitations to the data used and obtained from the TF1 software package. For example, the values use the data given in Tables 2.5 and 2.12 for nearly 20 polymers. As noted earlier, constant-value specific heats of crystalline polymers do not accurately reflect the temperature-dependent enthalpic changes with temperature. The "view factor" is obtained from the arithmetic used to obtain Fig. 3.29. While this view factor is appropriate to calculate time-dependent average sheet temperature, it does not incorporate local temperature effects, due either to edge effects or zonal heating. And the software does not allow for time-dependent heater or air temperatures. And as noted below, the convection boundary condition uses a linearized form for the radiant heat flux. As a result, the TF1 software should be considered only as a way of understanding the relative effects of the various parameters such as emissivity, air temperature, sheet-to-heater distance.

© 1996 Carl Hanser Verlag. All rights reserved.
No unauthorized disclosure or reproduction; licensed to purchaser only.

$$T_N(\theta + \delta\theta) = Fo\left[2 \cdot T_{N-1}(\theta) - \left(2 - \frac{1}{Fo}\right)T_N(\theta)\right] \tag{3.67}$$

The surface element temperature is given as:

$$T_1(\theta + \delta\theta) = Fo\left[T_2(\theta) + Bi \cdot T_\infty + \left(\frac{1}{2Fo} - 1 - Bi\right)T_1(\theta)\right] \tag{3.68}$$

where Bi is a differential Biot number:

$$Bi = (h + h_r) \cdot \frac{\delta x}{k} \tag{3.69}$$

Since the equations are explicit, the method of solution is quite simple with the nodal temperatures at time $\theta + \delta\theta$ being determined from those at time θ. Again, time step $\delta\theta$ is determined from the stability criterion for the Fourier number, Fo. Example 3.32 illustrates the application of these equations to the relative effect of heater temperature on time to heat the sheet. The time associated with the lower forming temperature is the time required for the centerline to reach this temperature. The time associated with the upper forming temperature is the time required for the sheet surface to reach this temperature.

Example 3.32 Heating Time for ABS and HDPE Polymers

Consider heating either ABS or HDPE sheet 30 in × 30 in × 0.060 in using top and bottom heaters 10 in from the sheet surface. The heater temperature is 500°F. The quiescent air temperature is 200°F. The initial sheet temperature is 80°F. The sheet and heater emissivities are 0.9. Determine the times required for the sheet to reach the lower forming temperature, the normal forming temperature and the upper forming temperature.

The lower, normal and upper forming temperatures are 260°F, 295°F and 360°F for both ABS and HDPE. From the arithmetic of Section 3.15 or from TF1, the following information is obtained:

Polymer	Times (s)		
	LFT	NFT	UFT
ABS	75.3	98.9	>160
HDPE	119.0	158.6	>251
HDPE/ABS ratio	1.58	1.60	~1.59

Note: In Example 3.2, it was determined that the time required to heat HDPE to these temperatures was approximately 2 to $2\frac{1}{2}$ times that for ABS. For this example, the values are about $1\frac{1}{2}$ times. There are two reasons for this discrepancy. The computer model assumes a temperature-independent average specific heat rather than a temperature-dependent enthalpy. And the computer model includes radiation and convection boundary conditions that alter the times required to obtain *internal* temperatures that exceed the forming temperature conditions.

© 1996 Carl Hanser Verlag. All rights reserved.
No unauthorized disclosure or reproduction; licensed to purchaser only.

Example 3.33 shows how air temperature and heater temperature affect overall heating cycle times using the computer-aided program. Note the dramatic effect of oven air temperature on the time required to heat the sheets to the normal forming temperatures. Example 3.34 shows the effect of heater temperature variation of $\pm 20°F$ on the total heating times. The variation for this example is $\pm 10\%$ on the total time. Example 3.35 illustrates the effect of sheet-to-heater spacing on the total heating times. As noted, the view factor is strongly dependent on this spacing. With increased spacing, the heaters see less of the sheet and so the total heating time increases. Example 3.36 shows the effect of downgaging on total heating time. As expected, heating times are quite dependent on sheet thickness. At relatively low heater temperature, the heating time decreases in proportion to the sheet thickness decrease. At relatively high heater temperature, the effect should be more dramatic[1].

Example 3.33 Effect of Heater and Air Temperature on Time-Dependent Heating Rates for ABS and HDPE

Using the information of Example 3.33, determine the heating rates for ABS and HDPE for heater temperatures of 500°F and 800°F. Then, with heaters at 500°F, determine the effect of 100°F and 200°F oven air temperature.

The results from Section 3.15 or TF1 are tabulated:

Polymer	Times (s) at 200°F Air Temperature					
	LFT		NFT		UFT	
Heater Temp	500°F	800°F	500°F	800°F	500°F	800°F
ABS	75.3	23.4	98.9	26.7	>160	33.3
HDPE	119.0	35.6	158.9	42.7	>251	57.3

Polymer	Times (s) at 500°F Heater Temperature					
	LFT		NFT		UFT	
Air Temp	200°F	100°F	200°F	100°F	200°F	100°F
ABS	75.3	104.9	98.9	151.8	>160	>281
HDPE	119.0	166.1	158.9	243.1	>251	>441

[1] Recall however that the convection heat transfer boundary condition used to generate this arithmetic assumes that the radiant heat flux can be approximated by a linear equation in temperature difference between the radiant heater and the sheet temperature.

© 1996 Carl Hanser Verlag. All rights reserved.
No unauthorized disclosure or reproduction; licensed to purchaser only.

Example 3.34 Effect of Small Changes in Heater Temperature on Time-Dependent Heating Rates for ABS and HDPE

Using the information of Example 3.32, determine the heating rates for ABS and HDPE for heater temperature of 480°F, 500°F and 520°F.

The results from Section 3.15 or TF1 are tabulated:

	Polymer			Times (s)					
	LFT			NFT			UFT		
Heater Temp	480°F	500°F	520°F	480°F	500°F	520°F	480°F	500°F	520°F
ABS	83.7	75.3	68.2	112.6	98.9	87.9	>184	>160	>142
HDPE	132.1	119.0	107.4	180.4	158.9	140.9	>289	>251	>220

Example 3.35 Sheet-to-Heater Spacing for ABS and HDPE

Determine the effect on heating time for ABS and HDPE of Example 3.32 if the sheet-to-heater spacing is 5 in, 10 in, or 15 in.

The results from Section 3.15 or TF1 are tabulated:

	Polymer			Times (s)					
	LFT			NFT			UFT		
Spacing	5	10	15	5	10	15	5	10	15
ABS	65.1	75.3	83.5	84.1	98.9	111.3	>135	>160	>180
HDPE	102.2	119.0	132.0	134.6	158.9	178.5	>211	>251	>284

Example 3.36 The Effect of Downgaging on Heating Times for ABS and HDPE

Using the information of Example 3.32, determine the heating rates for ABS and HDPE for sheets of 0.060 in, 0.054 in (10% reduction in thickness) and 0.048 in (20% reduction in thickness).

The results from Section 3.15 or TF1 are tabulated:

	Polymer			Times (s)					
	LFT			NFT			UFT		
Sheet Tk	0.048	0.054	0.060	0.048	0.054	0.060	0.048	0.054	0.060
ABS	59.5	67.4	75.3	78.6	88.8	98.9	>126	>143	>160
HDPE	94.7	106.8	119.0	126.6	142.5	158.9	>201	>226	>251

© 1996 Carl Hanser Verlag. All rights reserved.
No unauthorized disclosure or reproduction; licensed to purchaser only.

The Radiant Boundary Condition

The arithmetic given above and the commercial computer software program, TF1, assumes a pseudo-linear radiant heat transfer coefficient, h_r. This assumption is unnecessary [39]. The radiation (only) boundary condition at the surface node "1" of Fig. 3.54 is:

$$\rho c_p \frac{dx}{2}\frac{dT_1}{d\theta} = \frac{k}{dx}(T_2 - T_1) + \{\sigma F F_g\}(T_\infty^{*4} - T_1^{*4}) \tag{3.70}$$

where T_∞^* and T_1^* are the absolute temperatures of the heater and the surface node, respectively. The term $\{\sigma F F_g\}$ combines the view factor, emissivity constants and Stefan-Boltzmann constant. This equation is nonlinear in T_1. For computational purposes, it is locally linearized by writing:

$$T_1^{*4}(\theta + \delta\theta) \approx T_1^{*3}(\theta) \cdot T_1^*(\theta + \delta\theta) \tag{3.71}$$

where $T_1^*(\theta)$ is the old value of T_1^*. This allows the finite difference equation for the radiant (only) boundary condition to be written as:

$$T_1(\theta + \delta\theta) = 2Fo\left[T_2(\theta) + \left(\frac{1}{2Fo} - RT_1^{*3}(\theta) - 1\right)T_1(\theta) + RT_\infty^{*4}\right] \tag{3.72}$$

where $R = \{\sigma F F_g\}dx/k$, with similarities to the Biot number, Bi of Equation 3.10. R is sometimes called the radiation Biot number.

If the convection boundary condition is now included, the explicit finite difference version of the boundary condition for the one-dimensional transient heat conduction heat transfer problem is:

$$T_1(\theta + \delta\theta) = 2Fo\left[T_2(\theta) + \left(\frac{1}{2Fo} - RT_1^{*3}(\theta) - Bi - 1\right)T_1(\theta) + Bi \cdot T_a + R \cdot T_\infty^{*4}\right] \tag{3.73}$$

Again, T* refers to an absolute temperature.

3.16 Guidelines for Determining Heating Cycles

Guidelines for setting up processing parameters on a new polymer are presented in Chapter 2. This section focuses on energy management for a new polymer. Estimates of energy consumption, heater temperature and heating cycle time are needed for cost estimation. The best sources for this information are resin suppliers and extruders. Experimental data on homologous polymers are quite useful and may be available from the supplier of the new polymer or its competitors. Carefully documented prior observations, particularly from extruders, are also valuable aids in estimating needed data. If these sources cannot provide the information, certain guidelines can be extracted from the information in this chapter.

© 1996 Carl Hanser Verlag. All rights reserved.
No unauthorized disclosure or reproduction; licensed to purchaser only.

The Biot Number

Heating rate guidelines depend on whether the sheet is considered thin-gage or heavy-gage. These definitions are partially quantified in terms of the Biot number, $Bi = hL/k$. The Biot number is the ratio of energy input to the sheet surface to that conducted to the sheet interior. If $Bi < 0.1$, the sheet is usually considered as thin-gage. If $Bi > 1$, the sheet is considered as heavy-gage.

Thin-Gage Guidelines

When $Bi < 0.1$, the sheet is considered thin from a heat transfer viewpoint. The sheet surface temperature is not significantly greater than either the centerline or average sheet temperature. Surface blistering, degradation and burning are not considered primary concerns. Energy input to the sheet surface controls the cycle time. Therefore, radiant heating provides the most efficient means of heating[1]. To minimize cycle time, the maximum net energy exchange should occur in a wavelength range where the polymer has the greatest absorptivity. This usually implies high heater temperatures and short cycle times. Technically, the most efficient mode of heating is *constant heat flux*. The effective heat transfer coefficient is typically in the range of 0.06 to 0.12 $kW/m^2 \cdot °C$ or 10 to 20 $Btu/ft^2 \cdot h \cdot °F$. Energy transfer is dominated by radiation that is as much as 10 times the natural convection contribution. As a first approximation, convection effects can be ignored. For thin sheet such as those used in blister and bubble packaging, the heating cycle time is proportional to the film thickness. The lumped-parameter model discussed in Section 3.11 is used to predict average sheet temperature during thin-gage heating. It ignores temperature gradients through the sheet and so yields only average temperature values. Cycle time is determined when the average temperature reaches the normal forming temperature. From net energy balances, about 50% of the electric power supplied to the radiant heaters is actually used to heat the sheet to its forming temperature.

Heavy-Gage Guidelines

The rate of heating of heavy-gage sheet is governed by the maximum allowable surface temperature. For heavy-gage sheet, $Bi > 1$. Energy transmitted to the surface from the environment must be conducted to the sheet interior. If the rate of conduction is low compared with the input energy rate, the sheet surface temperature may reach an undesirable level. Thus, highly efficient heating methods may in fact be undesirable. Constant surface temperature or declining heat flux methods are preferred. Forced hot air convection ovens are used to heat very heavy-gage sheet.

[1] However, for very thin sheet, radiant transmission *through* the sheet may be a controlling feature. As a result, alternate heating means, such as direct conduction, contact or trapped sheet heating, are recommended.

© 1996 Carl Hanser Verlag. All rights reserved.
No unauthorized disclosure or reproduction; licensed to purchaser only.

Relatively low surface temperatures imply relatively low input energy levels, manifested as relatively low values of the effective convection heat transfer coefficient. Typical values are on the order of 0.005 to 0.03 $kW/m^2 \cdot °C$ or 1 to 5 $Btu/ft^2 \cdot h \cdot °F$. Cycle times are controlled by conduction into the sheet and therefore are proportional to the square of the sheet thickness. Traditional distributed parameter one-dimensional transient heat conduction equations are used to predict the heating rates. Overall energy efficiency is relatively low at about 20% to 30%. Heat losses to surroundings and low conversion efficiencies when heating air are considered the primary reasons. And equilibration times are also proportional to the square of the sheet thickness.

Intermediate-Gage Guidelines

If the Biot number value is between 0.1 and 1, the sheet has intermediate gage with regard to heat transfer. Typically, the heating cycle time, θ, is proportional to the sheet thickness, L, to a power,

$$\theta \propto L^n \tag{3.74}$$

where $1 < n < 2$[1]. Radiant heating dominates the heating methods, with heater temperatures set substantially below the region where optimum energy absorption occurs. Heater temperature values are usually dictated by the upper forming temperature, sheet blistering, discoloration, degradation and/or burning. The energy conversion efficiency is usually between 30% and 50%. Distributed parameter one-dimensional transient heat conduction equations are used to predict heating cycle times.

3.17 References

1. H. Dominighaus, *Plastics for Engineers: Materials, Properties, Applications*, Hanser Publishers, Munich (1993), Figure 24, p. 47.
2. F. Kreith, *Principles of Heat Transfer*, 2nd Ed., International Textbook Co., Scranton PA (1965), Figure 5-1, p. 199.
3. F. Kreith, *Principles of Heat Transfer*, 2nd Ed., International Textbook Co., Scranton PA (1965), p. 142.
4. F. Kreith, *Principles of Heat Transfer*, 2nd Ed., International Textbook Co., Scranton PA (1965), pp. 128-132.
5. J. Frados, Ed., *Plastics Engineering Handbook*, 4th Ed., Van Nostrand Reinhold, New York (1976), pp. 278-281.
6. W. McConnell, "Industrial Thermoforming Symposium and Workshop", SPE Thermoforming Division, Arlington TX, 12-14 March 1985, Distributed Handout.
7. F. Kreith, *Principles of Heat Transfer*, 2nd Ed., International Textbook Co., Scranton PA (1958), Appendix A-4.

[1] Again, for thin-gage heating, $n = 1$. For heavy-gage heating, $n = 2$.

© 1996 Carl Hanser Verlag. All rights reserved.
No unauthorized disclosure or reproduction; licensed to purchaser only.

8. F. Kreith, *Principles of Heat Transfer*, 2nd Ed., International Textbook Co., Scranton PA (1965), p. 215.
9. F. Brinken and H. Potente, "Some Considerations of Thermodynamics in Thermoforming", SPE ANTEC Tech. Papers, *24* (1978), p. 65.
10. J.L. Throne, *Plastics Process Engineering*, Marcel Dekker, New York (1979), pp. 714-715.
11. R.R. Kraybill, "Emission Efficiency of Reflector Materials for an Infrared Tubular Heater", SPE ANTEC Tech. Papers, *29* (1983), p. 466.
12. D. Weinand, "Modellbildung zum Aufheizen und Verstrecken beim Thermoformen", Doctoral Dissertation, Institut für Kunststoffverarbeitung (IKV), Aachen, 16 Jul 1987, Bild 4.9.
13. J.P. Holman, *Heat Transfer*, 4th Ed., McGraw-Hill Book Co., New York, 1976, Figure 8.8, pp. 284-288.
14. J.L. Throne, "Radiant Heat Transfer in Thermoforming", SPE ANTEC Tech. Papers, *41* (1995), p. 000.
15. D. Weinand, "Modellbildung zum Aufheizen und Verstrecken beim Thermoformen", Doctoral Dissertation, Institut für Kunststoffverarbeitung (IKV), Aachen, 16 Jul 1987, Bild 4.10.
16. N. Platzer, "Rigid Thermoplastic Sheeting", Mod. Plastics, *31*:11 (Nov 1954), pp3, 144.
17. N. Platzer, "Sheet Forming", in E.C. Bernhardt, Ed., *Processing of Thermoplastic Materials*, Reinhold, New York (1959), p. 485.
18. J.L. Throne, *Plastics Process Engineering*, Marcel Dekker, New York (1979), p. 657.
19. F. Kreith, *Principles of Heat Transfer*, 2nd Ed., International Textbook Co., Scranton PA (1965), pp. 129-135.
20. P.J. Schneider, "Conduction", in W.M. Rohsenow and J.P. Hartnett, Eds., *Handbook of Heat Transfer*, McGraw-Hill Book Co., New York, 1973, Figure 21, pp. 3-39.
21. A. Höger, *Warmformen von Kunststoffen*, Carl Hanser Verlag, Munich (1971), pp. 36-37.
22. H. Gross and G. Menges, "Influence of Thermoforming Parameters on the Properties of Thermoformed PP", SPE ANTEC Tech. Papers, *28* (1982), p. 840.
23. P.J. Schneider, "Conduction", in W.M. Rohsenow and J.P. Hartnett, Eds., Handbook of Heat Transfer, McGraw-Hill Book Co., New York, 1973, Figure 22e, pp. 3-39.
24. P.J. Schneider, "Conduction", in W.M. Rohsenow and J.P. Hartnett, Eds., *Handbook of Heat Transfer*, McGraw-Hill Book Co., New York, 1973, Figure 22a, pp. 3-39.
25. V.S. Arpaci, *Conduction Heat Transfer*, Addison-Wesley Publishing Co, Reading MA, 1966. See also references [2,13,20].
26. P.J. Schneider, "Conduction", in W.M. Rohsenow and J.P. Hartnett, Eds., *Handbook of Heat Transfer*, McGraw-Hill Book Co., New York, 1973, Figure 40a, pp. 3-67.
27. P.J. Schneider, "Conduction", in W.M. Rohsenow and J.P. Hartnett, Eds., *Handbook of Heat Transfer*, McGraw-Hill Book Co., New York, 1973, Figure 40b, pp. 3-67.
28. R.C. Progelhof and J.L. Throne, *Polymer Engineering Principles: Properties, Processes and Tests for Design*, Hanser Publishers, Munich (1993), Table 3.4, pp. 250-257.
29. R.C. Progelhof, J. Quintiere, J.L. Throne, "Temperature Distribution in Semitransparent Plastic Sheets Exposed to Symmetric, Unsymmetric, and Pulsed Radiant Heating and Surface Cooling", J. Appl. Polym. Sci., *17* (1973), p. 1227.
30. R.C. Progelhof, J. Franey, T.W. Haas, "Absorption Coefficient of Unpigmented Poly(methyl Methacrylate), Polystyrene, Polycarbonate, and Poly(4-methylpentene-1) Sheets", J. Appl. Polym. Sci., *15* (1971), p. 1803.
31. D. Weinand, "Modellbildung zum Aufheizen und Verstrecken beim Thermoformen", Doctoral Dissertation, Institut für Kunststoffverarbeitung (IKV), Aachen, 16 Jul 1987, Bild 3.13.
32. R.C. Progelhof, J. Franey, T.W. Haas, "Absorption Coefficient of Unpigmented Poly(methyl Methacrylate), Polystyrene, Polycarbonate, and Poly(4-methylpentene-1) Sheets", J. Appl. Polym. Sci., *15* (1971), p. 1806.
33. A. Höger, *Warmformen von Kunststoffen*, Carl Hanser Verlag, Munich (1971), Table 2, p. 31.
34. D. Weinand, "Modellbildung zum Aufheizen und Verstrecken beim Thermoformen", Doctoral Dissertation, Institut für Kunststoffverarbeitung (IKV), Aachen, 16 Jul 1987, Bild 3.14.
35. J. Florian, *Practical Thermoforming: Principles and Applications*, Marcel Dekker, New York (1987), p. 39.

© 1996 Carl Hanser Verlag. All rights reserved.
No unauthorized disclosure or reproduction; licensed to purchaser only.

36. J. Florian, *Practical Thermoforming: Principles and Applications*, Marcel Dekker, New York (1987), Chapter 2, "Components of the Thermoforming Process".
37. J.L. Throne, *TF1*, Integrated Design Engineering Systems, Inc., Laramie WY 82070, 1991.
38. D.R. Croft and D.G. Lilley, *Heat Transfer Calculations Using Finite Difference Equations*, Applied Science Publishers, London (1977).
39. D.R. Croft and D.G. Lilley, *Heat Transfer Calculations Using Finite Difference Equations*, Applied Science Publishers, London (1977), pp. 92-94.
40. F. Kreith, *Principles of Heat Transfer*, 2nd Ed., International Textbook Co., Scranton PA (1965), Table 5-1, pp. 215-216.
41. A.I. Brown and S.M. Marco, *Introduction to Heat Transfer*, McGraw-Hill Book Co., New York (1951), p. 68.
42. R.W. Singleton, "Electric Infrared: Textile Applications in the 1980's", Proceedings, AATCC National Technical Conference (1980), p. 201.
43. J.H. Perry, Ed., *Chemical Engineers' Handbook*, 4th Ed., McGraw-Hill Book Co., New York (1963), pp. 10-11 to 10-13.
44. H.R. Osmers, "Industrial Thermoforming Symposium and Workshop", SPE Thermoforming Division, Arlington TX, 12-14 March 1985, Distributed Handout.
45. R.C. Progelhof and J.L. Throne, *Polymer Engineering Principles: Properties, Processes and Tests for Design*, Hanser Publishers, Munich (1993), Table 6.17, p. 651.

© 1996 Carl Hanser Verlag. All rights reserved.
No unauthorized disclosure or reproduction; licensed to purchaser only.

4 Stretching the Sheet

© 1996 Carl Hanser Verlag. All rights reserved.
No unauthorized disclosure or reproduction; licensed to purchaser only.

4.1 Introduction

Once the plastic sheet temperature is within the forming window, it is ready to be stretched. There are many ways of stretching and prestretching the sheet, as detailed in Chapter 1. Vacuum, air pressure, mechanical aids such as plugs, rubber diaphragms, and combinations of these are used to shape the rubbery sheet against the mold surface. The extent to which a given polymer at a given temperature can be stretched limits the ways in which it can be thermoformed. Part design, especially local part wall thickness, depends on the extent of polymer deformation. Deep drawing, drawing into sharp corners, and replication of mold surface details such as patterns or lettering, require polymers that can be rapidly and uniformly stretched. Chapter 9 examines part design in greater detail.

This chapter focuses on the interaction between the forces available to stretch the rubbery sheet and the inherent nature of the rubbery plastic to resist these forces. This interaction, noted in Chapter 2, is directly related to the stress-strain-rate of strain behavior of the plastic at its forming temperature. Typically, at low temperatures, the plastic is quite stiff, does not stretch easily, and will not faithfully replicate the mold details under the modest forces available with simple vacuum forming. Higher forming forces are required when sheet temperatures are low. On the other hand, cycle times are short when sheet temperature is low, so economics favor low sheet temperatures. At high forming temperatures, the sheet is quite limp, is easily stretched and replicates the mold surfaces well at very modest forming pressures. But sagging and sheet surface discoloration can be serious problems, cycle times are increased, and part wall thickness uniformity is usually compromised.

Intuitively knowing when a sheet is hot enough for processing is an acquired skill. Sheet sag and sheet smoke are frequently considered as first-line visual indicators. As a plastic sheet is heated, it undergoes several phases of motion [1]:

- The sheet may momentarily *tighten* in a drum-head fashion. This tightening may be accompanied by some off-gassing from the sheet surface. The gas is usually vaporizing surface or adsorbed water. Since the sheet temperature at this point is usually only a few degrees above room temperature, the tightening is usually attributed to the last steps in sheet extrusion. In the case of heavy-gage sheet, the last step involves palletizing where the just-extruded and guillotined sheet is stacked on older sheet. Heat retention in the palletized stack can cause residual stresses in the individual sheets that are not attributable to the extrusion process, *per se*. A similar situation occurs with thin-gage sheet that is rolled. The rolling action may cause residual stresses called curl. This curl is relaxed out when the sheet is first heated. In addition, heat retention in the roll can also cause residual stresses that are not attributable to the extrusion process.
- As heating continues, the drum-tight state of the sheet is rapidly replaced by *sheet rippling* or "swimming". The sheet may also exhibit very rapid droop or sag and the sheet texture may change from glossy to matte at this time. During this time, the sheet temperature is passing through the glass transition temperature for

© 1996 Carl Hanser Verlag. All rights reserved.
No unauthorized disclosure or reproduction; licensed to purchaser only.

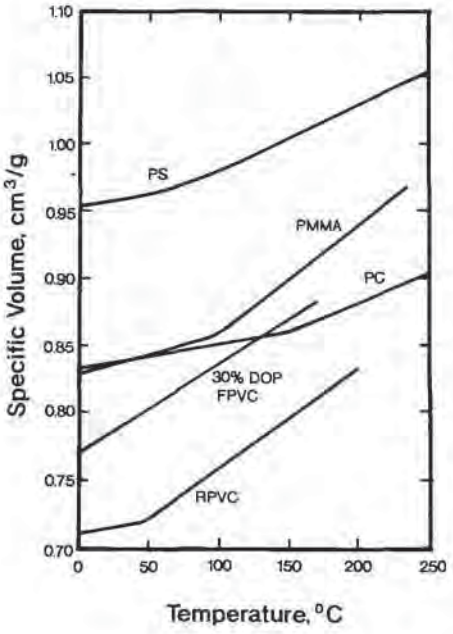

Figure 4.1 Temperature-dependent specific volume for several thermoplastics

amorphous polymers. For certain crystalline-tendency polymers such as PET, some surface crystallization may take place[1]. The swimming effect is apparently due to nonuniform residual stresses imparted in the sheet during the last stages of cooling the sheet. The sag is probably due to the decrease in density as the sheet passes through the glass transition temperature (Fig. 4.1) [3].

- As heating continues, the rippling state is frequently replaced with a second *tautness* in the sheet. Off-gassing or "smoking" may begin at this time, as well. The sheet temperature is usually above the glass transition temperature at this time. This state is directly attributable to sheet orientation during extrusion. At this time, the sheet may pull from the clamps. Careful observation of sheet tautness at this point may yield clues as to the balance in residual stresses in the MD and TD directions. In heavy-gage sheet forming, this balance may dictate the orientation of the sheet to the mold. The liberated gases may be external lubricants, processing aids, and other low boiling adducts. Since the sheet surface is now substantially hotter than the center, moisture and dissolved gas bubbles appear.
- Continued heating produces *sheet sag*. At this point, the tensile strength of the hot sheet is dropping rapidly and the force of gravity pulls the sheet into a catenary-like shape. As stated above, sag is universally used as an early indicator

[1] This crystallization is sometimes called "cold crystallization" [2]. It occurs above the glass transition temperature but below the crystalline melting point.

© 1996 Carl Hanser Verlag. All rights reserved.
No unauthorized disclosure or reproduction; licensed to purchaser only.

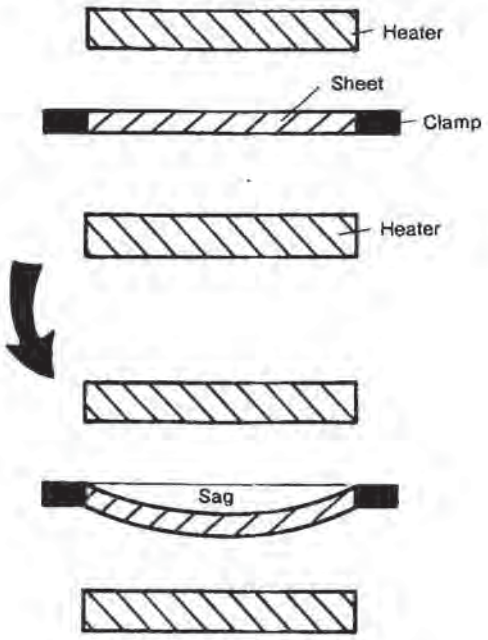

Figure 4.2 Schematic of sheet sag in thermoforming oven

that the sheet is ready to be formed. As seen below, sag is a measure of the temperature-dependent tensile strength of the polymer, in combination with sheet geometry. Since sag is so important to the forming process, it is discussed in detail in Section 4.9. Care must be taken when heating sheet beyond the early stages of sag. As seen in schematic in Fig. 4.2, sag dramatically changes the relationship of the sheet to the top and bottom heaters. The general effect is to change the local view factor between the heaters and the sheet. The center of the sag moves away from the top heaters and toward the bottom heaters. The heat flux becomes unbalanced, with more energy being transferred from the bottom heater. The results are different for thin-gage and heavy-gage sheet.

- For heavy-gage sheet, conduction from the sheet surface to its interior controls the general heating condition. As discussed in Chapter 3, energy inputs to the two surfaces of the sheet are usually controlled independently to ensure uniform energy distribution throughout the sheet thickness. Therefore, energy input to each sheet surface must be carefully controlled to prevent overheating or inadequate heating. When the sheet sags, it approaches the lower heater and retracts from the upper heater. Local energy input to the middle of the underside of the sheet increases dramatically and that to the top side decreases dramatically. This shifts the center of energy symmetry toward the lower surface of the middle of the

© 1996 Carl Hanser Verlag. All rights reserved.
No unauthorized disclosure or reproduction; licensed to purchaser only.

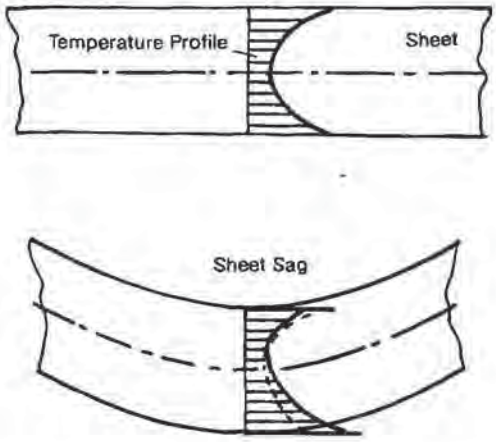

Figure 4.3 Characteristic shift in temperature profile through heavy-gage sheet during sagging

sheet toward the lower surface while the center of symmetry remains near the center of the sheet (Fig. 4.3).

- For thin-gage sheet, where energy input to the sheet surface controls the general heating condition of the sheet, the top-to-bottom energy uniformity is less important than the local change in view factor in the sagging center of the sheet. As the sagging sheet nears the lower heater, the view factor increases toward unity. Energy input is more intense and that area of the sheet heats more rapidly. The local sheet temperature may exceed the upper forming temperature of the polymer. If the polymer melt strength is particularly temperature sensitive, the sheet will flow apart and may drip into the heater. If the polymer degrades rapidly at this temperature, the sheet may blacken or ignite. Since sheet energy uptake is governed by the heater energy output, excessive sag and overheating may occur so quickly with certain polymers that degradation or fire cannot be prevented.

Again, sheet distortion and sag during heating is the result of the polymer responding to external forces of temperature and stress. This chapter lays the foundation for a technical understanding of the fundamental nature of polymer material deformation. Thermoplastic sheet at its forming temperature is considered as:

- A rubbery elastic solid,
- A highly viscous liquid, or
- Something in between.

Owing to the commercial interest in deforming polymers near their melt or softening temperatures, an extensive body of knowledge has been created on this topic. The stretching characteristics of thermoformable sheet are important since understanding the characteristics leads to a very basic understanding of polymer behavior during elongation.

© 1996 Carl Hanser Verlag. All rights reserved.
No unauthorized disclosure or reproduction; licensed to purchaser only.

In this chapter, elongational deformation of polymer sheet will be examined in great technical detail. The objective of this examination is a better understanding of the thermoforming process and how that relates to intelligent selection of the proper polymer for a given application. While the parts designer does not necessarily need to understand the specifics of the concepts presented to design quality parts, the material should be reviewed for general concepts.

4.2 The Stretching Concept

Stretching is elongational material deformation. All real materials, such as polymers, steel, wood and even concrete, stretch to some extent when forces are applied. For modest stretching, the extent of stretching or elongation is called *strain*, ϵ. For solids, strain is the polymer response to the applied force per unit cross-section, or *stress*, σ. For a thin membrane, stretching can be in one direction, uniaxial deformation. Or it can be in two directions or biaxial deformation. If the amount of biaxial stretching is the same in both directions, stretching is equal biaxial deformation.

The simplest uniaxial relationship is Hooke's law:

$$\sigma = E \cdot \epsilon \tag{4.1}$$

The proportionality is the elastic modulus, often called Young's modulus [4]. The units on σ and E are the same, either MPa or lb_f/in^2. The relationship in biaxial stretching is written as:

$$\sigma_i = \frac{E \cdot \epsilon_i}{(1 - \nu)} \tag{4.2}$$

where ν is Poisson's ratio and i is the strain direction ($i = 1,2$). Simply put, a Hookean material responds instantaneously to the applied load. So long as the load remains constant, the material retains a constant strain or elongation. When the load is removed, the material instantaneously returns to its unstrained state. Hooke's law adequately describes the small deformation response of most traditional materials such as metals and wood and is often pictured as a simple spring. For modest deformation levels, most solid materials respond in some fashion similar to that of Equation 4.1. When solids are strained to high levels, they may simply fracture, they may exhibit deviation from the Hookean relationship, or they may yield (Fig. 4.4[1]). Most polymers below their glass transition or melting temperatures show these general characteristics.

[1] As an example, if the solid material deforms in a Hookean manner to a given level of deformation, then yields to produce a continuous deformation under constant load, the material is called an *elastoplastic solid* [5].

© 1996 Carl Hanser Verlag. All rights reserved.
No unauthorized disclosure or reproduction; licensed to purchaser only.

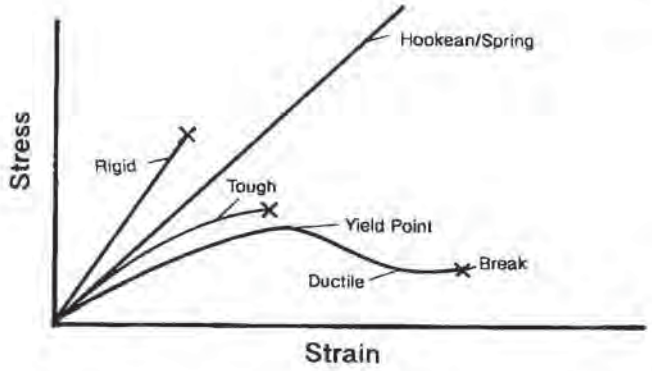

Figure 4.4 Characteristic stress-strain curves for thermoformable thermoplastics, compared with the classic purely elastic Hookean spring

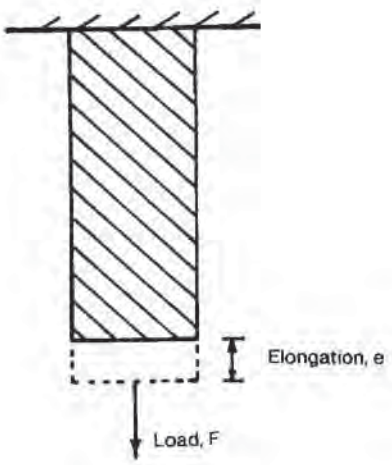

Figure 4.5 Tensile elongation under load [5]

For extensive deformation, consider the example of tensile loading (Fig. 4.5) [6]. The weight of the hanging sheet is given as:

$$W = \rho \cdot hbL \tag{4.3}$$

where ρ is the density of the sheet, h is its thickness, b is its width, henceforth assumed to be unity, and L is its length. The tensile strength is given as:

$$\sigma_o = \frac{W}{A} \tag{4.4}$$

where $A = bh$. Therefore the initial stress applied to the top of the sheet at the clamp is:

$$\sigma_o = \rho \cdot L_o \tag{4.5}$$

© 1996 Carl Hanser Verlag. All rights reserved.
No unauthorized disclosure or reproduction; licensed to purchaser only.

The local deformation, ϵ, per unit length of the sheet is given as:

$$\epsilon = \frac{\Delta L}{L} \tag{4.6}$$

The differential strain is uniform everywhere along the vertical sheet axis. Engineering strain, ϵ_{eng}, is given in terms of the initial sheet length, L_o:

$$\epsilon_{eng} = \frac{L - L_o}{L_o} = \frac{\delta}{L_o} = \lambda - 1 \tag{4.7}$$

where λ is the ratio of instant to initial length, L/L_o. Hencky strain or true strain, ϵ_{true}, is obtained by summing all differential strains over the sheet length:

$$\epsilon_{true} = \int_{L_o}^{L} \frac{dL}{L} = \ln\left(\frac{L}{L_o}\right) = \ln(\lambda) \tag{4.8}$$

For relatively low values of strain, $\epsilon \ll L_o$, engineering strain is a good approximation to true strain. At an engineering strain level of 20%, the error in approximating true strain is about 10%. Example 4.1 illustrates other values for engineering and true strain. The engineering strain value is always smaller than the true strain value.

Example 4.1 True and Engineering Strain

Determine values for true and engineering strain for $L = 1.1\ L_o$ and $L = 2\ L_o$.

True strain is given by Equation 4.8. Engineering strain is given by Equation 4.7.

For the first case, $L = 1.1\ L_o$. $\epsilon_{eng} = 0.1$ and $\epsilon_{true} = 0.095$. $\epsilon_{eng}/\epsilon_{true} = 1.15$.

For the second case, $L = 2\ L_o$. $\epsilon_{eng} = 1.0$ and $\epsilon_{true} = 0.693$. $\epsilon_{eng}/\epsilon_{true} = 1.44$. Engineering strain is always greater than true strain.

As with strain, there are two ways of defining stress. Engineering stress is the applied force per initial unit area:

$$\sigma_{eng} = \frac{F}{A_o} \tag{4.9}$$

True stress is the applied force per true or actual unit area, A_t:

$$\sigma_{true} = \frac{F}{A_t} \tag{4.10}$$

The initial stress is fixed by the length of the sheet and its density. As the sheet stretches, the weight remains constant, but L increases and h decreases, in proportion. The true stress on the sheet increases in proportion to its length, and the strain on the sheet increases, as well. It is apparent that engineering stress-strain, based on initial lengths and thicknesses, is easier to use for computational purposes. Regard-

© 1996 Carl Hanser Verlag. All rights reserved.
No unauthorized disclosure or reproduction; licensed to purchaser only.

less of whether engineering or true stress-strain relationships are considered, the functional relationship is:

$$\sigma = f(\epsilon;E(T)) = g(\lambda;E(T)) \tag{4.11}$$

where E(T) is some material proportionality, such as tensile modulus or the more complex multi-constant proportionalities of hyperelastic models such as the Ogden and Mooney-Rivlin models, discussed below. The stress-strain proportionality is temperature-dependent, decreasing with increasing temperature. As a result, increasing sheet temperature results in rapid increase in strain in the sheet.

In general, all solids behave as:

$$\sigma = f(\epsilon) \tag{4.12}$$

When fluids are shear-stressed, they continue to deform until the stresses are removed. The simplest relationship is Newton's law:

$$\sigma = \mu \cdot \dot{\epsilon} \tag{4.13}$$

where $\dot{\epsilon}$ is the time rate of change of strain, also called the strain rate. The proportionality, μ, is called the Newtonian viscosity or shear viscosity. The unit on the strain rate is s^{-1}. The units on μ are either MPa · s or $lb_f \cdot s/in^2$. For elongational flow, the equivalent uniaxial relationship is written as:

$$\sigma = \eta_e \cdot \dot{\epsilon} \tag{4.14}$$

where η_e is the extensional viscosity or the Trouton viscosity. For deformation-rate independent fluids in uniaxial extension, the Trouton viscosity is three times the Newtonian shear viscosity:

$$\eta_e = 3 \cdot \mu \tag{4.15}$$

For biaxial extension, the equation becomes:

$$\eta_e = 6 \cdot \mu \tag{4.16}$$

Most small molecule fluids are adequately described by Equations 4.4 and 4.5 [7]. As a rule, polymers do *not* follow Newton's law. In certain instances, polymer fluid response can be described adequately as non-Newtonian:

$$\sigma = \eta(\dot{\epsilon}) \cdot \dot{\epsilon} \tag{4.17}$$

For viscous-only polymer fluid response, the viscosity, $\eta(\dot{\epsilon})$ is considered to be deformation rate-dependent. For most polymers, the viscosity decreases with decreasing deformation rate. The intermolecular sliding is inhibited by steric factors and chain entanglements. Polymer fluids are considered to be viscoelastic fluids or *elastic liquids*. By viscoelasticity, it is meant that the polymer response to applied forces has both elastic and viscous characteristics:

$$\sigma = f(\epsilon,\dot{\epsilon}) \tag{4.18}$$

The arithmetic relationship between the applied stress, σ, and the polymer response, as ϵ and $\dot{\epsilon}$, is called the material *constitutive equation of state*. The study of polymer

© 1996 Carl Hanser Verlag. All rights reserved.
No unauthorized disclosure or reproduction; licensed to purchaser only.

Table 4.1 Relationship between Polymer Response and Extent of Deformation

Polymer behaviour	Small deformation	Large deformation	Small deformation rate	Large deformation rate
Viscosity	Not applicable	Not applicable	Newtonian or non-Newtonian	Newtonian or non-Newtonian
Elasticity	Hookean	neo-Hookean or rubber	Not applicable	Not applicable
Viscoelasticity	Linear	Nonlinear	Linear	Nonlinear

response to applied forces is called *rheology*[1]. The realm of viscoelasticity is usually separated into linear and nonlinear viscoelasticity. Linear viscoelasticity is restricted to polymer response to small deformations and small deformation rates. Material responses are usually position- or coordinate-independent. In nonlinear viscoelasticity, deformations and deformation rates are large. During stressing, the polymer is convected or moved far from its original position. As a result, there is great complexity in relating the time-dependent polymer response to the applied stress. Table 4.1 summarizes the general concepts of polymer viscoelasticity.

Before beginning the technical details of rubbery polymer sheet response to applied external loads, the following axiom applies:

Although hot rubbery polymers exhibit both solid rubbery and rubbery liquid characteristics, in the limit, thermoforming is a solid phase deformation process.

The importance of this axiom is seen in computer-aided design models for wall thickness calculations, discussed in detail in Chapter 9.

In thermoforming, the extent of sheet deformation depends on:

- Sheet temperature,
- Level of applied force,
- Level of molecular order and orientation, and
- General material constitutive equation of state.

[1] Details about rheology and its application to polymer processing in general can be obtained from many source-books. Some introductory books include:

S.L. Rosen, *Fundamental Principles of Polymeric Materials*, Wiley-Interscience, New York, 1982.
R.L. Crawford, *Plastics Engineering*, 2nd Ed., Pergamon Press, Oxford, 1987.
J.A. Brydson, *Flow Properties of Polymer Melts*, Van Nostrand Reinhold, New York, 1970.

More advanced books on rheology include:

C.D. Han, *Rheology in Polymer Processing*, Academic Press, New York, 1976.
A.G. Fredrickson, *Principles and Applications of Rheology*, Prentice-Hall, New Jersey, 1964.
C.J.S. Petrie, *Elongational Flows: Aspects of the Behaviour of Model Elastoviscous Fluids*, Pitman, London, 1979.
R.B. Bird, R.C. Armstrong, and O. Hassager, *Dynamics of Polymeric Liquids. Volume 1: Fluid Mechanics*, John Wiley & Sons, New York, 1977.

© 1996 Carl Hanser Verlag. All rights reserved.
No unauthorized disclosure or reproduction; licensed to purchaser only.

Table 4.2 Type of Viscosity Expected for Several Types of Plastic Processing[1]

Process	Type of extensional viscosity		
	Uniaxial	Uniform biaxial	Pure shear
Injection molding, radial flow			X
Blow molding			
Cylindrical parison			X
Spherical parison		X	
Fiber spinning	X		
Converging entry flows			
Rectangular die			X
Circular die	X		
Thermoforming[2]	X	X	X

[1] Adapted from [8], with permission of Society of Plastics Engineers
[2] Depends on particular configuration and whether plug assist is used

Above the glass transition temperature, T_g, most amorphous polymers have sufficient chain mobility to deform and even flow under load. For crystalline polymers above T_g, those chain segments that are not involved in the crystallite formations, either in the spherulites or capture in dendritic structures, can deform. The extent of deformation then depends on the polymer level of crystallinity. As an example, HDPE has a very high degree of crystallinity of about 90% and so cannot be thermoformed below its melt temperature. PVC, on the other hand, usually has a very low level of crystallinity of about 10% and so is usually thermoformed above its glass transition temperature just as if it is amorphous.

Thermoforming involves a complex mixture of extensional deformation processes, Table 4.2 [8]. In pneumatic sheet prestretching, the stretching is essentially uniform biaxial extension in the center of the bubble (Fig. 4.6) and nearly uniaxial extension at the clamp edge (Fig. 4.7). The deformation in the center of the bubble is essentially unconstrained orientation. Free-form blowing of skylights, blisters and

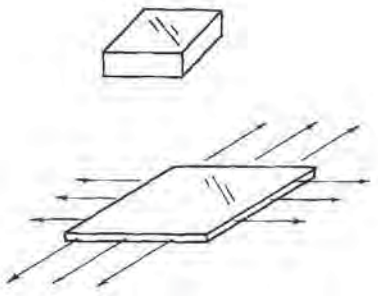

Figure 4.6 Characteristic biaxial stretching of membrane

© 1996 Carl Hanser Verlag. All rights reserved.
No unauthorized disclosure or reproduction; licensed to purchaser only.

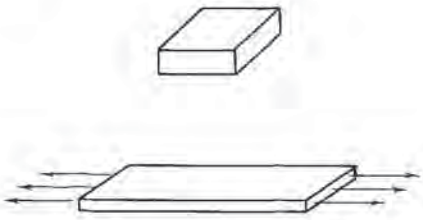

Figure 4.7 Characteristic uniaxial or tensile stretching of membrane

bubbles yields mostly biaxially stretched parts. When the sheet is mechanically stretched with plugs or web catchers, the plastic is uniaxially stretched between its solid anchor points. When the sheet contacts a mold surface almost immediately upon initiation of stretching, that portion of the sheet is uniaxially stretched. Under these conditions, the sheet is undergoing constrained orientation. Unconstrained deformation gives the clearest analysis of polymer behavior under load. It also provides a practical means for determining the thermoformability of a polymer and so is examined in detail shortly.

4.3 Polymer Hot Strength

As the polymer temperature increases, tensile strength and modulus decrease and elongation increases. This is true for amorphous and crystalline polymers alike. Simply put, polymer sheets should become rubbery when heated to the forming temperature. Typically, the tensile test is a standard procedure for measuring the strength of solid polymers[1]. From a uniaxial tensile test on a dogbone-shaped sample, the initial elongation under load yields the tensile modulus, elastic modulus or Young's modulus, E (Fig. 4.8). As the applied load increases, neck-down, yielding and extensive elongation occur. The polymer response becomes one of plastic yielding. The yield point is seen as the point where an abrupt change in strain occurs. Ductile and rubbery polymers continue to bear load while yielding. The sample fails at its ultimate tensile strength and ultimate elongation or elongation at break. Brittle polymers normally exhibit very little yielding before failing.

Standard Tensile Tests

According to the standard tensile test, ASTM D638, the test speed must be one of four standard values, according to the type of polymer being tested. And the gage

[1] The US standard is ASTM D638 with ASTM D618 as the conditioning procedure. The German standard is DIN 53455 and the international standard is ISO 527.

© 1996 Carl Hanser Verlag. All rights reserved.
No unauthorized disclosure or reproduction; licensed to purchaser only.

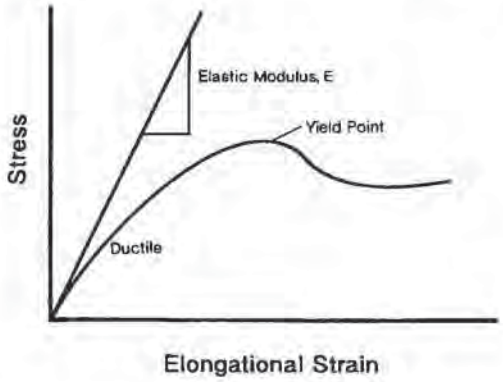

Figure 4.8 Characteristic stress-strain curve for a ductile polymer, showing tangent or elastic modulus

length must be one of two standard values, again according to the polymer. The four speeds are:

- Speed A is 0.05 in/min $\pm$ 25% for polymers with gage length of 2 in $\pm$ 0.01 in. This is an elongation rate of 2.5%/min or 0.0004 s^{-1}.
- Speed B is 0.2 in/min $\pm$ 25% for the same gage length. This is an elongation rate of 10%/min or 0.0017 s^{-1}.
- Speed C is 2.0 in/min $\pm$ 10% for polymers with gage lengths of 1 in $\pm$ 0.005 in or 2 in $\pm$ 0.01 in. For the shorter gage, this is an elongation rate of 200%/min or 0.033 s^{-1}.
- Speed D is 20 in/min $\pm$ 10% for polymers with gage length of 1 in $\pm$ 0.005 in. This is an elongation rate of 2,000%/min or 0.33 s^{-1}.

The sample strain rate, $\dot{\epsilon}$, in s^{-1}, mm/mm · s or in/in · s, is the slope of the elongation-time curve. Thermoforming is a high deformation rate process with momentary strain rates of 0.1 to 10 s^{-1} or higher. As seen above, the highest crosshead speeds on the shortest test specimen yield sustained strain rates of 0.33 s^{-1} [9,10]. In other words, even the highest laboratory speeds yield stress-strain data near the low end of the practical process strain rate.

The standard ASTM D638 test is a room temperature test. Thermoforming needs tensile data at the forming temperature. Hot tensile tests are difficult to carry out with any degree of reliability or confidence in the data. At elevated temperatures, uniaxial stretching is not confined to the neck-down portion of the dogbone sample. Grip slip or extrusion of the plastic from the grips is common. Sample conditioning at the desired temperature is arduous since the sample is usually quite limp and the grips and even the load cells conduct heat from the sample to the environmental chamber. Conditioning times of 12 minutes are recommended [9]. Appreciable annealing and strain relaxation can occur during thermal conditioning and initial elongation values under load, particularly initial values of Young's modulus, are

© 1996 Carl Hanser Verlag. All rights reserved.
No unauthorized disclosure or reproduction; licensed to purchaser only.

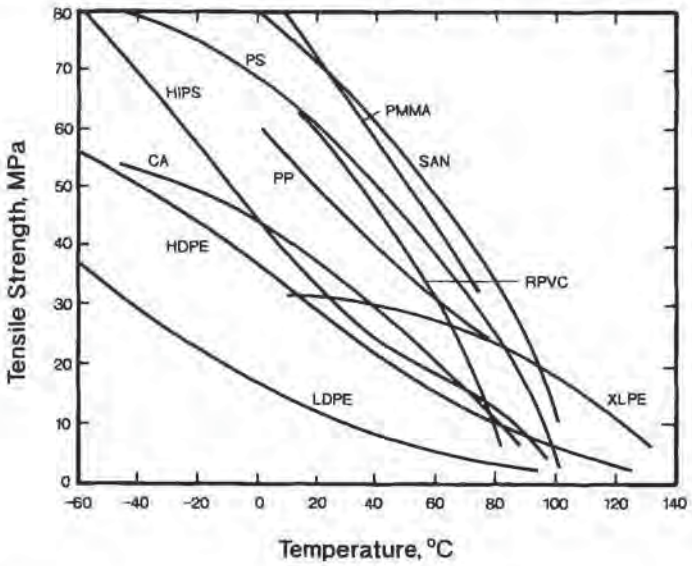

Figure 4.9 Temperature-dependent tensile strength for several thermoplastics. Figure adapted from [11] and used with permission of copyright owner

usually suspect. In short, high temperature tensile tests are difficult to master and may yield suspect data.

Nevertheless, hot tensile test data are quite important in the determination of the general formability of polymers. For example, the tendency for abrupt sheet sag is thought to be related to the rapid drop in tensile modulus with temperature [10]. Figures 4.9 and 4.10 [11,12] show the temperature-dependent tensile strengths for several crystalline and amorphous polymers. Figures 4.11 and 4.12 [13,14] show temperature-dependent moduli for several commodity and engineering polymers. It is hard to generalize about temperature-dependent properties of polymers. For example, in Fig. 4.9 [11], the tensile strength of amorphous high-impact polystyrene or HIPS has a relatively linear decrease in value with temperature, whereas amorphous unmodified polystyrene tensile strength decreases rapidly with increasing temperature. A similar comparison can be made for crystalline polychlorotrifluoroethylene or CTFE and crystalline polytetrafluoroethylene or PTFE. Again, although it is hard to generalize, filled polymers have higher low-temperature moduli but exhibit the same temperature dependencies as the unfilled polymers at higher temperatures. It is thought that the filler acts to dilute the polymer and to offer yielding defects at higher temperature.

Fibers, on the other hand, reinforce the polymer at higher temperatures. Thus, although the shape of the temperature dependent tensile property is the same as that for the neat polymer, the value is increased as the fiber loading is increased, to a point. The shape of the stress-strain curve is also important, as discussed shortly. If

© 1996 Carl Hanser Verlag. All rights reserved.
No unauthorized disclosure or reproduction; licensed to purchaser only.

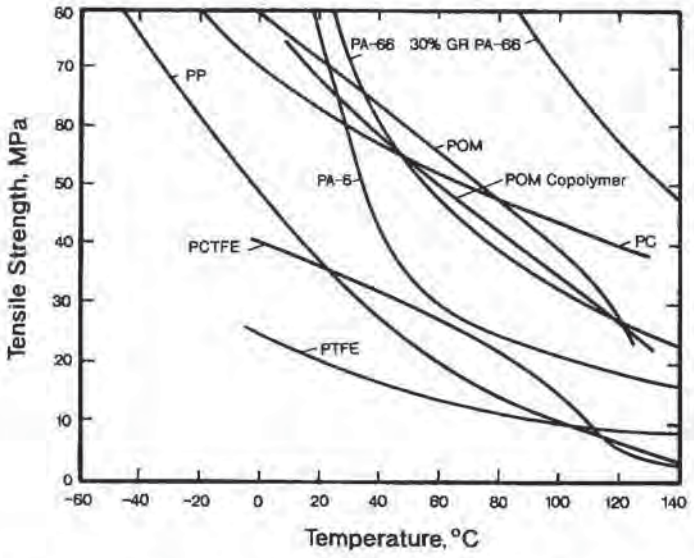

Figure 4.10 Temperature-dependent tensile strength for several thermoplastics. Figure adapted from [11,12] and used with permission of copyright owner

the polymer does not exhibit excessive yield, the parts produced from the polymer tend to have consistently uniform wall thicknesses, particularly in deep draw applications [10]. Crystalline polymers seem to process best if formed at temperatures within 10°C or 20°F of their melt temperatures.

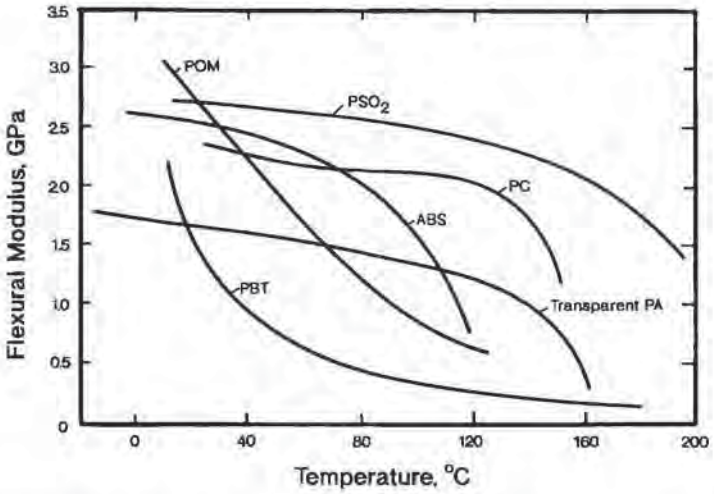

Figure 4.11 Temperature-dependent flexural modulus for several thermoplastics. Figure adapted from [13,14] and used with permission of copyright owner

© 1996 Carl Hanser Verlag. All rights reserved.
No unauthorized disclosure or reproduction; licensed to purchaser only.

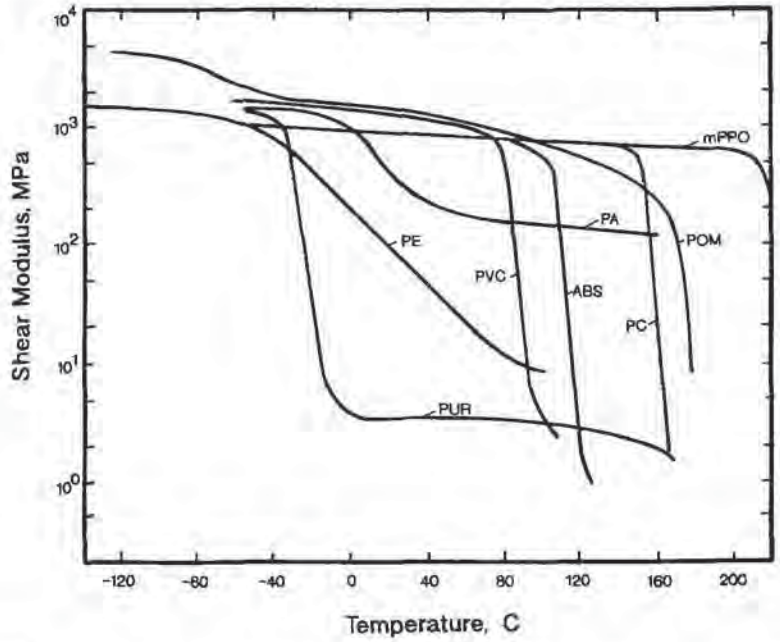

Figure 4.12 Temperature-dependent shear modulus for several thermoplastics. Figure adapted from [13,14] and used with permission of copyright owner

Hot Tensile Tests

Despite their problems, hot tensile tests have been used for years to bracket the forming regions of polymers [15]. There are two general approaches to hot tensile tests. The first employs a fixed rate of stretch. The ASTM D638 test run in a high-temperature environmental chamber is an example of a fixed stretching rate test. For this test, $\dot{\epsilon} = d\epsilon/d\theta = \text{constant}$ and the amount of force required to stretch the sample is measured as a function of deformation, yielding:

$$\sigma = f(\epsilon; \dot{\epsilon} \text{ fixed}) \tag{4.19}$$

If the polymer is simply an elastic solid, the rate of stretching is immaterial to the stress-strain curve. Thus:

$$\sigma = f(\epsilon \text{ only}) \tag{4.20}$$

On the other hand, if the polymer is viscoelastic, the generated stress-strain curves are functions of $\dot{\epsilon}$.

© 1996 Carl Hanser Verlag. All rights reserved.
No unauthorized disclosure or reproduction; licensed to purchaser only.

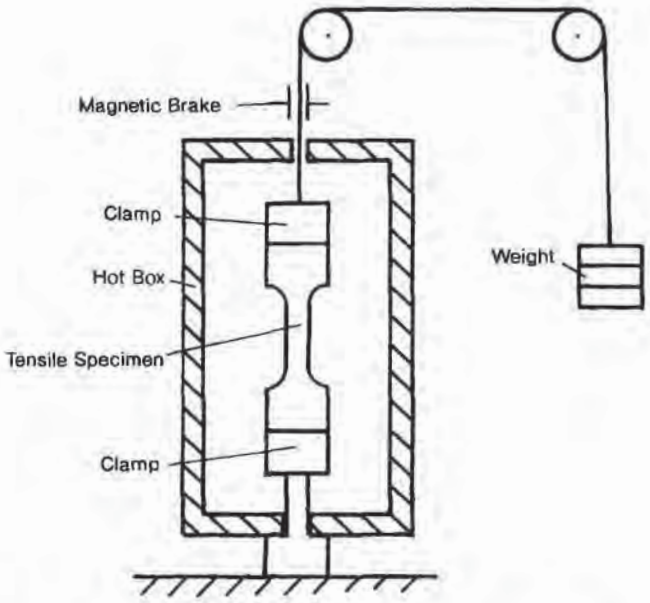

Figure 4.13 Schematic of hot tensile test apparatus with dogbone test specimen

Hot Creep Tests

Hot creep is another uniaxial test that has been used extensively to evaluate polymer candidates for thermoforming. In tensile creep, a fixed load, resulting in a fixed stress, $\sigma = \text{constant}$, is applied to the sample at temperature. The strain level, ϵ and the strain rate, $\dot{\epsilon}$ is then measured. Usually, creep is a long-term test, involving relatively low loads and temperatures [16]. Hot creep is a modification of this test. Here, a fixtured sample is placed in a high-temperature oven without load and allowed to reach isothermal temperature. A very high load is then instantaneously applied and a high speed film or video camera records the time-dependent elongation to break [17]. Figure 4.13 is a schematic of this simple test. Instantaneous strain rates of 5 s^{-1} or more are routinely measured this way. For this test, the following equation applies:

$$\sigma = \text{constant} = f(\epsilon;\dot{\epsilon}) \tag{4.21}$$

Although the test is simple, interpretation of the results can be difficult. Figure 4.14 is a schematic from an actual test sequence for one applied load value for rigid PVC or RPVC in the forming temperature range of 300°F to 350°F or 149°C to 177°C. As is apparent, the sample did not elongate appreciably at the lowest temperature and showed a very high rate of elongation at the highest temperature. The hot creep test yields temperature-dependent ultimate elongation values as well. In one reported experiment [17], the ultimate elongation or strain for rigid PVC or RPVC increased

© 1996 Carl Hanser Verlag. All rights reserved.
No unauthorized disclosure or reproduction; licensed to purchaser only.

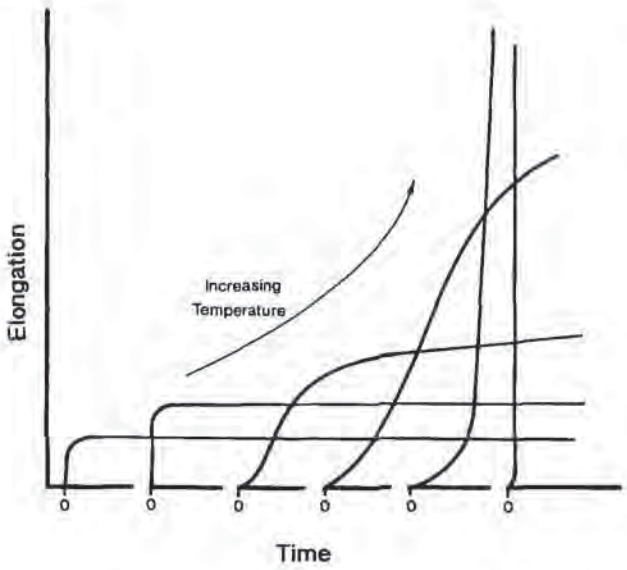

Figure 4.14 Characteristic of temperature-dependent elongation for hot tensile test

linearly from about 120% at 100°C to about 500% or so at 122°C, then dropped to about 300% or so at 140°C to 180°C. This indicates that local draw ratios for this PVC should not exceed about 3:1 to 4:1. The effect of strain hardening, owing to increasing strain rate at a given temperature is implicitly found in the hot creep test. Hot uniaxial creep test data are compromised by the same testing vagarities that occur in hot tensile testing. Nevertheless there is a strong indication that ultimate uniaxial strain can be related to areal draw ratios in simple geometries [17].

A strain rheometer has been developed recently in an effort to circumvent some of the difficulties with grip slip (Fig. 4.15) [18,19]. The device replaces the dogbone tensile bar with an injection molded O-ring. A section cut from an extruded thin-walled tube also works as a sample. The device employs a high-torque variable speed motor. A section of very high modulus aircraft cable connects the pulley attached to the motor to the sample. In turn the sample is attached to the load cell. The original device employed a load cell that was rigidly connected to the motor frame and was immersed in the hot silicone oil bath. A modified device uses a torque meter attached to the motor. The operation of the device is quite simple. The polymer O-ring sample is attached to round pins on the aircraft cable and the load cell. The entire assembly is lowered into hot silicone oil, and it reaches the hot oil temperature in about a minute or so. After a few moments, a slight tension is applied to the sample by the motor. The motor is then shut off and the desired motor speed selected. The motor is then switched on and the sample is stretched at constant strain rate. Elongation rates of up to 500%/s or 5 s^{-1} have been achieved although rates of 2.5%/s to 25%/s or 0.025 s^{-1} to 0.25 s^{-1} yield more reliable stress-strain curves.

© 1996 Carl Hanser Verlag. All rights reserved.
No unauthorized disclosure or reproduction; licensed to purchaser only.

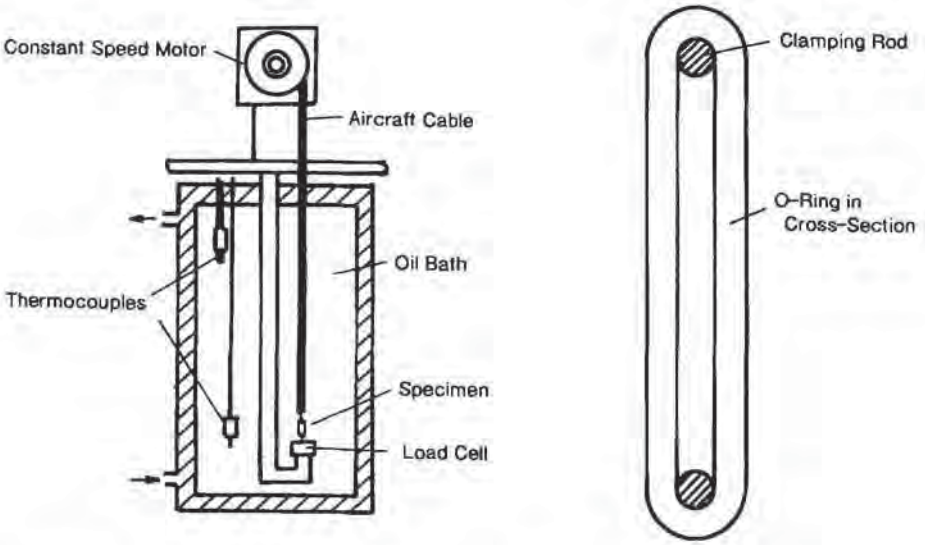

Figure 4.15 Tensile strain rheometer and O-ring-shaped test specimen [18,19]

The hot creep test is more sensitive than the hot tensile test to changes in polymer character at a given strain level and temperature. The hot tensile test provides a clearer picture for stress-strain behavior at high strain levels. However, hot creep and hot tensile tests do not predict processing conditions necessary for obtaining accurate mold replication. Prediction of sheet performance in practical draw-down situations cannot be obtained from these tests. Neither test system truly replicates the nature of biaxial sheet stretching so common in even the simplest thermoforming process. As a result, recent studies have focused on the development of biaxial stretching laboratory tests that more closely mirror reality. An important aspect of these efforts is to find and define useful material design parameters that are used to better evaluate the performance of a given polymer in a given stretching situation.

Other Stretching Tests

In addition to hot creep and hot tensile tests, sheet inflation experiments yield important information on biaxial membrane stretching. Two types of inflation devices have been used. The first uses a carefully gridded circular disk that is inflated at constant pressure [20], as shown in schematic in Fig. 4.16. A high-speed video or film camera is used to measure the biaxial stretching rate at the center or pole position of the disk. The results are used to determine constitutive constants in appropriate stress-strain equations, as discussed in Section 4.4. The second uses a long carefully gridded tube of polymer. The ends of the tube are either clamped in cylindrical fittings or pinched shut (Fig. 4.17). Inflation air at a fixed pressure is

© 1996 Carl Hanser Verlag. All rights reserved.
No unauthorized disclosure or reproduction; licensed to purchaser only.

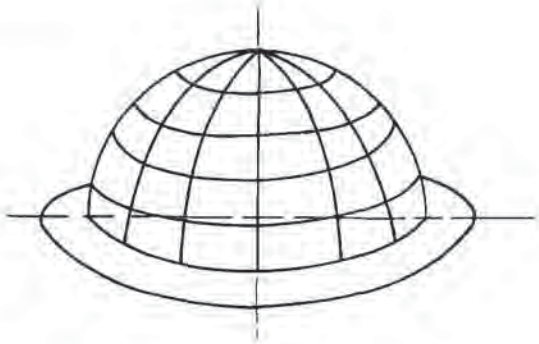

Figure 4.16 Schematic of biaxial stretching of disk by air inflation [20]

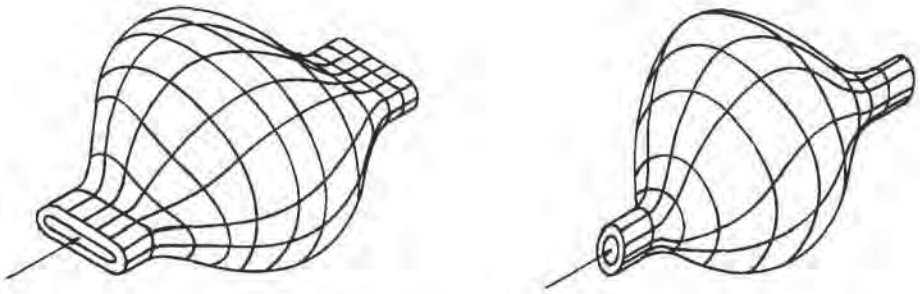

Figure 4.17 Schematics of biaxial stretching of tube by air inflation. Left figure shows flattened connection to air source. Right figure shows round connection to air source

introduced through a blow pin and the stretching rate in the middle of the tube is measured on high-speed video or film. This now-commercial device is used to obtain constants for constitutive equations [21,22]. And commercial isothermal tenter frame devices are used to determine forces required to biaxially orient thin films of 0.025 in or 0.64 mm or so [24,25].

Temperature-Dependent Viscosity for Amorphous Polymers

As noted earlier, once the temperature of an amorphous polymer exceeds its glass transition temperature, the polymer continues to become less and less rubbery and more and more fluid until it is a true liquid. Again, the relationship of stress to strain rate for a purely viscous fluid is:

$$\sigma = \mu \cdot \dot{\epsilon} \tag{4.13}$$

© 1996 Carl Hanser Verlag. All rights reserved.
No unauthorized disclosure or reproduction; licensed to purchaser only.

Table 4.3 Temperature Dependency of Shear Viscosity for Several Commercial Polymers [118]

Polymer	Shear rate (s^{-1})	$1/\beta_t$ (°C)	Trade name
Polymethyl methacrylate (PMMA)	100	24	Lucite 140
Polymethyl methacrylate (PMMA)	27	18	Plexiglass V100
Cellulose acetate (CA)	100	32	Tenite Acetate 036-H2
Nylon 6	100	60	Plaskin Nylon 8206
Nylon 66	100	56	Zytel 101 NC10
Polyethylene (LDPE)	100	85	Bakelite DYNH
Polyethylene (HDPE)	100	70	Alathon-10
Polystyrene (PS)	100	73	Styron 475
ABS	100	65	Cyclolac T
Polyvinyl chloride, rigid (RPVC)	40	51	Geon 8750
Polyvinyl chloride, flexible (FPVC)	100	40	Opalon 71329

where μ is a proportionality known as Newtonian viscosity. For polymers, the relationship is usually written as:

$$\sigma = \eta_e(\dot{\epsilon}) \cdot \dot{\epsilon} \tag{4.22}$$

where η_e is the strain-rate dependent elongational viscosity. For most amorphous polymers at low strain rates, the viscosity approaches a constant at low strain rates. This is usually written as:

$$\eta_e(\dot{\epsilon}) \rightarrow \eta_{e,o} \text{ as } \dot{\epsilon} \rightarrow 0 \tag{4.23}$$

where $\eta_{e,o}$ is the zero-elongational rate viscosity[1]. It is thought that the $\eta_{e,o}$ viscosity of any amorphous polymer at its glass transition temperature is about 1.0 GPa · s. As the polymer temperature increases, the viscosity decreases in an Arrhenius fashion:

$$\eta_{e,1} = \eta_{e,2} \cdot \exp\left[\frac{E_\epsilon}{R}\left(\frac{1}{T_2} - \frac{1}{T_1}\right)\right] \tag{4.24}$$

Usually the Arrhenius activation energy, E_ϵ, is determined from temperature-dependent shear viscosity measurements and so is listed as $E_{\dot{\gamma}}$. Figure 4.18 shows stress- and temperature-dependent shear viscosity for polymethyl methacrylate [26]. Equation 4.24 is also written in an empirical fashion as an Arrhenius-like equation:

$$\eta_{e,1} = \eta_{e,2} \cdot \exp[\beta_\epsilon(T_2 - T_1)] \tag{4.25}$$

where $1/\beta_\epsilon$ represents "the number of degrees that the polymer temperature must be raised at constant shear rate in order to decrease the viscosity by a factor of 1/e." [27]. Values for the equivalent $1/\beta_t$ coefficient are given in Table 4.3 for several

[1] Zero-extensional rate viscosity is the asymptotic elongational viscosity. Zero-shear rate viscosity is the asymptotic shear viscosity. Shear viscosity is easier to measure than elongational viscosity. The elongational viscosity is usually considered to be proportional to the shear viscosity, particularly at zero-state conditions. Since it is the *zero-state* condition that is most important, it is assumed that this proportionality is in effect in the rest of this section.

© 1996 Carl Hanser Verlag. All rights reserved.
No unauthorized disclosure or reproduction; licensed to purchaser only.

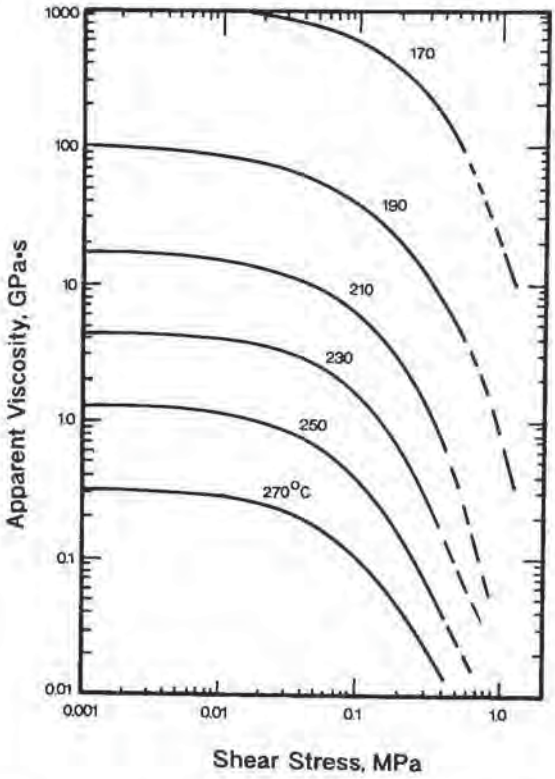

Figure 4.18 Temperature- and shear stress-dependent viscosity for polymethyl methacrylate, PMMA [26]

polymers. The WLF equation is an alternate to the Arrhenius temperature dependency. It is written as:

$$\log \frac{\eta_{\dot{\epsilon},o}(T)}{\eta_{\dot{\epsilon},o}(T_g)} = -\frac{C_1 \cdot (T - T_g)}{C_2 + (T - T_g)} \tag{4.26}$$

where C_1 and C_2 are the WLF constants for a given polymer, Table 3.16. Example 4.2 illustrates the application of these expressions for prediction of temperature-dependent zero-state viscosity. The zero-state viscosity of a polymer at its glass transition temperature cannot be accurately measured. Instead, the values are extrapolated using the Arrhenius-like equation or WLF expression.

Example 4.2 The Hypothetical Zero-Strain Rate Viscosity of Polymethyl Methacrylate at Its Glass Transition Temperature

From Fig. 4.18, determine the $1/\beta_{\dot{\epsilon}}$ factor for the molding grade of PMMA. Then, determine the C_1 and C_2 constants of the WLF equation. Finally, determine the zero-shear viscosity for PMMA at 105°C for each of these equations.

© 1996 Carl Hanser Verlag. All rights reserved.
No unauthorized disclosure or reproduction; licensed to purchaser only.

From Fig. 4.18, the zero-shear viscosities at three temperatures are:

$$\eta_o(270°C) = 310 \text{ Pa} \cdot \text{s}$$

$$\eta_o(230°C) = 4{,}400 \text{ Pa} \cdot \text{s}$$

$$\eta_o(190°C) = 102{,}000 \text{ Pa} \cdot \text{s}$$

The Arrhenius-like Equation 4.25 is written as:

$$\ln [\eta_{e,1}/\eta_{e,2}] = \beta_\epsilon (T_2 - T_1)$$

$$\ln [102000/310] = 5.80 = \beta_\epsilon (270 - 190) = 80 \cdot \beta_\epsilon$$

$$1/\beta_\epsilon = 13.8$$

Table 4.3 shows a range in values for equivalent $1/\beta_\epsilon$ from 18 to 24 for shear rates of 27 to 100 s^{-1}.

The WLF coefficients are obtained from Equation 4.26:

$$\log\left[\frac{\eta_{e,o}\,(T)}{\eta_{e,o}\,(T_g)}\right] = -\frac{C_1 \cdot (T - T_g)}{C_2 + (T - T_g)}$$

At 190°C:

$$\log_{10} [102000/\eta_{e,o}(T_g)] = -\frac{C_1(190 - 105)}{C_2 + (190 - 105)}$$

At 230°C:

$$\log_{10} [4400/\eta_{e,o}(T_g)] = -\frac{C_1(230 - 105)}{C_2 + (230 - 105)}$$

At 270°C:

$$\log_{10} [310/\eta_{e,o}(T_g)] = -\frac{C_1\,(270 - 105)}{C_2 + (270 - 105)}$$

These are written as:

$$5.0086 = A - 85 \cdot C_1/[C_2 + 85]$$

$$3.6435 = A - 125 \cdot C_1/[C_2 + 125]$$

$$2.4914 = A - 165 \cdot C_1/[C_2 + 165]$$

Eliminating A from the first two and the first and third:

$$1.3651 = \frac{125 \cdot C_1}{C_2 + 125} - \frac{85 \cdot C_1}{C_2 + 85}$$

$$2.5172 = \frac{165 \cdot C_1}{C_2 + 165} - \frac{85 \cdot C_1}{C_2 + 85}$$

Solving each for C_1:

$$1.3651 = C_1\left[\frac{125}{C_2 + 125} - \frac{85}{C_2 + 85}\right]$$

$$2.5172 = C_1\left[\frac{165}{C_2 + 165} - \frac{85}{C_2 + 85}\right]$$

© 1996 Carl Hanser Verlag. All rights reserved.
No unauthorized disclosure or reproduction; licensed to purchaser only.

Eliminating C_1:

$$\left[\frac{165}{C_2+165}-\frac{85}{C_2+85}\right]=1.8440\left[\frac{125}{C_2+125}-\frac{85}{C_2+85}\right]$$

$$C_2=347.7$$

Substituting:

$$C_1=20.08$$

These values are compared with $C_1 = 17.7$, $C_2 = 52.6$ for PMMA from Table 3.16.

The value of $A = \log_{10}[\eta_{e,o}(T_g)]$ is obtained by substitution:

$$5.0086=A-\frac{85\cdot C_1}{C_2+85}=A-\frac{85\cdot 20.08}{347.7+85}$$

$$A=8.953 \text{ or}$$

$$\eta_{e,o}(T_g)=0.897\times 10^9 \text{ Pa}\cdot\text{s}=0.897 \text{ GPa}\cdot\text{s}$$

For the Arrhenius-like results, the hypothetical viscosity at $T_g = 105°C$ is:

$$\eta_{e,105}=4400\cdot\exp[230-105)/13.8]$$

$$\eta_{e,105}=37.8 \text{ MPa}\cdot\text{s}=0.038 \text{ GPa}\cdot\text{s}$$

[It is reported that $\eta_{e,o}(T_g)\approx 1$ GPa · s for all amorphous polymers at their glass transition temperatures. It is apparent that the WLF equation yields a viscosity value similar to the expectation. The Arrhenius-like expression does not.]

Keep in mind that in thermoforming, stretching is primarily a solid polymer deformation action. The elastic character of the polymer dominates. Nevertheless, the hot rubbery strength of the polymer is frequently compared with its hot *melt* strength. The actual viscosity value of a polymer is less important than the temperature dependency of the viscosity. If the value of $1/\beta_\epsilon$ is very small, the polymer viscosity drops very rapidly with temperature. Since a wide rubbery plateau is sought for thermoforming, polymers with small $1/\beta_\epsilon$ values should have narrower forming windows than those with large $1/\beta_\epsilon$ values. Examples 4.3, 4.4 and 4.5 illustrate how the zero-state viscosity might be used for thermoforming.

Example 4.3 Determination of the Viscosity for Polystyrene in the Thermoforming Window

Determine the zero-state viscosity of polystyrene at its lower, average, and upper forming temperatures. Use the Arrhenius-like Equation 4.25.

The Arrhenius-like equation is:

$$\eta_{e,1}=\eta_{e,2}\cdot\exp[\beta_\epsilon(T_2-T_1)]$$

The relevant temperatures for PS are:
$T_g = 105°C$, $T_L = 127°C$, $T_A = 149°C$, $T_U = 182°C$. The viscosity of PS at 210°C is 9000 Pa · s and $1/\beta_\epsilon$ for polystyrene from Table 4.3 is 73.

© 1996 Carl Hanser Verlag. All rights reserved.
No unauthorized disclosure or reproduction; licensed to purchaser only.

$$\eta_{e,127} = \eta_{e,210} \cdot \exp[(210 - 127)/73] = 28{,}060 \text{ Pa} \cdot \text{s}$$

$$\eta_{e,149} = \eta_{e,210} \cdot \exp[(210 - 149)/73] = 20{,}760 \text{ Pa} \cdot \text{s}$$

$$\eta_{e,182} = \eta_{e,210} \cdot \exp[(210 - 182)/73] = 13{,}210 \text{ Pa} \cdot \text{s}$$

Example 4.4 Comparison of Polystyrene and ABS Viscosities in the Thermoforming Window

Determine the zero-state viscosity of ABS at its lower, average, and upper forming temperatures. Use the Arrhenius-like Equation 4.45. Then compare the results with Example 4.3 for PS.

The Arrhenius-like equation is:

$$\eta_{e,1} = \eta_{e,2} \cdot \exp[\beta_\epsilon(T_2 - T_1)]$$

The relevant temperatures for ABS are:
$T_g = 105°C$, $T_L = 127°C$, $T_A = 146°C$, $T_U = 182°C$. The viscosity of ABS at 190°C is 43,000 Pa · s and $1/\beta_\epsilon$ for ABS from Table 4.3 is 65.

$$\eta_{e,127} = \eta_{e,190} \cdot \exp[(190 - 127)/65] = 113{,}300 \text{ Pa} \cdot \text{s}$$

$$\eta_{e,146} = \eta_{e,190} \cdot \exp[(190 - 146)/65] = 84{,}600 \text{ Pa} \cdot \text{s}$$

$$\eta_{e,182} = \eta_{e,190} \cdot \exp[(190 - 182)/65] = 48{,}600 \text{ Pa} \cdot \text{s}$$

ABS has about four times the viscosity of PS across the entire forming window. This implies that the forming forces need to be about four times greater for ABS and that ABS sag should be less of a problem than PS sag.

Example 4.5 Predicting the Forming Window From Viscosity Measurements

A new polymer is known to have a $1/\beta_\epsilon$ value of 20°C. If its viscosity at 300°C is 2,000 Pa · s, determine its approximate forming temperature range. Assume that "best forming viscosity" is 40,000 Pa · s and that the "forming range for viscosity" is a factor of 2.

From the information given, the approximate viscosity at the upper forming temperature is about 25,000 Pa · s and that at the lower forming temperature is about 50,000 Pa · s. The Arrhenius-like equation is:

$$\eta_{e,1} = \eta_{e,2} \cdot \exp[\beta_\epsilon(T_2 - T_1)]$$

Applying this equation three times and solving for the temperatures:

$$2{,}000 = 25{,}000 \cdot \exp[(T_U - 300)/20]$$

$$2{,}000 = 40{,}000 \cdot \exp[(T_A - 300)/20]$$

$$2{,}000 = 50{,}000 \cdot \exp[(T_L - 300)/20]$$

$T_U = 250°C$, $T_A = 240°C$, $T_L = 235°C$. Potentially, this polymer has a very narrow forming window of 15°C.

© 1996 Carl Hanser Verlag. All rights reserved.
No unauthorized disclosure or reproduction; licensed to purchaser only.

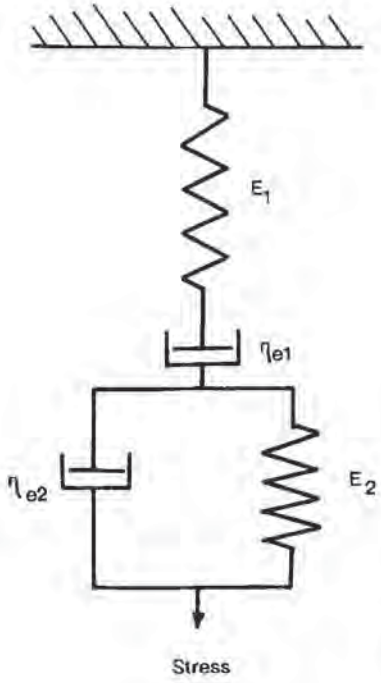

Figure 4.19 Maxwell-Voigt mechanical analog of linear viscoelasticity [29]

Dynamic Mechanical Testing

Dynamic mechanical testing is used to determine the relative importance of the elastic and viscous aspects of polymers [28]. If the polymer response to applied load can be considered as linear viscoelastic, then simple spring-and-dashpot models serve to illustrate the response. The spring represents the elastic or fully recoverable portion of the response and the dashpot represents the viscous or fully dissipative portion of the response. Figure 4.19 [29] is an example of a four-parameter element, having the Maxwell viscoelastic model of a spring and dashpot in series, in series with a Voigt-Kelvin model of a spring and dashpot in parallel. The response of the four-element model to an instantaneously applied constant stress, σ, is shown in Fig. 4.20 [30]. When the load is applied in a periodic, sinusoidal fashion, the elastic portion of the model responds instantaneously. The phase angle between the input and response is therefore zero. The phase angle for the purely viscous portion is always $\pi/2$ radians or the viscous portion is always 90° out of phase (Fig. 4.21) [31]. The four-element model, representing linear viscoelastic response, shows a response with a phase angle that is somewhere between 0° and 90°. The sinusoidal strain displacement of the polymer is given as:

$$\alpha = \alpha_o \sin(\omega\theta) \tag{4.27}$$

© 1996 Carl Hanser Verlag. All rights reserved.
No unauthorized disclosure or reproduction; licensed to purchaser only.

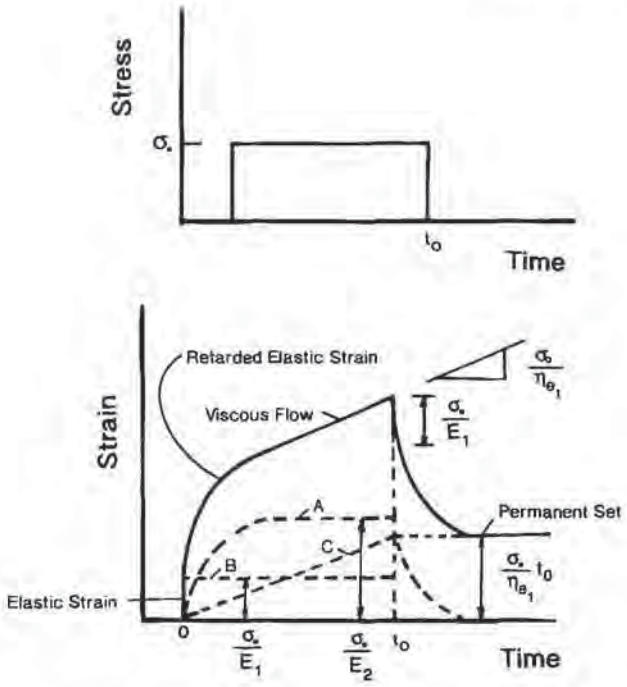

Figure 4.20 Response of Maxwell-Voigt mechanical analog of Fig. 4.19 to step-change in applied tensile load [30]

where α_o is the amplitude of the displacement, ω is the frequency, and θ is time. The response to the strain displacement is usually written in complex terms as:

$$\tau^* = \tau' + i \cdot \tau'' \tag{4.28}$$

where τ^* is the complex stress, τ' is the real component of the stress and τ'' is called the imaginary component of the stress. Four functions are associated with polymer response to sinusoidal load.The *complex modulus*, G^* is given as:

$$G^* = (\tau^*/\alpha) = (\tau'/\alpha) + i \cdot (\tau''/\alpha) \tag{4.29}$$

This is also written as:

$$G^* = G' + i \cdot G'' \tag{4.30}$$

The real or in-phase portion of the modulus, G', is called the *storage modulus*. It represents that portion of the inputted energy that is elastically recovered. The imaginary or out-of-phase portion of the modulus, G'', is called the *loss modulus*. It represents that portion of energy that is dissipated. The ratio of the loss modulus to storage modulus is the *loss tangent*, *loss factor* or *tan* δ. It is written as:

$$\tan \delta = \tau''/\tau' = G''/G' \tag{4.31}$$

© 1996 Carl Hanser Verlag. All rights reserved.
No unauthorized disclosure or reproduction; licensed to purchaser only.

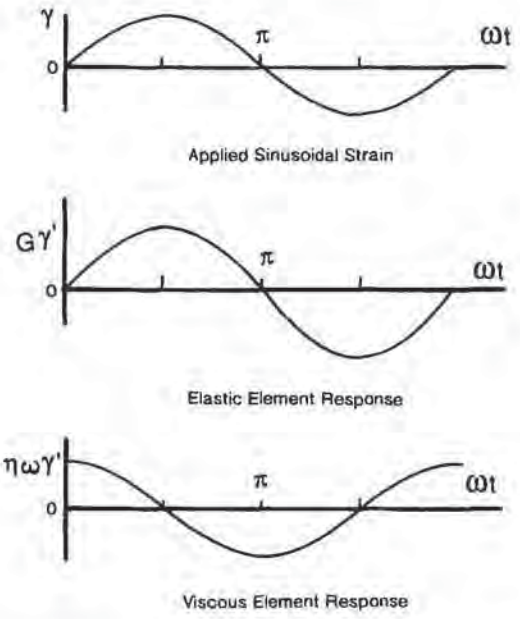

Figure 4.21 Response of elastic and viscous portions of Maxwell-Voigt mechanical analog to sinusoidal tensile load [31]

At constant temperature, polymer response changes with changing frequency. At very high loading frequencies, $\omega \rightarrow$ large, most polymers appear glassy. Thus, the storage modulus, G′ is large, the loss modulus, G″ is small and tan δ is small. At very low loading frequencies, $\omega \rightarrow$ small, many polymers appear rubber-like. Thus, G′ is small, G″ is small, and tan δ is moderately small. At intermediate frequencies, the storage modulus, G′ is decreasing with increasing frequency. The loss modulus, G′ on the other hand, goes through a maximum. The value of tan δ also goes through a maximum, as shown in Fig. 4.22 [32].

This analysis holds for constant frequency, changing temperature conditions as well. At very low temperatures, polymers appear glassy. At elevated temperatures, polymers appear rubbery. At intermediate temperatures, polymers exhibit loss in rigidity and increased viscous dissipation. The test used to obtain the temperature-dependent complex modulus is called dynamic mechanical analysis or thermomechanical analysis, DMA or TMA [33]. Typically, only G′, the storage modulus and tan δ, the loss factor are measured. G″, the loss modulus is obtained from Equation 4.31. Figure 4.23 shows classic TMA curves for polycarbonate [34]. As is expected, 30% glass-reinforced PC has a much greater modulus than that for unreinforced PC. However, at or about 140°C, both materials experience rapid drops in G′. Simultaneously, tan δ for both polymer species shows a rapid increase, indicating a

© 1996 Carl Hanser Verlag. All rights reserved.
No unauthorized disclosure or reproduction; licensed to purchaser only.

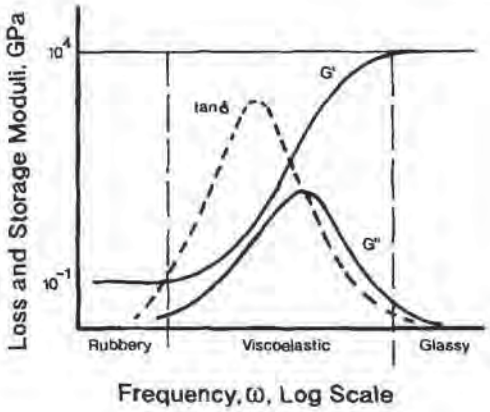

Figure 4.22 Frequency-dependent response of elastic and viscous portions of Maxwell-Voigt mechanical analog to applied sinusoidal tensile load [32]. The loss tangent, tan $\delta = G''/G'$

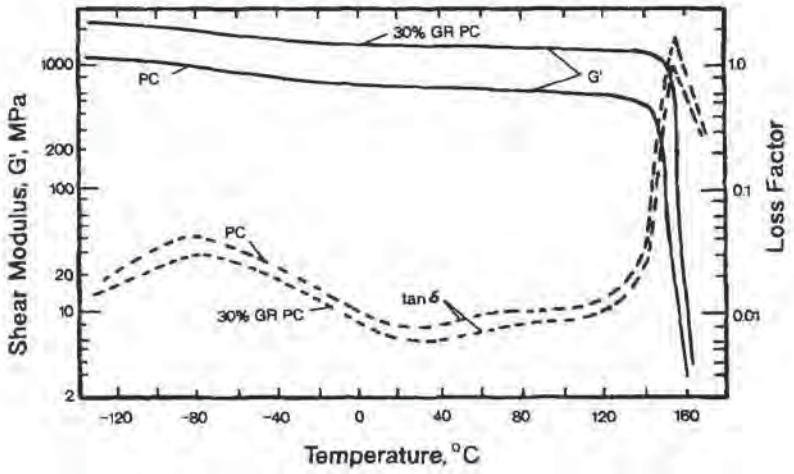

Figure 4.23 Temperature-dependent shear modulus and loss factor for unreinforced and 30% glass-reinforced polycarbonate, PC. Figure redrawn from [34] and used by permission of copyright owner

rapid increase in G". In a word, in this temperature range, the polymer is becoming more viscous and less elastic. The glass transition temperature of PC is listed as 150°C. Figure 4.24 shows the effect of molecular weight on transitions for PS [35] and Fig. 4.25 shows the effect of crystalline level on transitions for polyethylene [36].

© 1996 Carl Hanser Verlag. All rights reserved.
No unauthorized disclosure or reproduction; licensed to purchaser only.

4.4 Stress-Strain-Rate of Strain—Theory

The time-dependent elastic nature of polymers at the thermoforming temperature is understood in terms of solid or fluid behavior. There are two acceptable ways of including time dependency in the typical stress-stain analysis of a solid. One method is to alter conventional rheological stress-strain rate viscosity models to include solid-like behavior at high strain rates [37]. The other is to include some time dependent factor in a typical stress-strain relationship of a solid. Both are simplified approaches to the general cases of viscoelastic mechanical analyses [38-40]. The common methods for determining polymer strain-strain rate response to applied stretching stresses include extensional rheometry [37,41], biaxial or bubble inflation of a tube or sheet [21-23,42], biaxial stretching of a blown film [43], free blowing of a preform [44], uniaxial stretching of fibers [41], and creep experiments [9,17,45].

Creep experiments are the easiest tests to conduct. These tests yield information on polymer response to constant low-level load at isothermal conditions [9,14,45-47]. Rate-dependent terms are considered negligible. At room temperature, many polymers follow a near-ideal strain-hardening ductile material creep rupture response to constant load:

$$\sigma = \sigma_o \exp(m \cdot \epsilon) = \sigma_o \cdot e^m \cdot \lambda \tag{4.32}$$

where σ is instant stress, σ_o is the initial stress, ϵ is the elongational strain, and m is the straining-hardening factor. If the polymer is ideally ductile, $m = 1$. It has been shown that $0.92 < m < 1.6$ for many polymers at strain-rate levels of less than $0.0333\ s^{-1}$, Table 4.4 [47]. At high loading levels and/or elevated temperatures, creep rates are so high that measuring and conditioning errors make accurate interpreta-

Table 4.4 Strain Hardening Constants for Several Polymers[1]

$\sigma = \sigma_0 e^{m\epsilon}$

Polymer	Strain rate (s^{-1})	From plot [47] σ_0 (MPa)	(lb_f/in^2)	m	From least squares σ_0 (MPa)	(lb_f/in^2)	m
POM, Delrin	0.00027	67.9	9850	1.12	65.8	9539	1.312
POM, Delrin	0.0027	68.95	10000	1.19	68.3	9910	1.257
PA-66, nylon	0.0027	49.6	7200	0.919	51.5	7468	0.894
mPPO, Noryl	0.0027	48.3	7000	1.061	48.8	7079	1.06
PVC	0.0027	38.6	5600	0.974	38.0	5518	1.029
PE	0.0333	7.93	1150	1.182	8.26	1198	1.144
PP	0.0133	12.93	1875	1.103	13.0	1889	1.102
PE	0.0333	13.5	1960	1.182	13.4	1943	1.169
PTFE	NR	10.34	1500	1.58	10.3	1495	1.603
PTFE	NR	12.41	1800	1.203	12.51	1815	1.203

[1] Adapted from [47], by permission of copyright owner

NR = Not reported

© 1996 Carl Hanser Verlag. All rights reserved.
No unauthorized disclosure or reproduction; licensed to purchaser only.

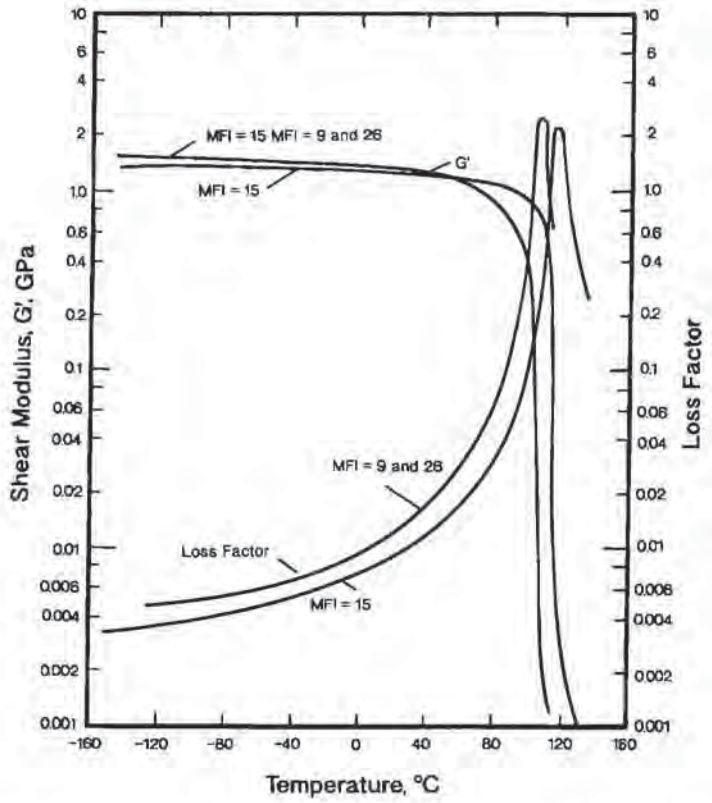

Figure 4.24 Temperature-dependent shear modulus and loss factor for two molecular weights of polystyrene, PS. Figure redrawn from [35] and used by permission of copyright owner

tion difficult or impossible [9,17]. Time-dependent behavior has been added to the creep model as [48-50]:

$$\sigma = \sigma_o \cdot f(\epsilon) \cdot g(\theta) \tag{4.33}$$

For amorphous polymers such as PMMA and HIPS, at normal forming temperatures, the data favor an ideal elastic or non-strain-hardening, model, Table 4.5 [49]:

$$\sigma = \sigma_o \cdot \epsilon^m \cdot \theta^n \tag{4.34}$$

HIPS appears to have little time-dependent behavior, with $n \approx 0$. On the other hand, ABS/PVC and PVC exhibit substantial strain-hardening at processing temperatures (Fig. 4.26) [17]. Recent studies on polypropylene show that the time-dependent coefficient can be either positive or negative, depending on the nature and size of spherulites (Fig. 4.27) [51].

So long as the polymer deforms uniformly during uniaxial stretching, its isothermal ultimate tensile strength is obtained from:

$$T^* = \sigma_o \cdot \exp[(m-1) \cdot \epsilon_f] \tag{4.35}$$

© 1996 Carl Hanser Verlag. All rights reserved.
No unauthorized disclosure or reproduction; licensed to purchaser only.

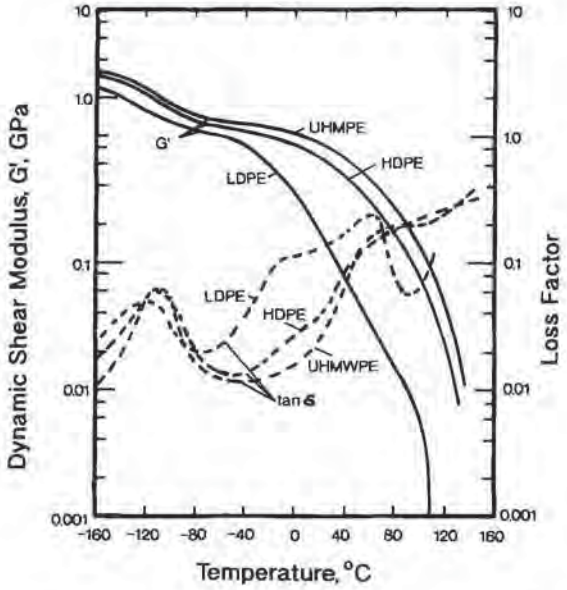

Figure 4.25 Temperature-dependent shear modulus and loss factor for three types of polyethylene. Figure redrawn from [36] and used by permission of copyright owner

where ϵ_f is the true strain at fracture. If $m \approx 1$, as is the case for most polymers in Table 4.3, $T^* \approx \sigma_o$. As noted in Figs. 4.9 and 4.10, polymer tensile strength decreases with temperature. Tensile strength values for most polymers at normal vacuum forming temperatures are in the 0.07 to 0.7 MPa or 10 to 100 lb_f/in^2.

For truly elastic polymers, the classic temperature-dependent stress-strain curves usually appear as shown in Fig. 4.28. At low temperatures, the polymer is purely elastic. Its modulus is very high and its ultimate strain is very low. As the temperature increases, a small amount of plastic deformation occurs before the polymer breaks. The modulus decreases with increasing temperature. At a slightly higher temperature, the polymer may show a distinct yielding. The higher strain regions beyond the yield point are characterized by localized drawing or necking.

Table 4.5 Stress-Strain Behavior of Two Plastics in Biaxial Extension[1]

$\sigma = \sigma_0 \epsilon^m \theta^n$

Polymer	n	m
PMMA	−0.05	1.0
HIPS	−0.33	1.1

[1] Adapted from [49], with permission

© 1996 Carl Hanser Verlag. All rights reserved.
No unauthorized disclosure or reproduction; licensed to purchaser only.

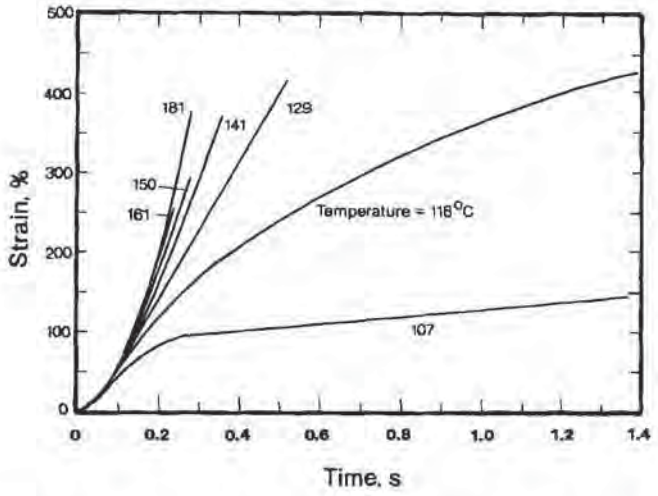

Figure 4.26 Temperature-dependent strain rate for rigid polyvinyl chloride, RPVC [17]

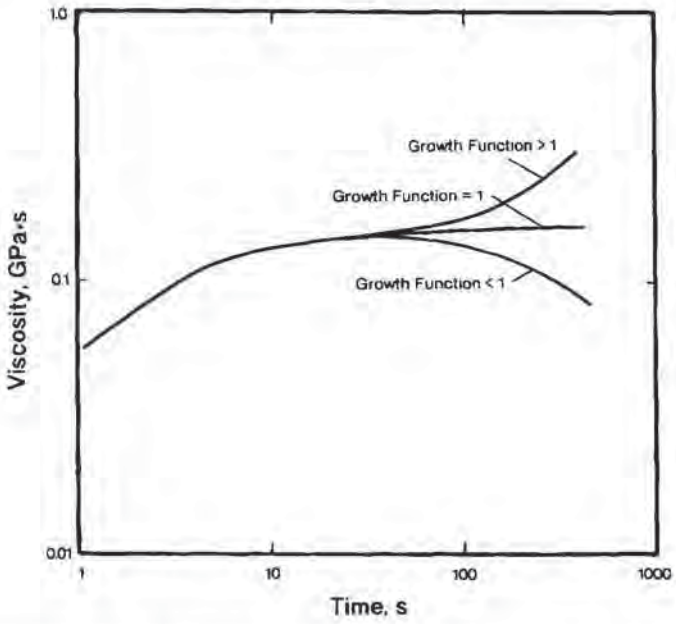

Figure 4.27 Schematic of time-dependent viscosity for polyolefin polymers that exhibit various strain rate effects [51]

© 1996 Carl Hanser Verlag. All rights reserved.
No unauthorized disclosure or reproduction; licensed to purchaser only.

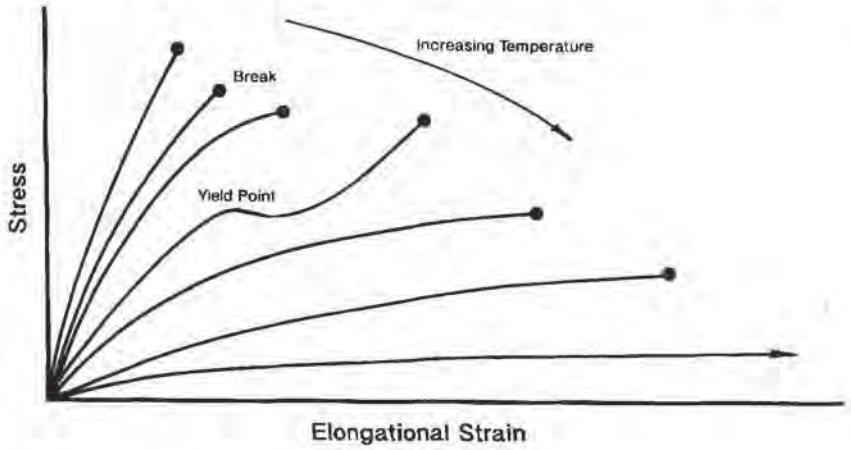

Figure 4.28 Characteristic temperature-dependent stress-strain curves

Not all polymers neck. As the temperature increases, the ultimate elongation increases rapidly. There is an upper limit to the temperature of course. When the polymer cannot sustain any applied force without extensive plastic deformation and fracture, it is considered a fluid.

Figure 4.29 shows the interrelationship between the polymer response to applied load and the forming window. As expected, the amount of force required to draw the polymer sheet to a given extent is highest at the lower forming temperature. This implies that the depth of draw or areal draw ratio increases with increasing

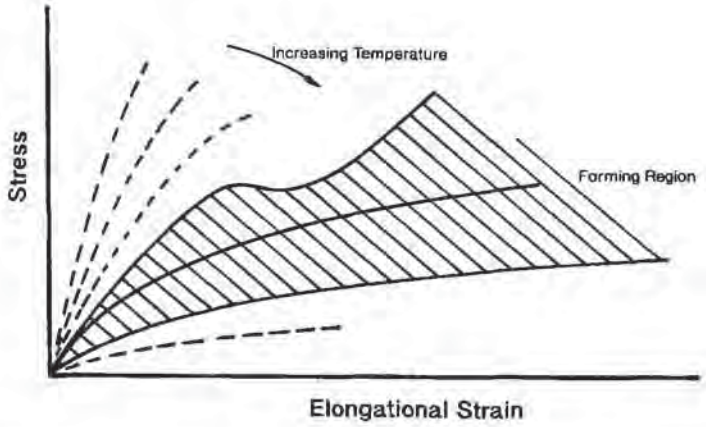

Figure 4.29 Characteristic overlay of forming temperature on temperature-dependent stress-strain curves

© 1996 Carl Hanser Verlag. All rights reserved.
No unauthorized disclosure or reproduction; licensed to purchaser only.

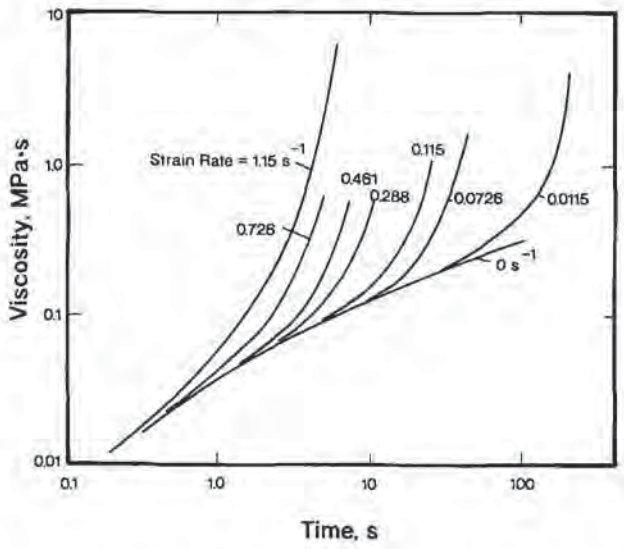

Figure 4.30 Strain-rate dependent extensional viscosity for high-density polyethylene, HDPE, at 180°C. Figure adapted from [37]

temperature. At the upper forming temperature, draw uniformity gives way to localized flow and the areal draw ratio then abruptly decreases with increasing temperature.

When the processing temperature is substantially above T_g for an amorphous polymer or T_m for a crystalline one, the polymer is a fluid. Behavior under load is correctly considered in terms of elongational viscosity. Isothermal elongational viscosity usually increases with increasing time (Fig. 4.30). At very low strain rates, $\eta_e \propto \theta^n$, where $n < 1$, Table 4.6 [49]. Isochronous biaxial elongational viscosities of olefins at forming temperature and very low strain rates of 0.000015 to 0.006 s^{-1} are inversely proportional to strain rate [46]. As the strain rate increases, the apparent viscosity deviates from the asymptote at earlier and earlier times. As seen in Fig. 4.31 [17], for LDPE at 2 seconds, the polymer has a viscosity about 15 times greater at a strain rate of $\dot{\epsilon} = 1\ s^{-1}$ than at $\dot{\epsilon} = 0$. At this same rate at 10 s, the elongational viscosity is about 1000 times greater. In short, the polymer is rapidly becoming solid-like in its response to applied load. Example 4.6 continues this analysis. In terms of true stress and true strain, $\epsilon = \dot{\epsilon} \cdot \theta$, the data show an initial linear region, a yield region, then strain hardening and fracture (Fig. 4.32) [37]. In other words, both amorphous and crystalline polymers behave as elastic liquids at typical thermoforming temperatures [52]. The extent of elasticity is important in determining the formability of the polymer in question.

© 1996 Carl Hanser Verlag. All rights reserved.
No unauthorized disclosure or reproduction; licensed to purchaser only.

Table 4.6 Biaxial Extensional Viscosities for Olefins at Very Low Strain Rates[1]

Polymer	Strain rate, $\dot{\epsilon}$ ($\times 10^{-6}\ s^{-1}$)	Viscosity (GPa · s)
PP, 0.003 in	2310	4.99
Unoriented[2]	196	71.6
	19.1	762
PP, 0.0015 in	2260	6.51
Unoriented	219	50.9
	15.1	719
PP, 0.003 in	5110	28.1
	262	496
	28.8	4150
Ethylene-propylene	181	890
copolymer,	24.3	6310
0.003 in		

[1] Adapted from [49], with permission
[2] Least squares fit, $\eta = 0.015/\dot{\epsilon}$

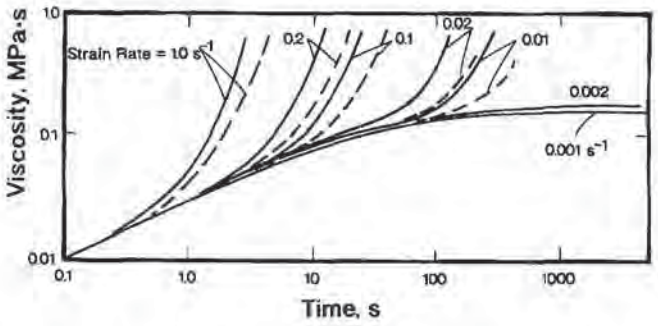

Figure 4.31 Comparison of experimental and theoretical strain-rate dependent extensional viscosity for low-density polyethylene, LDPE. Solid lines are theory. Dashed lines are experiment. Figure adapted from [39], and used with permission of John Wiley and Sons, Inc.

Example 4.6 Time-Dependent Strains for LDPE

From Fig. 4.31, at a strain rate of $\dot{\epsilon} = 0.1\ s^{-1}$, determine the time required to achieve the same level of stiffness as is achieved for $\dot{\epsilon} = 1\ s^{-1}$ in 2 s. Repeat for a strain rate of $\dot{\epsilon} = 0.01\ s^{-1}$.

From Fig. 4.31, the stress at $\dot{\epsilon} = 0.1\ s^{-1}$ is about 15 times greater than that for $\dot{\epsilon} = 0$ at 12 s. The stress at $\dot{\epsilon} = 0.01\ s^{-1}$ is about 15 times greater than that for $\dot{\epsilon} = 0$ at about 100 s.

© 1996 Carl Hanser Verlag. All rights reserved.
No unauthorized disclosure or reproduction; licensed to purchaser only.

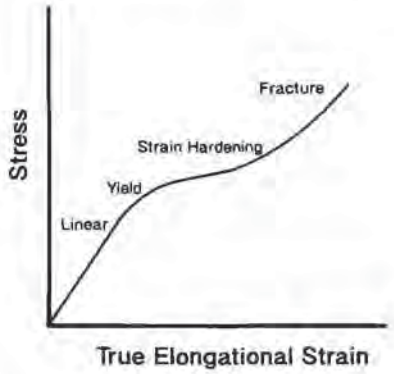

Figure 4.32 Schematic of various stages in the straining of a ductile polymer. Figure adapted from [37], and used with permission of John Wiley and Sons, Inc.

Elasticity—A Rationalization

When a thermoformed shape is placed in an environment having a temperature substantially greater than T_g and a temperature typically approaching that of its forming temperature, the shape returns to a flat sheet. A recovery rate of 90% in less than 0.002 s has been measured [53]. It is argued therefore that thermoforming is a solid phase deformation process. A contrary argument [40,54] is that this response is proper for a highly strained elastic liquid as well as a purely elastic membrane. Sheet stretching behavior is best viewed in terms of relative orders of magnitude of process times and polymer memory. Consider the simple series spring-and-dashpot model of a linear viscoelastic material, the Maxwell fluid (Fig. 4.33) [55]. If this simple model is strained to a fixed value, $\epsilon = \epsilon_o$, and $\dot{\epsilon} = 0$, the Maxwell element response is:

$$\sigma = \sigma_o \cdot \exp[-E\theta/\eta_e] \tag{4.36}$$

where E is the tensile or elastic modulus of the spring, η_e is the elongational viscosity of the dashpot and $\sigma_o = E \cdot \epsilon_o$. The retardation time, $\theta_p = \eta_e/E$, is a characteristic of the polymer. Creep data are used to obtain values for this retardation time. At low strain rates, $\dot{\epsilon} \approx 0$, the tensor stress-strain-rate-of-strain elastic liquid equation reduces to a simple relationship between stress and retardation [56]:

$$\sigma = 6G\theta_p \cdot \dot{\epsilon} \cdot [1 - \exp(-\theta/\theta_p)] \tag{4.37}$$

For long times, $\theta \to \infty$ and:

$$\sigma \to 6G\theta_p \cdot \dot{\epsilon} = \mu \cdot \dot{\epsilon} \tag{4.38}$$

The model yields the Trouton-Newton form for a *purely viscous fluid*. At high strain rates, on the other hand, $\dot{\epsilon} \to \infty$:

$$\sigma \to G\left[\left(1 + \frac{\delta}{2}\right) \cdot \exp(2\dot{\epsilon}\theta) - \frac{\delta}{2} \cdot \exp(4\dot{\epsilon}\theta)\right] \tag{4.39}$$

The term δ is proportional to the ratio of second to first normal stress difference of the polymer and its value is always negative or zero [40]. The model predicts that

© 1996 Carl Hanser Verlag. All rights reserved.
No unauthorized disclosure or reproduction; licensed to purchaser only.

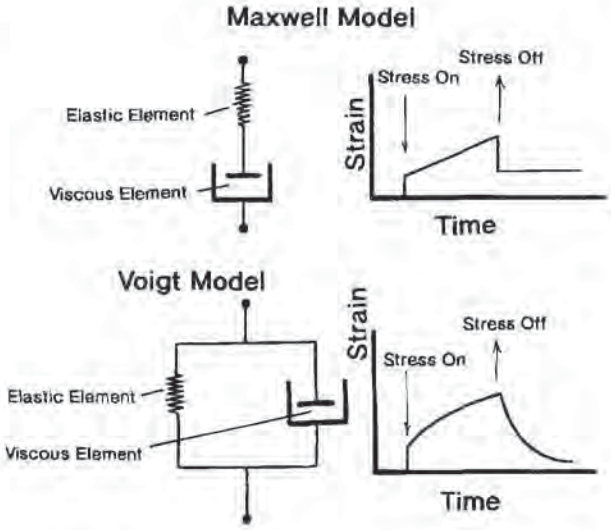

Figure 4.33 Responses of the Maxwell series mechanical analog of polymer linear viscoelasticity [top] and Voigt parallel mechanical analog of polymer linear viscoelasticity [bottom] to instantaneous change in applied tensile load

under constant deformation rate, stress increases exponentially with time. In other words, at high strain rates, the rate of stress increase is greater than the rate of internal material stress relaxation. The polymer therefore behaves as if it is an *elastic solid* [40,57]. It is highly unlikely that constant biaxial deformation can be sustained or is desirable in conventional thermoforming. Deformation rates have been measured that, for the most part, decrease with time [40]. For *constant velocity stretching*, deformation rate decreases with time [40]. This helps stabilize the initially rapidly growing stress.

As noted, retardation times are obtained from creep experiments. Usually these values decrease monotonically with increasing temperature, as seen schematically in Fig. 4.34. discontinuity in the retardation time curve for PP occurs at 110°C or 230°F [45]. This is attributed to a deformation mechanism change on the molecular level. The importance of creep data in parts design has produced a substantial library of information [58]. If temperature-dependent retardation times are not available for a given polymer, approximate values can be obtained at any temperature [48] from:

$$\theta_p(T) = \frac{\eta_o(T)}{G(T)} \tag{4.40}$$

where η_o is the zero-shear viscosity and G is the tensile modulus or the initial slope of the stress-strain curve. If the processing time is less than θ_p by a factor of about 10, the material behaves as an elastic membrane. Snap-back thermoforming depends on elastic membrane response, for instance. If the processing time is greater than θ_p by a factor of about 10, the polymer should behave as an elastic liquid. Pressure

© 1996 Carl Hanser Verlag. All rights reserved.
No unauthorized disclosure or reproduction; licensed to purchaser only.

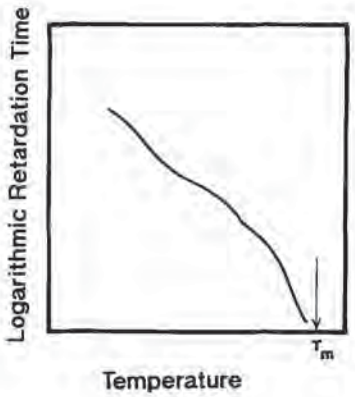

Figure 4.34 Characteristic temperature-dependent retardation time for linear viscoelastic polymers

forming, coining, and high surface replication depend to some degree on plastic or anelastic polymer response. Example 4.7 illustrates some of these aspects. As a point of reference, instantaneous stretching rates of 2.4 s^{-1} are recorded for 0.100 in or 2.5 mm HIPS sheet [59] and rates up to 26.8 s^{-1} are reported for 0.060 in or 1.25 mm PP [60].

Example 4.7 Stretching Rate and Retardation Time for ABS

Determine the retardation time for ABS at 120°C.

The tensile modulus of ABS at 120°C is 80 $lb_f/in^2 = 0.55$ MPa. The viscosity for ABS is obtained from Example 4.4:

$$\eta_{e,120} = \eta_{e,190} \cdot \exp[(190 - 120)/65] = 126{,}200 \text{ Pa} \cdot \text{s}$$

The retardation time, $\theta_p(120°C) = 126200/(0.55 \times 10^6) = 0.23$.

If the stretching rate is substantially greater than $1/\theta_p = 4.4$ s^{-1}, ABS should behave as an elastic solid. If the stretching rate is substantially less than 4.4 s^{-1}, ABS should behave as an elastic liquid.

Strain Energy Function[1]

Principal stresses in elastic solids are defined in terms of the strain energy function, W:

$$\sigma_i = \frac{\partial W}{\partial \lambda_i} \tag{4.41}$$

[1] The stress-strain analysis that follows is applicable to large elongational levels. As a result, the analysis is sometimes called *hyperelastic analysis*, in contrast with linear models used to describe elastic solid response to low elongation levels typically found in structural analysis.

© 1996 Carl Hanser Verlag. All rights reserved.
No unauthorized disclosure or reproduction; licensed to purchaser only.

where λ_i is the extension ratio in the ith direction (i = 1,2,3). ∂W is the incremental amount of work done by the solid when it is stretched an incremental amount $\partial\lambda$ under stress, σ. In general, the strain energy function is written in terms of three principal invariants of the Cauchy strain tensor [40,45,61], as:

$$W = W(I,II,III) \tag{4.42}$$

where:

$$I = \lambda_1^2 + \lambda_2^2 + \lambda_3^2 \tag{4.43}$$

$$II = \lambda_1^{-2} + \lambda_2^{-2} + \lambda_3^{-2} \tag{4.44}$$

$$III = \lambda_1^2 \cdot \lambda_2^2 \cdot \lambda_3^2 \tag{4.45}$$

A stress-strain energy expression is written in terms of these invariants as:

$$\sigma_i = \left(\frac{\partial W}{\partial I}\right)\left(\frac{\partial I}{\partial \lambda_i}\right) + \left(\frac{\partial W}{\partial II}\right)\left(\frac{\partial II}{\partial \lambda_i}\right) + \left(\frac{\partial W}{\partial III}\right)\left(\frac{\partial III}{\partial \lambda_i}\right) \tag{4.46}$$

For an incompressible solid, $\lambda_1 \cdot \lambda_2 \cdot \lambda_3 = 1$, or III = 1. The last term of Equation 4.46 is zero. For *uniaxial stretching*, $\lambda_1 = \lambda$, $\lambda_2 = \lambda_3 = \lambda^{-1/2}$. Therefore, this equation is written as:

$$\sigma\lambda = \left(\lambda^2 - \frac{1}{\lambda}\right) \cdot \left[2\left(\frac{\partial W}{\partial II}\right) + \frac{2}{\lambda}\left(\frac{\partial W}{\partial I}\right)\right] \tag{4.47}$$

In this equation, $\sigma\lambda$ is the tensile stress and σ is the force per unit area of unstrained cross-section. For *equal biaxial stretching*, $\lambda_1 = \lambda_2 = \lambda$, $\lambda_3 = \lambda^{-2}$. The equation is written as:

$$\sigma\lambda = \left(\lambda^2 - \frac{1}{\lambda^4}\right) \cdot \left[2\left(\frac{\partial W}{\partial II}\right) + 2\lambda^2\left(\frac{\partial W}{\partial I}\right)\right] \tag{4.48}$$

The bracketed terms in Equations 4.47 and 4.48 represent the specific elastic solid response, in this case polymeric response, to applied load. The exact form for W(I,II) depends to a great degree on curve-fitting elongational data. Several models follow.

The Rivlin Form for the Strain Energy Function

Fifty years ago, the following simple power-law form for W was proposed, to predict elongational response of rubber to stress [62,63]:

$$W(I,II) = \sum_{i,j} C_{ij}\,(I-3)^i \cdot (II-3)^j \tag{4.49}$$

The neo-Hookean solid yields one of the simplest forms for W:

$$W = C_{ij}(I-3) = C_{10}(I-3) \tag{4.50}$$

The second strain invariant is usually added in one of several ways. The Rivlin-Saunders[1] version is the most general form [64]:

[1] This is sometimes just called the Rivlin model.

© 1996 Carl Hanser Verlag. All rights reserved.
No unauthorized disclosure or reproduction; licensed to purchaser only.

$$W = C_{ij}(I - 3) + f(II - 3) \tag{4.51}$$

The Mooney version assumes a linear function for f(II)[1]:

$$W = C_{01}(I - 3) + C_{10}(II - 3) \tag{4.52}$$

Other Rivlin-type forms are found in Table 4.7. Representative strain energy function coefficients for several polymers are given in Table 4.8.

The uniaxial and biaxial forms for the elastic stress-strain equation are obtained by differentiating the W-function and substituting into Equations 4.47 and 4.48, respectively. Consider the simple Mooney version. $\partial W/\partial I = C_{01}$ and $\partial W/\partial II = C_{10}$. The Mooney stress-strain functions for uniaxial and equal biaxial extension are:

$$\sigma\lambda = \left(\lambda^2 - \frac{1}{\lambda}\right) \cdot \left[2 \cdot C_{01} + \frac{2}{\lambda} \cdot C_{10}\right] \tag{4.53}$$

$$\sigma\lambda = \left(\lambda^2 - \frac{1}{\lambda^4}\right) \cdot [2 \cdot C_{01} + 2 \cdot \lambda^2 \cdot C_{10}] \tag{4.54}$$

These equations are used to curve-fit rubbery elastic sheet deformation, and C_{01} and C_{10} are the curve-fitting constants. Further, since stress-strain relationships are temperature-sensitive, $C_{01} = C_{01}(T)$ and $C_{10} = C_{10}(T)$. In the limit, as the strain goes to zero, the constants are defined in terms of an elastic modulus [59]:

$$\frac{E}{6} = \frac{\partial W}{\partial I} + \frac{\partial W}{\partial II} \tag{4.55}$$

For the Mooney form for W:

$$\frac{E}{6} = C_{01} + C_{10} \tag{4.56}$$

For the Schmidt model, Table 4.7, $E/6 = C'_{01}$, where the prime denotes a different value for the first constant [59,131,132]. For HIPS and PS, predicted modulus values range from 427 to 1192 MPa or 62 to 173 lb_f/in^2. Measured values range from 310 to 3900 MPa or 45 to 566 lb_f/in^2, with errors ranging from -100% to $+50\%$. If the temperature dependency of the polymer modulus is known or is accurately measured, a good approximation of the temperature dependencies of the strain function coefficients can be obtained.

For many polymers, $\partial W/\partial I \gg \partial W/\partial II$ [69]. For the Mooney model, as an example, $C_{01} \gg C_{10}$. The curves are approximated best with the new-Hookean model (Fig. 4.35). For vulcanized natural rubber, the value for C_{10} is about 0.05 to 0.15 times the value for C_{01} [70]. If $C_{01} = 0$, C_{10} equals the elongational, tensile or elastic modulus, G. The neo-Hookean model works best at low levels of deformation, at or just above the linear viscoelasticity region [59,71]. The Schmidt, Mooney and higher order versions of the Rivlin model work best at very high levels of deformation. Schmidt recognized that although his sheet was being deformed rapidly to large deformation, it was not isothermal and was not being deformed at a constant rate. Funt, on the other hand, correlated PP isochronous creep data best with $C_{10} = 0$ [45].

[1] This is sometimes called the Mooney-Rivlin model.

© 1996 Carl Hanser Verlag. All rights reserved.
No unauthorized disclosure or reproduction; licensed to purchaser only.

Table 4.7 Strain Energy Density Forms for Polymers and Elastomers

Name	Form	Material	Source of data	Comments
Neo-Hookean	$W = C_{10}(I-3)$	Natural rubber	Treloar [63]	Uniaxial stretching
		PMMA	Williams [65]	
Mooney	$W = C_{10}(I-3) + C_{01}(II-3)$	Vulcanized natural rubber	Mooney [66]	Uniaxial stretching
			Treloar [63]	
		HIPS	Schmidt [59]	
Funt	$W = C_{01}(II-3)$	PP	Funt [5]	Creep
Schmidt	$W = C_{10}(I-3) + C_{02}(II-3)^2$	HIPS	Schmidt [59]	Bubble inflation (gross)
Mooney-Rivlin	$W = C_{10}(I-3) + C_{01}(II-3) + C_{11}(I-3)\cdot(II-3)$	PVC	Warnecke/Frankenhauser [67]	Uniaxial tensile
Three-parameter Signiorini	$W = C_{10}(I-3) + C_{01}(II-3) + C_{20}(I-3)^2$	EPDM	Warnecke/Frankenhauser [67]	Uniaxial tensile
Third-order	$W = C_{10}(I-3) + C_{01}(II-3) + C_{11}(I-3)\cdot(II-3) + C_{20}(II-3)^2$	PVC, EPDM	Warnecke/Frankenhauser [67]	Uniaxial tensile

© 1996 Carl Hanser Verlag. All rights reserved.
No unauthorized disclosure or reproduction; licensed to purchaser only.

Table 4.8 Typical Strain-Energy Function Coefficients for Rubbery Solids

$C_1 = C_{10} = \partial W/\partial I$
$C_2 = C_{01} = \partial W/\partial II$
$C_3 = C_{02} = 2(\partial W/\partial II) \cdot (II - 3)$

Polymer	Temperature (°C)	C_1 (MPa)	C_2 (MPa)	$C_3 \times 10^6$ (MPa)	Source	Comments
HIPS	123.3[1]	0.0758	–	0.001179		No representative values
HIPS	124.7	0.08598	–	0.001331	[68]	for Mooney C_2 given
HIPS	124.4	0.14445	–	0.002234		
Vulcanized Natural rubber	25.0	0.1618	0.0147[2]	–	[63]	Data on rubber, by Rivlin and Saunders
PP	A = 165-T	0.0	0.080 · A	–	[45]	Creep data is source
Cellulose acetate	NR	0.1236	–	3400	[68]	No temperature given, C_3 value seems high

[1] About 29°C higher at pole than at edge
[2] Average value. Range is 0.010 to 0.022. Value decreases with increasing value of II
NR = Not reported

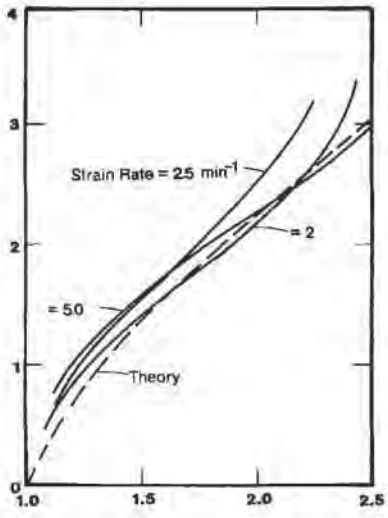

Figure 4.35 Tensile stress-strain behavior of polymethyl methacrylate, PMMA, at 160°C. Theory assumes tensile modulus = 130 lb_f/in^2 or 0.9 MPa and Mooney-Rivlin model with $C_2 = 0$. Figure adapted from [69], and used with permission of Ellis Horwood Ltd., copyright owner

The Ogden Form for the Strain Energy Function

It is apparent that the more constants that are available for curve-fitting, the more accurate the model will be in imaging the data. Figure 4.36 compares several Rivlin-type models with experimental data on PVC and EPDM [72, 129-130]. The agreement with experimental data is only satisfactory, even with a three-constant model. Ogden [61,73-75] proposed replacing the general Rivlin strain energy function model, Equation 4.49, with:

© 1996 Carl Hanser Verlag. All rights reserved.
No unauthorized disclosure or reproduction; licensed to purchaser only.

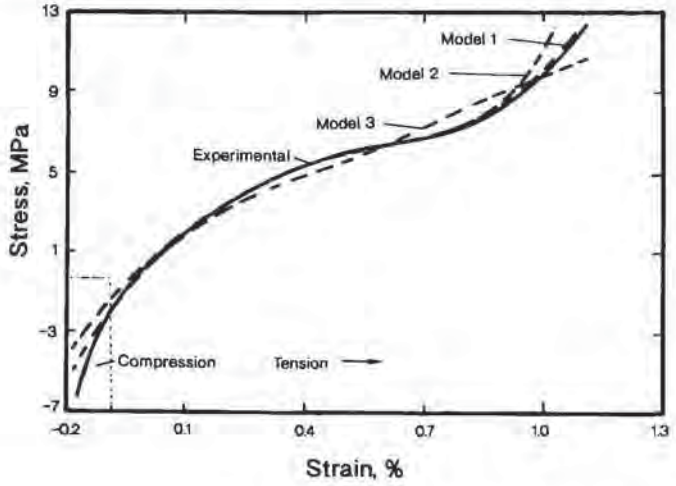

Figure 4.36 Comparison of experimental stress-strain data with several types of Rivlin constitutive equations. Figure adapted from [72]

$$W = \sum_{n=1}^{m} \frac{\mu_n}{\alpha_n} \cdot (\lambda_1^{\alpha_n} + \lambda_2^{\alpha_n} + \lambda_3^{\alpha_n} - 3) \tag{4.57}$$

Here α_n and μ_n are the Ogden curve-fitting constants. Although m is unbounded, its value is practically restricted to no more than 3, thus yielding 2, 4 or 6 constants. It has been shown that bubble dynamics are stable for $n = 1$ when $\alpha_1 > 3$. When $n = 2$, $\alpha_1 = 2$ and $\alpha_2 = -2$, the result is the Mooney model (Equation 4.52).

Although the Ogden model is based on the strain energy function relationship to principal invariants, the values of α_n are not restricted to integer values, as with the Rivlin version. There is some theoretical justification for the integer values of α_n [63,76]. However, the primary justification for the Rivlin version of a sum of principal invariant effects on the strain energy function is "[a] considerable simplification of the theory..." [77]. Certainly if the linearized Rivlin model is acceptable, the semi-empirical Ogden model is also acceptable.

Viscoelastic Models

Models for viscoelasticity are much more complex than elastic models. Most models employ coordinates that translate, rotate and distort with the fluid element under stress. As noted above, Equations 4.33 and 4.34 describe one simple way of including time-dependent polymer properties with traditional stress-strain relationships [48-50]:

$$\sigma = \sigma_o \cdot f(\epsilon) \cdot g(\theta) \tag{4.33}$$

or:

$$\sigma = \sigma_o \cdot \epsilon^m \cdot \theta^n \tag{4.34}$$

© 1996 Carl Hanser Verlag. All rights reserved.
No unauthorized disclosure or reproduction; licensed to purchaser only.

Correctly, the constitutive equation for a viscoelastic fluid must contain the concept of an imperfect or fading memory [78]. The general integral form for fading memory viscoelasticity is [79]:

$$\sigma(\theta) = \int_0^\theta \mu(\theta - \theta')\, h(I,II)\, B(\theta,\theta')\, d\theta' \tag{4.58}$$

where $\mu(\theta - \theta')$ is the relaxation factor or memory function:

$$\mu(\theta - \theta') = \sum_{i=1}^{N} \frac{G_i}{\lambda_i} \exp[-(\theta - \theta')/\lambda_i] \tag{4.59}$$

and G_i and λ_i are material parameters. h(I,II) is a damping function of the two strain invariants, usually written as the Wagner form [80]:

$$h(I,II) = [1 + a\sqrt{(I-3)\cdot(II-3)}]^{-1/2} \tag{4.60}$$

In biaxial stretching, h(I,II) is written as:

$$h(\epsilon) = [a \exp(2\epsilon) + (1-a)\exp(m\epsilon)]^{-1} \tag{4.61}$$

where $\epsilon(\theta) = \ln L(\theta)$, $a = \exp(-2\epsilon_o)$, and ϵ_o and m are measured constants for a given polymer. $L(\theta)$ is the stretch ratio, related to time θ'. $B(\theta,\theta')$ is the Finger strain tensor for deforming coordinates [81]. Temperature is included in the G_i material parameters as:

$$G_i(T) = G_i(T_o) \cdot \exp[-\beta(T - T_o)] \tag{4.62}$$

where T_o is a reference temperature and β is an Arrhenius-like parameter. The K-BKZ constitutive equation is used to describe the biaxial deformation of a viscoelastic sheet [82,83,119-123]. For biaxial plane stretching, the principal stresses in the $i = 1,2$ directions are given as:

$$\sigma_{ii} = \int_0^\theta \mu(\theta - \theta') \cdot h(\epsilon) \cdot [L_1^2(\theta,\theta') - L_2^2(\theta,\theta')]\, d\theta'$$

$$+ h(\epsilon(\theta)) \cdot [L_1^2(\theta) - L_2^2(\theta)] \cdot \int_{-\infty}^{0} \mu(\theta - \theta')\, d\theta' \tag{4.63}$$

where $L_i(\theta,\theta')$ is the stretch ratio at time θ related to time θ'. The K-BKZ model is used to shape the time-dependent elongational viscosity curves of the type shown in Figs. 4.26 and 4.30. Typically, only the first term of the memory function is needed:

$$\mu(\theta - \theta') = \frac{G}{\lambda} \exp[-(\theta - \theta')/\lambda] \tag{4.64}$$

This simplifies Equation 4.63 and allows strain recovery experiments to be used to obtain the necessary parameters [84].

© 1996 Carl Hanser Verlag. All rights reserved.
No unauthorized disclosure or reproduction; licensed to purchaser only.

As will be seen in Chapter 9, the viscoelastic characteristics of polymers are secondary to their pure elastic characteristics when predicting wall thickness variation in thermoforming[1].

4.5 Available Stress-Strain Data

Although there is a plethora of models to predict large deformation of solid and viscoelastic membranes, there is a dearth of temperature-dependent stress-strain-rate of strain data. This section records some of the available data. Typical room temperature data are shown in Fig. 4.37 [87]. The relationship between creep data and stress-strain curves is shown in Fig. 4.38 [88]. Typically, tensile strain or sample elongation is determined as a function of time for a given load or stress. When the data are replotted in terms of stress and strain, time is the parameter and the data are referred to as isochronous stress-strain. Figures 4.39 [89], 4.40, 4.41, and 4.42

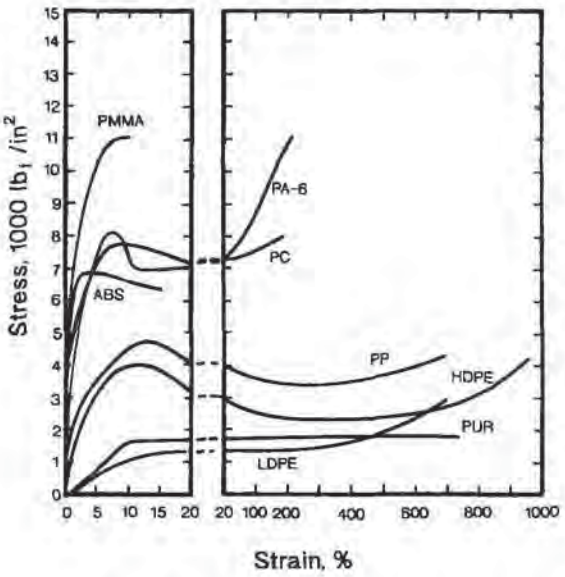

Figure 4.37 Room-temperature stress-strain data for several thermoplastics [87]

[1] Wineman [85,86] notes that if the membrane is an elastoviscous solid under fixed applied pressure, the membrane dimensions eventually reached fixed equilibrium values. If it is a viscoelastic fluid, on the other hand, the polymer will continue to creep. Since practical processing times are usually very small when compared with viscoelastic material times, long-term fluid effects are usually ignored in all but certain plug-assist conditions.

© 1996 Carl Hanser Verlag. All rights reserved.
No unauthorized disclosure or reproduction; licensed to purchaser only.

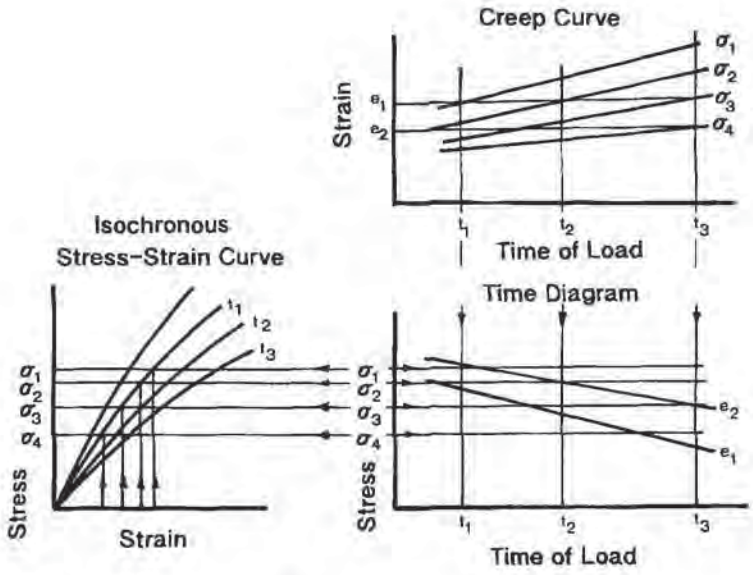

Figure 4.38 Interrelationship between isochronous stress-strain, creep and time-dependent stress [88]

[90-92] show isochronous stress-strain curves for amorphous RPVC and PMMA, and crystalline HDPE, LDPE and PP, respectively. These curves are for temperatures below T_g for the amorphous polymers and T_m for the crystalline ones.

Stress-strain curves at elevated temperatures for several polymers are given in the attached figures:

- SAN in Fig. 4.43 [93],
- P homopolymer in Fig. 4.44 [94],
- PMMA in Fig. 4.45 [95],
- PET in Fig. 4.46 [96],
- ABS in Fig. 4.47 [97],
- PS in Fig. 4.48 [98],
- ASA terpolymer in Fig. 4.49 [99],
- PTFE in Fig. 4.50 [100],
- FEP in Fig. 4.51 [101],
- Nylon 6 or PA-6 in Fig. 4.52 [102],
- Nylon 66 or PA-66 in Fig. 4.53 [103],
- PBT in Fig. 4.54 [104], and
- Polyimide in Fig. 4.55 [105].

As is apparent, most of the data are for engineering and high performance polymers. There are few data for commodity polymers such as PVC and PE. Unfortunately, commodity polymers make up the bulk of the polymers thermoformed today.

© 1996 Carl Hanser Verlag. All rights reserved.
No unauthorized disclosure or reproduction; licensed to purchaser only.

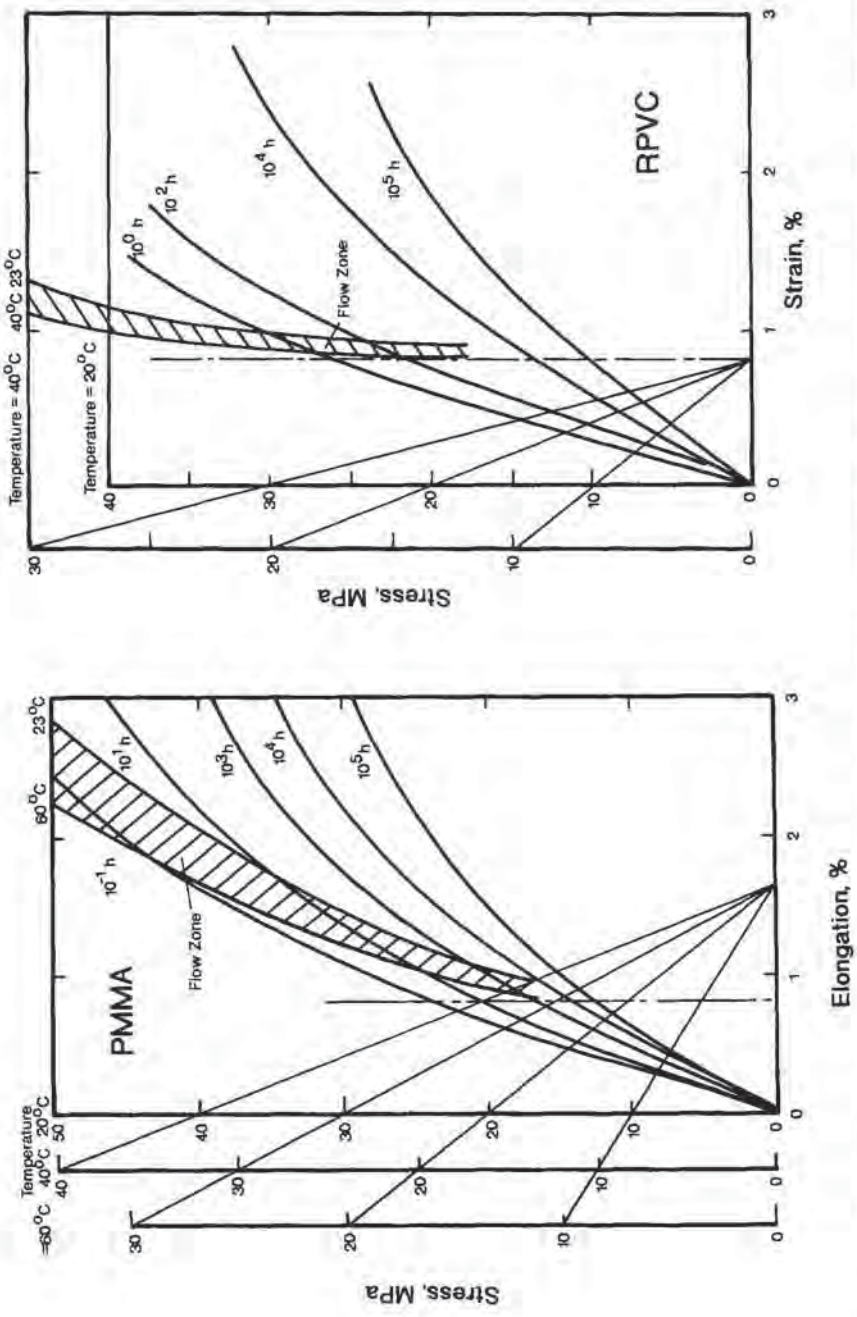

Figure 4.39 (left) Time-dependent isochronous stress-strain for rigid polyvinyl chloride, RPVC. (right) Polymethyl methacrylate, PMMA. Figures redrawn from [89] and used with permission of copyright owner

© 1996 Carl Hanser Verlag. All rights reserved.
No unauthorized disclosure or reproduction; licensed to purchaser only.

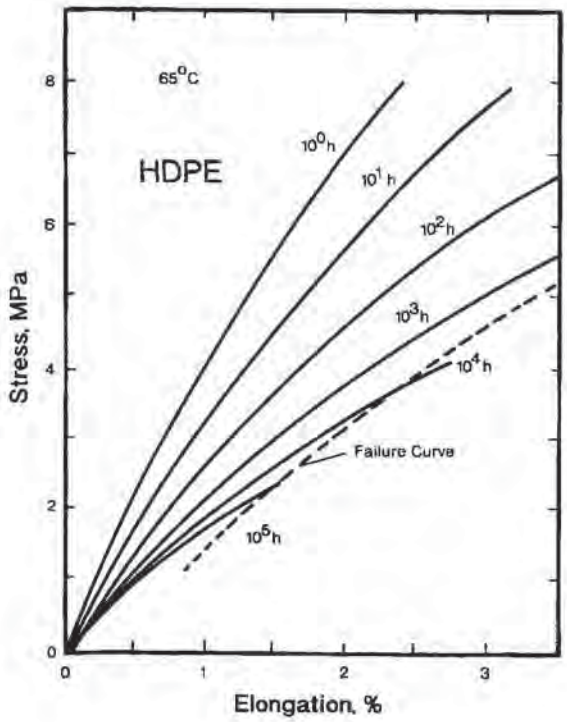

Figure 4.40 Time-dependent stress-strain curve for high-density polyethylene, HDPE at 65°C. Figure redrawn from [90] and used with permission of copyright owner

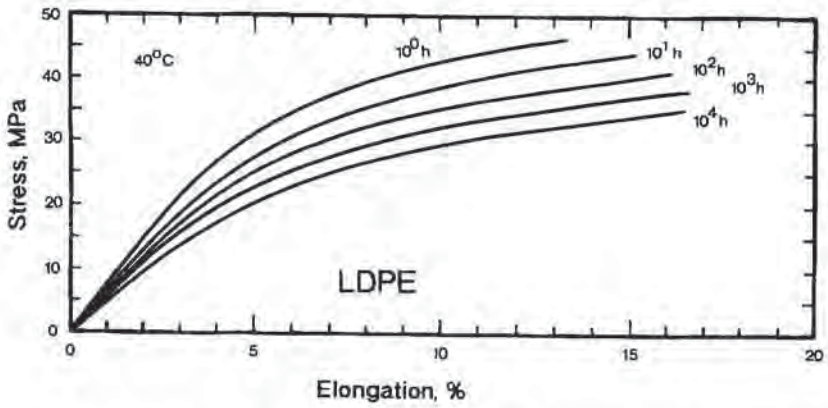

Figure 4.41 Time-dependent stress-strain curve for low-density polyethylene, LDPE at 40°C. Figure redrawn from [91] and used with permission of copyright owner

© 1996 Carl Hanser Verlag. All rights reserved.
No unauthorized disclosure or reproduction; licensed to purchaser only.

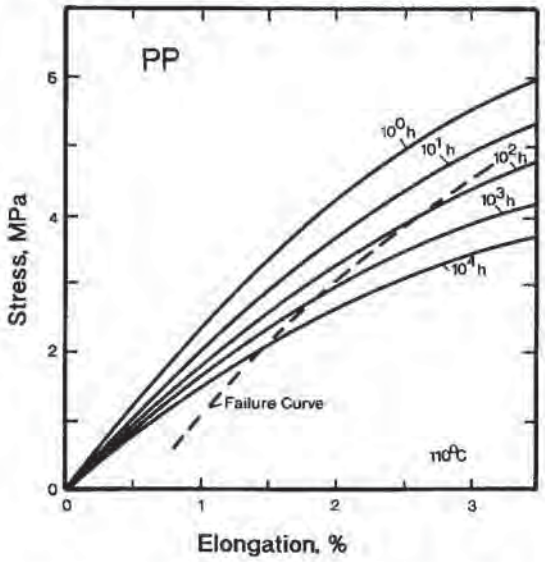

Figure 4.42 Time-dependent stress-strain curve for polypropylene, PP at 110°C. Figure redrawn from [92] and used with permission of copyright owner

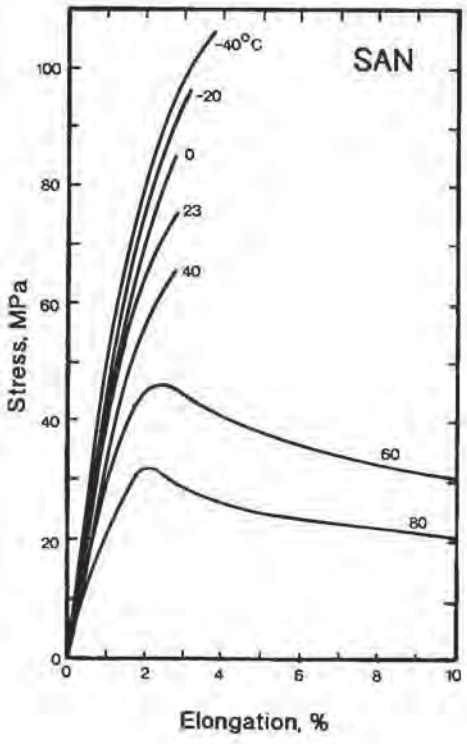

Figure 4.43 Temperature-dependent stress-strain curves for SAN. Figure redrawn from [93] and used with permission of copyright owner

© 1996 Carl Hanser Verlag. All rights reserved.
No unauthorized disclosure or reproduction; licensed to purchaser only.

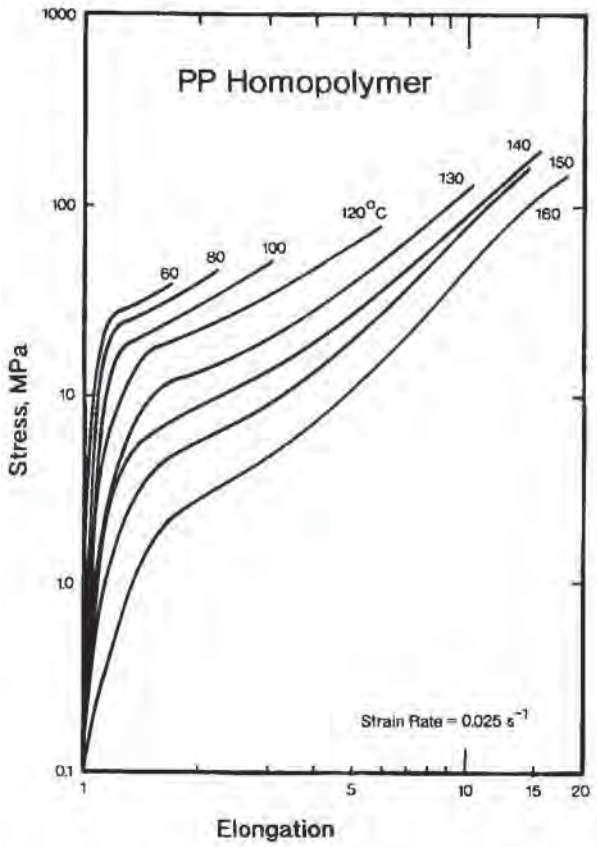

Figure 4.44 Temperature-dependent stress-strain curves for polypropylene, PP, homopolymer [94]

The method of fitting a model to the stress-strain data depends on the method used to obtain the data [106,124-128,133]. It is apparent that fitting uniaxial data with a neo-Hookean model is substantially easier and less arduous than fitting nonuniform biaxial data with a 4- or 6-constant Ogden model.

Sensitivity of Models

Two aspects of polymer response to applied load remain for discussion:

- The first deals with the sensitivity of the values of the curve-fit constants for any model to stress-strain prediction and then to the variation in wall thickness of the formed part. This will be addressed in Chapter 9 on the design of thermoformed parts.

© 1996 Carl Hanser Verlag. All rights reserved.
No unauthorized disclosure or reproduction; licensed to purchaser only.

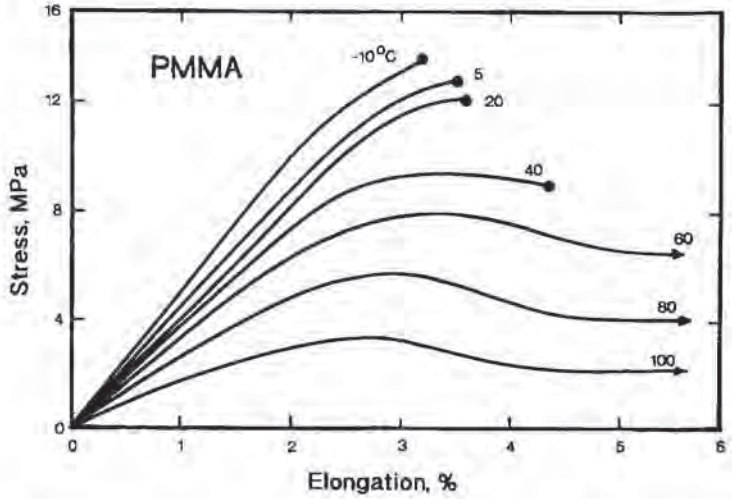

Figure 4.45 Temperature-dependent stress-strain curves for polymethyl methacrylate, PMMA. Figure redrawn from [95] and used with permission of copyright owner

- The second deals with the accuracy required of the models in the prediction of wall thicknesses of production quality thermoformed parts. This will be addressed in Chapter 10, on production quality control.

Obviously, if the day-to-day forming process conditions are not under control, the accuracy of wall thicknesses of formed parts will be poor. As a result, substantial effort to achieve great accuracy in the prediction of wall thicknesses is unwarranted. However, even with the most carefully controlled forming operation, it appears that no single rubbery solid model can describe the behavior of a polymer sheet undergoing nonisothermal high-speed, large scale deformation. Some guidelines are obtained, however, by beginning with the simplest model, the neo-Hookean model, for illustration.

4.6 The Importance of Polymer Material Properties[1]

A typical thermoforming process applies near-instantaneous, near-constant differential pressure to the rubbery sheet to deform it. If the pressure is insufficient or if the

[1] In [135], this section was titled "A Material Parameter, $\phi(T)$". Although $\phi(T)$ was identified as a material parameter related to the derivative of the strain energy function with respect to the first principal invariant of the Cauchy strain tensor, the analysis that followed used the neo-Hookean version of this derivative. More importantly, the relationship between $\phi(T)$ and the Mooney constants was not clear.

© 1996 Carl Hanser Verlag. All rights reserved.
No unauthorized disclosure or reproduction; licensed to purchaser only.

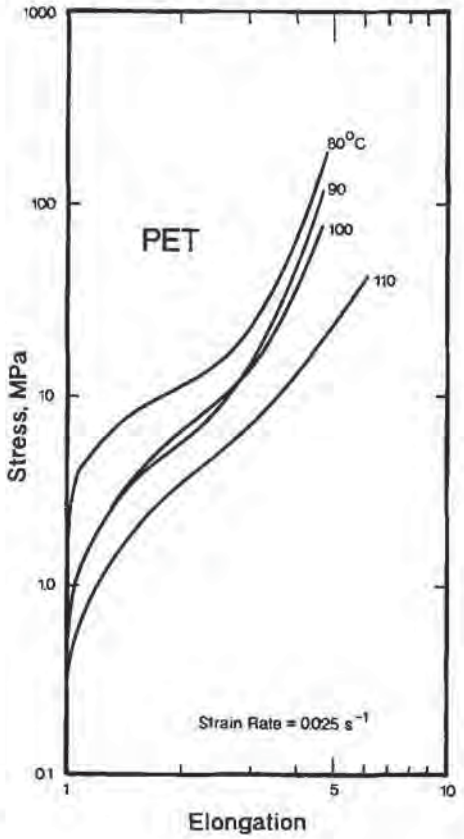

Figure 4.46 Temperature-dependent stress-strain curves for polyethylene terephthalate, PET [96]

sheet is not soft enough, the sheet will not distort fully to fill the mold or will not replicate the mold details. Earlier sections focused on the basic polymer response to applied load. There is a logical solid mechanistic approach to development of the parameters that are used to determine proper processing conditions for a given material [69,107]. As seen in Appendix 4.I, the neo-Hookean relation between the elongational or tensile elastic modulus, G, and the inflation pressure, P, for a uniform disk of radius a and initial thickness h_o, forming a dome of δ units above the horizontal is [107]:

$$\frac{Pa}{2h_o} \approx \frac{4C_{10}(\delta/a)}{1+(\delta/a)^2} = \frac{4G(\delta/a)}{1+(\delta/a)^2} \tag{4.I.10}$$

The modulus G is temperature-dependent, G(T), and has the units of MPa or lb_f/in^2. G(T) is determined by heating a sheet of radius a and initial thickness h_o to a fixed, uniform temperature, then measuring the extent of bulging, (δ/a), as a function of applied pressure. The analysis is dependent on all neo-Hookean assumptions and is inaccurate at the clamped sheet edge [107]. If the deforming sheet has a constant thickness everywhere:

© 1996 Carl Hanser Verlag. All rights reserved.
No unauthorized disclosure or reproduction; licensed to purchaser only.

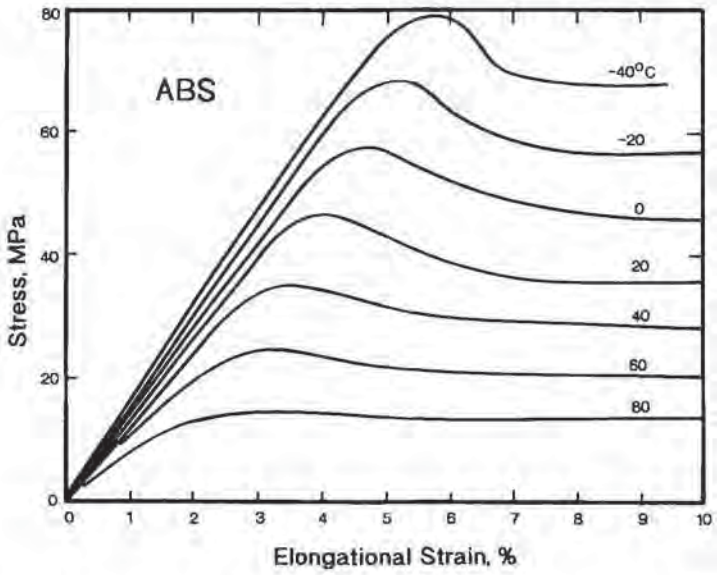

Figure 4.47 Temperature-dependent stress-strain curves for ABS. Figure redrawn from [97] and used with permission of copyright owner

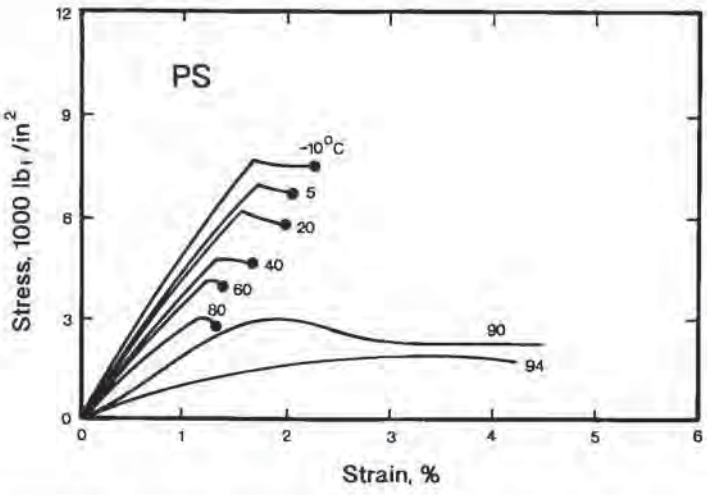

Figure 4.48 Temperature-dependent stress-strain curves for polystyrene, PS. Figure redrawn from [98] and used with permission of copyright owner

© 1996 Carl Hanser Verlag. All rights reserved.
No unauthorized disclosure or reproduction; licensed to purchaser only.

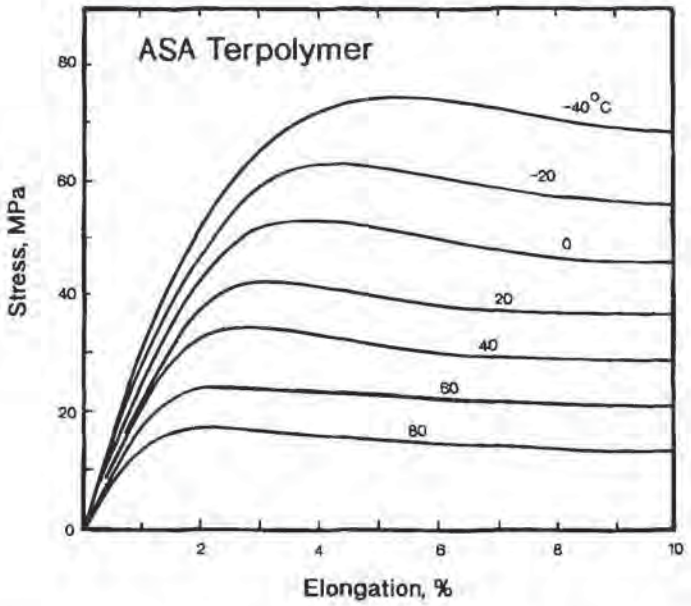

Figure 4.49 Temperature-dependent stress-strain curves for ASA terpolymer. Figure redrawn from [99] and used with permission of copyright owner

$$\lambda_h = [1 + (\delta/a)^{-2}] \tag{4.65}$$

$$\lambda_l = [1 + (\delta/a)^2] \tag{4.66}$$

At a maximum value of $\lambda_l = 2.59$, $(\delta/a) = 1.26$, and an approximate relationship between the applied pressure and the neo-Hookean modulus becomes:

$$P_{max} \approx \sqrt{3} \cdot G(T)\left(\frac{8h_o}{a}\right) \tag{4.67}$$

Unfortunately, experiments indicate that biaxially stretched sheet does not have constant thickness, a fundamental assumption in Equation 4.I.10 [50,68].

This analysis is extended to constrained biaxial deformation as sheet draw-down into a cone or funnel of wall angle α. The polymer not in contact with the wall is biaxially stretching as $\lambda_l = \lambda_\theta$ and $r_o = a$:

$$\frac{r}{a} = \left(\frac{r_o}{a}\right)^{\cos\alpha} \tag{4.68}$$

The thickness is:

$$\lambda_t = \frac{h}{h_o} = \frac{1}{\lambda_\theta^2} = \left(\frac{r}{r_o}\right)^2 = \left(\frac{r}{a}\right)^{2(\sec\alpha - 1)} \tag{4.69}$$

© 1996 Carl Hanser Verlag. All rights reserved.
No unauthorized disclosure or reproduction; licensed to purchaser only.

The pressure is:

$$P = 4G(T)\left(\frac{h_o}{r}\right)g(\alpha) \tag{4.70}$$

where:

$$g(\alpha) = \sin\alpha \cdot \left[1 - \frac{\sin^6\alpha}{8(1-\cos\alpha)^3}\right] \tag{4.71}$$

Note that $g(\alpha)$ is a geometric factor. If s is the distance down the cone side from the cone opening to the point where the sheet leaves the cone wall (Fig. 4.56):

$$\frac{r}{a} = 1 - \frac{s}{2\tan\alpha} \tag{4.72}$$

$$\frac{h}{h_o} = \left[1 - \frac{s}{a\tan\alpha}\right]^{\sec\alpha - 1} \tag{4.73}$$

$$P = 4G(T)\left(\frac{h_o}{a}\right)\frac{g(\alpha)}{\left[1 - \frac{s}{a\tan\alpha}\right]} \tag{4.74}$$

Examples 4.8 and 4.9 derive the expressions for commercial funnels where $\alpha = 60°$ and cylindrical or straight walled molds, where $\alpha = 90°$.

Example 4.8 Neo-Hookean Draw-Down into a 60° Funnel

Determine the pressure-modulus relationship for a neo-Hookean polymer being drawn into a 60° funnel.

From Equation 4.71, $g(\alpha) = 0.5$. The dimensionless radius is given by Equation 4.72 as:

$$\frac{r}{a} = 1 - 0.577\left(\frac{s}{a}\right)$$

The wall thickness is given by Equation 4.73 as:

$$\frac{h}{h_o} = \left(\frac{r}{a}\right)^2$$

And the pressure-modulus relationship from Equation 4.74 is:

$$P = 2G\left(\frac{h_o}{a}\right)\left[\frac{1}{1 - 0.577(s/a)}\right]$$

© 1996 Carl Hanser Verlag. All rights reserved.
No unauthorized disclosure or reproduction; licensed to purchaser only.

Example 4.9 Neo-Hookean Draw-Down into a Straight-Wall Can

Determine the pressure-modulus relationship for a neo-Hookean polymer being drawn into a can having 90° walls.

The wall thickness is given by Equation 4.73 as:

$$\frac{h}{h_o} = \exp\left(-\frac{2s}{a}\right)$$

And the pressure-modulus relationship from Equation 4.74 is:

$$P = 2G\left(\frac{h_o}{a}\right)\left[1 - 0.125\ \exp\left(-\frac{6s}{a}\right)\right]$$

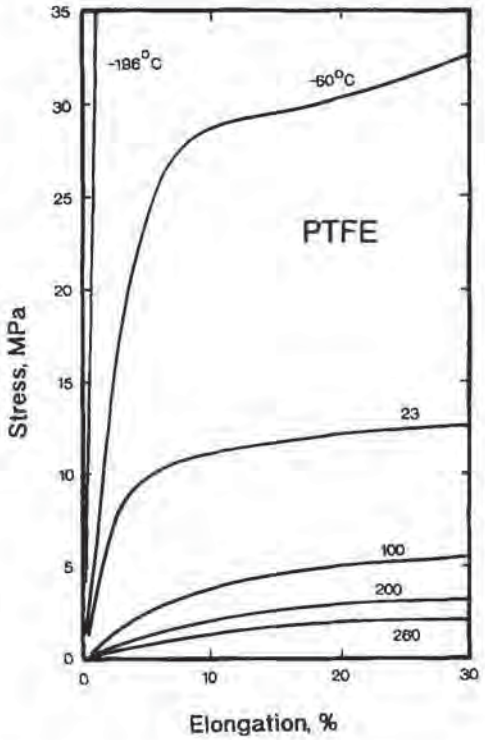

Figure 4.50 Temperature-dependent stress-strain curves for polytetrafluoroethylene, PTFE. Figure redrawn from [100] and used with permission of copyright owner

© 1996 Carl Hanser Verlag. All rights reserved.
No unauthorized disclosure or reproduction; licensed to purchaser only.

The general form for the pressure equation is:

$$P = G(T) \cdot \left(\frac{h_o}{a}\right) \cdot g \tag{4.75}$$

where g is the general form for the geometry of the mold. The deformation pressure is directly proportional to both the neo-Hookean modulus and the relative sheet thickness, h_o/a. If the pressure is fixed by the process, as with vacuum forming where $P < 0.1$ MPa or 15 lb_f/in^2, the ability to deform a sheet of specific thickness into a specific shape or depth of draw, s/a, depends entirely on the temperature-dependent modulus:

$$G(T) = \frac{P}{(h_o/a) \cdot g} \tag{4.76}$$

As seen in Figs. 4.11 and 4.12, G(T) decreases with increasing temperature. To form thicker sheets in the same mold and with the same pressure as thinner sheet, the sheet temperature must be increased. This is true for any geometry and any predetermined applied pressure (Fig. 4.57).

As shown in Example 4.10 for a straight-walled mold, there is good agreement between the forming pressure, measured modulus and the temperature where extensive elongation begins. This supports the view that the simple neo-Hookean model has value in determining the minimum forming temperature. Note also that if the polymer type, sheet thickness, mold geometry and applied pressure are known, G(T) establishes a minimum value for the forming temperature. Example 4.11 illustrates the minimum value for the straight-walled mold.

Example 4.10 Comparison of Calculated and Experimental Moduli for PVC

Determine the maximum value for the neo-Hookean modulus for vacuum forming PVC into an $\alpha = \pi/2$ straight-walled can and compare the results with the experimental data of Table 4.9.

For the data in Table 4.9, the applied stress, $\sigma = 426$ lb_f/in^2 or 2.9 MPa. The initial sheet thickness, $h_o = 0.040$ in or 1 mm and the mold diameter, $a = 1$ in or 25 mm. For a straight-walled cavity, from Example 4.9, the depth of draw is no longer an important element once $s/a > 0.5$. As a result, the equation is written as:

$$P \approx 4G(T) \cdot \left(\frac{h_o}{a}\right)$$

For simple vacuum forming, $P < 0.1$ MPa or 15 lb_f/in^2. As a result:

$$G(T) = \frac{0.1 \text{ MPa}}{4 \cdot (1/25)} = 0.626 \text{ MPa} = 91.9 \text{ } lb_f/in^2$$

© 1996 Carl Hanser Verlag. All rights reserved.
No unauthorized disclosure or reproduction; licensed to purchaser only.

As seen in Table 4.9, the modulus of PVC at 110°C is 93.6 lb_f/in^2 or 0.65 MPa and the measured elongation at this temperature is substantially greater than that at 100°C.

Example 4.11 The Minimum Forming Temperature for PVC

Determine the minimum forming temperature for PVC for the data in Example 4.10.

The maximum applied pressure occurs when the geometric parameter, g, is maximum. This occurs when $s/a = 0$. At this condition:

$$P_{max} = 4G(T)\left(\frac{h_o}{a}\right) \cdot 0.875$$

Again, for the vacuum forming case, Example 4.10, $P < 0.1$ MPa or 14.7 lb_f/in^2.

$$G(T) = \frac{0.1 \text{ MPa}}{4 \cdot 0.875 \cdot (1/25)} = 0.71 \text{ MPa} = 105 \text{ lb}_f/\text{in}^2$$

As seen in Table 4.9, if the sheet temperature is less than 110°C, the sheet will not begin to draw since the experimental G(T) is greater than 105 lb_f/in^2.

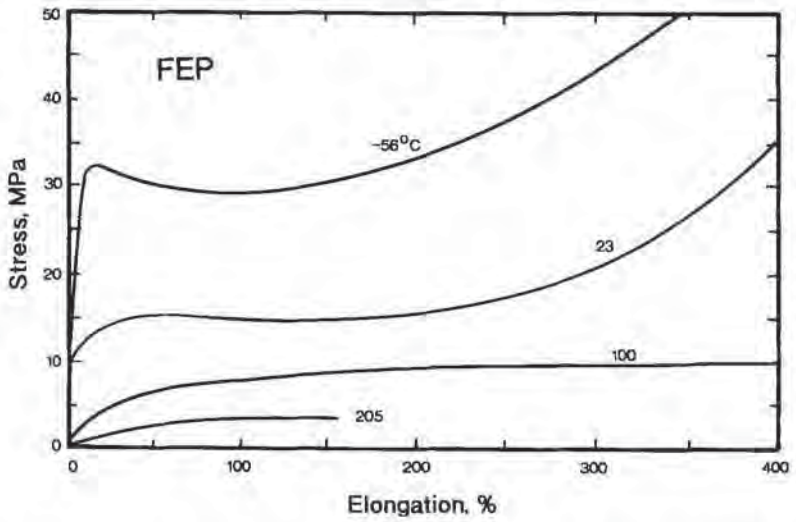

Figure 4.51 Temperature-dependent stress-strain curves for fluoroethylene polymer, FEP. Figure redrawn from [101] and used with permission of copyright owner

© 1996 Carl Hanser Verlag. All rights reserved.
No unauthorized disclosure or reproduction; licensed to purchaser only.

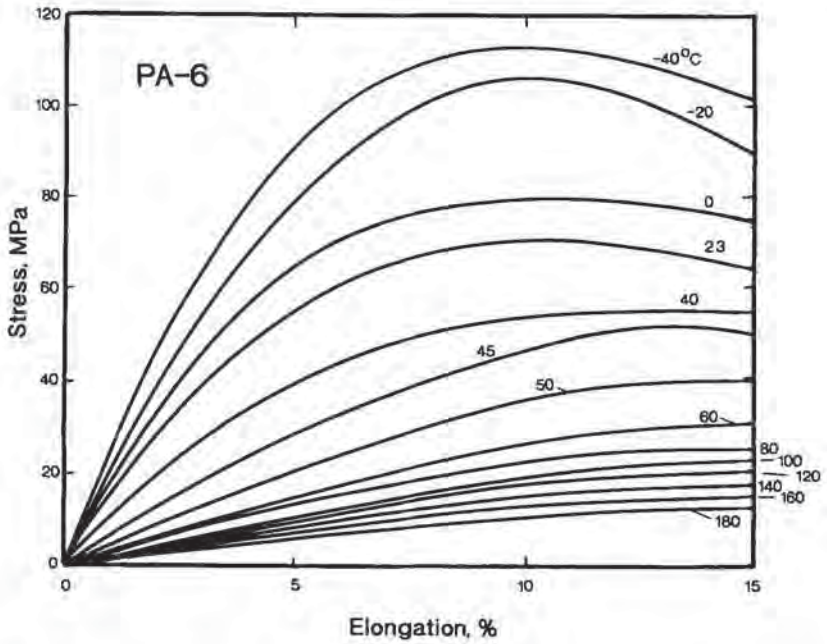

Figure 4.52 Temperature-dependent stress-strain curves for nylon 6, polycaprolactam, PA-6. Figure redrawn from [102] and used with permission of copyright owner

One definition for the thermoforming window then is:

The minimum thermoforming window is the temperature range from the value below which the sheet is too stiff to deform under applied pressure to that above which the sheet can be easily deformed to a draw ratio, s/a, greater than 0.5.

In the examples, the forming window using this definition is a few degrees, at best. Increasing the temperature above this minimum forming window allows the sheet to be formed at much lower pressure. The practical upper limit on formability is still the point where the sheet is plastically drawn to rupture.

Table 4.9 Creep Data and Measured Modulus for PVC [17] (PVC at stress, $\sigma = 426$ lb$_f$/in^2 or 2.9 MPa)

Temperature (°C)	ϵ (measured)	Modulus G(T) (MPa)	(lb$_f$/in^2)
98	1.2	1.5	214
100	1.45	1.6	187
110	3.6	0.65	93.6
118	3.6	0.65	93.6

© 1996 Carl Hanser Verlag. All rights reserved.
No unauthorized disclosure or reproduction; licensed to purchaser only.

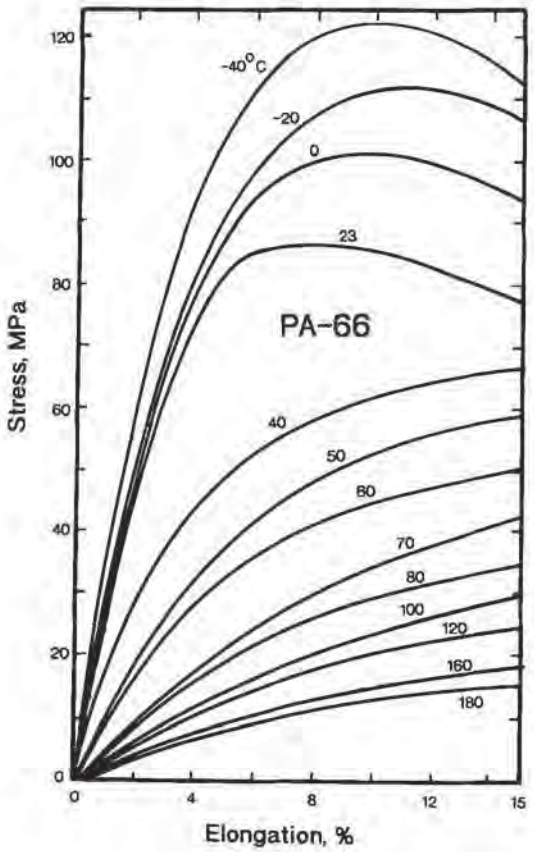

Figure 4.53 Temperature-dependent stress-strain curves for nylon 66, polyhexamethylene adipamide, PA-66. Figure redrawn from [103] and used with permission of copyright owner

4.7 Practical Aspects of Stretching

As noted, there are many ways of generating stretching data on plastics. G(T), the neo-Hookean modulus, is one material property extracted from an analysis that uses a simple isothermal stress-strain model. Several precautions are important. Creep data over a relatively wide range in temperatures are easy to obtain, but normally yield uniaxial stretching data at *fixed stress*. The effect of strain-rate-dependency is masked or missing. Further Treloar [108] cautions against using uniaxial data to predict biaxial performance. He notes that for rubber, experiments that

> "...cover only one type of strain may, and usually do, appear to conform to [a given strain-energy function] equation. [However,] they provide very little real evidence regarding the form of the strain energy function in general strain, and any use of them is an unwarranted extrapolation."

© 1996 Carl Hanser Verlag. All rights reserved.
No unauthorized disclosure or reproduction; licensed to purchaser only.

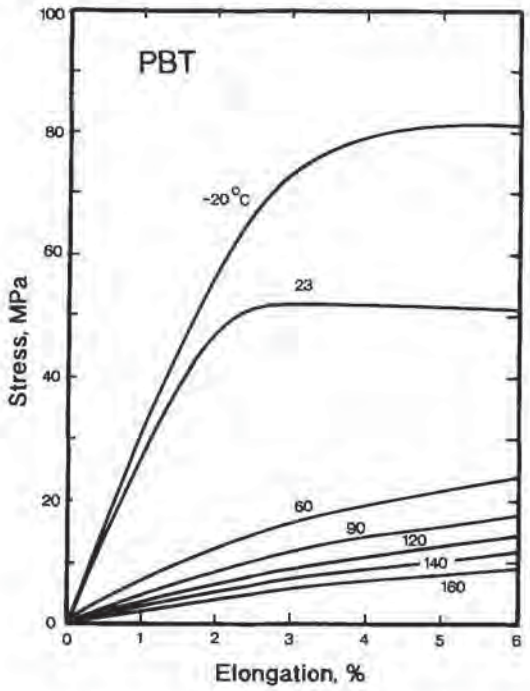

Figure 4.54 Temperature-dependent stress-strain curves for polybutylene terephthalate, PBT. Figure redrawn from [104] and used with permission of copyright owner

Example 4.12 shows the relationship between uniaxial and uniform principal invariants for a Mooney-type solid at a fixed strain. It is apparent that the importance of curve-fitting constants changes from one stretching mode to another. For one very specific type of fluid, called a "simple fluid" [20], a relationship between uniaxial extension and uniform biaxial extension is obtained.

Example 4.12 Uniaxial and Uniform Biaxial Strain for a Mooney-Type Solid

Consider uniaxial extension of a Mooney-type solid, where $\lambda = 7$. Determine values for the first and second strain invariants and their ratios, at the same stress level.

For uniaxial stretching, $\lambda_1 = \lambda$, $\lambda_2 = \lambda_3 = \lambda^{-1/2}$. I and II are:

$$I = \lambda^2 + 2 \cdot \lambda^{-1} = 49.29$$

$$II = 1/\lambda^2 + 2 \cdot \lambda = 14.02$$

$$I/II = 3.52$$

© 1996 Carl Hanser Verlag. All rights reserved.
No unauthorized disclosure or reproduction; licensed to purchaser only.

For uniform biaxial stretching, $\lambda_1 = \lambda_2 = \lambda$, $\lambda_3 = 1/\lambda^2$. I and II are:

$$I = 2 \cdot \lambda^2 + 1/\lambda^4 = 98.0$$

$$II = 2/\lambda^2 + \lambda^4 = 2401$$

$$I/II = 0.041$$

In order for biaxial extension data to be relevant [109], inflation experiments must be at isothermal, uniform constant rate conditions. Practical stretching rates are rarely achieved under these conditions. When practical rates are used [46,49,59], inflation rates are not constant and the sheet may not be isothermal. It has been cautioned [110] that the natural process time for inflation may be so short

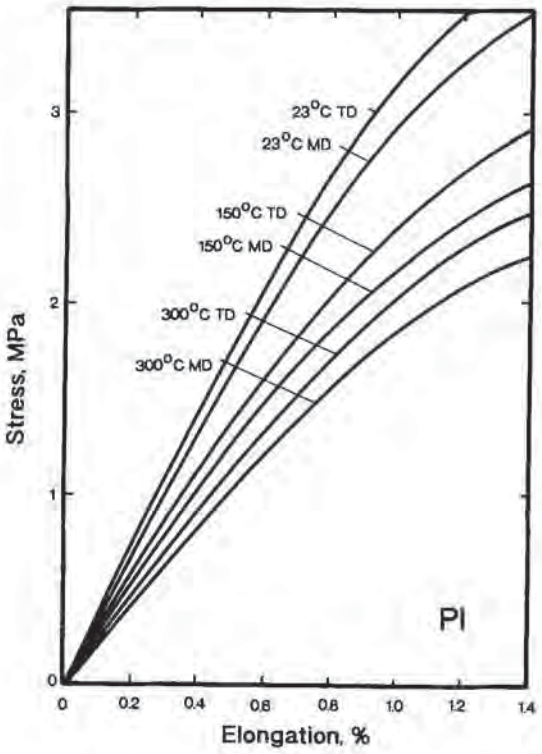

Figure 4.55 Temperature-dependent stress-strain curves for polyimide, PI. Figure redrawn from [105] and used with permission of copyright owner

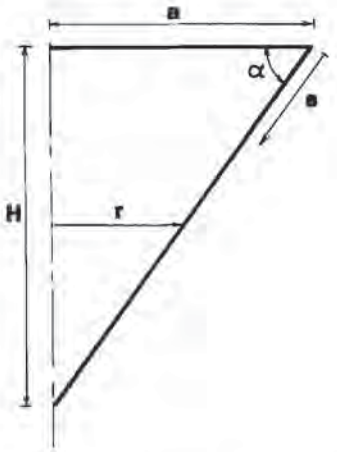

Figure 4.56 Geometric factors for a conical female mold

© 1996 Carl Hanser Verlag. All rights reserved.
No unauthorized disclosure or reproduction; licensed to purchaser only.

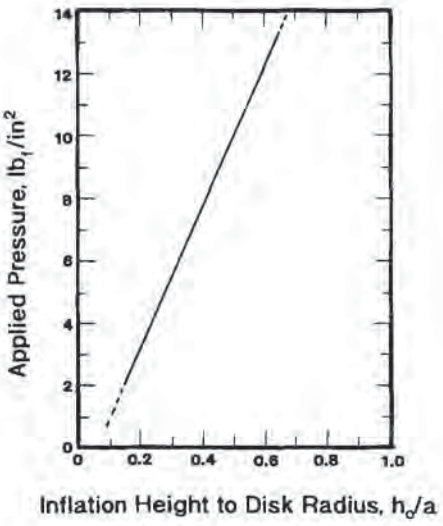

Figure 4.57 Elastic deformation as a function of inflation pressure for polyisobutylene [46]. Redrawn figure used by permission of Society of Rheology

that the polymer may never behave as a fluid in dynamic steady state elongation. It appears, then, that elastic liquid and viscoelastic solid models serve only as clues or signposts in thermoforming. No current analytical model should be used *a priori* to predict the thermoformability of a given polymer. Even with advent of finite element analysis to the solution of the large deformation, the thin membrane problem today cannot yield forming ranges. Practical methods of comparing the performance of one polymer with another must remain relatively empirical for the time being.

Funnel Test

Biaxially constrained stretching into a funnel is a relatively simple way of obtaining qualitative information about G(T). Figure 4.58 is the coordinate for thermoforming into a cone of diameter d and angle, α, at time θ, as a sheet of initial thickness h_o is being drawn into a cone to a depth of h. The sheet is in contact with the cone surface for a diagonal distance or slant height, s. The sheet is divided into a frustum of a cone and spherical cap. That portion of the sheet that is not in contact with the cone surface forms a spherical cap of radius $R = d/2$ and r is the indeterminate radius at the bottom of the frustum of the cone. The frustum area is:

$$A_f = \pi(R + r)[(R - r)^2 + h_f^2]^{1/2} \tag{4.77}$$

where $h = R \tan \alpha$ and h_f is given as:

$$h_f = h(1 - r/R) \tag{4.78}$$

© 1996 Carl Hanser Verlag. All rights reserved.
No unauthorized disclosure or reproduction; licensed to purchaser only.

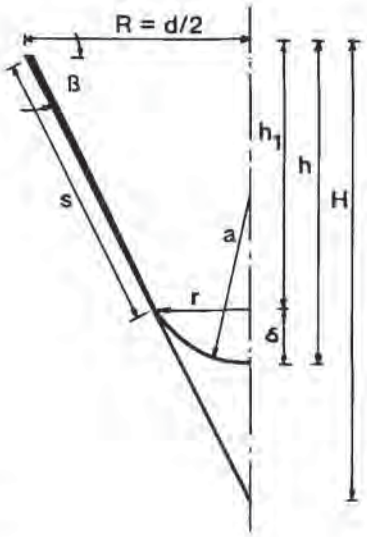

Figure 4.58 Geometric factors for draw-down into a conical female mold

The area of the spherical cap is:

$$A_{cap} = 2\pi a\delta \tag{4.79}$$

where δ is given as:

$$2a\delta = r^2 + \delta^2 \tag{4.80}$$

Therefore:

$$A_{cap} = \pi(r^2 + \delta^2) \tag{4.81}$$

Now $r = a \cos \alpha$ and $\delta = a(1 - \sin \beta)$. As a result:

$$A_{cap} = 2\pi r^2\left[\frac{1 - \sin \alpha}{\cos^2 \alpha}\right] \tag{4.82}$$

The total area in terms of r is:

$$A_{total} = \frac{\pi R^2}{\cos \alpha} + \frac{2\pi r^2}{\cos \alpha} \cdot \left[1 - 2\left(\frac{1 - \sin \alpha}{\cos \alpha}\right)\right] \tag{4.83}$$

The reduced thickness of the sheet at the frustum-spherical cap intersection, at s, is given as:

$$\frac{t}{t_o} = \left(1 + \frac{\cos \alpha}{2}\right)\left[1 - \left(\frac{2s}{a}\right) \cos \alpha\right]^{\sec \alpha - 1} \tag{4.84}$$

For a cone angle of $\alpha = 60°$ or $\pi/3$:

$$\frac{t}{t_o} = \left(\frac{3}{4}\right) \cdot \left[1 - \frac{s}{d}\right] \tag{4.85}$$

© 1996 Carl Hanser Verlag. All rights reserved.
No unauthorized disclosure or reproduction; licensed to purchaser only.

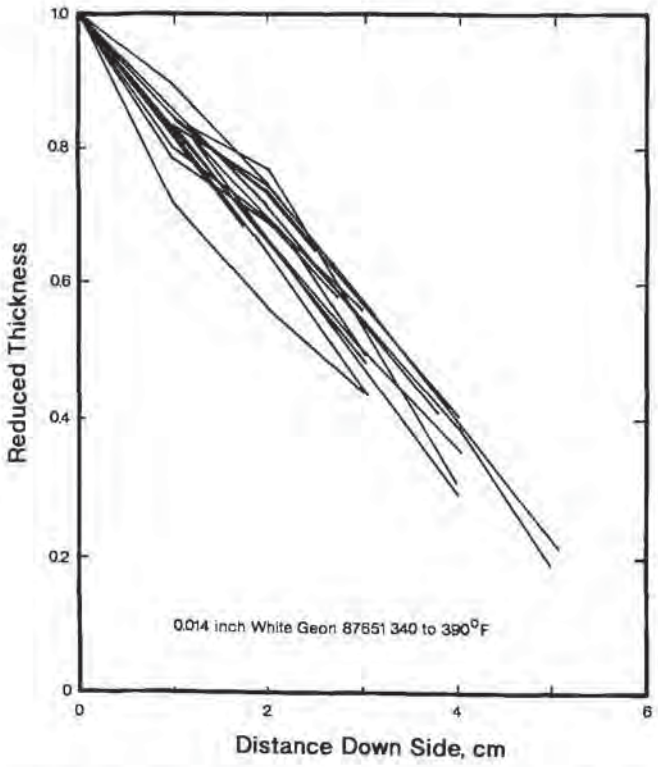

Figure 4.59 Measured thicknesses of 0.014-inch polyvinyl chloride, PVC sheet drawn into a 60° conical female mold. Initial sheet temperature range is 340°F to 390°F

Figure 4.59 shows the repeatability of reduced thickness as a function of slant distance, s, for 0.014 in or 0.36 mm RPVC sheet formed into a 2.5 in or 64 mm diameter, 60° cone at sheet temperatures from 340 to 390°F or 171 to 199°C. The thickness shown is $(4t/3t_o)$. As expected, the reduced thickness is linear with s/d with the data scattering about the linear line and the intercept at about 6.4 cm.

The experimental procedure is as follows. An isothermal sheet is stretched using either vacuum or positive air pressure (Fig. 4.60). Sheet temperature and differential pressure are accurately measured. Positive air pressure is easier to control than vacuum [21]. The funnel temperature should be substantially below the polymer T_g so that the sheet freezes instantaneously on contact with the funnel surface. The surface should be relatively smooth to allow good seal between the sheet and the surface. In practice, once the sheet contacts the surface, it does not slide [111]. At a given temperature and applied differential pressure, deformation occurs to a depth s/a, where s is the point along the funnel surface where the sheet last touches it. If s cannot be determined, $s + \delta$ is measured and δ is calculated from $\delta = a(1 - \sin \alpha)$.

© 1996 Carl Hanser Verlag. All rights reserved.
No unauthorized disclosure or reproduction; licensed to purchaser only.

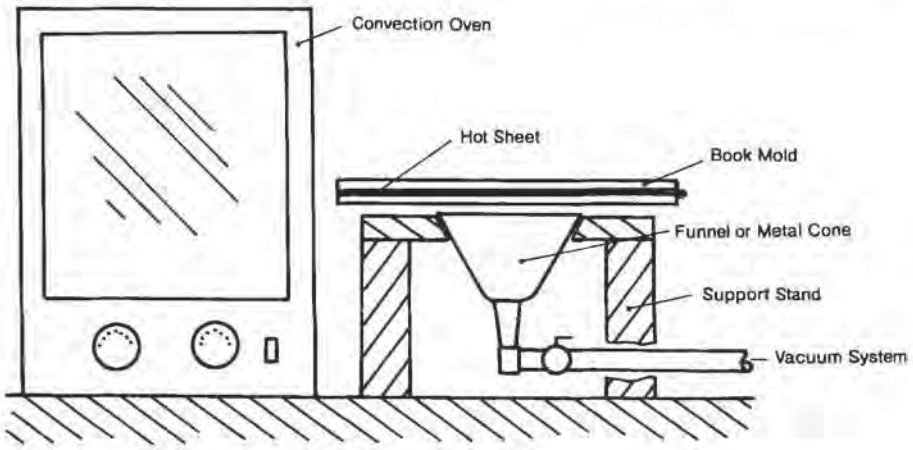

Figure 4.60 Laboratory-scale draw-down apparatus

Furthermore, t/t_o is easily measured at every point along the part surface and compared with s/a at any set of conditions. All polymer in the cone should be accounted for with a simple material balance:

$$\text{Volume} = \int_0^s 2\pi rt\, dr + 2\pi R\delta t(s) \tag{4.86}$$

If the measured values of t/t_o do not exactly agree with calculated values, the measured values should be used. G(T) is determined once P, T, t/t_o, and t_o/a are known. Figure 4.61 shows the reduced thickness of the cap as a function of sheet temperature for 0.014 in or 0.36 mm thick RPVC drawn into a 60° or $\pi/3$ cone. The data in Fig. 4.62, where the applied vacuum was fixed at 9 lb_f/in^2 or 0.06 MPa, show the characteristic Arrhenius temperature dependency of G(T) for two types of RPVC polymer.

Note that extension ratios for draw down into a 60° cone are initially rather small with λ_θ and λ_l values of only 2.4 when the sheet has been drawn a distance of $h/a = 1$. Values rapidly increase as the polymer is drawn into the tip of the cone. Maximum values of $\lambda \approx 11$ are achieved when $h/a > 1.5$.

A straight-walled cylinder has been used as a test mold [112], but draw-down is extreme. High pressure and rapid rate-of-pressurization of the sheet on the funnel can lead to premature diaphragm rupture. Results from these types of experiments should be used only to roughly define processing parameters such as pressure and temperature for any given polymer grade, for a given ratio of sheet thickness to part dimension. These experiments suffer many of the same limitations on interpretation as fiber spinning and film blowing processes [41,113].

© 1996 Carl Hanser Verlag. All rights reserved.
No unauthorized disclosure or reproduction; licensed to purchaser only.

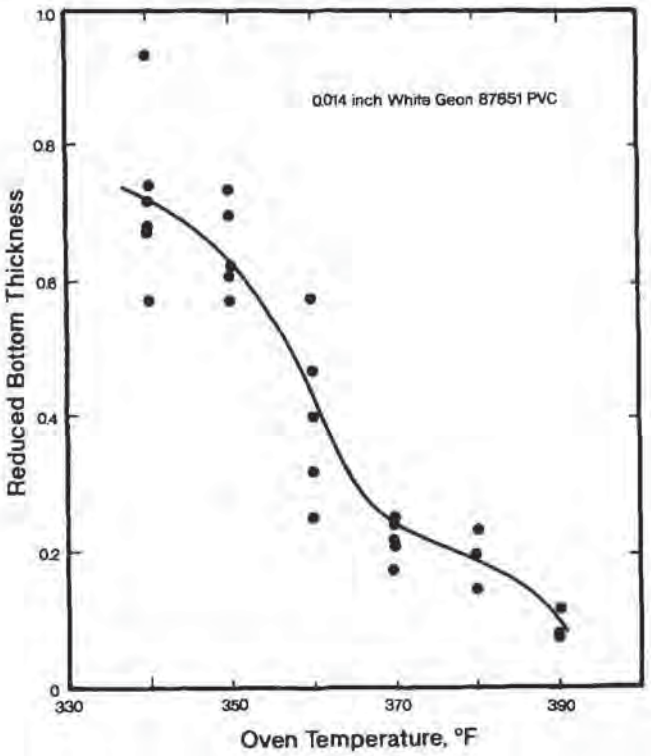

Figure 4.61 Measured temperature-dependent bottom free-surface sheet thickness for 0.014-in polyvinyl chloride, PVC sheet drawn into 60° conical female mold

4.8 Bursting Conditions

Rapid biaxial stretching is common thermoforming practice for thin-gage sheet. Instantaneous strain rates of up to 30 s^{-1} have been reported at the pole during bubble blowing. As noted earlier, for elastic liquids at constant stress or constant applied pressure, polymer deformation rate increases without bound. This can result in membrane rupture. An interesting relation between applied pressure and bursting time has been proposed in terms of an elastic liquid response to applied stress, σ [22]:

$$\sigma = \eta_e \cdot \dot{\epsilon} \tag{4.87}$$

where η_e is the biaxial extensional viscosity and $\dot{\epsilon}$ is the principal biaxial strain rate. Now:

$$\sigma \approx \frac{P}{2}\left[\left|\frac{a}{2h_o}\right| + \left|\frac{a}{2h_b}\right|\right] \tag{4.88}$$

© 1996 Carl Hanser Verlag. All rights reserved.
No unauthorized disclosure or reproduction; licensed to purchaser only.

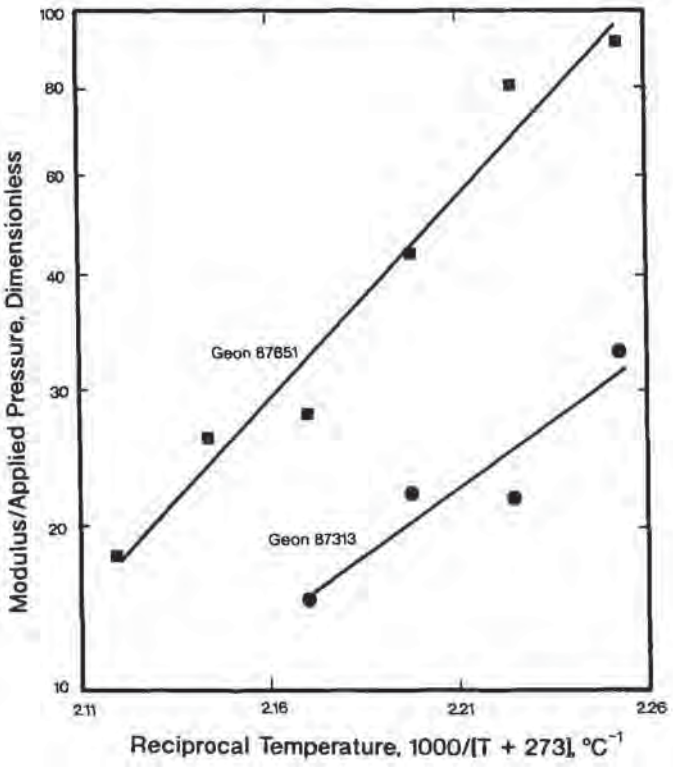

Figure 4.62 Comparison of temperature-dependent tangent modulus-to-applied pressure ratio for two polyvinyl chlorides, PVCs

$$\dot{\epsilon} \approx \left(\epsilon_b - \frac{\epsilon_o}{\theta_b}\right) \tag{4.89}$$

R is the radius of the cap of the bubble, h is the membrane thickness, P is the constant applied pressure, θ_b is the time to burst, and subscripts o and b represent the initial and bursting conditions. This is rewritten as:

$$P\theta_b \approx \eta_e \cdot \left[\frac{(\epsilon_b - \epsilon_o)}{\left[\left|\frac{a}{2h_o}\right| + \left|\frac{a}{2h_b}\right|\right]}\right] \tag{4.90}$$

Note that $(1/\theta_b)$ is a strain-rate-like term with units of s^{-1} and $(P\theta_b)$ is a viscosity-like term with units of $MPa \cdot s$ of $lb_f \cdot s/in^2$. If the term in the large brackets $[\cdots]$ in Equation 4.90 is essentially constant, $(P\theta_b)$ is proportional to η_e, the biaxial extensional viscosity. A comparison of bursting time data and viscosity data for room-temperature bubble inflation of polyisobutylene rubber is given in Fig. 4.63. If the biaxial extensional viscosity is essentially inversely proportional to strain rate

© 1996 Carl Hanser Verlag. All rights reserved.
No unauthorized disclosure or reproduction; licensed to purchaser only.

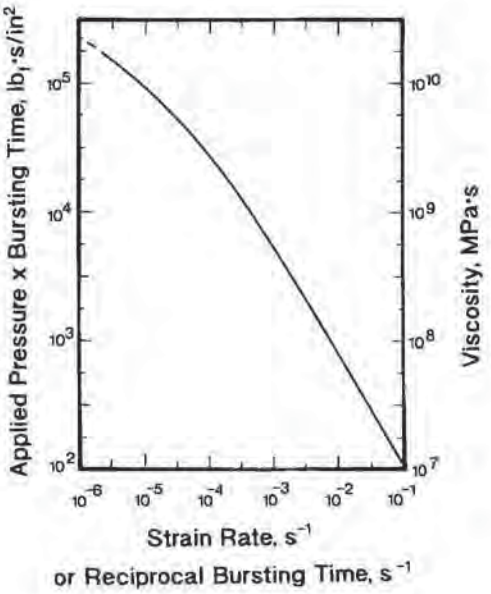

Figure 4.63 Comparison of bursting time with viscosity for polyisobutylene rubber [46]. Redrawn figure used with permission of society of rheology

[46], the bursting time is independent of applied pressure. Moreover, even if a direct comparison is fortuitous, the effect of sheet temperature on bursting time is found by applying an Arrhenius-type temperature correction factor:

$$(P\theta_b)(T) = A \exp[-E_{vis}/RT] \tag{4.91}$$

where A is a pre-exponential constant, E_{vis} is a viscous energy of activation for biaxial extension and R is the gas constant.

Bursting should be of concern only in the early stages of bubble deformation. At later stages, the process approaches one of constant velocity, and the falling sheet temperature helps to stabilize the bubble against rupture. Sheet splitting is a similar problem seen in constrained deep drawing into rather sharp corners. Perforation of sheet nibs or nipples during draw-down into oversized vacuum holes can also be analyzed in terms of this bursting phenomenon.

4.9 Sheet Sag

When a polymer sheet is clamped in a frame and heated, it begins to sag. If the extruded sheet has some residual stress, the initial sag will be reduced as the sheet temperature increases. If the sheet has substantial residual stress, the initial sag is

© 1996 Carl Hanser Verlag. All rights reserved.
No unauthorized disclosure or reproduction; licensed to purchaser only.

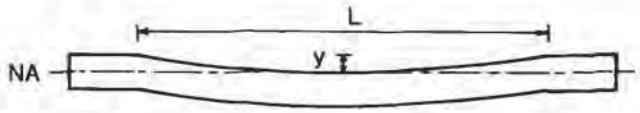

Figure 4.64 Geometric factors for initial sheet sag for a linear sheet element

minimal and the sheet may be pulled from its frame. This initial stage has been discussed earlier in this chapter. When the sheet is quite hot, sag is appreciable, as shown in schematic in Fig. 4.2. The mechanics of sag are divided into initial sag, where the neutral axis remains in the sheet, and tensile sag, where the sag is appreciable.

Initial Sag

For initial sag, the neutral axis or the boundary between compressive stress and tensile stress, remains in the polymer sheet, as shown in Fig. 4.64. Maximum tensile strain occurs on the lower sheet surface and maximum compressive strain occurs on the upper sheet surface. There are two general cases:

- For an rectangular sheet clamped along all edges, Fig. 4.64, the initial sag is given as [114]:

$$y = -\frac{\beta q L^4}{E(T)h^3} \tag{4.92}$$

where y is the extent of sag, in mm or in, q is the weight of the sheet, in kg/m^2 or lb/in^2, L is the sheet span in inches or mm, E(T) is the temperature-dependent modulus, in MPa or lb_f/in^2, h is the sheet thickness, in mm or in, and β is a function of the sheet length to width, Table 4.10. The sheet weight, $q = \rho h$ where ρ is the density of the polymer, kg/m^3 or lb/ft^3. The sheet width is temperature-dependent, $L = L(T)$, since all polymers have finite thermal expansion coefficients. However this effect is small when compared with the temperature dependency of the modulus (Figs. 4.11 and 4.12). Since b increases with temperature and E decreases with temperature, the overall effect is an increase in initial sag with increasing temperature. For continuous sheet clamped along two edges, $\beta = 0.1421$. For a square sheet clamped along four edges, $\beta = 0.0444$. The initial sag for the square sheet, as found in cut-sheet forming, is less than one-third that of the continuous sheet, as is typical of roll-fed forming.

Example 4.12 illustrates the method of calculating initial sag.

- For a circular disk clamped along the radius, Fig. 4.65, the initial sag is given as [115]:

$$y = \frac{3qd^4}{16E(T)h^3}\frac{(5+\nu)}{(1-\nu)} \tag{4.93}$$

© 1996 Carl Hanser Verlag. All rights reserved.
No unauthorized disclosure or reproduction; licensed to purchaser only.

Table 4.10 Scale Factor for Sheet Sag Equation [114]

Sheet length / Sheet width	β
1.0	0.0444
1.2	0.0616
1.4	0.0770
1.6	0.0906
1.8	0.1017
2.0	0.1110
3.0	0.1335
4.0	0.1400
5.0	0.1417
∞	0.1421

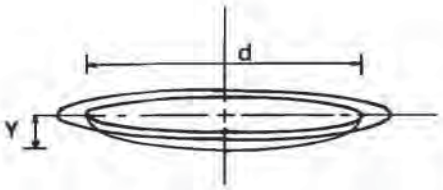

Figure 4.65 Geometric factors for initial sheet sag for a circular disk

where ν is Poisson's ratio. This example is most useful when determining the extent of draw-down into vacuum or vent holes. A form of this equation is used in Chapter 6 to predict the initial draw of sheet into a vent hole of diameter d.

Tensile Sag

When the neutral axis is no longer within the sheet thickness, the entire sheet is under tension. As described above, the polymer elongates under tensile loading according to:

$$\sigma = f(\epsilon;E(T)) \tag{4.94}$$

If the polymer is simply hanging vertically, as seen in Fig. 4.5, the engineering stress is given as:

$$\sigma_{eng} = \frac{W}{A_o} \tag{4.95}$$

where $A_o = bh_o$, where b is the unit width and h_o is the initial sheet thickness. W is the weight of the sheet, $W = \rho bh_oL_o$. If the sheet stretches uniaxially as would be the case if the vertical sheet is heated, the weight of the polymer remains fixed and

© 1996 Carl Hanser Verlag. All rights reserved.
No unauthorized disclosure or reproduction; licensed to purchaser only.

so does the engineering stress. The elongation increases and the temperature-dependent proportionality, E(T) decreases in proportion. The analysis of a sagging sheet follows this logic but includes the important fact that the sheet is supported on both ends. There are two models used for suspended elements. Both are developed for the hanging of cable in civil engineering and are adapted here for an infinitely long sheet supported on two edges. The arithmetic follows.

The Catenary Sag

The classic one-dimensional strength of materials case, typical of a roll-fed sheet held along two sides, is the catenary (Fig. 4.66) [116]. The sheet has a horizontal T_o tension at its origin ($x = 0, y = 0$). T is its tension at coordinates (x,y) along the sheet surface. The vertical supported load is the weight of the section of sheet length s. For a sheet of unit width and length weighing μ kg/m or lb/ft, the load is μs. The sheet unit weight, μ is related to the sheet thickness by:

$$\mu \text{ (per unit width and length)} = \rho h \tag{4.96}$$

where ρ is the sheet density, lb_f/ft^3 or kg/m^3 and h is the sheet thickness in inches or mm. This is resolved as:

$$T \sin \theta = \mu s \tag{4.97}$$

$$T \cos \theta = T_o \tag{4.98}$$

The extent of deflection, y, below the horizontal is given as:

$$\frac{d^2y}{dx^2} = \frac{\mu s}{T_o} \tag{4.99}$$

where x is the distance from the center of the catenary. Since $(ds)^2 = (dx)^2 + (dy)^2$, this is written as:

$$\frac{d^2y}{dx^2} = \frac{\mu}{T_o}\left[1 + \left(\frac{dy}{dx}\right)^2\right]^{1/2} \tag{4.100}$$

The arc length then is:

$$s = \frac{T_o}{\mu} \sinh\left(\frac{\mu x}{T_o}\right) \tag{4.101}$$

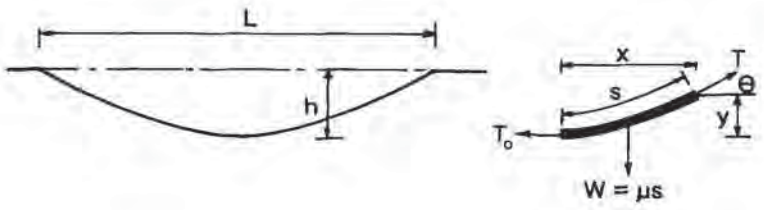

Figure 4.66 Geometric factors for catenary sag of a linear sheet element. Figure adapted from [116]

© 1996 Carl Hanser Verlag. All rights reserved.
No unauthorized disclosure or reproduction; licensed to purchaser only.

The extent of deflection, y, is given as:

$$y = \frac{T_o}{\mu}\left(\cosh \frac{\mu x}{T_o} - 1\right) \tag{4.102}$$

And the tension on the sheet is given as:

$$T(x) = T_o \cosh \frac{\mu x}{T_o} = T_o + \mu y \tag{4.103}$$

The total sheet length, S, is given as:

$$S = \int_0^{L/2} s\, dx = \frac{T_o}{\mu} \cosh\left(\frac{\mu L}{2T_o}\right)^{-1} \tag{4.104}$$

where L is the initial sheet span.

Although the solution is quite compact, there is difficulty applying Equations 4.102 through 4.104 to sagging sheet in thermoforming. For example, as the sheet begins to sag, its span, given as S, increases. Since the total sheet weight remains constant, the sheet must therefore thin. As the sheet thins, the local unit weight of the sheet, given as μ, decreases in proportion.

Parabolic Sag

The parabolic model is simpler than the catenary model but less exact. It assumes that the load, μ, is uniformly applied along the *horizontal* plane of the sheet (Fig. 4.67) [117]. Again, $\mu = \rho h$ is assumed. The describing equations are:

$$T \sin \theta = \mu x \tag{4.105}$$

$$T \cos \theta = T_o \tag{4.106}$$

The equation describing the curve of the sheet under these conditions is:

$$\frac{dy}{dx} = \frac{\mu x}{T_o} \tag{4.107}$$

with the parabolic solution being:

$$y = \frac{\mu x^2}{2T_o} \tag{4.108}$$

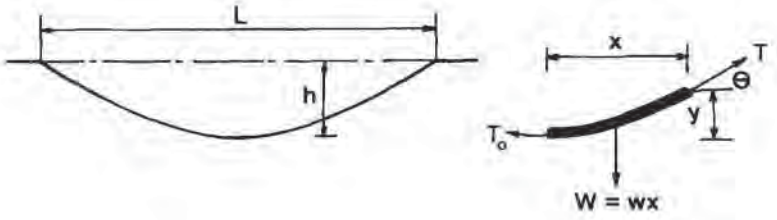

Figure 4.67 Geometric factors for parabolic sag of a linear sheet element. Figure adapted from [117]

© 1996 Carl Hanser Verlag. All rights reserved.
No unauthorized disclosure or reproduction; licensed to purchaser only.

The tension at the origin ($x = 0, y = 0$) is:

$$T_o = \frac{\mu L^2}{8Y} \tag{4.109}$$

where Y is the maximum sag. The maximum tension in the sheet is:

$$T_{max}(x = L/2) = \frac{\mu L}{2}\left[1 + \frac{L^2}{16Y^2}\right]^{1/2} \tag{4.110}$$

Note that it requires an infinite force to hold a sheet of finite thickness in the horizontal plane, $Y = 0$. And the value for the sagged length of the sheet is obtained from:

$$\frac{S}{L} = \left[\frac{1}{2}\frac{1}{(4Y/L)}\right]\left\{\frac{4Y}{L}\left[\left(\frac{4Y}{L}\right)^2 + 1\right]^{1/2} + \ln\left(\frac{4Y}{L} + \left[\left(\frac{4Y}{L}\right)^2 + 1\right]^{1/2}\right)\right\} \tag{4.111}$$

When the sag-to-span ratio, Y/L, is small, the parabolic sag equations are satisfactory approximations to the catenary equations and substantially easier to manipulate. Plots of Y/L and S/L as functions of $\mu L/2T_o$ are given in Fig. 4.68. The curves deviate at $\mu L/2T_o > 1$ or so. A cross-plot of the ratio of S/L to Y/L for parabolic and catenary sag shows essentially identical shapes for values of Y/L greater than about 0.1 (Fig. 4.69). S/L approaches a value of 2(Y/L) for sag levels greater than $Y/L = 2$.

Relating Sag to Hot Sheet Strength

The catenary relationship between T_{max}, the tension at the gripped edge of the sheet, and T_o, the tension at ($x = 0, y = 0$) is obtained from:

$$T_{max} = T_o + \mu S = T_o + \left(\frac{\mu_o \cdot h}{h_o}\right) \cdot \left(\frac{h_o \cdot L}{h}\right) = T_o + \rho h_o L \tag{4.112}$$

or T_{max} is a constant factor greater than T_o, regardless of the extent of stretching. On the other hand, for the parabolic relationship:

$$T_{max}^2 = T_o^2 + \frac{\mu^2 L^2}{4} \tag{4.113}$$

Again, $\mu = \mu_o \cdot (h/h_o)$ and $(h/h_o) = (S/L)^{-1}$ as before. Since T_{max} is assumed to be constant and equal to the tensile stress of the polymer, this equation is solved for T_o as:

$$T_o^2 = T_{max}^2 - \mu_o^2 \frac{L^2}{4}\left(\frac{L}{S}\right)^2 \tag{4.114}$$

Unlike Equation 4.112 for the catenary, T_o is not constant but a function of the length of the sagged sheet, which in turn is a function of the vertical extent of sag, Y/L, according to Equation 4.107. So long as S/L is small, the effect of sag on the value of T_o is small and $\mu \approx \mu_o$. As the sag becomes more significant, the basic premises used to develop the parabolic equations are no longer valid.

© 1996 Carl Hanser Verlag. All rights reserved.
No unauthorized disclosure or reproduction; licensed to purchaser only.

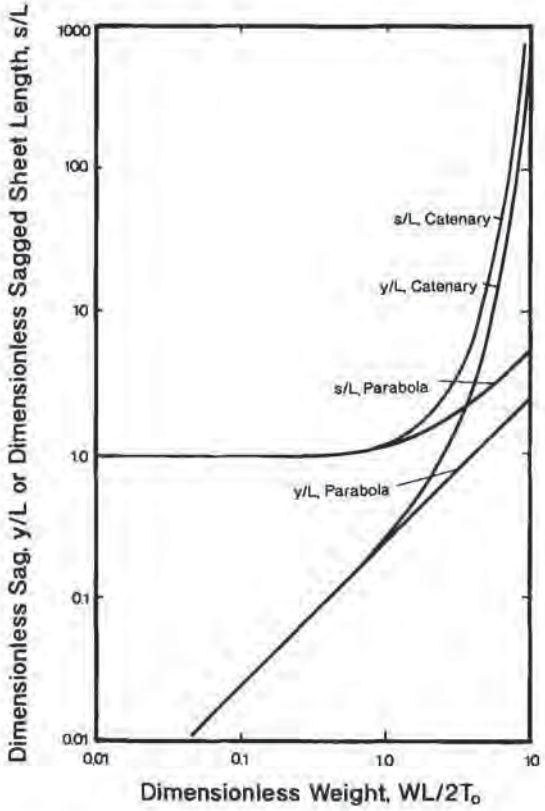

Figure 4.68 Dimensionless extent of sag as function of sheet dimensionless weight for catenary and parabolic sag

From Equation 4.113:

$$T_o^2 = \frac{\mu^2 L^4}{64Y^2} = \frac{\mu_o^2 L^4}{64Y^2}\left(\frac{h}{h_o}\right)^2 \tag{4.115}$$

Again, since T_{max} is constant, Equation 4.114 is written as:

$$\frac{2T_o}{\mu_o L} = \left(\frac{L}{4Y}\right)\left(\frac{2T_{max}}{\mu_o L}\right)\left[1 + \left(\frac{L}{4Y}\right)^2\right]^{-1/2} \tag{4.116}$$

This relationship also shows T_o as a function of Y/L.

The hot strength of the polymer, in terms of the engineering stress at the grip, is written as $\sigma = T_{max}/A$ where A is the initial cross-section of the sheet, $A = h_o \cdot b$. As a result, a measured property, the tensile strength of the polymer, is directly related to the measured response, sag, for both the catenary and parabolic models [134]. Example 4.14 illustrates the relationship between the catenary and parabolic models. Examples 4.15 and 4.16 illustrate the effect of sheet temperature on sheet sag.

© 1996 Carl Hanser Verlag. All rights reserved.
No unauthorized disclosure or reproduction; licensed to purchaser only.

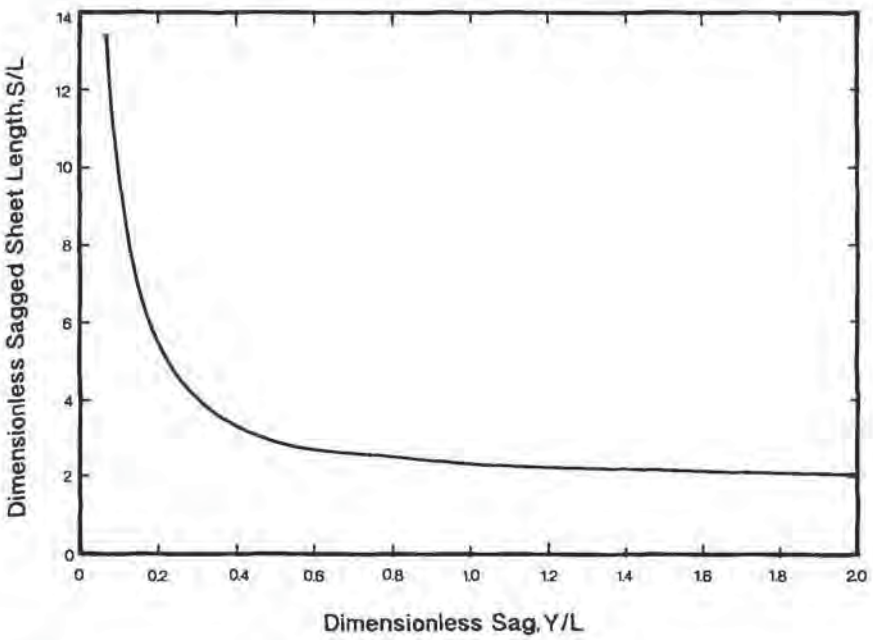

Figure 4.69 Dimensionless sheet length as function of dimensionless extent of sag. Catenary and parabolic curves coincide

Example 4.13 Initial Sag of Polypropylene Sheet

Consider a 0.250-in thick polypropylene sheet at 100°C. The modulus of the sheet is 10 MPa or 1500 lb_f/in^2 and its Poisson's ratio is 0.35. Determine the extent of sag if a 10 × 10 in sheet is clamped on all sides and then only on two sides. Determine the equivalent sag if a 10-in disk is being heated.

The extent of sag is obtained from Equation 4.92. The density of PP is 0.91 $g/cm^3 = 56.8\ lb/ft^3 = 0.0329\ lb/in^3$. $q = 0.0329 \cdot h$. Therefore for the sheet clamped on all sides, $\beta = 0.0444$:

$$y = \frac{0.0444 \cdot 0.0329 \cdot h \cdot 10^4}{1500 \cdot h^3} = \frac{0.0444 \cdot 0.0329 \cdot 10^4}{1500 \cdot 0.25^2} = 0.156 \text{ in}$$

For the sheet clamped on two sides, $\beta = 0.1421$, and $y = 0.500$ in[1].

The extent of sag of a disk is obtained from Equation 4.93:

$$y = \frac{3 \cdot 0.0329 \cdot h \cdot 100 \cdot (5 + 0.35)}{16 \cdot 1500 \cdot h^3} = 0.0542 \text{ in}$$

[1] Correctly, when the value of y calculated using this equation exceeds the half-thickness of the sheet, the equation should not be used to predict sag.

© 1996 Carl Hanser Verlag. All rights reserved.
No unauthorized disclosure or reproduction; licensed to purchaser only.

Example 4.14 Parabolic and Catenary Sag

Consider the sag of a 0.100 in thick by 48 in wide plastic sheet having a density of 62.4 lb/ft³. The tensile stress on the sheet at the grip is 10 lb/in². Determine the sag as given by the parabolic and catenary sag equations.

Consider the sag in catenary terms first. The tension in the sheet at the grip is given in Equation 4.112 in terms of the tension, T_o at $(x = 0,\ y = 0)$, written as:

$$T_{max} = T_o + \rho h_o L$$

$$\frac{2T_{max}}{\mu L} = \frac{2\sigma}{\rho L} = \frac{2T_o}{\mu L} + 2$$

$$\frac{2T_o}{\mu L} = \frac{2\sigma}{\rho L} - 2 = \frac{2 \cdot 10}{0.0361 \cdot 48} - 2 = 9.54$$

$$\eta = \left(\frac{2T_o}{\mu L}\right)^{-1} = 0.1048$$

For the catenary sag model, $(Y/L)_{cat} \approx 0.0265$ and $Y_{cat} = 1.27$ in.

For the parabolic sag concept:

$$\frac{2T_{max}}{\mu_o L} = \frac{2\sigma}{\rho L} = 11.54$$

As seen in Fig. 4.72, the S/L-to-Y/L ratio for the catenary model has nearly the same dependency on Y/L as the parabolic model.

If $(Y/L)_{para} \approx 0.0265$ and if $\mu \approx \mu_o$:

$$\frac{2T_o}{\mu L} = \frac{L}{4Y} = \frac{1}{4 \cdot 0.0265} = 9.43$$

Note that $2T_{max}/\mu_o L - 2T_o/\mu L = 11.54 - 9.43 = 2.11$ or approximately the same value as for the catenary problem[1]. In other words, for this case, there probably is not a substantial difference in the sag predicted by parabolic and catenary equations.

[1] The reader is warned that this may be a self-fulfilling prophecy in that an incorrect value is used for Y/L. Please review the comments in the text at this point.

© 1996 Carl Hanser Verlag. All rights reserved.
No unauthorized disclosure or reproduction; licensed to purchaser only.

Example 4.15 Effect of Temperature on Sheet Sag

Consider the polymer of Example 4.14. Consider the stress given in the example to be at 200°C. The polymer elongational energy of activation is 20,000 kcal/mol. Determine the tensile stress at 230°C and determine the extent of sag at 230°C. Repeat the analysis for a sheet temperataure of 240°C.

The Arrhenius form is given as:

$$\sigma = \sigma_o \exp\left[\frac{E}{R}\left(\frac{1}{T} - \frac{1}{T_o}\right)\right]$$

where the temperatures are absolute. From the values given:

$$\sigma_{230} = 10 \cdot \exp\left[\frac{20000}{1.987}\left(\frac{1}{230+273} - \frac{1}{200+273}\right)\right] = 10 \cdot \exp(-1.269)$$

$$= 2.81 \text{ lb/in}^2$$

$$\frac{2T_o}{\mu L} = \frac{2 \cdot 2.81}{0.0361 \cdot 48} - 2 = 1.243$$

$$\eta = \left(\frac{2T_o}{\mu L}\right)^{-1} = 0.804$$

For catenary sag, $Y/L \approx 0.215$ and $Y_{cat} \approx 10.3$ in. From Fig. 4.73, $S/L \approx 5.12\,(Y/L)$ or $S/L \approx 1.10 = (h/h_o)^{-1}$.

For parabolic sag, assume:

$$\frac{2T_o}{\mu L} = \frac{L}{4Y} \approx 1.243$$

Therefore, $Y/L \approx 0.201$ and $Y_{para} \approx 9.65$ in[1]. The sheet sag has increased by about 700% in 30°C.

Now consider the effect at 235°C. $\sigma_{235} = 2.31$ lb/in^2. For catenary sag, $2T_o/\mu L = 0.663$ and $\eta = 1.508$. For catenary sag, $Y/L \approx 0.463$ or $Y_{cat} = 22.2$ in. For parabolic sag, $Y/L \approx 0.36$ or $Y_{para} \approx 17.3$ in. The extent of sag has more than doubled in 5°C.

[1] This value is suspect since μ has not been adjusted by the 10% decrease in sheet thickness

Example 4.16 The Importance of Temperature-Dependent Hot Strength on Sag

Consider two polymers exhibiting the same extent of sag of 9.65 in for a 48-in sheet span at 230°C as given in Example 4.15. Assume that Polymer A has an elongational energy of activation value of 20,000 and B has a value of 10,000. Determine the extent of sag at 235°C.

$$\sigma_{A,230} = \sigma_{B,230} = 2.81.$$

© 1996 Carl Hanser Verlag. All rights reserved.
No unauthorized disclosure or reproduction; licensed to purchaser only.

$\sigma_{A,235} = 2.31$ in Example 4.15. For catenary sag, $2T_o/\mu L = 0.663$ and $\eta = 1.508$. For catenary sag, $Y/L \approx 0.463$ or $Y_{cat} = 22.2$ in.

$$\sigma_{B,235} = 2.55 \text{ from Example 4.15}$$

$$\frac{2T_o}{\mu L} = \frac{2 \cdot 2.55}{0.0361 \cdot 48} - 2 = 0.942$$

$$\eta = \left(\frac{2T_o}{\mu L}\right)^{-1} = 1.061$$

For catenary sag, $Y/L \approx 0.305$ and $Y_{cat} \approx 14.6$ in.

The results are tabulated as follows:

	$(Y/L)_{230}$	$(Y)_{230}$	$(Y/L)_{235}$	$(Y)_{235}$
Polymer A	0.201	9.65	0.463	22.2
Polymer B	0.201	9.65	0.305	14.6

It is apparent that Polymer B is substantially stiffer at 235°C than Polymer A and that this should be visibly apparent in the relative extents of sag.

Some interesting insights to sheet sag are obtained by reviewing the parabolic and catenary models. For example, the tension on the sheet increases in proportion to the sheet thickness—through the value for μ—and in proportion to the square of the span[1]. S/L varies between 1.0 and 2Y/L as Y/L varies between 0 and ∞ (Fig. 4.69). Note that the thickness of the sheet decreases from a value of h for $Y/L = 0$ to a value of h/2 or $S/L = 2$ at a value of $Y/L \approx 0.8$[2]. When $Y/L \approx 1.9$, $S/L \approx 4$ and the sagged sheet thickness is about 1/4 its original thickness. But, minor sagging does not appreciably reduce the sheet thickness. Even when the sheet has sagged $Y/L = 0.2$, S/L is just 1.1 and the sagged sheet thickness is still more than 90% of its original thickness.

Sag—A Comment

The parabolic model is simpler to use than the catenary model and satisfactory for small values of Y/L. For larger values of Y/L, the catenary model is more accurate. The catenary and parabolic sag models are simplistic. They assume that the sheet is

[1] As noted in Equation 4.85 for initial sheet sag, the extent of sag was proportional to the fourth-power of the span.

[2] Note that this assumes that the sheet is thinning uniformly across the sagging span. In reality, the tension on the sheet is varying from the minimum at mid-span to maximum at the clamped edges. As a result, an isothermal sheet should stretch more in the clamped edges. In general, the sheet tends to be cooler in the vicinity of the clamped edges, and so uniform sheet stretching is a reasonable assumption.

© 1996 Carl Hanser Verlag. All rights reserved.
No unauthorized disclosure or reproduction; licensed to purchaser only.

essentially infinite in length. Large deformation of two-dimensional sheet and axisymmetric sheet is best solved using finite element analysis, as described in Chapter 7, on part design.

4.10 References

1. J. Florian, *Practical Thermoforming: Principles and Applications*, Marcel Dekker, Inc., New York (1987), pp. 122-125.
2. R.C. Progelhof and J.L. Throne, *Polymer Engineering Principles: Properties, Processes, Tests for Design*, Hanser Publishers, Munich (1993), p. 104.
3. H. Domininghaus, *Plastics for Engineers: Materials, Properties, Applications*, Hanser Publishers, Munich, (1993).
4. R.C. Progelhof and J.L. Throne, *Polymer Engineering Principles: Properties, Processes, Tests for Design*, Hanser Publishers, Munich (1993), p. 196.
5. R.C. Progelhof and J.L. Throne, *Polymer Engineering Principles: Properties, Processes, Tests for Design*, Hanser Publishers, Munich (1993), p. 293.
6. R.C. Progelhof and J.L. Throne, *Polymer Engineering Principles: Properties, Processes, Tests for Design*, Hanser Publishers, Munich (1993), Figure 3.4, p. 193.
7. C.J.S. Petrie, *Elongational Flows*, Pitman, London (1979), p. 93, p. 4.
8. C.D. Denson, "Implications of Extensional Flow in Polymer Fabrication Processes", Polym. Eng. Sci., *13* (1973), p. 125.
9. V.E. Malpass and C.H. White, "Laboratory Comparison of the Thermoforming Properties of Two ABS Materials", in P.F. Bruins, Ed., *Basic Principles of Thermoforming*, Gordon and Breach, New York (1973), p. 103.
10. V.E. Malpass and J.T. Kempthorn, "Comparison of Polyolefin Thermoforming by Hot Tensile Testing", SPE ANTEC Tech. Papers, *32* (1986), p. 63.
11. H. Saechtling, *International Plastics Handbook for the Technologist, Engineer and User*, 2nd Ed., Hanser Publishers, Munich (1987), Figure 110A, p. 417.
12. H. Saechtling, *International Plastics Handbook for the Technologist, Engineer and User*, 2nd Ed., Hanser Publishers, Munich (1987), Figure 110B, p. 417.
13. H. Domininghaus, *Plastics for Engineers: Materials, Properties, Applications*, Hanser Publishers, Munich (1993), p. 506.
14. H. Domininghaus, *Plastics for Engineers: Materials, Properties, Applications*, Hanser Publishers, Munich (1993), p. 208.
15. V.E. Malpass and C.H. White, "Laboratory Comparison of the Thermoforming Properties of Two ABS Materials", in P.F. Bruins, Ed., *Basic Principles of Thermoforming*, Gordon and Breach, New York (1973), p. 105.
16. R.C. Progelhof and J.L. Throne, *Polymer Engineering Principles: Properties, Processes, Tests for Design*, Hanser Publishers, Munich (1993), Section 6.5, "Solid Mechanical Properties: Long-Time Tests".
17. R.L. Harris and P.F. Bruins, "A New Technique for Predicting Optimum Thermoforming Conditions", in P.F. Bruins, Ed., *Basic Principles of Thermoforming*, Gordon and Breach, New York (1973), p. 81.
18. D. Weinand, "Modellbildung zum Aufheizen und Verstrecken beim Thermoformen", Doktor-Ingenieur Dissertation, Rheinisch-Westfälische Technische Hochschule Aaachen (Institut für Kunststoffverarbeitung) (1987), Bild 5.1.
19. D. Weinand, "Modellbildung zum Aufheizen und Verstrecken beim Thermoformen", Doktor-Ingenieur Dissertation, Rheinisch-Westfälische Technischen Hochschule Aaachen (Institut für Kunststoffverarbeitung) (1987), pp. 74-79.
20. J.M. Dealy, "On the Relationship Between Extensional Viscosities for Uniaxial and Biaxial Extension", Trans. Soc. Rheol., *17* (1973), p. 255.

© 1996 Carl Hanser Verlag. All rights reserved.
No unauthorized disclosure or reproduction; licensed to purchaser only.

21. C.D. Denson and R.J. Gallo, "Measurement on the Biaxial Extension Viscosity of Bulk Polymers: The Inflation of a Thin Polymer Sheet", Polym. Eng. Sci., *11* (1971), p. 174.
22. D.D. Joye, G.W. Poehlein and C.D. Denson, "A Bubble Inflation Technique for the Measurement of Viscoelastic Properties in Equal Biaxial Extensional Flow. II", Trans. Soc. Rheol., *17* (1973), p. 287.
23. D.D. Joye, G.W. Poehlein and C.D. Denson, "A Bubble Inflation Technique for the Measurement of Viscoelastic Properties in Equal Biaxial Extensional Flow", Trans. Soc. Rheol., *17* (1973), p. 421.
24. R.J. Arenz, R.F. Landel and K. Tsuge, "Miniature Load-Cell Instrumentation for Finite-Deformation Biaxial Testing of Elastomers", Exp. Mech., *15* (1975), pp. 114-120.
25. S. Peng and R. Landel, "Viscoelastic Response of a Highly Filled Polymer", NASA Tech. Brief., *16*:3 (Mar 1992), p. 135.
26. N.G. McCrum, C.P. Buckley, and C.B. Bucknall, *Principles of Polymer Engineering*, Oxford University Press, Oxford (1988), Figure 7.13, p. 281.
27. J.M. McKelvey, Polymer Processing, John Wiley & Sons, New York (1962), p. 45.
28. R.C. Progelhof and J.L. Throne, *Polymer Engineering Principles: Properties, Processes, Tests for Design*, Hanser Publishers, Munich (1993), pp. 565-569.
29. R.C. Progelhof and J.L. Throne, *Polymer Engineering Principles: Properties, Processes, Tests for Design*, Hanser Publishers, Munich (1993), Figure 3.28.
30. R.C. Progelhof and J.L. Throne, *Polymer Engineering Principles: Properties, Processes, Tests for Design*, Hanser Publishers, Munich (1993), Figure 3.29.
31. R.C. Progelhof and J.L. Throne, *Polymer Engineering Principles: Properties, Processes, Tests for Design*, Hanser Publishers, Munich (1993), Figure 3.40.
32. R.C. Progelhof and J.L. Throne, *Polymer Engineering Principles: Properties, Processes, Tests for Design*, Hanser Publishers, Munich (1993), Figure 3.42.
33. G. Kampf, *Characterization of Plastics by Physical Methods: Experimental Techniques and Practical Application*, Hanser Publishers, Munich (1986), Chapter 4, "Thermoanalytic Methods".
34. H. Domininghaus, *Plastics for Engineers: Materials, Properties, Applications*, Hanser Publishers, Munich (1993), Figure 371, p. 427.
35. H. Domininghaus, *Plastics for Engineers: Materials, Properties, Applications*, Hanser Publishers, Munich (1993), Figure 113, p. 194.
36. H. Domininghaus, *Plastics for Engineers: Materials, Properties, Applications*, Hanser Publishers, Munich (1993), Figure 11, p. 39.
37. C.W. Macosko and J.M. Lorntson, "The Rheology of Two Blow Molding Polyethylenes", SPE ANTEC Tech. Papers, *19* (1973), p. 461.
38. Z. Tadmor and C.G. Gogos, *Principles of Polymer Processing*, John Wiley & Sons, New York (1979), "Elongational Flows", Section 6.8, p. 184.
39. R.B. Bird, R.C. Armstrong and O. Hassager, *Dynamics of Polymeric Liquids*, Vol. 1, John Wiley & Sons, New York (1977), p. 451.
40. J.L. White, "Theoretical Considerations of Biaxial Stretching of Viscoelastic Fluid Sheets with Application to Plastic Sheet Forming", Rheol. Acta, *14* (1975), p. 600.
41. C.J.S. Petrie, *Elongational Flows*, Pitman, London (1979), p. 93, Section 3.3, "Spinning and Related Flows".
42. J. Meissner, "A Rheometer for Investigation of Deformation-Mechanical Properties of Plastic Melts Under Defined Extensional Straining", Rheol. Acta, *8* (1969), p. 78.
43. C.D. Han and J.Y. Park, "Studies on Blown Film Extension. I: Experimental Determination of Elongational Viscosity", J. Appl. Polym. Sci., *19* (1975), p. 3257.
44. L. Erwin, H. Gonzolez and M. Pollock, "Analysis and Experiments in Blow Molding of Oriented PET Bottles", SPE ANTEC Tech. Papers, *29* (1983), p. 807.
45. J.M. Funt, "An Analysis of the Rheology of Polypropylene Below Its Melting Point", Polym. Eng. Sci., *15* (1975), p. 817.
46. K.C. Hoover and R.W. Tock, "Experimental Studies on the Biaxial Extensional Viscosity of Polypropylene", Polym. Eng. Sci., *16* (1976), p. 82.
47. S. Bahadur, "Strain Hardening Equation and the Prediction of Tensile Strength of Rolled Polymers", Polym. Eng. Sci., *13* (1973), p. 266.

© 1996 Carl Hanser Verlag. All rights reserved.
No unauthorized disclosure or reproduction; licensed to purchaser only.

48. P.I. Vincent, "Short-Term Strength and Impact Behaviour", in R.M. Ogorkiewicz, Ed., *Thermoplastics: Properties and Design*, John Wiley & Sons, Ltd., London (1974), p. 72.
49. M.O. Lai and D.L. Holt, "The Extensional Flow of Poly(Methyl Methacrylate) and High-Impact Polystyrene at Thermoforming Temperatures", J. Appl. Polym. Sci., *19* (1975), p. 1209.
50. M.O. Lai and D.L. Holt, "Thickness Variation in the Thermoforming of Poly(Methyl Methacrylate) and High-Impact Polystyrene Sheets", J. Appl. Polym. Sci., *19* (1975), p. 1805.
51. D. Hylton, Laboratory Techniques for Predicting Material Thermoformability: A Review, SPE ANTEC Tech. Papers, *37* (1990), pp. 580-583.
52. A.S. Lodge, *Elastic Liquids*, Academic Press, London (1964), p. 99.
53. L.R. Schmidt and J.F. Carley, "Biaxial Stretching of Heat-Softened Plastic Sheets: Experiments and Results", Polym. Eng. Sci., *15* (1975), p. 51.
54. T. Alfrey, Jr., "Plastics Processing and Fabrication Problems Involving Membranes and Rotational Symmetry", SPE Trans., *5*:4 (Apr 1965), p. 68.
55. J.A. Brydson, *Flow Properties of Polymer Melts*, Van Nostrand Reinhold, New York (1970), pp. 18-19.
56. R.B. Bird, R.C. Armstrong and O. Hassager, *Dynamics of Polymeric Liquids*, Vol. 1, John Wiley & Sons, New York (1977), p. 83.
57. C.J.S. Petrie, *Elongational Flows*, Pitman, London (1979), p. 65.
58. R.C. Progelhof and J.L. Throne, *Polymer Engineering Principles: Properties, Processes, Tests for Design*, Hanser Publishers, Munich (1993), p. 655.
59. L.R. Schmidt, *Biaxial Stretching of Heat-Softened Plastic Sheets*, PhD Thesis, University of Colorado, Boulder CO (1972).
60. H. Gross and G. Menges, "Influence of Thermoforming Parameters on the Properties of Thermoformed PP", SPE ANTEC Tech. Papers, *28* (1982), p. 840.
61. R.W. Ogden, "Large Deformation Isotropic Elasticity—on the Correlation of Theory and Experiment for Incompressible Rubberlike Solids", Proc. Roy. Soc. London *A326* (1972), pp. 565-584.
62. L.R.G. Treloar, "Elasticity of a Network of Long-Chain Molecules", Trans. Faraday Soc., *39* (1943), pp. 241f.
63. L.R.G. Treloar, *The Physics of Rubber Elasticity*, Oxford University Press, Oxford (1958).
64. R.S. Rivlin and D.W. Saunders, "Free Energy of Deformation of Vulcanized Rubber", Trans. R. Soc. Lond., *A243* (1951), pp. 251f.
65. J.G. Williams, "A Method of Calculation for Thermoforming Plastics Sheets", J. Strain Anal., *5* (1970), p. 49.
66. M. Mooney, "Theory of Large Elastic Deformations", J. Appl. Phys, *11* (1940), pp. 582-592.
67. H.J. Warnecke and B. Frankenhauser, "Montage von Kunststoffschlauchen mit Industrieroboter", Kunststoffe, *78* (1988), pp. 440-444.
68. L.R. Schmidt and J.F. Carley, "Biaxial Stretching of Heat-Softened Plastic Sheets Using an Inflation Technique", Int. J. Engng. Sci., *13* (1975), p. 563.
69. J.G. Williams, "A Method of Calculation for Thermoforming Plastics Sheets", J. Strain Anal., *5* (1970), p. 52.
70. L.R.G. Treloar, *The Physics of Rubber Elasticity*, Oxford University Press, Oxford (1958), p. 162.
71. L.R.G. Treloar, *The Physics of Rubber Elasticity*, Oxford University Press, Oxford (1958), p. 169.
72. H.J. Warnecke and B. Frankenhauser, "Montage von Kunststoffschlauchen mit Industrieroboter", Kunststoffe, *78* (1988), Figure 5, pp. 440-444.
73. R.W. Ogden, *Non-Linear Elastic Deformations*, Ellis Horwood Ltd., West Sussex, England (1984).
74. W. Song, "Large Deformation Finite Element Analysis for Polymer Forming Processes", PhD Dissertation, McMaster University, Hamilton ON Canada (1993), Section 4.2.1.
75. K. Kouba, O. Bartos, and J. Vlachopoulos, "Computer Simulation of Thermoforming in Complex Shapes", Poly. Eng. Sci., *32* (1992), pp. 699-704.
76. A.E. Green and J.E. Adkins, *Large Elastic Deformations and Non-Linear Continuum Mechanics*, Oxford (1960), p. 26.
77. A.E. Green and J.E. Adkins, *Large Elastic Deformations and Non-Linear Continuum Mechanics*, Oxford (1960), p. 85.

© 1996 Carl Hanser Verlag. All rights reserved.
No unauthorized disclosure or reproduction; licensed to purchaser only.

78. B.D. Coleman, H. Markovitz and W. Noll, *Viscometric Flows of Non-Newtonian Fluids*, Springer, New York (1966), pp. 37-41.
79. K. Kouba and J. Vlachopoulos, *T-FORMCAD: A Finite Element Software Package for Thermoforming and Blow Molding*, Accuform Co., Ltd, and CAPPA-D, McMaster University, Hamilton ON Canada L8S 4L7.
80. M.H. Wagner, "A Constitutive Analysis of Extensional Flows of Polyisobutylene", J. Rheol., *34* (1990), pp. 943-958.
81. R.B. Bird, R.C. Armstrong and O. Hassager, *Dynamics of Polymeric Liquids*. Volume 1. Fluid Mechanics, John Wiley & Sons, New York (1977), p. 430.
82. K. Kouba and J. Vlachopoulos, "Modeling of 3D Thermoforming", SPE ANTEC Tech. Papers, *38* (1992), pp. 114-116.
83. R.I. Tanner, *Engineering Rheology*, Clarendon Press, Oxford (1985).
84. R.B. Bird, R.C. Armstrong, and O. Hassager, *Dynamics of Polymeric Liquids*. Volume 1. Fluid Mechanics, John Wiley & Sons, New York (1977), p. 107.
85. A. Wineman, "On Axisymmetric Deformations of Nonlinear Viscoelastic Membranes", J. Non-Newt. Fluid Mech., *4* (1978), pp. 249-260.
86. A. Wineman, "On the Simultaneous Elongation and Inflation of a Tubular Membrane of BKZ Fluid", J. Non-Newt. Fluid Mech., *6* (1979), pp. 111-125.
87. H. Saechtling, *International Plastics Handbook for the Technologist, Engineer and User*, 2nd Ed., Hanser Publishers, Munich (1987), Figure 109, p. 416.
88. H. Saechtling, *International Plastics Handbook for the Technologist, Engineer and User*, 2nd Ed., Hanser Publishers, Munich (1987), Figure 111, p. 418.
89. H. Saechtling, *International Plastics Handbook for the Technologist, Engineer and User*, 2nd Ed., Hanser Publishers, Munich (1987), Figure 112, p. 419.
90. H. Domininghaus, *Plastics for Engineers: Materials, Properties, Applications*, Hanser Publishers, Munich (1993), Figure 14.
91. H. Domininghaus, *Plastics for Engineers: Materials, Properties, Applications*, Hanser Publishers, Munich (1993), Figure 15.
92. H. Domininghaus, *Plastics for Engineers: Materials, Properties, Applications*, Hanser Publishers, Munich (1993), Figure 42.
93. H. Domininghaus, *Plastics for Engineers: Materials, Properties, Applications*, Hanser Publishers, Munich (1993), Figure 129, p. 206.
94. D. Weinand, "Modellbildung zum Aufheizen und Verstrecken beim Thermoformen", Doktor-Ingenieur Dissertation, Rheinisch-Westfälische Technische Hochschule Aaachen (Institut für Kunststoffverarbeitung (1987), Bild 5.2.
95. R.C. Progelhof and J.L. Throne, *Polymer Engineering Principles: Properties, Processes, Tests for Design*, Hanser Publishers, Munich (1993), Figure 6.25.
96. D. Weinand, "Modellbildung zum Aufheizen und Verstrecken beim Thermoformen", Doktor-Ingenieur Dissertation, Rheinisch-Westfälische Technische Hochschule Aaachen (Institut für Kunststoffverarbeitung (1987), Bild 5.3.
97. H. Domininghaus, *Plastics for Engineers: Materials, Properties, Applications*, Hanser Publishers, Munich (1993), Figure 153, p. 228.
98. R.C. Progelhof and J.L. Throne, *Polymer Engineering Principles: Properties, Processes, Tests for Design*, Hanser Publishers, Munich, 1993, Figure 6.29.
99. H. Domininghaus, *Plastics for Engineers: Materials, Properties, Applications*, Hanser Publishers, Munich (1993), Figure 171, p. 245.
100. H. Domininghaus, *Plastics for Engineers: Materials, Properties, Applications*, Hanser Publishers, Munich (1993), Figure 242, p. 313.
101. H. Domininghaus, *Plastics for Engineers: Materials, Properties, Applications*, Hanser Publishers, Munich (1993), Figure 260, p. 328.
102. H. Domininghaus, *Plastics for Engineers: Materials, Properties, Applications*, Hanser Publishers, Munich (1993), Figure 295, p. 374.
103. H. Domininghaus, *Plastics for Engineers: Materials, Properties, Applications*, Hanser Publishers, Munich (1993), Figure 296, p. 374.

© 1996 Carl Hanser Verlag. All rights reserved.
No unauthorized disclosure or reproduction; licensed to purchaser only.

104. H. Domininghaus, *Plastics for Engineers: Materials, Properties, Applications*, Hanser Publishers, Munich (1993), Figure 403, p. 456.
105. H. Domininghaus, *Plastics for Engineers: Materials, Properties, Applications*, Hanser Publishers, Munich (1993), Figure 492, p. 534.
106. R.H. Finney and A. Kumar, "Development of Material Constants for Nonlinear Finite-Element Analysis", Rubber Chem. Tech., *61* (1988), pp. 879-891.
107. J.G. Williams, *Stress Analysis of Polymers*, John Wiley & Sons, New York (1973), pp. 211-220.
108. L.R.G. Treloar, *The Physics of Rubber Elasticity*, Oxford University Press, Oxford (1958), p. 170.
109. C.J.S. Petrie, *Elongational Flows*, Pitman, London (1979), p. 90, p. 210.
110. S. Middleman, *Fundamentals of Polymer Processing*, McGraw-Hill Book Co., New York (1977), p. 48.
111. R. Allard, J.-M. Charrier, A. Ghosh, M. Marangou, M.E. Ryan, S. Shrivastava and R. Wu., "An Engineering Study of the Thermoforming Process: Experimental and Theoretical Considerations", Paper presented at First Annual Meeting, Polym. Proc. Soc., Akron OH, 28-29 March 1984.
112. M.J. Stephenson and M.E. Ryan, "Experimental Study of Thermoforming Dynamics", SPE ANTEC Tech. Papers, *40* (1994), pp. 844-849.
113. S. Middleman, *Fundamentals of Polymer Processing*, McGraw-Hill Book Co., New York (1977), p. 49.
114. R.J. Roark and W.C. Young, *Formulas for Stress and Strain*, Fifth Ed., McGraw-Hill Book Co., New York (1975), Table 26, p. 386.
115. R.J. Roark and W.C. Young, *Formulas for Stress and Strain*, Fifth Ed., McGraw-Hill Book Co., New York (1975), p. 363, Example 10b.
116. J.L. Meriam, *Mechanics: Part I Statics*, John Wiley and Sons, Inc., Chapman & Hall, Ltd., London (1952), Figure 52, p. 184.
117. J.L. Meriam, *Mechanics: Part I Statics*, John Wiley and Sons, Inc., Chapman & Hall, Ltd., London, (1952), Figure 51.
118. J.M. McKelvey, *Polymer Processing*, John Wiley & Sons, New York (1962), p. 41.
119. M.C. Boyce and E.M. Arruda, "An Experimental and Analytical Investigation of the Large Strain Compressive and Tensile Response of Glassy Polymers", Polym. Eng. Sci., *30* (1990), pp. 1288-1298.
120. H.G. DeLorenzi and H.F. Nied, "Finite Element Simulation of Thermoforming and Blow Molding", in A.I. Isayev, Ed., *Modeling of Polymer Processing*, Carl Hanser Verlag, Munich (1991), Chapter 5.
121. W.N. Song, F.A. Mizra and J. Vlachopoulos, "Finite Element Analysis of Inflation of An Axisymmetric Sheet of Finite Thickness", J. Rheol., *35* (1991), pp. 93-111.
122. K. Kouba, O. Bartos and J. Vlachopoulos, "Computer Simulation of Thermoforming in Complex Shapes", Polym. Eng. Sci., *32* (1992), pp. 699-704.
123. H.F. Nied, C.A. Taylor and H.D. DeLorenzi, "Three-Dimensional Finite Element Simulation of Thermoforming", Polym. Eng. Sci., *30* (1990), pp. 1314-1322.
124. S.D. Batterman and J.L. Bassani, "Yielding, Anisotropy, and Deformation Processing of Polymers", Polym Eng. Sci., *30* (1990), PP. 1281-1287.
125. S. Bahadur, "Strain Hardening Equation and the Prediction of Tensile Strength of Rolled Polymers", Polym. Eng. Sci., *13* (1973), pp. 266-272.
126. M.J. Miles and N.J. Mills, "The Deep Drawing of Thermoplastics", Polym. Eng. Sci., *17* (1977), pp. 101-110.
127. G.W. Halldin, "Solid-Phase Flow Behavior of Polymers", Polym. Eng. Sci., *25* (1985), pp. 323-331.
128. K. Nakamura, K. Imada and M. Takayanagi, "Solid State Extrusion of Isotactic Polypropylene Through a Tapered Die. I. Phenomenological Analysis", Int. J. Polym. Mat., *2* (1972), pp. 71-88.
129. G. Menges and D. Weinand, "Modellierung des Verstreckprozesses beim Warmformen", Kunststoffe *78* (1988), pp. 456-460.
130. K. Kouba, M.O. Ghafur, J. Vlachopoulos and W.P. Haessly, "Some New Results in Modelling of Thermoforming", SPE ANTEC Tech. Papers, *40* (1994), pp. 850-853.

© 1996 Carl Hanser Verlag. All rights reserved.
No unauthorized disclosure or reproduction; licensed to purchaser only.

131. L.R. Schmidt and J.F. Carley, "Biaxial Stretching of Heat-Softened Plastic Sheets: Experiments and Results", Polym. Eng. Sci., *15* (1975), pp. 51-62.
132. L.R. Schmidt and J.F. Carley, "Biaxial Stretching of Heat-Softened Plastic Sheets Using an Inflation Technique", Int. J. Eng. Sci., *13* (1975), pp. 563-568.
133. D. Hylton, "Laboratory Techniques for Predicting Material Thermoformability: A Review", SPE ANTEC Tech. Papers, *37* (1990), pp. 580-583.
134. C. Cruz, Jr., "The Sag Process in Modified Polypropylene", SPE ANTEC Tech. Papers, *40* (1994), pp. 854-858.
135. J.L. Throne, *Thermoforming*, Carl Hanser Verlag, Munich (1987), pp. 110–112.

Appendix 4.1 Biaxial Stretching of an Elastic Membrane[1]

Consider the biaxial extension of a rubbery solid membrane of initial thickness h_o and radius a, inflated with a differential pressure P. The extensional stress-strain equations for a Mooney-type polymer are:

$$\sigma_l = 2(C_{10} + C_{01} \cdot \lambda_\theta^2) \cdot \left(\lambda_l^2 - \frac{1}{\lambda_l^2 \cdot \lambda_\theta^2}\right) \tag{4.I.1}$$

$$\sigma_\theta = 2(C_{10} + C_{01} \cdot \lambda_l^2) \cdot \left(\lambda_\theta^2 - \frac{1}{\lambda_l^2 \cdot \lambda_\theta^2}\right) \tag{4.I.2}$$

C_{01} and C_{10} are the Mooney constants, and l and θ are the in-sheet or meridional and angular or hoop direction coordinates (Fig. 4.70). N is the force acting on the membrane, $N = \sigma \cdot h$, σ is the local stress and h is the local thickness. The radius from the center axis is r, $\lambda_h = h/h_o$, $\lambda_\theta = r/r_o$, and $\lambda_l = (\lambda_h \cdot \lambda_\theta)^{-1}$. The angle of the membrane from the horizontal is β and δ is the cap height above the horizontal plane. Thus $r/R = \sin\beta$, where R is the radius of the spherical cap (Fig. 4.71). At the top of the dome:

$$\lambda_h = \frac{h}{h_o} = \frac{1}{1 + (\delta/a)^2} \tag{4.I.3}$$

For $C_{01} \ll C_{10}$ and $\lambda_l, \lambda_h \gg 1$, or for large deformations of a neo-Hookean solid:

$$\sigma_l \approx 2C_{10} \cdot \lambda_l^2 \tag{4.I.4}$$

$$\sigma_\theta \approx 2C_{10} \cdot \lambda_\theta^2 \tag{4.I.5}$$

The forces acting on the membrane are:

$$N_l = \sigma_l \cdot h = \frac{\sigma_l \cdot h_o}{\lambda_l \cdot \lambda_\theta} \approx 2C_{10} \cdot h_o \cdot \left(\frac{\lambda_l}{\lambda_\theta}\right) \tag{4.I.6}$$

$$N_\theta = \sigma_\theta \cdot h = \frac{\sigma_l \cdot h_o}{\lambda_l \cdot \lambda_\theta} \approx 2C_{10} \cdot h_o \cdot \left(\frac{\lambda_\theta}{\lambda_l}\right) \tag{4.I.7}$$

Now $N_l \cdot N_\theta = (2C_{10}h_o)^2 = N_o^2$, a constant. Further, stress equilibrium yields $N_l = N_o$. Therefore, $N_\theta \equiv N_l$. A hoop stress condition is:

$$\frac{\sigma_l h_o}{N_l} = \frac{PR}{2} \tag{4.I.8}$$

[1] Adapted from Williams [107], by permission of Ellis Horwood, Ltd., copyright owner.

© 1996 Carl Hanser Verlag. All rights reserved.
No unauthorized disclosure or reproduction; licensed to purchaser only.

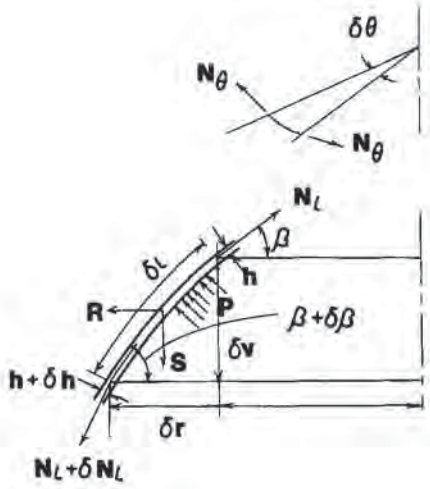

Figure 4.70 Membrane stretching geometry. Adapted from [107] and used with permission of Ellis Horwood, Ltd., copyright owner

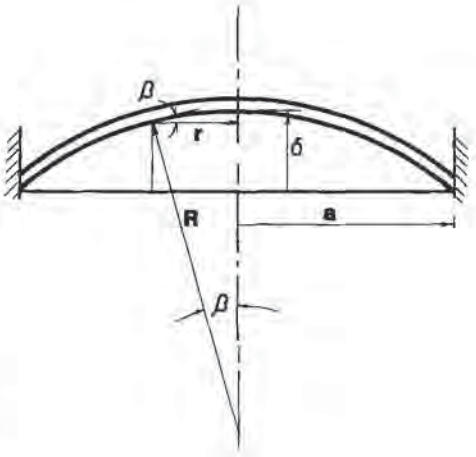

Figure 4.71 Geometry of stretched cap or dome. Adapted from [107] and used with permission of Ellis Horwood, Ltd., copyright owner

As a result:

$$\sigma_1 = \lambda_1^2 \cdot \frac{PR}{2h_o} \approx 2C_{10} \cdot \lambda_1^2 \tag{4.I.9}$$

And since $R = R(a,\delta)$ above:

$$\frac{Pa}{2h_o} \approx \frac{4C_{10}(\delta/a)}{1+(\delta/a)^2} = \frac{4G(\delta/a)}{1+(\delta/a)^2} \tag{4.I.10}$$

where G is the elastic modulus of the new-Hookean polymer, $G = C_{10}$. This is the neo-Hookean relationship between applied pneumatic pressure, P, and the extent of deformation, given as δ/a.

© 1996 Carl Hanser Verlag. All rights reserved.
No unauthorized disclosure or reproduction; licensed to purchaser only.